Spray Processes in Optical Diesel Engines - Air-Entrainement and Emissions

Chartier, Clement

2012

Spray Processes in Optical Diesel Engines

Air-Entrainment and Emissions

Clément Chartier

Doctoral Thesis

Division of Combustion Engines
Department of Energy Sciences
Faculty of Engineering
Lund University

LUND UNIVERSITY

ISBN 978-91-7473-297-9
ISRN LUTMDN/TMHP-12/1087-SE
ISSN 0282-1990

Division of Combustion Engines
Department of Energy Sciences
Faculty of Engineering
Lund University
P.O. Box 118
SE-22100 Lund
Sweden

Printed in Sweden by Tryckeriet E-huset, Lund, April 2012

Abstract

Internal combustion engines have been an important technological field for more than a century. It has had an important impact on society through improved transportation and industrial applications. However, concerns about environmental effects of exhaust gases and utilization of oil resources have pushed development of combustion engines towards cleaner combustion and higher efficiencies.

The diesel engine is today an interesting solution in terms of fuel economy. However, emissions of pollutants such as soot particles are still a major concern for diesel engines. The combustion process in diesel engines is far from fully understood and there are many to questions to be answered about emissions formation and oxidation within the combustion chamber. The objective of this work is it to gain knowledge on in-cylinder processes related to engine-out emissions. More specifically, the focus is set on understanding the connections between spray processes and the formation of pollutants such as soot particles and unburned hydrocarbons by using optical diagnostics. Engines modified for optical studies allowing optical access to the combustion chamber have been used in the different investigations presented in this thesis. Even though engines are complex systems with interacting sub-systems, such as turbochargers and after-treatment devices, the focus of this work is solely on the in-cylinder processes. The focus of this thesis is fuel-jet mechanisms related to air-entrainment and emission formation. The different investigations conducted in this work can be divided in two main categories. First, air-entrainment in fuel jets and its coupling to emissions formation were studied in different optical engines. Previous results in the field, often obtained in constant volume combustion vessels, were used for prediction calculations and comparison between free jets and jets in engine environment. Secondly, multiple injection strategies were investigated to reduce engine-out emissions of soot and unburned hydrocarbons and also to stabilize combustion in cold conditions.

The results presented in this thesis can be divided into two main categories; air entrainment in fuel jets and multiple injection strategies. The first part regards air entrainment upstream of the lift-off length as well as in the interaction between adjacent jets. The second part presents multiple injections strategies as a tool for combustion stabilization in cold conditions and emissions reduction.

Populärvetenskaplig sammanfattning

Att kunna resa och transportera gods är en del av människors vardag i dagens samhälle. De flesta av dessa transportmedel använder förbränningsmotorer på grund av deras flexibilitet, låga totalkostnad och långa räckvidd. Utsläpp i olika former är en oönskad biprodukt av förbränningsmotorer som är skadlig både för människor och för miljön. Dieselmotorer är idag bland de mest energieffektiva motorerna och har relativt låga well-to-wheel utsläpp av koldioxid. Motorer har utvecklats under mer än hundra år och blivit betydligt renare när det gäller avgasutsläpp. Ändå finns det fortfarande skadliga ämnen i avgaserna som kväveoxider, obrända kolväten, sotpartiklar, kolmonoxid och koldioxid. Dagens utveckling fokuserar på att sänka dessa utsläpp för att klara framtida utsläppskrav, som t.ex. Euro VII som förväntas träda i kraft innan 2020, samtidigt som bränsleförbrukningen måste minskas. Man har idag betydande kunskap om förbränningen i dieselmotorer, men det finns fortfarande mycket kvar att förstå om detaljerna i förbränningsrummets processer. Aktiv forskning om förbränningsprocessen förbättrar förutsättningarna för att utveckla effektivare och renare motorer.

Denna avhandling syftar till att bidra till förståelsen av dieselförbränning och koppla den till bildning av utsläpp. Ett av de huvudområden som täcks är bildning av sotpartiklar under förbränningen. Andra forskare har visat vikten av att blanda in mycket luft i den bränsle-spray som sprutas in i förbränningsrummet för att minska sotbildningen. Det är förhållandet mellan bränsle och luft som avgör om sot ska bildas eller inte. Avhandlingen beskriver hur moderna insprutningssystem kan öka luftinblandningen och därmed sänka mängden sotpartiklar i avgaserna under den nivå som är mätbar med konventionella instrument. I avhandlingen visas det också hur närliggande bränslesprayer kan påverka varandra och bidra till minskad luftinblandning och ökad inblandning av varma förbränningsgaser i sprayen. Detta resulterar i att risken för sotbildning ökar markant.

Användning av flera insprutningar under samma förbränningscykel har visat sig kunna bidra till minskade utsläpp av både sot och obrända kolväten. Genom att spruta in lite extra bränsle mot slutet av förbränningen så kan man öka temperaturen och bilda hydroxylradikaler vilket kan hjälpa till att oxidera det sot som har bildats tidigare under förbränningen. Dessutom kan man under vissa förutsättningar blanda in för mycket luft i sprayen. I extrema fall kan bränslet då inte förbrännas helt, vilket ger obrända kolväten i avgaserna och orsakar sämre

bränsle-effektivitet. Också här kan en extra insprutning användas, men för att skapa bränslerikare blandningar i områden där luftmängden var för hög. Resultaten visar att dessa områden antänds efter den andra insprutningen vilket leder till 20 % minskning av de obrända kolvätena i de studerade fallen. Slutligen har en studie i denna avhandling visat hur multipla insprutningar markant kan förbättra startegenskaper hos dieselmotorer under kalla vinterförhållanden. Genom att dela upp bränslemängden i flera insprutningar blir förångningsprocessen mindre energikrävande och temperaturen i förbränningsrummet kan hållas på en rimlig nivå för antändningen.

Acknowledgments

There are many persons that I would like to thank for their contributions to this work. First of all, my supervisor, Öivind Andersson, who has been a great support in all aspects involved in Ph.D. studies. His dedication to sharing knowledge and methods has been highly motivating during these years. *Merci!*

Rolf Egnell who was my supervisor at the beginning of this thesis has brought many ideas and has been a great source of inspiration. Some say he owns every single model Citroën has made!

I would also like to thank my co-supervisor Professor Bengt Johansson who always has ideas and useful answers about combustion engines.

I am also grateful to my colleagues from the combustion physics department for their expertise on laser diagnostics and collaboration in our measurement campaigns. It is always a special moment when engines and lasers happen to work at the same time. I also want to acknowledge our technicians, especially Jan-Erik Nilsson and Kjell Jonholm, for having kept the lab in perfect condition along the years.

A great thanks to the industrial members of the GenDies group for a very fruitful collaboration. Their guidance on future research subjects and open-mindedness to suggestions contribute largely to making this project very pleasant and motivating.

Two years ago, I had the opportunity to stay for three months as a guest researcher at Sandia national labs in Livermore. I am very thankful to all the persons who made this visit possible both in Lund and at Sandia. It was a very enriching period where I have had the chance to meet accessible and inspiring persons. A special thanks to Mark Musculus, Mohan Bobba and Dave Cicone for their hospitality, support and ideas. They made everything possible in order to help me finish the experiments in time before the end of my stay, and it worked out.

I would like to thank all my colleagues and friends at the division of combustion engines for making the daily life at work more enjoyable. I sincerely appreciate the good daily discussions and laughs, thank you for all that!

Last but not least, I would like to thank my parents and family for being a great source of inspiration and for their support throughought my studies. Special thanks to my better half Ann-Sofie for her love and patience with me, especially in the last few months!

List of Publications

Paper I

Analysis of Smokeless Spray Combustion in a Heavy-Duty Diesel Engine by Combined Simultaneous Optical Diagnostics

Clément Chartier[1], Ulf Aronsson[1], Öivind Andersson[1], Rolf Egnell[1], Robert Collin[2], Hans Seyfried[2], Mattias Richter[2], Marcus Aldèn[2]
[1]*Division of Combustion Engines, Lund University, Sweden*
[2]*Division of Combustion Physics, Lund University, Sweden*

SAE Technical Paper 2009-01-1353

Paper II

Effect of Injection Strategy on Cold Start Performance in an Optical Light-Duty DI Diesel Engine

Clément Chartier, Ulf Aronsson, Öivind Andersson, Rolf Egnell
Division of Combustion Engines, Lund University, Sweden

SAE International Journal of Engines, 2010 2:431-442

Paper III

Effects of Post-Injection Strategies on Near-Injector Over-Lean Mixtures and Unburned Hydrocarbon Emission in a Heavy-Duty Optical Diesel Engine

Clément Chartier[1], Öivind Andersson[1], Bengt Johansson[1]
Mohan K. Bobba[2], Mark P. Musculus[2]
[1]*Division of Combustion Engines, Lund University, Sweden*
[2]*Sandia National Laboratories Livermore, CA, United States*

SAE International Journal of Engines, 2011 4:1978-1992

Paper IV

Influence of Jet-Jet Interactions on the Lift-Off Length in an Optical Heavy-Duty DI Diesel Engine

Clément Chartier, Ulf Aronsson, Öivind Andersson, Rolf Egnell, Bengt Johansson
Division of Combustion Engines, Lund University, Sweden

Submitted to International Journal of Engine Research

Paper V

Air Entrainment in Wall-Jets using SLIPI in a Heavy-Duty Diesel Engine

Clément Chartier[1], Johan Sjöholm[2], Elias Kristensson[2], Yann Gallo[1], Öivind Andersson[1], Mattias Richter2, Marcus Aldén[2] and Bengt Johansson[1]
[1]*Division of Combustion Engines, Lund University, Lund, Sweden*
[2]*Division of Combustion Physics, Lund University, Lund, Sweden*

Submitted to SAE Powertrains, Fuels & Lubricants Meeting, September 18-20, 2012, Malmo, Sweden

Paper VI

Planar Laser-Diagnostics of Soot and OH with Post-Injections in a Heavy-Duty LTC Diesel Engine

Mohan K. Bobba[1], Clément Chartier[2], Bengt Johansson[2], Öivind Andersson[2], and Mark P. B. Musculus[1]
[1]*Sandia National Laboratories Livermore, CA, United States*
[2]*Division of Combustion Engines, Lund University, Sweden*

Proceedings of THIESEL 2010 Conference on Thermo- and Fluid Dynamic Processes in Diesel Engines, Valencia, Spain, September 14-17 2010.

Other publications

Heat Release Comparison Between Optical and All-Metal HSDI Diesel Engines

Ulf Aronsson, Clément Chartier, Uwe Horn, Öivind Andersson, Bengt Johansson, Rolf Egnell
Division of Combustion Engines, Lund University, Sweden

SAE Technical paper 2008-01-1062

Analysis of the Correlation Between Engine-Out Particulates and Local Φ in the Lift-Off Region of a Heavy Duty Diesel Engine Using Raman Spectroscopy

Ulf Aronsson[1], Clément Chartier[1], Öivind Andersson[1], Rolf Egnell[1], Johan Sjöholm[2], Mattias Richter[2], Marcus Aldén[2]
[1]*Division of Combustion Engines, Lund University, Sweden*
[2]*Division of Combustion Physics, Lund University, Sweden*

SAE International Journal of Fuels and Lubricants October 2009 vol. 2 no. 1 645-660

Analysis of EGR Effects on the Soot Distribution in a Heavy Duty Diesel Engine using Time-Resolved Laser Induced Incandescence

Ulf Aronsson[1], Clément Chartier[1], Öivind Andersson[1], Johan Sjöholm[2], Rikard Wellander[2], Mattias Richter[2], Marcus Aldén[2], Paul C. Miles[3]
[1]*Division of Combustion Engines, Lund University, Sweden*
[2]*Division of Combustion Physics, Lund University, Sweden*
[3]*Sandia National Laboratories Livermore, CA, United States*

SAE International Journal of Engines, 2010, 3(2), 137-155.

Impact of Mechanical Deformation due to Pressure, Mass, and Thermal Forces on the In-Cylinder Volume Trace In Optical Engines of Bowditch Design

Ulf Aronsson, Hadeel Solaka, Clément Chartier, Öivind Andersson and Bengt Johansson
Division of Combustion Engines, Lund University, Sweden

SAE paper 2011-26-0082

Challenges for In-cylinder High-Speed Two-Dimensional Laser-Induced Incandescence Measurements of Soot

Johan Sjöholm[1], Rikard Wellander[1], Henrik Bladh[1], Mattias Richter[1], Per-Erik Bengtsson[1], Marcus Aldén[1], Ulf Aronsson[2], Clément Chartier[2], Öivind Andersson[2], Bengt Johansson[2]
[1]*Division of Combustion Physics, Lund University, Sweden*
[2]*Division of Combustion Engines, Lund University, Sweden*

SAE International Journal of Engines, 2011, 4(1):1607-1622.

Lift-off and stabilization of n-heptane combustion in a diesel engine with a multiple-hole nozzle injector

Rickard Solsjö[1], Mehdi Jangi[1], Clément Chartier[2], Öivind Andersson[2] and Xue-Song Bai[1]
[1]*Division of Combustion Fluid Mechanics, Lund University, Sweden*
[2]*Division of Combustion Engines, Lund University, Sweden*

Accepted at "The Combustion Institute, 34th International Symposium on Combustion", PROCI-D-12-00837, 2012.

Quantitative in-cylinder fuel measurements in a heavy-duty diesel engine using Structured Laser Illumination Planar Imaging (SLIPI)

Johan Sjöholm[1], Clément Chartier[2], Elias Kristensson[1], Edouard Berrocal[1], Yann Gallo[2], Mattias Richter[1], Öivind Andersson[2], Marcus Aldén[1], Bengt Johansson[2]
[1]*Division of Combustion Physics, Lund University, Sweden*
[2]*Division of Combustion Engines, Lund University, Sweden*

Accepted for publication at COMODIA conference on Combustion Modeling and Diagnostics, Fukuoka, Japan, July 23-26 2012.

Nomenclature

ATDC	After Top Dead Centre
CAD	Crank Angle Degree
CAFE	Corporate Average Fuel Economy
CI	Compression Ignition
CO	Carbon monoxide
CO_2	Carbon Dioxide
COV	Coefficient Of Variation
DPF	Diesel Particulate Filter
EGR	Exhaust Gas Recirculation
EOI	End of Injection
EU	European Union
FID	Flame Ionization Detector
GHG	Green House Gases
UHC	Unburned Hydro Carbon
IMEP	Indicated Mean Effective Pressure
LIF	Laser Induced Fluorescence
LII	Laser Induced Incandescence
LOL	Lift-Off Length
LTC	Low Temperature Combustion
MK	Modulated Kinetics
NO_X	Nitrogen Oxides
PAH	Poly-Aromatic Hydrocarbons
PCI	Premixed Compression Ignition
PPC	Partially Premixed Combustion
PPCI	Partially Premixed Compression Ignition
PM	Particulate Matter
RPM	Revolutions Per Minute
SI	Spark Ignited
SLIPI	Structured-Light Illumination Planar Imaging
SOI	Start of Injection
TDC	Top Dead Center
UE15	European Union with 15 countries (between 1995 and 2004)
UV	Ultra Violet

Table of Contents

Chapter 1

Introduction

1.1 Background

1.1.1 The diesel engine, an interesting solution?

Internal combustion engines have been an important technological field for more than a century. It has had an important impact on society through improved transportation and industrial applications. Although the basic principle of the four-stroke engine has not changed since Beau de Rochas' patent in 1862, four-stroke engines have continuously been under development and still are. Reliability and output performance were the main domains of improvement until the second half of the twentieth century; whereafter the focus has shifted to exhaust gas emissions and fuel consumption [1].

Concerns about the effects of green house gases (GHG) on climate change has brought carbon dioxide (CO_2), a major GHG, to the front scene of emissions discussions. A recent analysis showed that 23 % of the UK's carbon dioxide emissions in 2008 originate from internal combustion engines used in transportation, compared to 14 % in 1980 [2]. These figures are representative of most western countries and show the need for research towards more fuel-efficient engines and other technologies leading to lowered carbon dioxide emissions.

Due to its higher fuel efficiency, the diesel engine is indeed an interesting solution in the search for more energy efficient transports. Furthermore, it has shown to become cleaner in terms of exhaust emissions for every generation developed during the past decades. However, as will be discussed later, stringent emissions

legislations are still challenging for the diesel engine and highlight the need for cleaner combustion and advanced after-treatment systems.

1.1.2 An important place in the automotive sector

Diesel engines are dominant in the heavy-duty sector, both on land and at sea, due to their lower specific fuel consumption and higher specific torque performance compared to gasoline engines. For light-duty applications, the share of diesels varies largely in time and location but a significant increasing trend is observed. In the European Union (UE15), 51.9 % of passenger car registrations were diesels in January 2009 whereas they represented a share of only 29 % in 1999 [3]. The geographical disparities are large. In Sweden, for example, this share evolved from 7.2 to 40 % during the same period and from 54.3 to 70.3 % in Belgium [3]. However, despite differences in absolute market share levels and increase rates, all countries within the UE15 show a growing interest in light-duty diesel vehicles.

Diesel engines have seen significant improvements in terms of driving comfort and performance in the last decade, contributing to this trend. However, in the context of CO_2 emissions reductions and unstable fuel prices, the higher fuel efficiency of the diesel engine compared to spark-ignited (SI) engines, increasing fuel prices and changing tax policies can be assumed to be part of the factors behind this trend.

The low fuel consumption of the diesel engine compared to its competitors was one major goal of Rudolf Diesel when developing his compression ignition concept in the 1890's [4]. The part load pumping losses of diesel engines are significantly lower compared to SI since the intake airflow is not throttled. This is because the diesel engine works with excess air. Excess air also increases the polytropic exponent which is directly coupled to the thermodynamic efficiency of the diesel cycle. Furthermore, as fuel is injected towards the end of the compression stroke and relies on auto-ignition to start the combustion, knocking is not an issue. For this reason, the compression ratio of diesel engines is higher compared to SI engines. A higher compression ratio increases the thermodynamic efficiency and contributes to the higher brake efficiency of the diesel engine.

1.2 Objectives and Scope of the thesis

The main goal of this thesis it to gain knowledge on in-cylinder processes related to engine-out emissions. More specifically, the focus is set on understanding the connections between spray processes and the formation of pollutants such as soot

particles and unburned hydrocarbons by using optical diagnostics. Air-entrainment in fuel jets is a central topic in this thesis and was investigated for a variety of conditions. This work was performed in close collaboration with the automotive industry and addresses essential topics for future engine developments.

The scope of this thesis includes fuel-jet mechanisms related to air-entrainment and emissions formation in direct-injected compression-ignition engines. The types of engines concerned in this work are four-stroke heavy- and light-duty diesel engines. Even though engines are complex systems with interacting sub-systems, such as turbochargers and after-treatment devices, this work solely deals with the in-cylinder processes. The main combustion type studied is spray-driven combustion and in some cases low-temperature combustion with short positive ignition-dwells.

The different investigations conducted in this work can be divided in two main categories. First, air-entrainment in fuel jets and its coupling to emissions formation was studied in optical engines. Previous results in the field, often obtained in constant volume combustion vessels, were used for prediction calculations and comparison between free jets and jets in an engine environment. Secondly, multiple-injection strategies were investigated to reduce engine-out emissions of soot and unburned hydrocarbons (UHC) and also to stabilize combustion in cold conditions.

1.3 Approach

In this work, measurements in optical engines were the main investigation tools to answer scientific questions about fuel-jets. The usage of a variety of techniques, from natural chemiluminescence to advanced laser-diagnostics, gave general and detailed information about diesel combustion. Advanced laser-diagnostics were employed in several studies in collaboration with the division of combustion physics at Lund University. The focus of this group is to develop and implement such techniques, but their research is not primarily focused on the engine processes themselves. The main advantage of such collaborations is to merge knowledge from two fields of expertise in a single project. Discussions between the two groups about upcoming combustion investigations lead to the development of new or existing laser-diagnostics. Advanced laser techniques will be described in greater detail in Chapter 3. In most cases, modifications to the optical engines, such as piston geometry, optical access or cooling setup were made prior to new studies. The combustion physics group implemented their techniques in the optical engines whereas the combustion engine group focused on engine related

questions. As essential complements to optical measurements, in-cylinder pressure sampling, heat release calculations and exhaust gas analysis were performed as well.

1.4 Thesis contributions

As will be explained in greater detail later in this thesis, this work deals with a variety of aspects of combustion in compression-ignition engines and presents novel insights about:

- Air-entrainment in fuel jets prior to the lift-off region and lift-off length stabilization in an optical engine.
- Air-entrainment in confined wall-jets in a heavy-duty optical engine.
- Fuel evaporation issues and combustion stabilization after start at low ambient temperatures using multiple injection strategies.
- Reductions of engine-out soot and unburned hydrocarbons emissions using different post-injection strategies.

Chapter 2

Diesel combustion

2.1 General concept

Diesel engines, which are also called compression-ignition engines (CI), work according to the four-stroke cycle for most applications. The two-stroke cycle is commonly used for large-bore marine diesel engines but this type of engine is outside the scope of this thesis.

During the first phase of diesel combustion, the intake charge is compressed and the fuel is injected directly into the cylinder at the end of the compression stroke. High gas temperature resulting from the compression triggers autoignition of the air-fuel mixture near top dead center (TDC). The time elapsed between the start of injection (SOI) and start of combustion is referred to as the ignition delay. This corresponds to the time between 'SOI' and the start of 'Premixed combustion' in Figure 1. It is caused by the need of the air-fuel mixture to reach a high temperature, typically above 800 K, for ignition to occur.

When mixture temperatures and local stoichiometry are right in some regions of the cylinder, the combustion starts spontaneously. This causes pressure and temperature to rise globally in the cylinder, which causes ignition in other regions. This part is called the premixed combustion phase of the combustion and corresponds to the peak in rate of heat release shown in Figure 1.

Depending on the length of the ignition delay, the quantity of premixed fuel will vary. As a consequence the amount of heat released in the premixed combustion phase is largely depending on the ignition delay.

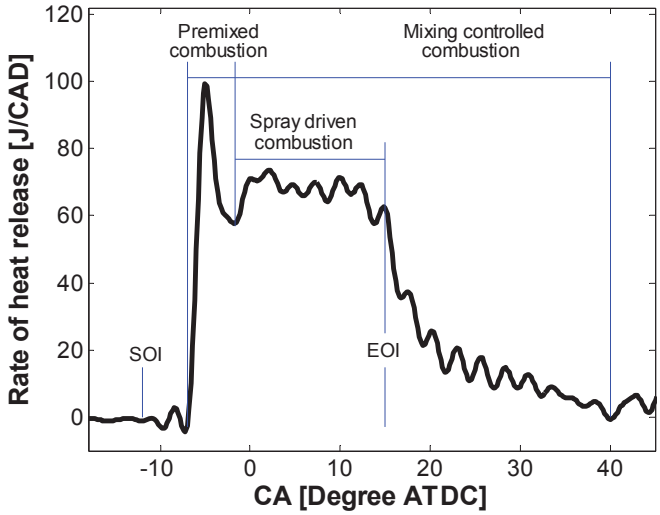

Figure 1: *Typical rate of heat release for conventional diesel combustion [5].*

A large amount of heat released in the premixed phase usually causes a high pressure derivative since the auto-ignition of premixed mixtures is very rapid. The high pressure derivative results in the characteristic diesel engine sound.

The third phase of diesel combustion is known as the spray-driven combustion or quasi-steady diffusion combustion, in this phase fuel burns as it is injected, evaporated, mixed with air and ignited. After the end of injection (EOI), the late combustion phase takes place.

Both the spray driven and the late combustion phases are part of the mixing controlled combustion phase. As will be explained in Chapter 2, the mixing process of air into the fuel jet limits the combustion rate in this phase.

2.2 Spray processes

2.2.1 The quasi-steady jet

The spray driven phase of diesel combustion presented in the previous section is important for conventional diesel combustion since it is often where most of the heat release takes place. A conceptual model describing combustion in quasi-steady diesel jets was presented by Dec in 1997. It is based on laser-diagnostic studies under certain operating conditions [6]. It gives a general mental image, shown in Figure 2, which is useful in research and development of diesel combustion systems. Liquid fuel emanating from the nozzle vaporizes and mixes

into a combustible but fuel-rich mixture. The equivalence ratio is an important concept for air entrainment. It relates the fuel-to-air mass ratio to the stoichiometric fuel-air mass as shown in Eq.1.

$$\phi = \frac{\left({}^{Fuel}/_{Air}\right)_{actual}}{\left({}^{Fuel}/_{Air}\right)_{stoichiometric}} \qquad (1)$$

The fuel rich mixture in beige in Figure 2 normally has a local fuel-air equivalence ratio, ϕ, between two and four. A narrow, light-blue zone of fuel-rich premixed combustion surrounds this mixture. Soot formation starts in the product gas from this region if the local equivalence ratio is above a value of about two [7]. The soot formation process continues in the downstream regions (dark blue and red-yellow in the figure) and soot particles increase in number and size until they reach the head of the jet.

A hot diffusion flame is located at the periphery of the jet where OH is observed and it is hypothesized that most of the thermal NO is formed in this region. This high temperature envelope around the jet is also where soot is oxidized by OH-radicals. The distance between the nozzle orifice and the most upstream part of the OH envelope is referred to as the lift-off length.

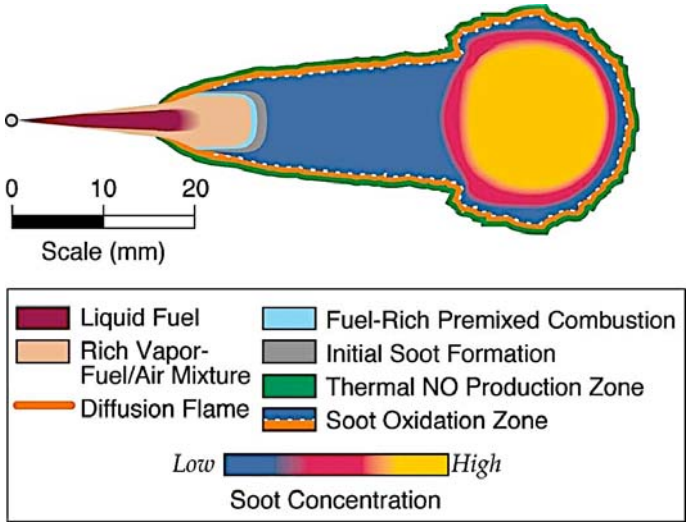

Figure 2: *Conceptual model of a quasi-steady diesel jet by Dec. Reproduced from [6]*

It should be noted that the conceptual model was based on measurements at given operating conditions. Use of exhaust gas recirculation (EGR), change in nozzle dimensions, injection pressure, fuel properties or in-cylinder conditions will affect this picture in terms of the sizes or precise locations of certain zones.

Modern diesel engines are equipped with high-pressure fuel pumps capable of pressures in the range of 2000 bar or 2500 bar, for light- and heavy-duty applications, respectively. It makes it possible to inject the fuel mass required for full load operation with relatively small nozzle orifices in the range of 0.1 to 0.2 mm. Small orifices and high injection pressures enhance atomization, i.e. break-up of liquid fuel into droplets. This results in a large total droplet area, leading to rapid vaporization up to the saturation limit. This means that vaporization cannot be enhanced by finer atomization. Instead, more air has to be mixed into the volume in order to go below the saturation limit. Spray vaporization under diesel conditions is thereby mixing-limited, rather than limited by atomization [8]. This has been found under conditions in modern engines with common diesel fuel. Low volatility fuels, high viscosity fuels, larger nozzle holes, very low injection pressures or in-cylinder densities would likely shift the limiting process from mixing to atomization.

2.2.2 Air-entrainment in fuel jets

Since the spray-vaporization process is mixing-limited for modern diesel engine conditions, it is important to understand how the surrounding air mixes into fuel jets. An expression for equivalence-ratio predictions in steady jets was developed by Naber and Siebers using an idealized model of a free-jet [8]. The model gives a prediction of the cross-section average equivalence ratio $\bar{\phi}$. The model assumed constant spreading angle α, radially uniform velocity and fuel concentration profiles to derive this expression from conservation of mass and momentum principles:

$$\bar{\phi}(x) = \frac{2\left(Air/Fuel\right)_{stoichiometric}}{\sqrt{1+16\left(\frac{x}{x^+}\right)^2}-1}, \qquad (2)$$

where, x is the downstream axial location and x^+ is a characteristic length defined as:

$$x^+ = \sqrt{\frac{\rho_f}{\rho_a}}\frac{d\sqrt{C_a}}{tan(\alpha/2)}, \qquad (3)$$

where ρ_a and ρ_f are the ambient and fuel densities, respectively, d the physical nozzle hole diameter and C_a the area contraction coefficient. The spreading angle of the model jet, α depends only on ρ_a and ρ_f.

Based on these expressions, the jet's mean equivalence-ratio can be calculated at any downstream distance x from the nozzle. Furthermore, the reciprocal of that equivalence ratio relationship (x100) gives the quantity of air entrained at any location up to the lift-off length as a percentage of the total air required to burn the fuel being injected. It is referred to as the percentage of stoichiometric air ζ_{st}, with:

$$\zeta_{st}(\%) = \frac{100}{\bar{\phi}} \qquad (4)$$

In order to better understand the effect of different engine parameters on air-entrainment up to the lift-off length, a simple parametric calculation is shown in Figure 3 as an example. A baseline case was used with 1000 bar injection pressure, 140 µm nozzle hole diameter, 20 kg/m^3 ambient density and European diesel fuel with a density of 840 kg/m^3 at 15°C, which is typical of mid-load light-duty engine conditions. For comparison, one parameter only was varied at a time; all others not indicated for each curve are the same as for the baseline case.

It appears clearly that according to Siebers expression, the injection pressure has no effect on air-entrainment. Increasing ambient density leads to a significant increase in air-entrainment as does decreasing the nozzle-hole size.

The trend in modern diesel engines is pointing towards smaller nozzle holes and higher boost pressures with better inlet charge cooling leading to higher ambient densities. These technical choices improve the air-entrainment in the jet and therefore contribute to reductions in engine-out emissions of soot as will be presented later in this chapter.

As mentioned previously, the distance between the nozzle orifice and the most upstream part of the OH envelope in Figure 2 is referred to as the lift-off length and is an important parameter for air-entrainment in diesel jets. The air-entrainment rate into the central parts of the jet is the largest along this portion and the equivalence-ratio reached in the lift-off region influences the soot production processes.

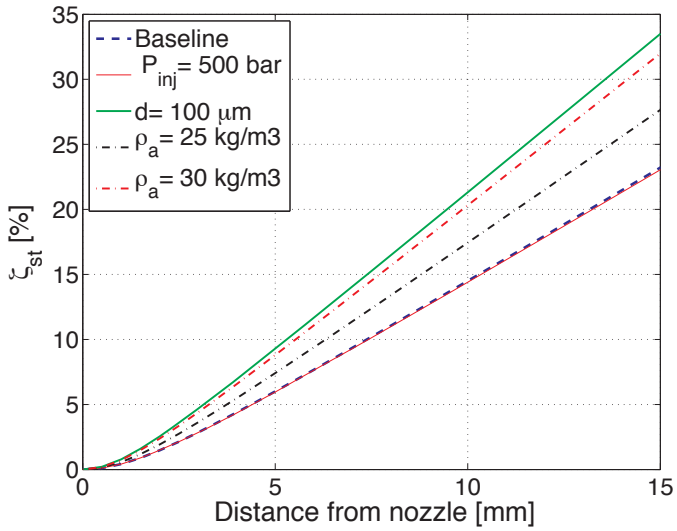

***Figure** 3: The percentage of stoichiometric air entrained in the jet versus distance from the nozzle for several parameters variations compared to a baseline case (1000 bar injection pressure, 20 kg/m³ ambient density, 140 μm nozzle hole diameter, and European diesel fuel).*

Air-entrainment into the jet still occurs downstream of the lift-off region but, as the diffusion flame consumes a significant amount of oxygen; it does not tend to affect the equivalence ratio in the inner region of the jet. It has been shown that reaching a ϕ value below two at lift-off reduces drastically the soot formation rate in the jet [7,9,10]. Therefore, it is of interest to maximize air-entrainment in the jet and especially along the lift-off section of the jet.

An empirical expression was established by Pickett *et al.* [11] to predict the lift-off length, *H*:

$$H \propto T_a^{-3.74} \rho_a^{-0.85} d^{0.34} U Z_{st}^{-1} \quad , \qquad (5)$$

where T_a is the ambient gas temperature, ϱ_a is the ambient density, d is the nozzle hole diameter, U is the fuel velocity at the nozzle exit and Z_{st} is the stoichiometric mixture fraction which is the ratio of the fuel mass to the total mass at stoichiometric conditions.

It appears clearly that the ambient temperature is the dominant factor for lift-off stabilization. The linearity regarding jet velocity U means that changes in the injection pressure will change the lift-off length. Even though it was seen previously that increasing injection pressure does not affect the air-entrainment rate in the jet, it will increase the lift-off length and therefore lengthen the

portion of the jet where no flame surrounds the jet. This will lead to more air entrained in the jet in total up to the lift-off length and therefore a lower ϕ value in this region.

As described above, aiming at higher entrainment rates in the jet is an essential key in reducing soot formation by obtaining leaner fuel-air mixtures. However, if the mixture becomes too lean, i.e. below approximately ϕ =0.5, the lower ignitability limit is reached and combustion cannot be sustained.

This situation has been identified to possibly occur after the end-of-injection where a rapid leaning-out of the mixtures is observed in the tail of the jet [12]. Applying the conservation of momentum flux principle to sections of the jet, the decreasing fuel flow coming from the nozzle after EOI is compensated by radial air-entrainment into the jet. Air-entrainment rates after EOI was shown to be as high as 2.5 times the steady-jet entrainment-rate [12]. Increased air-entrainment leads to loss of axial velocity and stagnant over-lean mixtures close to the nozzle. As a result, unburned hydrocarbons emissions (UHC) are rising in the exhaust gases [12]. Therefore, air-entrainment in the jet has to be maximized to reduce soot formation but without exceeding a certain threshold after end of injection otherwise ignition becomes impossible to achieve.

2.3 Emissions

2.3.1 Emissions legislations

In order to limit the environmental impact of combustion engines, authorities in different regions of the world define acceptable limits for exhaust emissions. The main regulations of harmful emissions for diesel engines concern NO_x (NO and NO_2), carbon monoxide (CO), unburned hydrocarbons (UHC), and particulate matter (PM). PM is a general category for all liquid or solid particles found in exhaust-gases. As discussed later in this chapter, soot is the most important component of PM for diesel engines.

Table 1 and 2 present the on-road European regulations for light and heavy-duty diesel vehicles, respectively. Similar standards are found in other regions of the world.

Carbon dioxide was previously an unregulated emission from internal combustion engines. However, concerns about greenhouse gases emissions have grown in the past decade. A recent EU regulation for passenger cars fixes a fleet average CO_2 target of 130 g/km during the European test cycle by 2015 and 95 g/km by 2020.

This target is modulated with vehicle mass and lighter cars have lower CO_2 targets while heavier cars have higher CO_2 targets [19]. Similar regulations exist in the United States under the name Corporate Average Fuel Economy (CAFE) for both passenger cars and light trucks ($<$ 4500 kg) [20]. However, regulations on fuel economy for heavy-duty engines do not exist yet. Nevertheless, CO_2 emissions are coupled to fuel consumption, which is of central interest for most heavy-duty applications because of its large effect on the total cost of ownership for such vehicles.

The regulations are getting more challenging for every step and significant reductions of harmful pollutants have been achieved during the past twenty years. Combined efforts of research and development on both in-cylinder pollutant control and after-treatment have permitted fulfilment of the latest regulation levels. For example, Diesel Particulate Filters (DPF) are becoming more common to control the PM emissions.

Table 1: *EU emission standards for diesel passenger cars, g/km [19]*

Tier	Date	CO	HC+NO_x	NO_x	PM	PN *[#/km]*
Euro I	1992.07	2.72	0.97	-	0.14	-
Euro II, IDI	1996.01	1.0	0.7	-	0.08	-
Euro II, DI	1996.01	1.0	0.9	-	0.10	-
Euro III	2000.01	0.64	0.56	0.50	0.05	-
Euro IV	2005.01	0.50	0.30	0.25	0.025	-
Euro Va	2009.09	0.50	0.23	0.18	0.005	-
Euro Vb	2011.09	0.50	0.23	0.18	0.005	$6.0x10^{11}$
Euro VI	2014.09	0.50	0.17	0.08	0.005	$6.0x10^{11}$

Table 2: *EU emission standards for heavy-duty diesel engines, g/kWh [19]*

Tier	Date	CO	HC	NOx	PM	PN *[#/kWh]*
Euro I	1992, $<$ 85 kW	4.5	1.1	8.0	0.612	-
	1992, $>$ 85 kW	4.5	1.1	8.0	0.36	-
Euro II	1996.10	4.0	1.1	7.0	0.25	-
	1998.10	4.0	1.1	7.0	0.15	-
Euro III	2000.10	2.1	0.66	5.0	0.10 0.13[a]	-
Euro IV	2005.10	1.5	0.46	3.5	0.02	-
Euro V	2008.10	1.5	0.46	2.0	0.02	-
Euro VI	2013.01	1.5	0.13	0.4	0.01	$6.0x10^{11}$

a - for engines of less than 0.75 dm^3 swept volume per cylinder and a rated power speed of more than 3000 min^{-1}

The filters can help meet the regulations, which are specifying a mass of PM, but may displace the size distribution towards smaller particles. These small particles, in the nanometer range, are potentially harmful for respiratory systems [21] and a particle number (PN) emission limit of 600 billion per kilometer for light-duty and per kWh for heavy-duty is effective for the *Euro VI* stage [19].

2.3.2 In-cylinder pollutants formation and oxidation

Traditionally, diesel combustion research has focused on the mechanisms behind particulate and NO_x emissions, as these have been considered as the major pollutants. Particulates are the combination of soot and other liquid- or solid-phase materials that are collected when exhaust gases pass through a filter. It is typically estimated that in diesel engines more than 50 % of the particulate matter is soot. Therefore, soot is the main particulate constituent of interest in this thesis. The other main sources of particulate matter are partially burned fuel and lubricant oil, bound water, wear metals and fuel-derived sulphate [13].

The formation of soot from vaporized fuel involves five main processes shown in Figure 4. First, pyrolysis where the fuel molecule structure is modified without being oxidized, even in the presence of oxygen. These altered fuel molecules become soot precursors such as poly-aromatic hydrocarbons (PAH). Pyrolysis is temperature dependant and its rate increases with temperature.

Soot precursors will then go through the nucleation process to form nuclei. This phase consists of additions of small hydrocarbons to larger aromatic molecules. These particle nuclei are small and represent only a small fraction of the total soot mass. It is the surface growth phase that adds mass to the previously obtained nuclei. Hydrocarbons in gas-phase are added to the surface of the small soot particles and they represent most of the mass of the final soot particle.

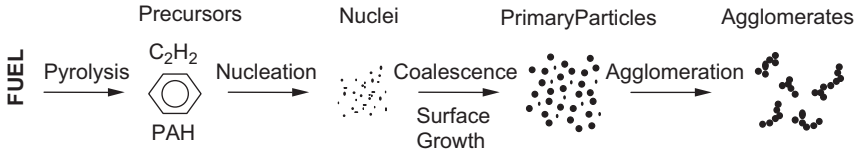

Figure 4: *Schematic diagram of the steps in the soot formation process from gas phase to solid agglomerated particles. Reproduced from [13].*

Finally, these soot particles are combined through the coalescence and agglomeration phases. The coalescence process leads to larger spherical soot particles from the collision of smaller spherical particles whereas the agglomeration phase forms groups or chains of primary particles [13].

The soot formation process in itself is only half of the mechanism behind engine-out soot emissions. The oxidation process will transform most of the formed soot into CO or CO_2 before the exhaust valves open.

More than 90 % of the formed soot is oxidized before leaving the combustion chamber in modern light-duty engines as shown in [14]. Oxidation can take place at any time in the process described above. Soot precursors as well as nuclei or agglomerates can be oxidized.

The second main pollutant in diesel engines is NO_x. There are three main mechanisms for NO_x-formation in combustion. First, fuels containing organic nitrogen can form so-called fuel-NO_x. Secondly, NO_x can be formed in rich zones through the so-called prompt mechanism. Finally, NO_x can be formed by reactions between N_2 and O_2 in the air. This mechanism is sensitive to temperature and is therefore called thermal NO_x. It has a fast formation rate at high temperature. Fast cooling rates during expansion cause a freezing of the reactions. Thermal NO_x is generally the dominant source in diesel combustion. The reactions describing thermal NO_x formation are given by the extended Zeldovic-mechanism [1]:

$$O + N_2 \rightleftharpoons NO + N \tag{6}$$

$$N + O_2 \rightleftharpoons NO + O \tag{7}$$

$$N + OH \rightleftharpoons NO + H \tag{8}$$

As seen in the formation processes for both soot and NO_x, temperature is an important factor for the formation of pollutants. The local equivalence-ratio is also central in the soot formation process, as richer mixtures will have a higher soot formation rate.

These two parameters, i.e. temperature and equivalence ratio, were used in simulation work by Akihama *et al.* and gave a major insight into soot and NO_x

production mechanisms, notably by using the so-called ϕ-T *map* introduced by Kamimoto and Bae [15,16].

Following a fuel element downward from the top along the conventional diesel path in blue for 21 % inlet O_2 in Figure 5, it is seen that the mixture grows leaner and hotter during the ignition delay, due to mixing with ambient gases. In this case, ignition occurs when ϕ has reached a value close to three. The ignition of premixed mixtures causes a steep temperature increase, as seen in Figure 5, until the start of the mixing controlled phase of the combustion, i.e. the diffusion combustion. Soot forms when a fuel element passes through the soot formation zone, which is located approximately between the temperatures 1600 and 2400 K, and a ϕ-value greater than two.

During the mixing-controlled phase, the theoretical fuel element follows the adiabatic flame temperature corresponding to the ambient oxygen concentration, 21 % in this example. This phase gives peak combustion temperatures above 2600 K. NO_x is formed at these high temperatures when equivalence ratios are around stoichiometric conditions.

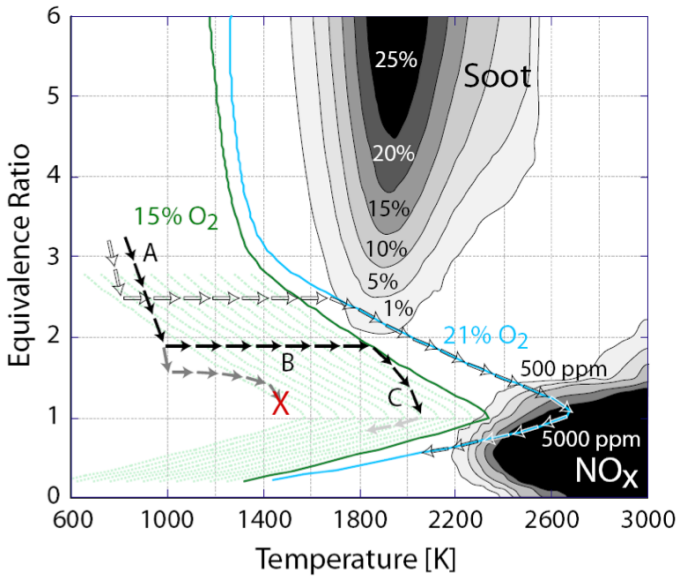

Figure 5: *Homogeneous reactor simulation results after 2 ms giving soot and NO_x formation zones in a ϕ-T map. Adiabatic flame temperature for the 21 % and 15 % oxygen conditions are indicated. Reproduced from [17].*

Finally, the late combustion phase features a temperature decrease and lean mixtures, with ϕ below unity. What is not seen in Figure 5 is the soot oxidation zone, characterized by low equivalence ratios and temperatures between 1400 and 2000 K [18]. The engine out soot level corresponds to the difference between the amounts of soot formed and oxidized. Engine-out soot emissions can thereby be decreased both by reducing soot formation and enhancing oxidation.

The NO_x formation reactions are frozen when the temperature drops in the expansion stroke. Since there is no significant in-cylinder oxidation of NO_x, this means that most of the NO_x formed survives until the exhaust valves open. Therefore, controlling NO_x emissions is a matter of reducing NO_x formation.

2.4 LTC: an alternative diesel concept

The idea of low temperature combustion (LTC) is based on reducing the combustion temperature to avoid the zones in the ϕ-T-space that have the highest production rates of soot and NO_x [22]. The LTC path in Figure 5 is represented by the black arrows. Reducing the combustion temperature is done using high rates of cooled EGR. The superior heat capacity of EGR compared to air reduces the temperature rise for a given heat release in the combustion chamber by lowering the adiabatic flame temperature [23]. Lower peak temperature during LTC operation permits avoidance of the thermal NO_x formation zone above 2200 K. Therefore, low engine-out NO_x emissions can be achieved.

EGR also slows down the kinetics by introducing inert gases in the mixture. Slower reactions cause the ignition delay to increase. A general definition for LTC concepts is when the combustion starts after the end of injection. Such positive ignition dwells enable larger degrees of premixing at start of combustion compared to spray driven cases. Together with the lower combustion temperature, higher degree of premixing permits avoidance of the soot formation region in the ϕ-T-space. In Figure 5, the start of combustion, corresponding to the segment “B” in the path of black arrows, is located below the equivalence ratio threshold of two. The longer ignition delay in LTC cases provides leaner mixtures at start of combustion compared to conventional diesel combustion.

However, significant drawbacks exist for LTC concepts, which raise new issues. High EGR rates can affect soot oxidation late in the cycle due to the low oxygen content in the cylinder and therefore soot emissions can be problematic until the EGR rate is high enough to prevent soot formation, which usually occurs in the range of 60 % [9,24]. Another major drawback of using higher EGR-rates is the

elevated levels of CO and UHC emissions, which are less problematic in conventional diesel cases using low dilution rates.

Emissions of CO and UHC arise by a number of possible mechanisms. Over-lean mixtures can be formed in some regions due to the slow reaction rates at lower combustion temperatures and the longer time available for mixing prior to ignition [25]. A local equivalence ratio below the ignitability limit, approximately ϕ=0.5, causes non-complete oxidation of the fuel and will cause CO and UHC emissions. However, both CO and UHC can originate from rich mixtures as well [26]. The increase is then due to insufficient access to oxygen and quenching in the fuel oxidation reactions, occurring below 1000 K [26], contribute to increased UHC emissions. Partially oxidized fuel deteriorates combustion efficiency, which is a further disadvantage.

LTC concepts are currently being investigated to further understand and minimize the drawbacks of these concepts while taking advantage of the low soot and NO_x emissions achievable. High EGR rates and early injections are found in concepts such as Partially Premixed Compression Ignition (PPCI) [26,27], Premixed Compression Ignition (PCI) [28] and Partially Premixed Combustion (PPC) [29,30]. Nissan pioneered LTC with their Modulated Kinetics (MK) concept using also high EGR rates but with late injections and high swirl [31,32].

Chapter 3

Diagnostics

3.1 Conventional diagnostics for combustion investigations

3.1.1 Heat-release analysis

Even though this work is performed using engines modified for optical access, they are also equipped with standard measurement devices similar to metal engines. A pressure transducer, often installed in the glow plug location, measures the pressure trace inside the cylinder. Knowing the volume of the combustion chamber as a function of the crankshaft position, the heat release during an engine cycle can be calculated from the pressure trace. Heat release analysis can give interesting information of the combustion process globally in the cylinder. Pressure and temperature are assumed uniform in the combustion chamber since the pressure trace measured in one point of the cylinder volume is the basis of heat release calculations. A brief description of heat release calculations is given in this section based on [1] and [33]. The first law of thermodynamics applied to the combustion chamber as an open system gives:

$$\frac{dQ}{dt} = \frac{dU}{dt} + \frac{dW}{dt} + \sum \dot{m}_i h_i \tag{9}$$

with dQ/dt being the heat added to the system per unit time (i.e heat released by the combustion minus heat transfer to the chamber walls). dU/dt represents the change in internal energy, dW/dt is the piston work per unit time. The last term represents mass flux across the system boundary with m_i and h_i representing the

mass and enthalpy, respectively, of an element i entering the system, such as injected fuel or flow into and out of the crevice regions.

The objective is to derive Eq.9 in order to express it as a function of volume and pressure. The internal energy, U, can be expressed as

$$U = mC_v T \tag{10}$$

where m is the mass in the system, C_v the specific heat at constant volume and T the temperature. Assuming the mass to be constant in the system, the derivative of the internal energy is

$$\frac{dU}{dt} = mC_v \frac{dT}{dt} \tag{11}$$

In order to express the temperature derivative with known parameters, the ideal gas law is employed. Likewise, the global temperature (i.e. for both burned and unburned gases) can be obtained by applying the ideal gas law to the pressure data acquired,

$$pV = mRT \tag{12}$$

Neglecting mass losses and considering R to be constant, the internal energy of the system per time unit can now be expressed as

$$\frac{dU}{dt} = \frac{C_v}{R}\left(p\frac{dV}{dt} + V\frac{dp}{dt} \right) \tag{13}$$

The second term in Eq.9, the work performed on the piston per time unit can be written as a function of cylinder pressure p and volume V as

$$\frac{dW}{dt} = p\frac{dV}{dt} \tag{14}$$

Neglecting mass exchange and inserting Eq.13 and Eq.14 in the expression for heat release (Eq.8) we obtain

$$\frac{dQ}{dt} = \frac{C_v}{R}\left(p\frac{dV}{dt} + V\frac{dp}{dt} \right) + p\frac{dV}{dt} \tag{15}$$

Making the assumption of an ideal gas, the constant R can be expressed as a function of the specific heats at constant pressure and volume:

$$R = C_p - C_v \tag{16}$$

The ratio of specific heats, γ, is given by

$$\gamma = \frac{C_p}{C_v} \tag{17}$$

Then, the first right hand term of Eq.15 can be expressed:

$$\frac{C_v}{R} = \frac{1}{\gamma - 1} \tag{18}$$

Eq.15 can be written as follows:

$$\frac{dQ}{dt} = \frac{\gamma}{\gamma - 1} p \frac{dV}{dt} + \frac{1}{\gamma - 1} V \frac{dp}{dt} \tag{19}$$

Heat transfer to the walls, dQ_{HT}/dt, can be estimated and added to Eq.19 in order to calculate the heat actually released by combustion. Assuming a uniform and constant wall temperature, we have

$$\frac{dQ_{HT}}{dt} = hA_{wall}(T_{gas} - T_{wall}) \tag{20}$$

where A_{wall} is the wall area and h is the heat transfer coefficient. The latter is estimated by an empirical relationship developed by Woschni [1]:

$$h = CB^{-0.2} p^{0.8} T^{-0.55} w^{0.8} \tag{21}$$

with C, a constant, B, the cylinder bore and w a characteristic speed given by

$$w = C_1 S_p + C_2 \frac{V_d T_r}{p_r V_r}(p - p_m) \tag{22}$$

Here, C_1 and C_2 are constants, S_p is the mean piston speed, V_d is the displacement volume, T_r, p_r and V_r are the temperature, pressure and volume at a reference

point (e.g. inlet valve closing or start of combustion). Finally, p_m is the pressure during a motored cycle at the same crank angle position as p.

Heat release calculations are based on numerous assumptions and estimations. The actual compression ratio is difficult to obtain with precision and has influence on volume calculations. Since volume is a major parameter in heat release calculations, such uncertainties can have a large impact on the heat release analysis. The volume calculations are based on geometrical data, but in reality the engine geometry can be changing due to temperature of the materials and gas pressure effects on the several engine parts such as piston and connecting rod. Previous studies in one of the heavy-duty engine used in this work showed a linear increase of the squish height with peak cylinder pressure. Deformations of the whole piston-connecting rod assembly (original connecting rod and piston, piston elongation and optical piston) where shown to increase the squish height by 1.65 mm at a TDC pressure of 87 bar [34]. The error introduced in the heat-release analysis can be corrected by rewriting the equation for in-cylinder volume as a function of crank angle degree with a spring constant taking into account the flexibility of the engine parts assembly [35].

Furthermore, the ratio of specific heats, γ, is often estimated for a given gas composition and temperature during the inlet stroke. Compression and combustion will change these parameters and thereby the actual value of γ during the engine cycle. Finally, the exact synchronization between the pressure and volume traces is of major importance for heat release calculations and can introduce large errors if it is not correct.

3.1.2 Exhaust gas analysis

The analysis of exhaust gases is an important aspect of engine investigations in the scope of this thesis. For many studies, the optical diagnostics results are correlated to exhaust emissions for understanding how the in-cylinder processes affect the emissions. Here follows a brief description of the measurement techniques used to measure the engine-out emissions that are investigated in this thesis, i.e. unburned hydrocarbons and PM.

Exhaust gases are ideally sampled close to the cylinder head in the exhaust pipe and pumped to the measurement devices through a heated line in order to avoid condensation of the hot exhaust gases. Condensation along the way would affect the measured concentration of the different substances of interest.

Unburned hydrocarbons are detected with a flame ionization detector (FID). Combustion of hydrocarbons forms electrons and positive ions. Therefore, by burning unburned hydrocarbons in an electric field formed between two electrodes, ionized carbon and free electrons are obtained. The carbon ions are positive and are thereby drawn to the negative electrode. As a result, a current is obtained and is proportional to the number of carbon atoms present. FIDs usually use a hydrogen-helium-air flame between the electrodes since it does not cause any ionization by itself that would interfere with the measurements. Calibration of the instrument is necessary to ensure accuracy of the obtained values. At first, pure nitrogen is pumped in the FID to zero the output value. Then, a calibration gas with a known UHC concentration is used and the value obtained is adjusted if necessary [36].

Smoke level is most often measured with a filter method. A sample volume of exhaust gas is drawn through a white filter paper. The reflection of the darkened filter is then measured with a light source and compared to the original reflection of the paper. A filtered smoke number (FSN) is then obtained in the range between zero, meaning that the reflection is unaltered by the exhaust sample, and ten, corresponding to zero reflection [36]. The FSN values can be related to the mass fraction of particles in the exhaust gases using empirical correlations [36, 37].

3.2 Potential and limitations of optical engines

3.2.1 Optical engines

Optical engines allow visual access to the combustion chamber and are valuable tools for combustion diagnostics. As a complement to combustion vessels, where fundamental spray and combustion studies can be conducted, optical engines provide an environment that is more engine-like in many respects for combustion investigations.

The optical access, usually on one of the cylinders only, is obtained by exchanging some metal parts of the combustion chamber with transparent material, often made in quartz. Different optical engine designs exist. Some only have access to the combustion chamber via an endoscope, which enables high load operation but limits the optical access. Today the design by Bowditch is one of the most common in optical engine research. It provides better optical access but is operable in a more limited load range. [38]. The work presented in this thesis was performed either in light- or heavy-duty optical engines of Bowditch design. The

engine-size does not affect the design principle significantly. Figure 6 presents schematics of an optical engine.

The lower part of the engine is not modified. A hollow piston elongation *(b)* is fixed on the original piston and an optical piston *(a)* is mounted on top of the elongation. Since only one of the cylinders is modified for optical studies, a mass of tungsten is mounted on top of other pistons to compensate for the mass increase of the optical piston and maintain the balancing.

The optical access from under the piston is obtained with a 45° mirror, not represented in the schematics, mounted fixed on the engine block inside the hollow piston elongation. Furthermore, a liner of quartz, or of metal with quartz windows, is mounted under the firedeck to permit optical access to the combustion chamber from the side. It enables viewing from the side but it is often used as optical path for lasers when using laser-diagnostics.

As a consequence of this optical liner design, the piston rings have to be mounted low on the optical piston crown in order not to pass over the junction between the main liner and the optical liner, see (a) in Figure 6.

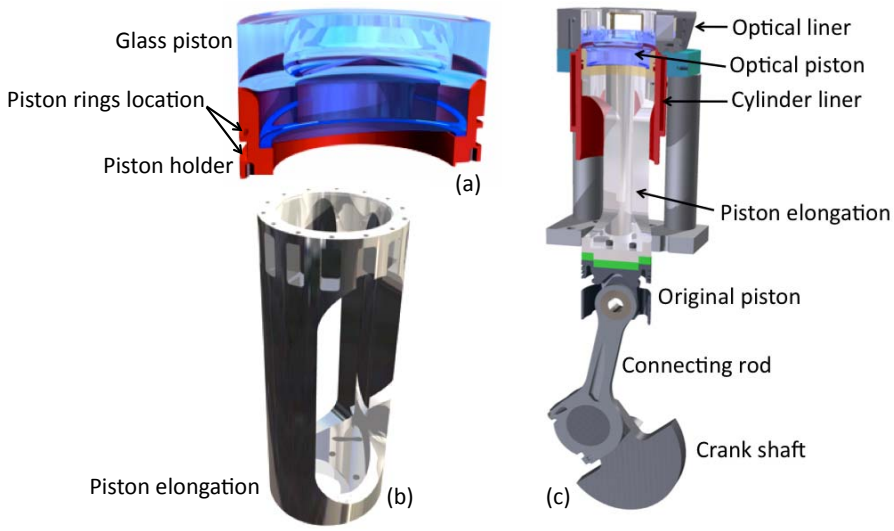

Figure 6: *Schematic of Bowditch-type optical engine with details of the optical piston (a), the piston elongation (b), and global view of the optical engine design (c).*

The piston glass can be made in various shapes and it is possible to replicate the original piston bowl geometry. A complex curved geometry introduces optical distortions in the images that need to be corrected with specific algorithms. Furthermore, sharp edges like in the case of a re-entrant bowl can cause very high local thermal stresses and may cause failure of the piston.

3.2.2 How realistic are studies of diesel combustion in optical engines?

The purpose of using optical engines to study combustion is to gain detailed knowledge on real engine combustion processes. Optical engines are among the most realistic equipment to reproduce the conditions of ordinary metal engines such as air flow-field during compression, expansion during combustion, jet-jet and jet-wall interactions.

However, due to mechanical properties of piston extension used in the Bowditch design and trade-offs made to provide optimal conditions for optical diagnostics, some divergences are introduced. It is justified to discuss the relevance of the results obtained in optical engines and their application to metal engines. This section will examine the main differences between the two types of engine and attempt to quantify the errors introduced as well as accounting for them when relating optical to metal engines results.

First of all, optical engines are often used on single-cylinder mode with simulated EGR and separated air-management systems for inlet air. Therefore, a large flexibility is given in terms of inlet pressure, temperature and gas composition. Such flexibility could be unrealistic in a production metal engine with fixed turbocharger, air-cooler and EGR system. The composition of EGR would for example depend on the combustion process in the engine whereas synthetic EGR used in optical engines is not coupled to the actual exhaust gases of the engine.

Dry EGR, either from a separate stoichiometric burner or pure nitrogen gas, was employed in this work. Figure 7 shows the impact of EGR on ignition delay in a light-duty optical diesel engine and the metal engine values are shown for reference. This EGR investigation was performed by Colban *et al.* at highly diluted conditions with 9 % mole fraction inlet O_2 [39]. The "simple" EGR is composed of air, nitrogen and CO_2. Then a few per cents of water by mass were added, as well as traces of CO and C_3H_8 to match the real EGR composition of the metal engine [39]. The specific heat-ratio is held constant for all EGR configurations.

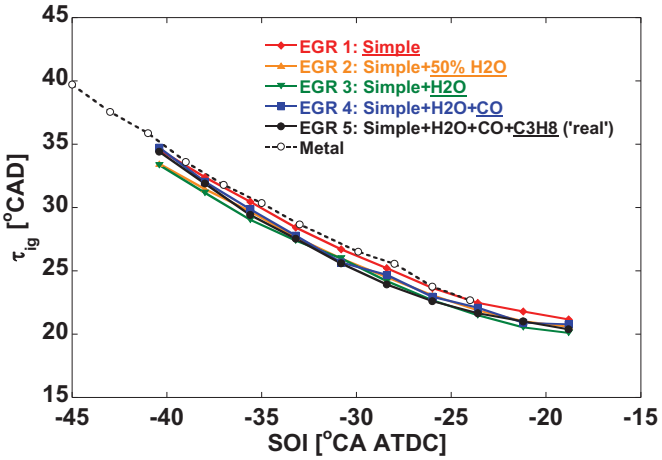

Figure 7: *Comparison of ignition delay for different compositions of simulated EGR in a light-duty optical engine at LTC conditions. Reproduced from [39].*

The trends in ignition delays are similar for all cases even though the absolute levels are lower for all optical engine cases. The addition of water reduces the ignition delay by roughly 1 CAD across the entire range of SOI compared to the baseline case. CO has a slightly lower effect on ignition delay than water and no effects were observed for C_3H_8. Since the specific heat-ratio is constant it appears that no major chemical effects of EGR components are observed. Using synthetic EGR in optical engine may therefore have a slight effect on ignition delay but the trends are expected to be relevant for metal engine cases.

Secondly, the load-speed range available in optical engines is limited due to mechanical concerns of certain parts. Optical liners or windows made of quartz cannot sustain the high pressures and pressure derivates that are common in the upper load range. Furthermore, the piston elongation and optical piston mounted on top of the original piston increase the oscillating mass significantly. In the case of the Scania D12 used in this work, the production metal engine has an oscillating mass of 5.2 kg per cylinder whereas it increases to 12 kg for the optical version. It implies 2.3 times larger mass-forces applied to the piston assembly. For this reason, the speed of optical engines is limited to low speed, and for practical reasons 1200 rpm is usually chosen. At this speed, a four-stroke cycle takes 100 ms, which is convenient for diagnostics with lasers often working at 10 Hz.

Third, as mentioned earlier in this chapter, previous studies have shown that the whole piston-assembly is compressed due to pressure forces at TDC. Therefore, a spring constant has to be used for the volume calculations used in the heat-release analysis in order to account for the error introduced by the ideal volume

trace. The impact of volume trace corrections for mechanical deformations on the motored rate of heat release is illustrated in Figure 8. Furthermore, the increase in squish height with pressure should be taken into account when defining the spray-target in the bowl wall. Emissions trends in CO and UHC for example could be deviating from metal engine cases since more fuel could be introduced in the squish region in the optical engine.

Fourth, since quartz is a much poorer heat conductor than aluminium and steel, heat losses are smaller in an optical engine compared to a metal version. These lower heat losses cause higher combustion-chamber wall temperatures and lead to a shorter ignition delay. This results in an earlier phasing of the premixed combustion leading to elevated NO_x emissions. Furthermore, the higher surface temperature gives a more efficient oxidation resulting in higher combustion efficiency.

A strategy to reduce the difference in combustion behaviour was identified in the light-duty engine used in this thesis [5]. By simply adjusting the inlet temperature, most quantities illustrated in Figure 9 could converge towards the metal engine results under non skip-fire conditions. This was achieved by increasing the inlet temperature in the metal engine by 8 %. However, despite a monotonous decreasing trend with inlet temperature, NO_x emissions are still higher in the optical engine.

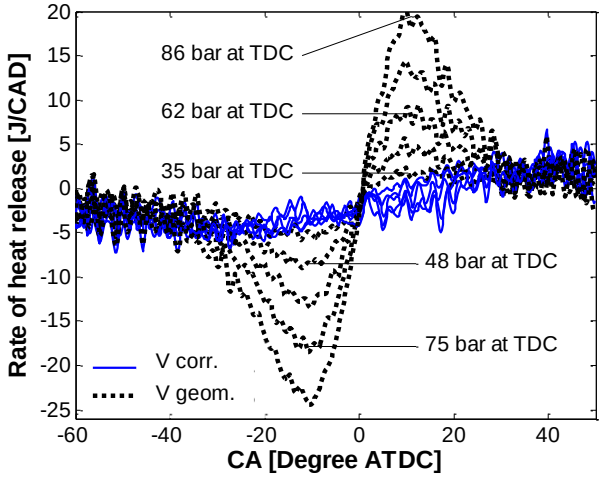

Figure 8: *Motored heat release traces for different TDC pressures. The dotted curves are calculated with the geometrical volume trace. The solid curves are calculated with corrected volume traces to account for squish-height changes. Reproduced from [35].*

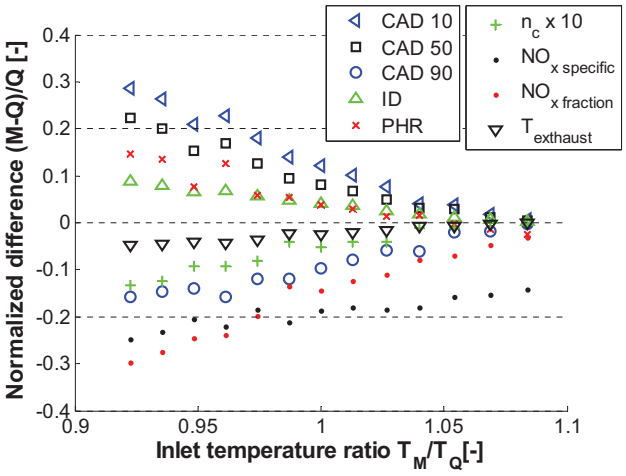

Figure 9: *The normalized difference between two engine configurations i.e. the quantity for an engine configuration with a metal piston crown (M) minus the same quantity for a similar configuration with a quartz piston crown (Q) divided with the quantity for the quartz configuration ((M-Q)/Q). The measures are; CAD at 10 % heat release, CAD at 50 % heat release, CAD at 90 % heat release, portion of premixed heat release (PHR), ignition delay (ID) [CAD], combustion efficiency (difference enlarged 10 times for clarity), specific NO_x emissions [$g/kWh_{indicated}$], NO_x mole fraction [ppm], and exhaust gas temperature [K]. Reproduced from [5].*

Another common approach is to limit the glass temperature by using skip-fire routines the engine. This leads to on the other hand to lower residual gas levels than continuous firing. It also makes it almost impossible to measure representative emissions from the engine. Matching to metal engine operating cases then has to be accomplished by matching the heat release rates.

Finally, diesel fuel contains a large number of components like poly-aromatic hydrocarbons that can disturb laser diagnostics. Indeed, many species present in diesel fuel can lead to unwanted laser-induced fluorescence signal or absorption when combustion intermediates are being investigated in the same wavelength domain. Therefore, diesel fuel is seldom used for optical measurements in engines. Single-component fuels like n-heptane or iso-octane are preferred since they don't absorb laser light in the UV region and therefore don't fluoresce if exposed to laser light in this wavelength region. N-heptane has been used in several studies of this thesis due to its cetane number being similar to diesel fuels. However, n-heptane has a lower density and therefore an enhanced air-entrainment is expected compared to diesel according to Siebers expressions detailed in Chapter 2 (Eq.2). Figure 10 illustrates the influence of fuel density on ζ_{st} (the percentage of the total air needed to produce a stoichiometric mixture).

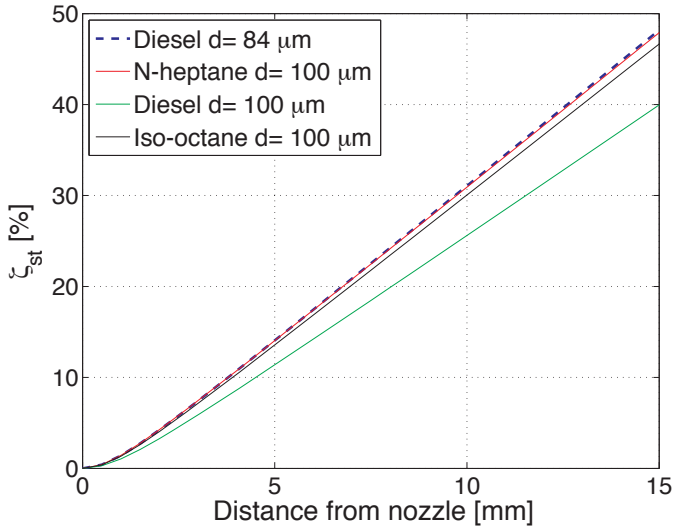

Figure 10: *The percentage of stoichiometric air entrained in the jet versus distance from the nozzle for several fuels and nozzle hole diameters at 2000 bar injection pressure and 25 kg/m^3 ambient density if not specified otherwise.*

It appears that using the same nozzle with 100 μm holes gives a significantly higher air-entrainment in n-heptane or iso-octane jets compared to diesel. To account for this difference in air-entrainment, similar air-entrainment would be obtained in a diesel jet with a 16 % smaller nozzle hole diameter for diesel compared to n-heptane. Therefore, the results presented with lower density fuels compared to diesel can be related knowing that similar air-entrainment would be obtained by decreasing the nozzle hole diameter.

3.3 Optical diagnostics

3.3.1 Passive optical diagnostics

Combustion emits natural luminosity in a broad wavelength domain since several components contribute to the total luminosity. A common example is the yellowish luminosity emitted from a log fire or burning candle. Sooting flames have a major part of their luminosity originating from glowing soot particles. Soot is considered as a black body since it absorbs and incandescently re-emits radiation in a characteristic, continuous spectrum. The emission spectrum of black bodies is wavelength and temperature dependent, as described by Planck's law,

$$E(\lambda,T) = \frac{2\pi hc^2}{\lambda^5 (e^{\frac{hc}{\lambda kT}} - 1)} \tag{22}$$

where λ is the wavelength of the emission, T temperature of the black body, h is Planck's constant, k is Boltzmann's constant and c is the speed of light in vacuum. A representation of black body radiation for several temperatures, typical of soot temperatures in combustion engines, is given in Figure 11.

The radiation intensity profile is broadband and its peak value is blue shifted, i.e. shifted towards shorter wavelengths, when the black body temperature increases. Furthermore, the peak intensity is significantly increasing with temperature. Therefore, black bodies appear to be black at ambient temperatures due to the low radiation intensity and shift towards blue color at higher temperature.

Given the broadband nature of black body radiation, and the fact that peak values are in the visible wavelength domain for combustion relevant temperatures, capturing soot luminosity can be done with a regular visible detector and a glass lens. A global estimation of soot luminosity during the combustion event can also be performed with photodiodes and filters for specific wavelengths.

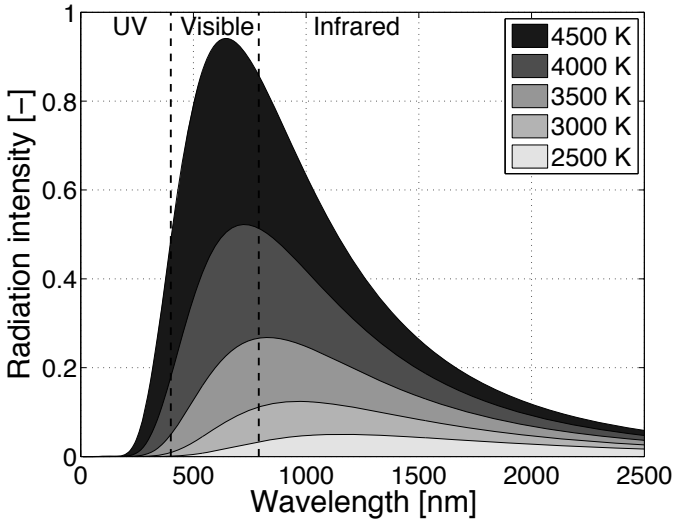

Figure 11: *Normalized black body radiation intensity according to Planck's law for different temperatures typical of soot temperatures in combustion engines. A characteristic of black body radiation is blue shifting with increasing black body temperature.*

Natural luminosity from soot is an important aspect in optical diagnostics of diesel combustion. However, other radiation, like chemiluminescence from excited radicals, are naturally emitted during combustion. A radical of major interest for chemiluminescence measurements of diesel combustion is the hydroxyl radical (OH). It indicates regions of high temperature and stoichiometric combustion [40,41]. The high temperature reactions produce a significant amount of the excited state of OH (OH*). The chemiluminescence emitted from OH* returning to its ground state produces a banded spectrum, unlike the broadband, continuous spectrum of soot mentioned previously. This banded spectrum has one of its strongest peaks near 310 nm [42,43]. A band pass filter centered around this wavelength can be employed to capture the distribution of OH on a UV sensitive camera.

Interferences from soot luminosity in the acquired OH-chemiluminescence signal can be an issue. Due to its broadband nature, natural luminescence from soot can be transmitted through a narrowband UV interference filter. This concern is greater at higher soot temperatures since its radiation in the UV region becomes stronger. Care must be taken to avoid misinterpreting the data, especially for highly sooting cases.

To avoid this problem, a camera equipped with a stereoscope can be used with an interference filter on one entrance and a neutral density filter on the other. This setup produces two simultaneous images of the combustion process that can be used to distinguish the much weaker OH-chemiluminescence from soot luminosity. In particular, the lift-off length can often be safely measured using OH-chemiluminescence, as the soot formation occurs in the product gas of the rich, partially premixed part of the flame, which is located downstream of the lift-off position.

Since no light source is employed for natural luminosity measurements, the signal is obtained from the integrated line of sight. For instance, this means that signal is acquired from the whole volume of a jet. This is another aspect to take into account when drawing conclusions from data obtained by these passive diagnostics.

The temperature dependence and the line of sight aspect of these measurement techniques are significant limitations. However, this type of diagnostic is a very useful tool for numerous diesel jet investigations, for example lift-off length determination.

3.3.2 Laser-based optical diagnostics

Laser diagnostics are more detailed and complex measurement techniques compared to the natural luminescence measurements. These active optical measurement techniques use external radiation sources, to generate signal from given species in a finite measurement volume. This volume can be a point, a line, a plane or a three dimensional region. Therefore, the line of sight aspect of the diagnostic is generally not an issue. Pulsed lasers, which are common in laser diagnostics, makes it possible to obtain a frozen picture of a transient combustion process. The short duration of the laser pulses together with short camera gates are contributing to suppressing background luminosity when collecting laser-induced signal. Two laser-based optical diagnostics will be presented in this section, laser induced incandescence and laser induced fluorescence, since they have been used in the work of this thesis. As mentioned in the introduction section, the advanced laser-diagnostics employed in several studies result of a collaboration with the division of combustion physics at Lund University. The focus of this group is to develop and implement such techniques, but their research is not primarily focused on the engine processes themselves.

Laser induced incandescence (LII) is a commonly used diagnostic technique aimed at visualizing soot volume fraction [44,45]. LII is created by a laser pulse heating particles to a temperature significantly higher than the surrounding medium. The upper limit of the soot particle temperature is about 4000 K. Above this temperature sublimation of small molecules (e.g. C_2 and C_3) from the soot particles prohibits further temperature increase. Since the laser heated soot particles are much hotter than the surrounding gas their emitted light spectra are blue shifted compared to the surrounding cooler particles. The blue shifted light is collected as the LII signal, usually at short wavelengths where the flame background luminosity is insignificant, since the black body radiation of soot particles is temperature dependent [40].

Controlling the level of the background luminosity is not the only concern for LII signal collection. The laser radiation used to heat up soot particles can have the side effect of exciting certain molecules, causing laser-induced fluorescence (LIF) as they relax to their ground state. Interferences from LIF can be collected together with the LII signal if the two signals have similar content and intensity, and lead to misinterpretation of the soot concentration. LII can be performed with a Nd:YAG laser at 1064 or 532 nm but the latter has been seen to cause LIF of poly-aromatic hydrocarbons in highly diluted conditions [46] and therefore 1064 nm can be preferred to avoid interferences.

Furthermore, LII signal can be affected in highly sooting combustion environments by two major problems: the extinction of the laser sheet by the soot particles and the attenuation, or trapping, of the signal while propagating from the measurement plane to the detector. Both of these effects are spatially inhomogeneous and, therefore, difficult to compensate for. However, improvements can be made for extinction problems by adjusting the fluence of the laser, i.e. the laser pulse energy divided by the cross-sectional area of the laser sheet. The LII signal is typically proportional to the laser fluence. A higher fluence yields a higher LII signal since soot particle temperatures become higher. This dependence on the fluence is the reason for extinction issues and can be suppressed if the laser fluence becomes high enough. Sublimation of soot particles then reduces the signal strength at the same rate as the increased fluence increases it. As a result the LII signal intensity becomes independent of the laser fluence. This regime is called the fluence plateau. Therefore, despite laser extinction by soot particles along the path of the laser sheet, LII can remain on the fluence plateau and provide in theory unaffected signal intensity. However, implementing LII for quantitative measurements in optical engines reveals that extinction remains a challenge for accurate measurements of the soot volume fraction.

Planar laser induced fluorescence (PLIF) imaging is a diagnostic technique for measuring distributions and potentially concentrations of species in the combustion process. A laser is used to excite given molecules which then spontaneously relax from their excited state to their ground state. Photons are emitted during the relaxation process and the wavelength of this fluorescence corresponds to the energy difference between the excited and relaxed energy levels. Usually fluorescence takes place at longer wavelength than the excitation wavelength. For example, OH-PLIF is often excited at 284 nm and signal is collected around 310 nm with appropriate filtering.

Excitation and fluorescence wavelengths are specific for a given molecule although overlapping absorption spectra of different species often overlap. For example, when exciting with 355 nm radiation, the fluorescence signal is likely to originate from several molecules present during combustion, e.g. formaldehyde and poly-aromatic hydrocarbons since they all absorb in the 355 nm wavelength region. In such cases, a spectrograph can be used in addition to the LIF capturing camera to spectrally differentiate the species. The very specific spectral fingerprint of the formaldehyde band spectrum between 380 and 450 nm is used to extract formaldehyde-LIF signal from the broadband PAH-LIF signal.

Performing quantitative LIF measurements in optical engines is a challenging task for several reasons. In flame studies, deexcitation through collision with

other molecule (collisional quenching) is the dominating source of uncertainty as it depends on both the local temperature and the chemical environment. Therefore, thorough calibration is required in order to account for the effect of these environmental parameters.

Chapter 4

Results and discussion

This chapter is divided in two main categories; air entrainment in fuel jets and multiple injection strategies. The first part regards air entrainment both upstream the lift-off length and in the interaction between adjacent jets. The second part presents multiple injections strategies as a tool for combustion stabilization in cold conditions and emissions reduction.

4.1 Air-entrainment and lift-off length

4.1.1 Smokeless spray combustion

The common image of conventional diesel combustion without EGR is a quasi-steady jet with soot formation and growth shortly after the lift-off region in the downstream direction [6]. The investigation presented in Paper I employed an operating condition similar to that investigated by Dec when developing his conceptual model, as presented in Figure 2. There were, however, three major differences compared to these conditions: smaller injector orifices, higher injection pressure and higher TDC density.

Despite the fact that it was not a LTC strategy for soot reduction, this operating case produced no smoke at all. Non-sooting mixing controlled combustion had previously been demonstrated in a pressurized combustion vessel when the equivalence ratio, ϕ, fell below approximately two [7,47]. However, demonstrations of this combustion mode in an optical engine have not been found in the literature. The current study can be seen as a complement to the previous studies in combustion vessels. The conceptual model was used as a reference for comparison.

The results obtained with combined simultaneous laser diagnostics revealed a significant difference in the soot formation process. Laser induced incandescence using 1064 nm laser radiation showed the absence of soot in the section of the jet between the lift-off region (16 mm from the nozzle) and the bowl wall (40 mm from the nozzle). However, high-speed line of sight natural-luminescence measurements showed the presence of soot close to the bowl wall along the bowl floor. The soot luminosity vanishes shortly after the CA50 timing.

These results imply that the soot formation process in the present case is much slower than the in the conceptual model case and is therefore visible only in the far downstream regions of the jet, i.e. in the recirculation zones. Furthermore, since no detectable levels of soot were found in the exhaust gases, this means that the soot oxidation process in the recirculation zones is complete.

The absence of soot in the section of the free part of the jet, i.e. before reaching the bowl wall, can be explained by lower local equivalence ratios in the center of the jet. Theoretical calculations using the air entrainment model by Naber and Siebers showed that the mean equivalence ratio across the jet section at lift-off is below 1.5. A threshold value of two was identified as the sooting threshold for diesel jets [7,16].

The high air entrainment rate in the present study compared to Dec's conceptual model can be explained by the parameters named earlier. Mainly, the smaller orifice diameter causes significant air entrainment increase. The higher ambient density is also affecting the air entrainment but to a lesser degree. Finally, the higher injection pressure is believed to reduce the residence time of a fuel element at a given location in the jet. A shorter residence time at a given soot formation rate will result in a lower overall soot production.

Fluorescence signal from 355 nm PLIF was not found upstream of the lift-off region when moving the laser sheet closer to the injector. The OH signal from OH-PLIF forms an envelope around the 355 nm PLIF signal and is found more upstream, i.e. at the lift-off region, as schematically shown in Figure 12.

Signal from 355 nm PLIF originates from the fluorescence of partially oxidized fuel (POF). This name gathers ketones, aldehydes (e.g. formaldehyde) and polyaromatic hydrocarbons (PAH). Formaldehyde is typically found in regions that have gone through low temperature reactions whereas PAH are found in fuel rich regions and are regarded as soot precursors [48].

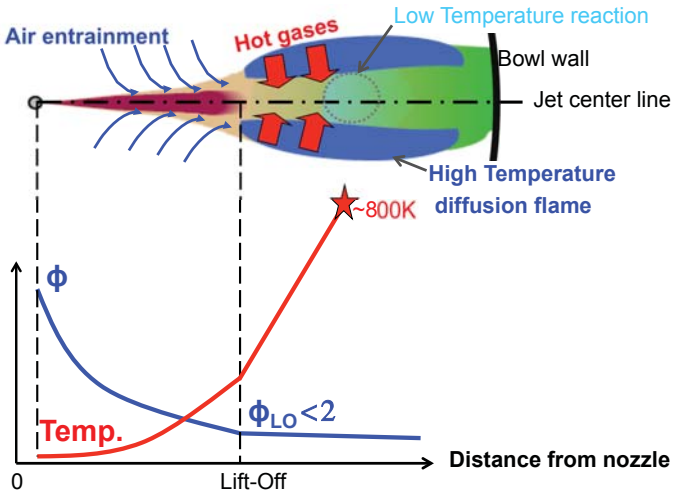

Figure 12: *Schematic of smokeless combustion with Φ-T evolution along the centerline of the jet.*

A spectral analysis of the signal would enable the differentiation between formaldehyde and PAH, although such measurements were not performed at the time of the experiments. However, given the relatively lean mixtures at lift-off (ϕ below 1.5), the absence of soot in the jet section, and the low intensity of the 355 nm PLIF signal, it is likely that PAH is not a dominating source of fluorescence in the present case.

The location of the first POF signal along the jet axis being downstream of the first detected OH implies that either the local equivalence ratio or the temperature is not appropriate for first stage ignition at the center of the jet at lift-off. Since the equivalence ratio calculated at lift-off is below a value of 1.5, temperature is an interesting parameter to investigate. The high temperature reaction zone (OH) at the periphery of the jet is likely to contribute with hot burned gases and raise the temperature of the jet inner mixtures until first-stage ignition is set as represented in Figure 12.

An additional important aspect of the current study that differs from the conceptual model is the utilization of a three-hole nozzle compared to eight holes in Dec's study. With three holes, the jets can be considered as isolated and jet-jet interactions are minimal until the end of injection for such a low load case. Closely spaced jets implies high temperature burned gases recirculating in the upstream direction between the jets and being entrained upstream of the lift-off length. This effect contributes to shortening the lift-off length since the jet mean temperature is higher and autoignition can occur earlier. However, the lift-off length of the present case is comparable with the one of Dec's study. The three-

hole nozzle of the present study provides less jet-jet interaction and entrainment of hot gases but higher TDC density and injection pressure compensate for it and the lift-off stabilizes approximately at the same location.

This study contributes to the knowledge in the field about quasi-steady jets for modern diesel engines. The higher air-entrainment in the jet compared to the case presented by Dec in 1997 explains the differences in soot formation behaviors. The enhanced air-entrainment is mainly due to the smaller nozzle hole size and the higher injection pressure provides a longer lift-off length as well as a shorter residence time for soot formation. This is the first time that smokeless spray driven combustion was demonstrated in an engine.

4.1.2 Impact of jet-jet interactions on the lift-off length

The importance of jet-jet interactions for diesel combustion was underlined in the previous section and will be discussed more in details in this part. The previously mentioned three-hole nozzle differs significantly from production nozzles found in engines today where six- to eight-hole nozzles are more common. The latter provide an inter-jet angle of 45° and lead to potentially stronger jet-jet interactions compared to three-hole nozzles for example.

In Paper IV, a first set of data was acquired using an 8 x 75 µm nozzle and performing high-speed OH-chemiluminescence measurements at 310 nm of the burning jets for different injection pressures. Figure 13 shows time-resolved lift-off length results for these cases. The length of the curves varies since data are plotted from the start of combustion to the end of injection.

There is no clear trend regarding the injection pressure but the general trend is of interest and similar for all five cases. The start of combustion takes place in the downstream regions, in the vicinity of the bowl wall, and thereafter the lift-off position travels back towards the injector. In this configuration, no quasi-steady phase of the lift-off length is seen; it is instead transient until the end-of-injection.

This trend was investigated using a combination of ambient gas temperatures and lift-off length predictions. As exposed in Chapter 2, the lift-off length is strongly dependant upon the temperature of the air entrained into the jet. The temperature and composition of the ambient air can vary significantly in a combustion chamber with burning jets whereas it tends to be more homogeneous in a combustion vessel.

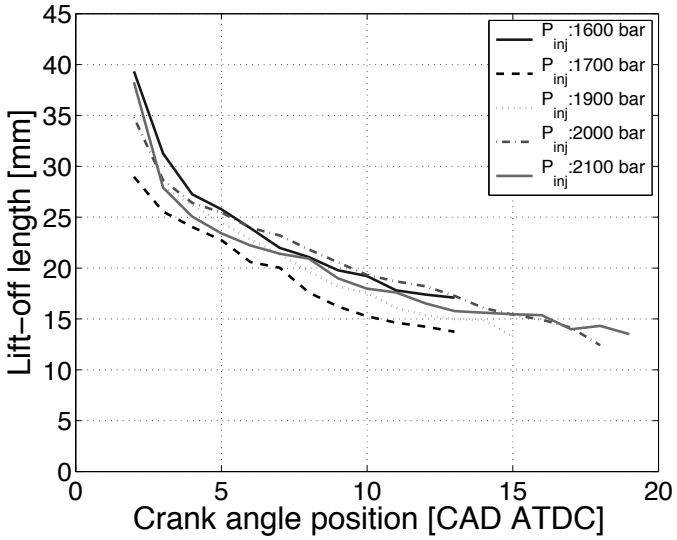

Figure 13: *Lift-off length measurements for single cycles at several injection pressure levels. The data are plotted from the start of combustion to the end of injection.*

In engine combustion chambers, burned gases with high temperature and low oxygen content are typically found at the head of the jet while unburned gases at comparatively lower temperature remain close to the injector.

However, this simplistic description of gas distribution is significantly affected by jet-wall and jet-jet interactions that tend to redirect burned gases towards the center of the combustion chamber. This location is critical since it is where the air is entrained in the jet between the nozzle and the lift-off position. The portion of hot burned-gases in this region will therefore strongly affect the lift-off length.

The empirical expression for lift-off length predictions by Pickett presented in Chapter 2 (Eq.5) can be used in two ways to investigate the observed trends in the lift-off length measurements.

First, the lift-off length can be predicted by calculating the gas temperature, density and stoichiometric mixture fraction from the in-cylinder pressure trace.

Secondly, the gas temperature needed to obtain a given lift-off length can be calculated by using the empirical expression backwards and inserting the measured lift-off length. This temperature is referred to as T_{needed}. The unburned gas temperature $T_{unburned}$ was calculated using a two-zone analysis as described in Paper IV and in [49]. The global gas-temperature T_{global} was calculated using the Ideal Gas Law and the sampled in-cylinder pressure, it comprises both burned and unburned gases.

Figure 14 shows the evolution of the three gas temperatures mentioned previously during the relevant timeframe for lift-off length observation in the 1600 bar case of Figure 13. The decreasing trend of the lift-off length observed before translates logically here in an increasing trend for T_{needed} with time. There is a strong similitude between T_{needed} and T_{global} whereas $T_{unburned}$ is lower and deviates clearly from the gas temperature needed to obtain the measured lift-off lengths.

The impact of the different gas temperatures mentioned previously on the lift-off length is illustrated in Figure 15. Predicted lift-off length using T_{global} and $T_{unburned}$ are compared to the measured lift-off data along the timeframe of observation. The largest difference observed between T_{global} and T_{needed} of about 10 % at 4 CAD ATDC gives a 40 % overprediction of the lift-off length. An overprediction remains until the end of injection but reaches below 5 % at later timings. Due to the large gap between T_{needed} and $T_{unburned}$, the overprediction in this case is extremely large.

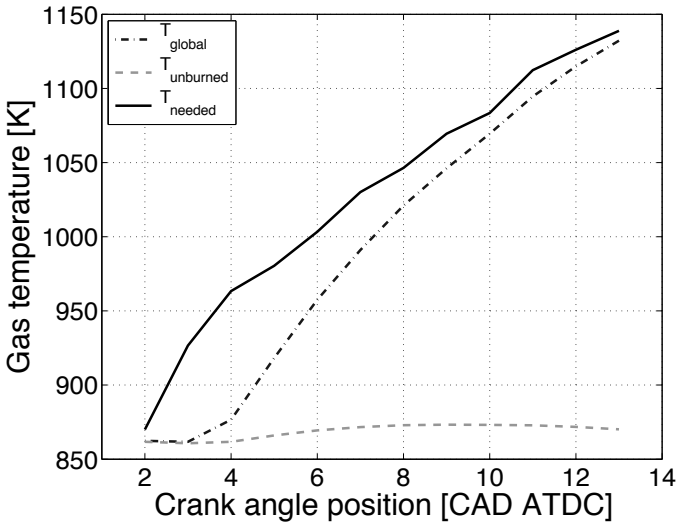

Figure 14: *Global, unburned and needed temperature for the observed lift-off length at 1600 bar injection pressure with an eight-hole nozzle. The global temperature is obtained by applying the ideal gas law to the sampled in-cylinder pressure whereas the unburned gas temperature is calculated using the assumption of an isentropic compression of the unburned gas [49]. The needed temperature is obtained by using Eq.5 and experimental lift-off length measurements.*

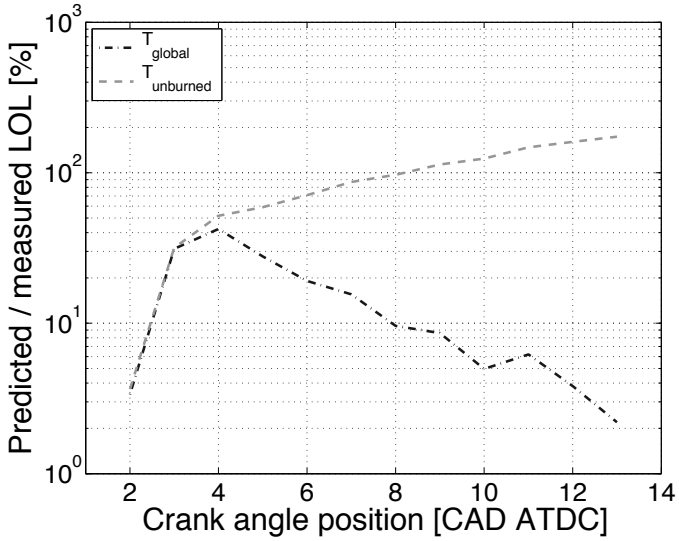

Figure 15: *Evolution of the ratio between the lift-off lengths calculated using the global or unburned gas temperature and using the needed temperature obtained from experimentally measured lift-off lengths.*

These observations indicate that the gas entrained upstream of the lift-off position is far from purely unburned. On the contrary, hot gases constitute globally a non-negligible portion of the entrained gas. These hot gases come from the high temperature reservoirs surrounding the jet as well as recirculating burned gases.

Furthermore, since the needed temperature deviates early from the unburned temperature it means than hot gases are rapidly moved towards the nozzle due to the recirculation zones formed between colliding jets along the bowl-wall. Different inter-jet angles are therefore expected to produce different intensities in the hot-gas recirculation patterns towards the nozzle. As a consequence, the temperature of entrained gas along the lift-off portion of the jet would be different and lead to variations in the lift-off length.

Two different nozzles were employed in order to further investigate the effect of jet-jet interactions on the lift-off length. Both nozzles have four holes with a nominal diameter of 100 µm, an umbrella angle of 146° and a flow rate of 37.2 pounds per hour (pph). One nozzle has 90° axially projected angles between the holes whereas the second one has three close holes with 45° in between and the forth hole separated by 135° on each side, as illustrated in Figure 16. This setup enables the comparison between different levels of jet-jet interactions and to measure the effect on the lift-off length.

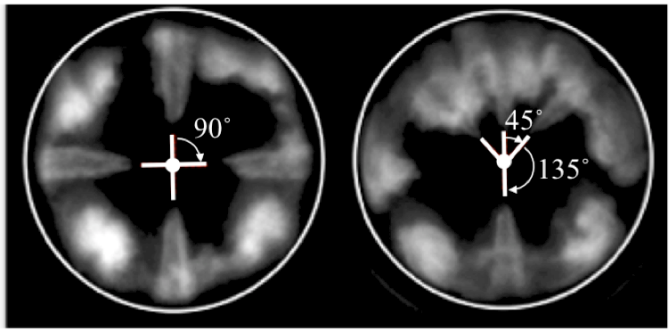

Figure 16: *Symmetrical (left) and asymmetrical (right) nozzle configurations.*

The effect of inter-jet spacing on the lift-off length is significant, as seen in Figure 17. Decreasing the angle between the jets leads to shorter lift-off lengths. This trend supports the hypothesis that jet-jet proximity enhances the recirculation of hot gases towards the nozzle. Based on these results, the entrained gas temperature is estimated to have increased on average by 4.8 % and 12.4 % by changing the inter-jet angle from 135° to 90° and 135° to 45° respectively.

If these observations are due to a larger portion of hot burned gases being entrained into in the jet, the oxygen content of the gas mixture should decrease and thereby lengthen the lift-off length. However, the dependence of the lift-off length on temperature is greater than oxygen content and therefore, the net effect is a shortened lift-off length with narrower inter-jet spacing.

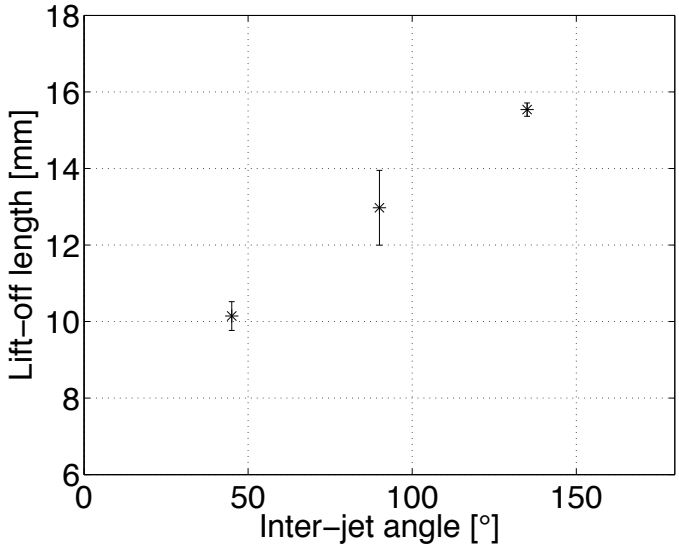

Figure 17: *Lift-off length as a function of inter-jet angle. The error bars represent the standard deviation of the measurement data.*

Moreover, hot gases from the reservoirs surrounding the jet are suspected to contribute to the shortening of the lift-off length. These gases are assumed to be hot due to heat transfer from the high temperature diffusion flame around the jet and not necessarily to be only burned gases.

Another way to affect the temperature of the entrained gases in the jet is to vary the inlet air temperature. By increasing it, both the global and unburned gas temperatures will increase. Figure 18 shows the interaction effect between inter-jet spacing and inlet temperature on the lift-off length. At larger inter-jet angles, the lift-off length becomes more sensitive to changes in inlet temperature. However, the effect of inter-jet angles becomes insignificant at higher inlet temperatures. A plausible explanation is that the gas temperature experienced by the jet at close inter-jet spacing is dominated by the burned gas temperature. The temperature variation in the unburned gas thereby becomes incapable of affecting the lift-off length.

The main contribution of this investigation to the field is to enable coupling of the empirical expression for lift-off length predictions developed in a combustion vessel to lift-off measurements in an optical engine. Jet-jet interactions leading to recirculation of hot gases towards the nozzle causing a shortened lift-off length were demonstrated. This observation implies that a larger inter-jet spacing is beneficial to ensure low equivalence ratios at the lift-off region, and therefore limit the soot formation process in diesel engines. However, at high ambient temperature conditions, the influence of jet-jet interactions becomes less important for the lift-off length.

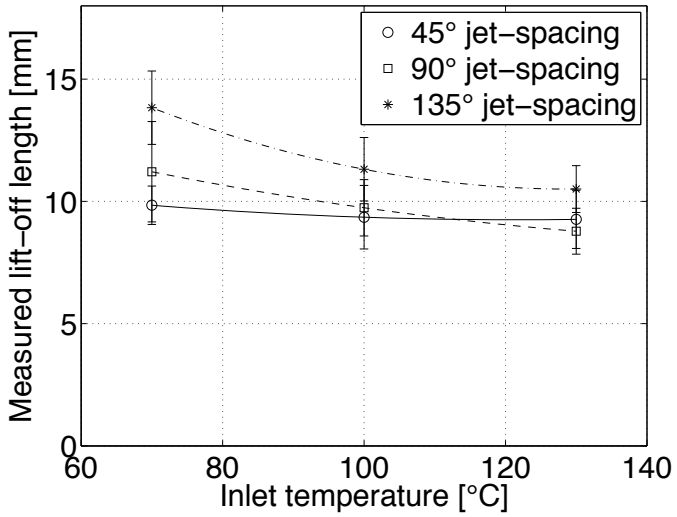

Figure 18: *Lift-off length vs. inlet temperature and inter-jet angle.*

Large-Eddy Simulations (LES) of the experimental cases presented here have been recently performed by Solsjö [50]. Similar trends in terms of shortening lift-off length with decreasing inter-jet angle were observed due to higher temperature of the entrained gas. Furthermore, the asymmetrical behaviour of the lift-off length in relation to the swirl direction was also noticed in the LES results. With ratios in the range of 12.5 to 18 % between the upswirl and downswirl side in the simulation, there is a good agreement with the experimental results.

4.1.3 Air-entrainment in colliding wall jets

Spray driven combustion in an engine is affected by the presence of the bowl-wall at some distance from the nozzle. Typically, the distance between nozzle and bowl-wall is in the range of 25 mm for light-duty and 45 mm for heavy-duty diesel engines.

As underlined in the previous section, when the jet interacts with the wall, a wall-jet is formed which travels along the bowl-wall. Eventually, two neighbouring wall-jets collide and form a recirculation zone, usually moving towards the nozzle. This chain of events is shown in Figure 19 for the asymmetrical nozzle (3+1) with quantitative fuel-LIF measurements using Structured-Light Illumination Planar-Imaging (SLIPI) in an optical heavy-duty diesel engine. These results are obtained in non-reacting conditions for the optical diagnostic purposes. More details on the laser-diagnostic method can be found in Paper V. The positions of the nozzle and of the four jets are illustrated in white color on the right side of the images. The height of the horizontal laser-sheet was fixed at the point where the centerline of the jet reaches the bowl wall, i.e. 1.4 mm above the flat bowl floor at TDC.

The same nozzles as in the lift-off length study described above were used for this investigation. The goal of this study is to gain knowledge on mixing in wall-jets since mixing is of importance in the downstream regions to enhance soot oxidation and therefore decrease engine-out soot emissions. The effect of inter-jet spacing (45° and 90°) as well as injection pressure (1500, 2000 and 2500 bar) was investigated for fixed inlet conditions and injection durations.

The average cross-sectional equivalence-ratio of the free-jet was extracted from the fuel-LIF results at 3 mm upstream of the bowl-wall over a 0.2 mm wide region. This region is illustrated in the sixth frame of Figure 19 as the region *"a"*. The equivalence-ratio at the start of the recirculation-zone was determined in a similar way, in region "b" for comparison with the free-jet.

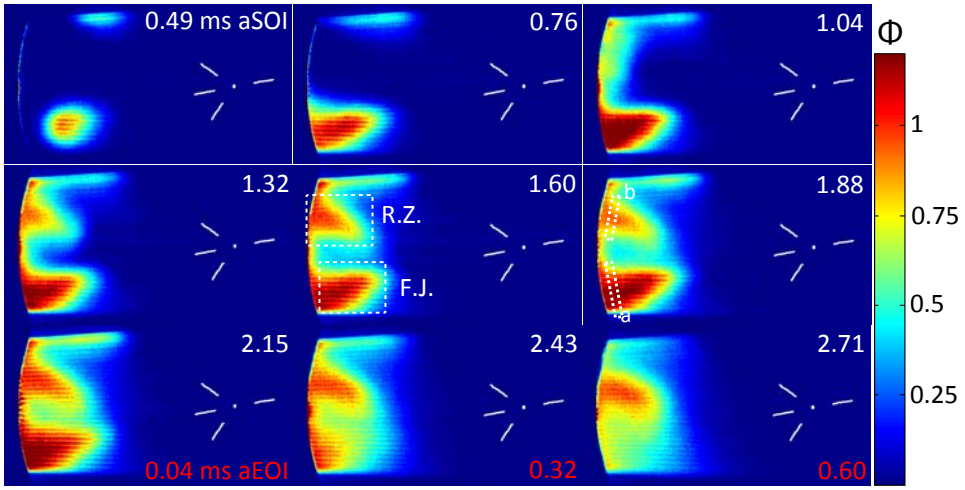

Figure 19: *Evolution of the ϕ-distribution in colliding wall-jets with an asymmetrical four-hole nozzle at 2000 bar injection pressure. The timing is indicated in each frame relative to the start of injection (aSOI) and end of injection (aEOI) when relevant. . The free part of the jet and the whole recirculation zone are indicated in the center frame as "F.J." and "R.Z." respectively. The color scale show the local equivalence ratio as indicated by the color bar to the right.*

The evolution of the equivalence-ratio in the free part of the jet is presented in Figure 20 for different injection pressures and an inter-jet angle of 45°. Overall, there is no significant difference between the three injection pressure cases. This confirms the expression by Siebers [8] shown in Eq.17, where the average ϕ in the jet cross-section has no explicit dependence on the injection pressure. At 1.04 ms aSOI, an increase in ϕ values is observed for all cases. This timing corresponds to the impact of the free-jet on the bowl-wall. A similar enrichment of the free-jet upon impact was observed by Bruneaux in a wall-jet experiment conducted at similar ambient conditions and injection pressures in a constant volume chamber [51].

After this increase, a brief stabilization is observed in Figure 20 before another raise can be noticed. It is more pronounced for the 2000 and 2500 bar cases compared to 1500 bar. The reason for this ϕ-bump is found in the results presented in Figure 19. The recirculation zone that started forming at 1.32 ms aSOI has grown and moved inward, towards the nozzle. Due to the downwards motion of the swirl in the frames of Figure 19, the recirculation zone is transported towards the free part of the jet and fuel-rich mixtures are being re-entrained in the jet instead of ambient gas. It is particularly visible in the frame at 2.15 ms aSOI. This phenomenon leads to higher fuel concentration in the jet and therefore higher Φ values.

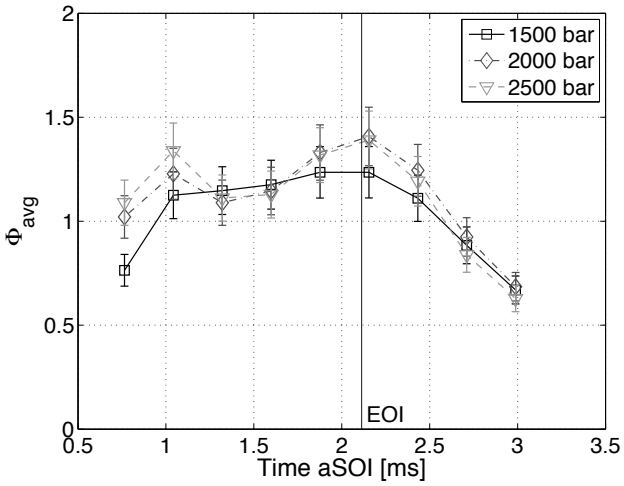

Figure 20: *Evolution of the cross-sectional average equivalence-ratio distribution for the free part of the jet at different injection pressures with 45° inter-jet spacing. The end-of-injection is indicated at 2.11 ms aSOI.*

The present conditions are non-reactive and it is reasonable to assume that little unburned fuel should be left at the tip of the recircualtion zone under reactive conditions. However, it is reasonable to assume that hot burned products would follow the same path from the tip of the recirculation into the jet. The low oxygen content of burned products would contribute to higher ϕ values in the jet and eventually increased soot formation rate.

Furthermore, recirculation of hot gases is expected to shorten the lift-off length and enhance the soot formation process as well. Pickett and López showed similar mechanism in confined jets with hot burned gases recirculation upstream in the jet and shortening the lift-off length. A significant effect on soot formation was observed in those cases [52].

Shortly after the end of injection, at 2.11 ms aSOI, a rapid decrase of ϕ is observed in Figure 20 for all cases. According to the free-jet theory by Siebers, a fuel element leaving the nozzle should reach the bowl-wall in 0.76, 0.67 and 0.60 ms in the 1500, 2000 and 2500 bar cases respectively under the present conditions. Even though the present injector does not provide top-hat injection profiles, the leaning-out of the jet after EOI at the bowl-wall location appears to be faster than the jet itself.

The same kind of observations were made by Musculus *et al.* [53,12] with toluene-LIF measurements in jets after EOI in a heavy-duty diesel engine. The entrainment wave theory proposed by these authors suggests a strong increase in air-entrainement into the jet to compensate for the loss of momentum-flux due to the absence of fuel flow after EOI. The entrainement wave was shown to travel downstream in the jet at up to 2.5 times the steady-jet speed and significantly decrease the axial velocity of the jet. The trend observed in Figure 20 after EOI indicates that a similar phenomenon is taking place in the present jet-investigation.

The evolution of the mean equivalence-ratio distribution at the start of the recirculation, named *R.Z*, is represented in Figure 21. Comparing the equivalence ratio before and after the wall-jet region can provide information about the mixing process in the wall jet compared to a free jet. Similar to the free-jet, little difference is observed between the different injection pressures. A similar ϕ-bump to the one described earlier is observed in Figure 21 after EOI. It indicates that the enriched mixtures in the free-part of the jet for 2000 and 2500 bar injection pressure are found after traveling along the bowl wall. The differences in timing for this enrichment to occur between the free-part of the jet and the recirculation zone is due to transport time in the wall-jet. Based on image processing of the data, the wall jet is estimated to travel at 26, 29 and 33 m/s for 1500, 2000 and 2500 bar respectively.

Furthermore, the fast leaning-out process observed in the free jet is apparently not transmitted through the wall-jet to the recirculation zone due to the axial-stagnation of the free-jet since only a slow decay in ϕ is observed.

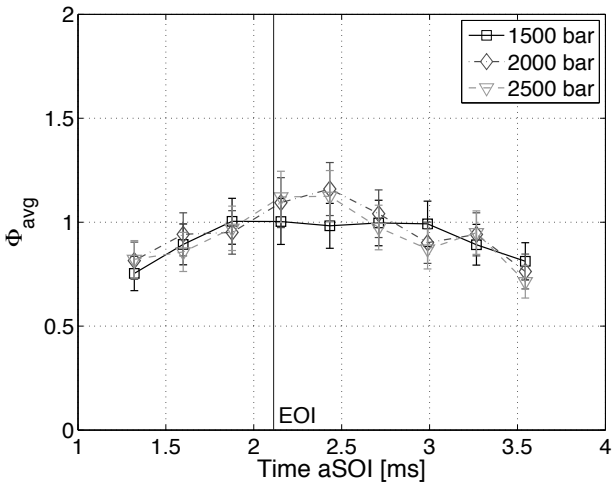

Figure 21: *Evolution of the local equivalence ratio at the start of the recirculation zone for the 45° inter-jet angle configuration.*

For the 90° inter-jet spacing cases, the trends presented in Figure 22 and 23 show once again the low impact of injection pressure on the equivalence ratios both in the free-jet and in the recircualtion-zone. The spread of ϕ values in the free-jet before EOI is larger compared to the 45° jet-spacing cases. However, a similar drop after EOI is observed for the free-jet, confirming the hypothesis of an strong leaning-out process after EOI.

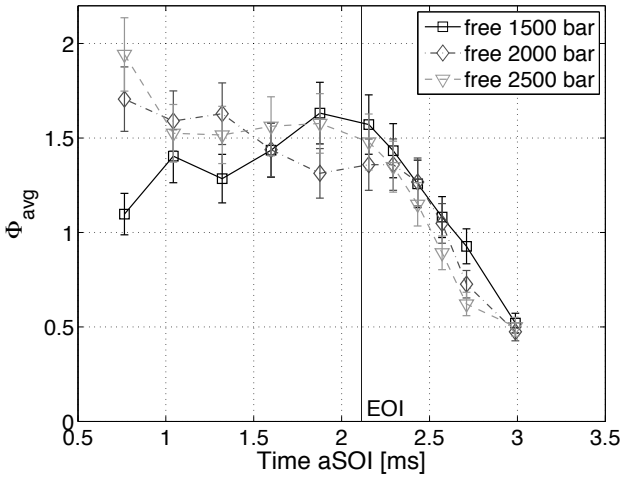

Figure 22: *Evolution of the cross-sectional average equivalence-ratio distribution for the free part of the jet at different injection pressures with 90° inter-jet spacing. The end-of-injection is indicated at 2.11 ms aSOI.*

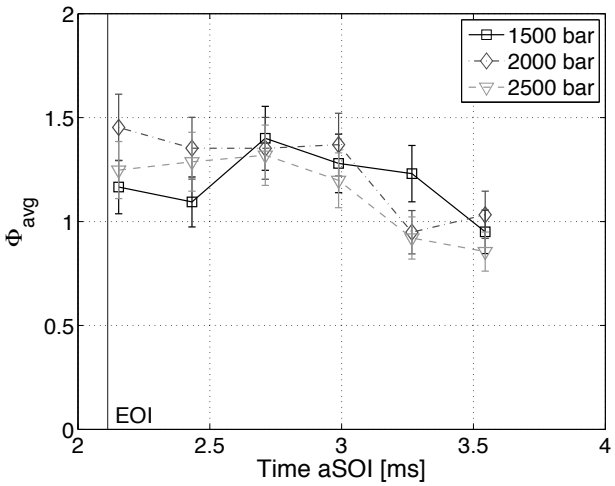

Figure 23: *Evolution of the local equivalence ratio at the start of the recirculation zone for the 90° inter-jet angle configuration.*

Figure 24 shows the ratio of the measured and predicted ϕ values at the start of the recirculation zone for different cases. The predicted values are obtained using Siebers' scaling law for free jets [8].

Note that the downstream distance is different for 45° and 90° inter-jet spacing cases due to the longer distance travelled by the wall-jet prior to the recirculation zone (53 mm from the nozzle for 45° and 74 mm for 90° inter-jet angle).

At the start of the recirculation zone, measured ϕ is ca. 15 % higher than the free-jet predictions by Siebers. The 90° inter-jet angle case with a longer portion of wall-jet has a significantly higher ϕ at the start of the recirculation zone compared to the free-jet, in the range of 45 %. The same trend is observed with the 45° inter jet-angle but to a lesser degree due to the shorter wall-jet section before the recirculation zone is formed. It implies a lower air entrainment rate in the wall-jet compared to free-jets. This observation goes against the hypothesis of increased mixing rates in wall-jets compared to a free jet.

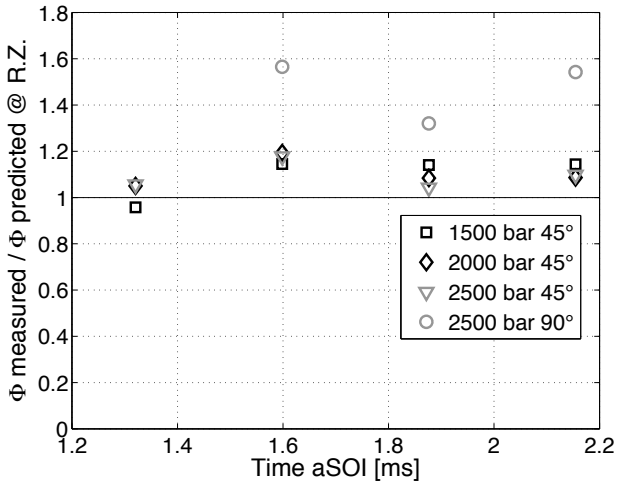

Figure 24: *Ratio between the measured ϕ values after the wall-jet and predicted ϕ values in a free-jet according to Siebers model at the same downstream distance corresponding to the beginning of the recirculation zone. The predicted values use the measured ϕ values from the free jet prior to wall impingement to calculate x^+.*

The novelty of this study is that the results show that in the present conditions, mixing is not enhanced in the wall-jet after impact on the bowl-wall independently of the injection pressure. The hypothesis of increased mixing in wall-jets with increasing injection pressure based on the observations by Bruneaux [51] is not confirmed in the confined conditions of the optical. Therefore, the hypothesis of increased mixing by increased turbulence upon interaction with the wall is not supported by the present results. On the other hand, the hypothesis of increased mixing due to larger surface area of the jet when impinging on a flat wall seems to explain the results presented in [51]. At a narrow inter-jet spacing (45°) interactions between the recirculation zone and the free part of the jet were observed in the optical engine, causing an enrichment of the jet. The fast-leaning-out process after EOI described by Musculus was identified in the free part of the jet but not transmitted through the bowl-wall to the recirculation zone. Such enhancement of the air-entrainment in the recirculation zone would be beneficial for late-cycle soot-oxidation processes taking place in this region.

4.2 Injection strategies: a combustion tuning tool

4.2.1 Cold-start

The trend in the development of diesel engines goes towards lower compression ratios in order to achieve low NO_x emissions and comply with stringent legislations. Furthermore, the specific power per displacement volume can be increased with lower equivalence ratios due to possible IMEP increase at a given peak pressure. A consequence of lower compression ratio is lower compression temperatures in the cylinder by the start of injection. This aspect becomes an issue when starting at low or very low ambient temperatures like in winter conditions since evaporation and auto-ignition of the diesel jets are dependent of the compressed gas temperature in the cylinder.

An investigation was performed in Paper II to better understand combustion stability issues at low ambient temperature. A light-duty optical diesel engine based on the Volvo D5 was modified for low temperature experiments. The inlet-air flow, fuel supply and engine coolant were cooled down to -20°C using heat exchangers in a bath of glycol-water mixture. Any of these three fluid flows could bypass the cooling loop and run at ambient temperature, i.e. 20°C. At first, start at ambient and cold conditions were investigated as a first approach to the cold start challenges. Then, investigating different injection strategies provided a promising method to counter evaporation and ignition issues at cold conditions.

Natural luminosity imaging showed that, with a single injection, the combustion does not spread to the whole piston bowl, see Figure 25. Only the jet closest to the glowplug in the downswirl direction is reacting fully. The localized combustion kernel is then transported downswirl along the bowl wall but no evidence of reaction is observed in the other six jets.

A factorial experiment was conducted to investigate the effects and interaction effects of engine block, fuel and inlet-air temperature on ignition and combustion stability.

Engine block temperature was found to be the most significant parameter for cold start optimization, both in terms of load achieved for a given injected fuel mass and of combustion phasing. Inlet air temperature was shown to be the second most significant factor, especially affecting load stability. However, heat transfer between the cylinder head and the inlet air can influence the real origin of the observed effects.

Fuel temperature at the high-pressure pump inlet was found to be a less significant factor for most responses. Similarly to the limitation mentioned above, the actual temperature of the injected fuel can be influenced due to heat transfer in the injection system. A detailed investigation of in-cylinder inlet air and injected fuel temperature would help studying the problem with more accuracy.

The relative position of the glow-plug and the nearest spray revealed that increasing the angle can improve combustion phasing stability and reduce the pressure derivative, i.e. combustion noise.

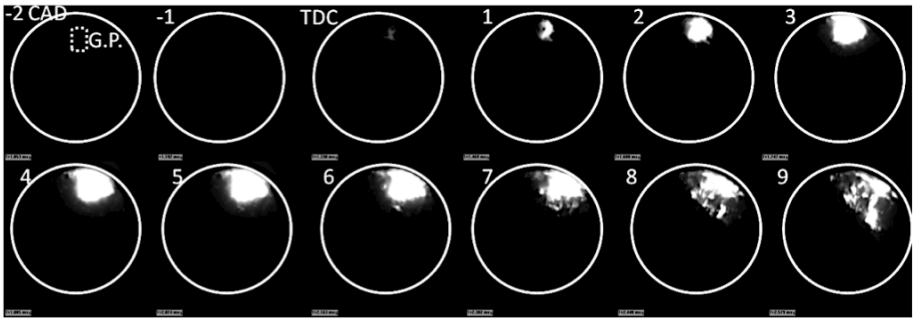

Figure 25: *High-speed natural luminosity imaging of a single injection case for start in low temperature conditions (-20°C) captured from under the piston. The glowplug location is indicated in the first frame and the timing in CAD ATDC in the upper-left corner of each image. The white circles indicate the piston bowl edge.*

The second part of the study was focusing on the investigation of injection strategies for improved cold start performance. Five different multiple injection strategies were analysed and compared to a single injection case. This was done using natural luminescence imaging and global temperature calculations, presented in Figure 26, from pressure trace measurements. The single injection case shows a large temperature drop due to the large amount of fuel to evaporate at once. Promising results were obtained when adding several pilot injections while keeping the total injected fuel mass constant.

The cases with one, two or three pilots show that more pilot injections move the temperature closer to dotted line corresponding to the motored case. It means easier evaporation for each pilot and as seen on the plot, earlier start of combustion. Shorter injections appear to be the key to improved fuel evaporation.

A strategy with three pilot injections was found to be the best configuration. The pilots were set with increasing fuel mass and it seems to be advantageous for better load stability and higher load. The natural luminescence results, shown in Figure 27, indicate that a more homogenous ignitable mixture is obtained with this injection strategy. Furthermore, combustion covers almost the whole piston bowl, compared to the case presented in Figure 25. It is probably a consequence of a reduced temperature drop due to an easier evaporation of the progressive pilots. These conditions allow the pilots to react early and thus release heat to compensate for the evaporative cooling.

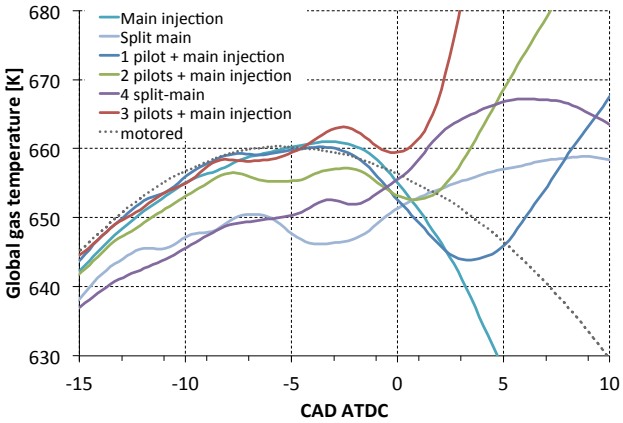

Figure 26: *Global in-cylinder temperature calculated from the pressure data for different injection strategies during cold start conditions.*

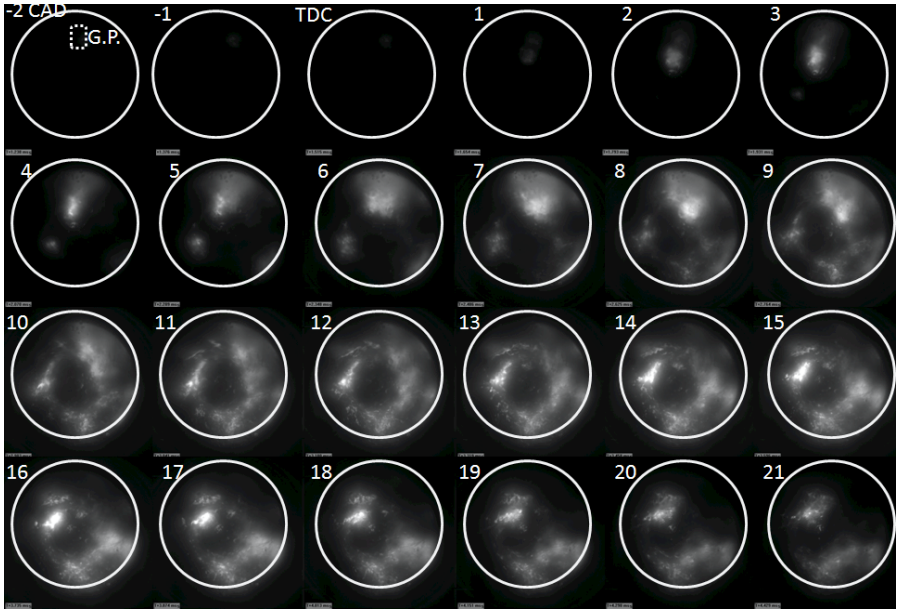

Figure 27: *High-speed natural luminosity imaging of a case with three increasing pilot and a main injection for start in low temperature conditions (-20°C) captured from under the piston. The glowplug location is indicated in the first frame and the timing in CAD ATDC in the upper-left corner of each image. The white circles indicate the piston bowl edge.*

This study of cold starting at low ambient temperature in an optical diesel engine was one of the first of this kind. Investigations of cold start during realistic conditions in optical engines are rare and few studies were found in the literature [54,55,56]. The unique aspects of the present study are the optical investigation of advanced injection strategies, their effects on after-start stability and the separation of the effects of engine block, fuel, and inlet air temperatures on after start stability. The main contributions of this study to the engine community are a better understanding of the cold start combustion with in-cylinder visualization and the multiple injection strategies developed to improve after-start stability. These results agree with those by Tomoda *et al.* published in 2010 [57] confirming the potential of multiple injections in cold start conditions due to the contribution of the early posts to the heat release and therefore globally enhancing fuel evaporation over a cycle.

Many technical issues were brought to light during the preliminary tests and specific procedures were progressively defined to assure the repeatability and quality of the measurements. Based on the technical knowledge acquired during this investigation, more specific diagnostics could be employed to explore cold starting and multiple injection strategies more in detail in future investigations. Mie scattering measurements on the liquid portion of the jets could for example

give insight in the wall-impingement and evaporation issues at low temperatures. Furthermore, 355 nm PLIF together with OH-PLIF could help characterize the zones were first and second stage ignition occur. Spectral analysis of the 355 nm PLIF signal would be suggested in order to differentiate formaldehyde from PAH in the fluorescence signal.

4.2.2 Pollutant reductions with multiple injections

Enrichment of locally over-lean regions with post-injections

Low temperature combustion is a concept aimed at reducing NOx and PM from diesel engines by dilution of the charge with large amounts of cooled EGR, as described in a previous section. However, drawbacks in terms of elevated UHC emissions are known for low load LTC conditions.

Previous studies have shown that over leaning of the jet after end of injection, due to enhanced air entrainment, results in mixtures too lean to ignite in the near-injector region [12]. This behavior is especially seen at low loads when the ignition dwell, i.e. time between end of injection and start of combustion, is large.

The objective of this study was to investigate the potential of post-injections to reduce UHC emissions originating from the near-nozzle overlean regions. The hypothesis is that post-injected fuel can locally increase the equivalence ratio and render the mixtures ignitable and therefore reduce UHC emissions from low load LTC. Issues with over-mixing after the end of the post injection, creating the same UHC problem, were solved by adjusting the post-injection parameters as described later in this section.

Combined laser diagnostics were used for indirect measurements of mixing. Combustion intermediates were used as indicators of the local stoichiometry. Formaldehyde can be found in regions ranging from fuel lean to fuel rich but it persists late in the cycle only in fuel lean regions [58]. Furthermore, OH concentrations are high in near-stoichiometric regions. Third, PAH is known as a soot precursor and is found in overall fuel rich regions [58]. Using combined OH and 355 nm PLIF, the different combustion intermediates can be imaged and give information about the local stoichiometry. Formaldehyde and PAH can be extracted from spectral analysis of the 355-PLIF fluorescence signal since formaldehyde has a particular spectrum with seven distinct peaks between 385 and 445 nm [58]. More details about the laser diagnostics are given in Paper III.

It was found that for a single injection, OH radicals are formed in the downstream regions close to the bowl wall and stagnate in this location late in the cycle as shown by the green signal in Figure 28. Formaldehyde, i.e. lean regions, are found after EOI around the injector in the center of the bowl as seen by the red signal in Figure 28. No sign of fuel rich regions were observed for this case.

Two different post-injection strategies were investigated. First, a post-injection strategy able to reduce measured exhaust UHC emissions was found to be achievable, though very sensitive to the settings of the post-injection. This case showed 20 % decrease in UHC emissions and repeatability tests showed good results. The post-injection for this case was closely spaced after the actual end of main injection, by one CAD. Rate of injection measurements showed that the momentum of the post injection is very low compared to the main injection and that the fuel mass delivered in the post only is small (1.8 mg). Pressure wave dynamics in the injector body and common rail system are suspected to cause this behavior since a one CAD shift in the start of post-injection, without changing the energizing time, gave a similar momentum as the main injection.

The small post-injection caused a sudden appearance of OH radicals in the upstream part of the jet by 9 CAD ATDC, as seen 2 CAD later in the right-hand frame of Figure 28. This observation indicates that second stage ignition was made possible close to the nozzle by the post-injected fuel, which must have raised the local equivalence ratio towards stoichiometry.

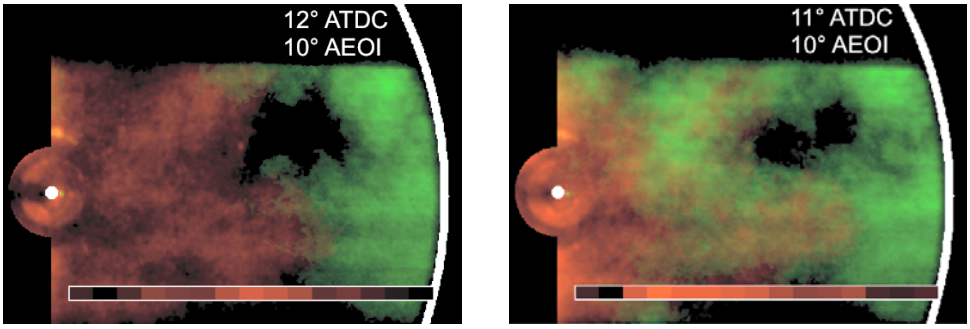

Figure 28: *Simultaneous OH (green) and 355 PLIF (red) images. The left frame is extracted from a sequence with the single injection whereas the right one is from the small post injection strategy. The timings are given relative to TDC and to the main EOI. The formaldehyde correlation bar indicates the similitude of the 355 PLIF signal to a formaldehyde reference spectrum. The darkest colors in the correlation bar indicate a low correlation whereas the brightest colors indicate that the LIF signal has a high probability of being formaldehyde-LIF signal.*

The second case of post-injection investigated shows the sensitivity of the local enrichment mechanism to changes in post injection strategy. The post-injection duration was kept constant but its start was delayed by one CAD. Exhaust measurements showed no influence of the post on UHC emissions for this case compared to the single injection. Furthermore, no OH radicals were seen closer to the injector. Instead the same trend as for the single injection was observed, see Figure 29.

The fuel lean regions in the center of the bowl remained lean, correlating with the unchanged UHC emissions. Rate of injection measurements showed that post-injected fuel mass was nine times higher than the small post case and the momentum was similar to the main injection.

A comparison of the two post-injection strategies suggests that the momentum is crucial. The post injection momentum should be low enough for the penetration to remain relatively short. The post-injected fuel should thereby remain in the near-injector region to enrich the over-mixed zones.

Higher momentum in the post would carry the post-injected fuel too far downstream. The discovery of the small post-injection strategy leading to exhaust UHC reduction is the result of a trial and error process on the engine.

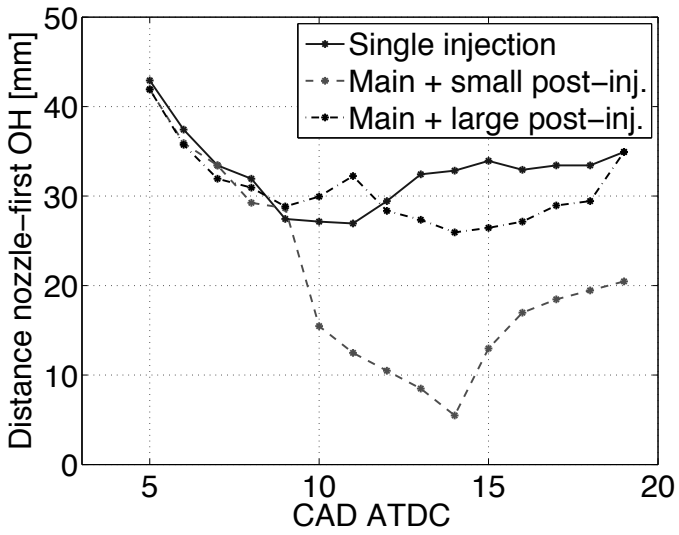

Figure 29: *Evolution of the OH-radicals downstream position relatively to the injector nozzle in the jet axis plane for the single injection compared to both investigated post-injection strategies.*

This strategy can be seen as using pressure dynamics in the fuel system to achieve such a small post injection. Injector dynamics is not a controlled variable and the transfer of this particular injection strategy to another engine might not be straightforward.

However, the working principle of the local enrichment by the post is valid and is the major novelty of this study and considered as a contribution to the development of LTC concepts by reducing one of their main drawbacks i.e., UHC emissions. Furthermore, the 20 % reduction in UHC emissions achieved by affecting the local equivalence ratio of the jet after EOI implies that at least 20 % of UHC originate from the leaning-out process of the entrainment wave in the present conditions. This insight in the origin of UHC emissions for LTC cases is a useful result for further development of this combustion concept.

Oxidation of soot by post-injections

The usage of post-injections to reduce UHC emissions presented in the previous section is not the most common strategy. Post-injections are mostly used in diesel engines to aim at reducing engine-out soot emissions [59,60,61,62]. The mechanisms behind this soot reduction effect are not well understood yet and can be of mainly two different types. First, the momentum of the post-injection can enhance mixing in the targeted soot cloud, as a mechanical effect. Increased mixing can make locally fuel-rich zones leaner and therefore decrease soot formation as well as enhance soot oxidation. Second, OH-radicals produced during combustion of the post-injected fuel can locally increase temperature and also oxidize soot particles since they are known as good soot-oxidizers [63].

A study was conducted, based on previous work by Bobba *et al.* [59], in order to investigate the origin of soot emissions reduction with post-injections. Figure 30 shows the identified soot emissions trends with different main and post timings at 35 % load in a heavy-duty optical engine The post-injected fuel mass represented 17 % of the total injected fuel mass for all cases.

The horizontal lines represent the soot level measured for the main-injection alone and the long main-injection. The latter is a longer main without post used to match the injected fuel mass of the case with combined main and post injections. The main-injection only case gives a reference to observe the sooting or soot-oxidation tendency of the post. For early main-injection timing (-15° ATDC), the post-injection appears to be producing soot leading to higher engine-out smoke compared to the long main case. But with sufficient post-injection retard, the exhaust smoke drops below the long main-injection level. The maximum soot-reduction benefit is realized when the post injection is introduced near 40° ATDC, irrespective of the timing of the main injection.

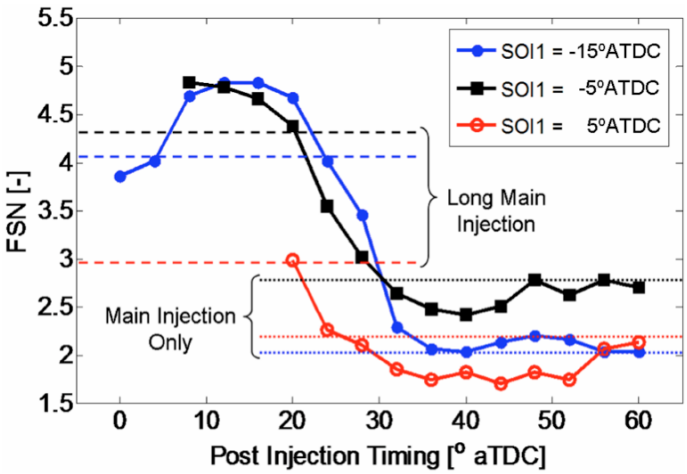

Figure 30: *Variation of exhaust smoke as post-injection timing is delayed into the expansion stroke for three main injection timings, reproduced from [59]. Smoke emissions for the main-injection only and for a longer main-injection with the same total fuel mass as with a post injection are also shown in the figure with dotted and dashed lines, respectively.*

For later main injections (especially for SOI1=5° ATDC), the smoke emissions dip below that of the main-injection only by as much as 15 % at the optimal retarded post-timing. Clearly, for late main injections, the post injections eliminate some of the soot produced from the main injection, implying some sort of interaction between injections.

The study presented in Paper VI investigates the soot and OH-radicals distributions for early and late main-injection timings with a post-injection at 36 CAD ATDC. Simultaneous LII at 1064 nm and OH-PLIF at 284 nm were employed in the squish region with the laser sheets entering through a side-window and signal acquisition performed from above through a removed exhaust-valve.

Results presented in Figure 31 show that the post-injected fuel produces OH-radicals in the squish region independently of the main-injection timing. However, with early main-injections, the soot is not present in the squish region Natural luminosity measurements showed that soot is located in the piston-bowl instead. As a consequence, no interaction is established between soot and OH radicals since their locations are not matching.

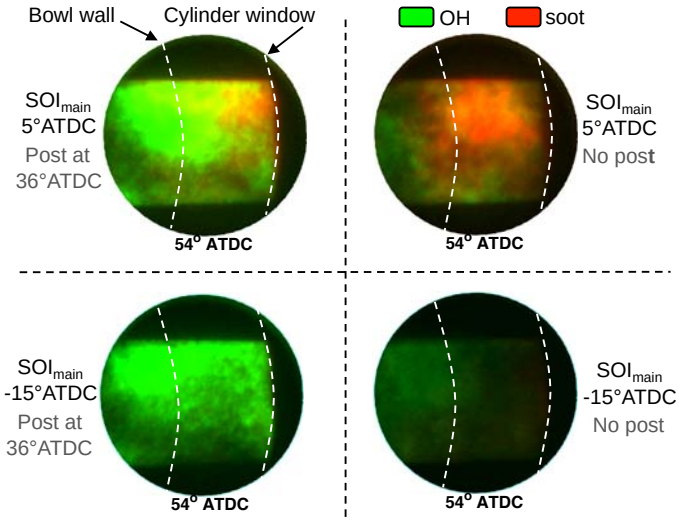

Figure 31: *Simultaneous LII (red) and OH-PLIF (green) in the squish region at 54 CAD ATDC, seen from above. Timings for the main and post-injections are indicated for each frame.*

With late main-injections however (first row in Figure 31), soot is present in the squish region and interacts with the OH-radicals formed during the combustion of the post. These observations correlate with the previous results showing the larger potential for soot reduction with late main-injections presented in Figure 30.

To summarize, this study showed the importance of targeting the soot region with the post-injected fuel in order to reduce engine-out soot emissions. Late main-injections tend to place the soot clouds in the squish region, making them easier targets for the post-injection. By comparing OH and soot distributions with and without post-injections it appears clearly that in-cylinder soot decreases where increasing OH-signal is observed, see Figure 32.

These results contribute to the knowledge of the soot reduction mechanism by post-injections and supports the hypothesis of OH-soot interaction for enhanced soot oxidation. They do not however discard the hypothesis of increased mixing due to the momentum of the post jet. This mixing-effect was doubtlessly underlying in the study, on parallel with the oxidation by OH process, but was out of the scope of this investigation.

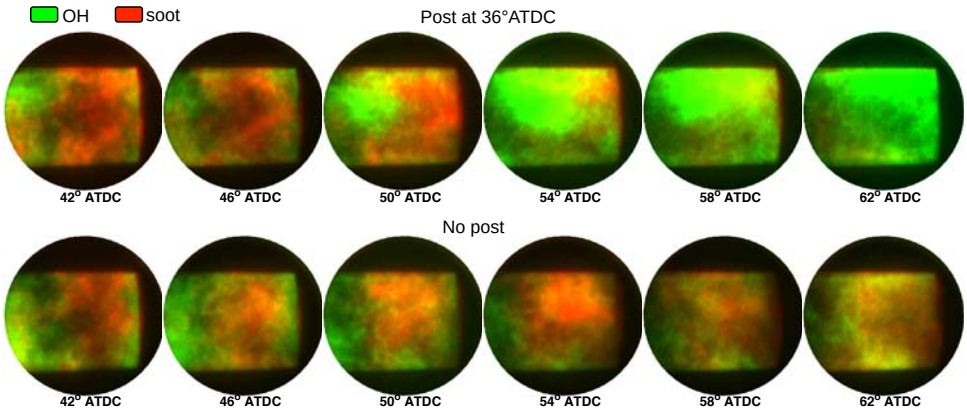

Figure 32: *Simultaneous LII (red) and OH-PLIF (green) in the squish region for the late main-injection case with and without post-injection.*

Chapter 5

Summary and Outlook

This concluding section is a summary of the main results obtained in this thesis. The contributions brought to the field are underlined and the limitations of the conclusions are also discussed.

5.1 Air entrainment and lift-off length

The several studies about air-entrainment in fuel jets in optical engines revealed that sufficient air-entrainment can lead to smokeless combustion. The smaller nozzle-hole diameter together with higher injection pressure and ambient density compared to the study underlying Dec's conceptual model gave a slightly different picture of the quasi-steady jet. Indeed, no soot was observed in the section of the burning jet despite the prediction of the conceptual model. Enhanced air entrainment in the jet up to the lift-off region prevents significant soot formation from occurring early in the jet. As a consequence, the soot formation occurs in the head vortices of the jet, in the recirculation zone. The net result is an engine-out soot level not detectable with the filtered smoke number method. These results were obtained without use of EGR and with a three-hole nozzle configuration. Therefore, the conditions for mixing oxygen into the fuel-jet are favourable compared to a standard eight-hole nozzle and lower oxygen level in the inlet air as when using EGR. Furthermore, a spectral analysis of the 355 nm-LIF signal was not performed. This could have given more detailed information about the origin of the signal, for example if it is due to PAH.

As mentioned above, jet-jet interactions can be of importance when observing air-entrainment and lift-off length in diesel jets. Results in this thesis showed the significant effect of inter-jet spacing on the lift-off length due to recirculation of

hot gases upstream of the lift-off region. When entraining these hot gases in the jet, auto ignition occurs earlier and the lift-off length is shortened. As a result, higher equivalence ratios are obtained at the lift-off length and higher soot formation is expected. A further study based on these results could use LII to couple the soot formation in the jet to the lift-off trends obtained when varying the inter-jet spacing.

The reason for the jets to interact and form recirculation zones is the presence of the piston-bowl wall in the downstream regions. Jets impact on the wall and travel along in the bowl until they collide and form a recirculation zone moving towards the nozzle. In this work, air-entrainment was found to lower in wall-jets compared to free-jets for a large range of injection pressure. Air-entrainment in wall jets was shown to have no significant dependence on the injection pressure in the optical engine unlike previous combustion vessel results where increased mixing with injection pressure was observed, likely due to an area increase upon impingement on a flat wall. The effect of swirl was noticed on these recirculation zones since they tend to follow the swirl motion. As a consequence, the recirculation zone tends to interact with the free part of the jet for closely spaced jets and cause enrichment of the mixtures in the whole jet downstream of this region. Furthermore, rapid leaning-out of the jet was observed after end of injection in the free part of the jet but this phenomenon was not transmitted to the recirculation zone by the wall jet. Unfortunately, few details could be gathered on the wall-jet in itself since the construction of the optical piston allows no clear optical access within 1.1 mm of the bowl wall. Therefore, for future measurements of wall jets, a different construction should be adopted or observation from above would give important information on the region close to the wall. Furthermore, experiments in combustion vessels with reproduction of the confined volume of wall-jets in engines would provide interesting complementary results about mixing in wall-jets.

5.2 Injection strategies: a combustion tool

Multiple injections have been used in several studies to help reducing engine-out emissions and also to improve combustion stability in cold conditions.

Cold starting properties were improved by using three pilot injections and a main to inject the desired fuel mass. By doing so, the evaporation process was spread over a longer time and did not cause a sudden temperature drop in the combustion chamber. By contributing to the heat release, the pilots compensated for the energy consumed during their evaporation. Further investigations on the different injection strategies proposed here could give more details on the different

processes involved. Mie scattering measurements on the liquid portion of the jets could for example give insight in the wall-impingement and evaporation issues at low temperatures. Furthermore, 355 nm PLIF together with OH-PLIF could help characterize the zones where first and second stage ignition occur. Spectral analysis of the 355 nm PLIF signal would be suggested in order to differentiate formaldehyde from PAH in the fluorescence signal.

Two measurement campaigns were performed to reduce engine-out emissions of soot and unburned hydrocarbons respectively. In the first study, the post injection was able to significantly reduce soot emissions by interaction between high temperature OH radicals and the soot clouds in the cylinder. The location of the soot is crucial for the determination of the timing of the post-injection in order to properly target the post on the soot. Complementing investigations would be needed to separate the effect of high temperature OH radicals and the mechanical mixing effects of post injections in the soot reduction mechanism.

In the second study, overlean regions close to the injector could be enriched by use of a small-post injection. Overlean regions contribute to engine-out emissions of UHC and by applying a post-injection strategy with a close short post, a 20 % decrease in UHC emissions was observed. These results were repeatable but very sensitive to the post-injection timing and duration. A further study could investigate these parameters in details using for example an injector with rate-shaping capabilities. Guidelines for the post-injection strategies reducing UHC emissions could be obtained and implemented in production engines if feasible.

References

1. Heywood, J.B., “Internal Combustion Engine Fundamentals”, McGraw-Hill Book Co, New York, US, 1988.

2. Taylor, A.M.K.P, ”Science review of internal combustion engines”, Energy Policy 36, 2008, pp. 4657-4667.

3. Diesel share in the European market from European Automobile Manufacturers Association, available at: http://www.acea.be/images/uploads/files/20090317_All.jpg 06/03/2012

4. Cummins, L., ”Internal Fire”, Carnot Press, Oregon, 2000.

5. Aronsson, U., “Processes in Optical Diesel Engines, Emissions Formation and Heat Release”, Doctoral thesis, Lund University, 2011.

6. Dec, J.E., ”A Conceptual Model of DI Diesel Combustion Based on Laser-Sheet Imaging”, SAE paper 970873, 1997.

7. Pickett, L.M. and Siebers, D.L., ”Soot Formation in Diesel Fuel Jets Near the Lift-Off Length”, International Journal of Engine Research, 7(2), 2006.

8. Siebers, D.L., ”Scaling Liquid-Phase Fuel Penetration in Diesel Sprays Based on Mixing-Limited Vaporization”, SAE paper 1999-01-0528, 1999.

9. Idicheria, C.A. and Pickett, L.M., ”Soot Formation in Diesel Combustion under High-EGR Conditions”, SAE paper 2005-01-3834, 2005

10. Pickett, L.M. and Siebers, D.L., ”Non-Sooting, Low Flame-Temperature Mixing-Controlled DI Diesel Combustion”, SAE paper 2004-01-1399, 2004

11. Pickett, L.M., Siebers, D.L. and Idicheria,C.A., “Relationship Between Ignition Process and the Lift-Off Length of Diesel Fuel Jets.”, SAE paper 2005-01-3843, 2005.

12. Musculus, M.P.B., and Kattke, K., “Entrainment Waves in Diesel Jets”, SAE paper 2009-01-1355, 2009

13. Tree, D.R., Svensson, K.I., “Soot processes in compression ignition engines”, Progress in energy and Science 33 (2007) pp. 272-309.

14. Andersson, Ö., “Diesel Combustion”, in “Handbook on Combustion vol 3”, Ed. Winter F., Wiley-VHC books, Weinheim 2010.

15. Kamimoto, T. and Bae, M., “High Combustion Temperature for the Reduction of Particulate in Diesel Engines”, SAE paper 880423, 1988.

16. Akihama, K., Takatori, Y., Inagaki, K., Sasaki, S. and Dean, A.M., ”Mechanism of the Smokeless Rich Diesel Combustion by Reducing Temperature”, SAE paper 2001-01-0655, 2001.

17. Miles P.C., Choi D., Pickett L.M., L.M., Singh, I.P. Henein, N., Rempelewert, B.H., Yun, H., and Reitz, R.D., “Rate-Limiting Processes in Late-Injection Low-Temperature Diesel Combustion Regimes”, Thiesel, Valencia, Spain, 2004.

18. Soot oxidation zone in the Φ-T map available at: http://www.dieselnet.com/tech/diesel_comb.html 13/03/2012

19. European emission standards. Available at: http://www.dieselnet.com/standards/ 13/03/2012.

20. National Highway Traffic Safety Administration. "2017-2025 Model Year Light-Duty Vehicle GHG Emissions and CAFE Standards: Supplemental" available at http://www.nhtsa.gov, 10/04/2012.

21. Ken-ichiro Inoue , Hirohisa Takano , Rie Yanagisawa , Seishiro Hirano , Takahiro Kobayashi , Yuji Fujitani , Akinori Shimada , Toshikazu Yoshikawa, ” Effects of inhaled nanoparticles on acute lung injury induced by lipopolysaccharide in mice”, Toxicology 238 (2007) 99–110.

22. Akihama, K., Takatori, Y., Inagaki, K., Sasaki, S. and Dean, A.M., ”Mechanism of the Smokeless Rich Diesel Combustion by Reducing Temperature”, SAE paper 2001-01-0655, 2001.

23. Pierpont, D. A., Montgomery, D. T. and Reitz, R. D., ”Reducing particulate and NOx using multiple injections and EGR in a D. I. diesel”. SAE paper 950217, 1995.

24. Alriksson, M., ”An Investigation of Low Temperature Combustion Using high Levels of EGR”, Licentiate thesis, Chalmers University of Technology, 2007.

25. Ekoto, I., Colban, W.F., Miles, P.C., Wook Park, S., Foster, D.E., Reitz, R.D., ”UHC Emissions Sources from a Light-Duty Diesel Engine Undergoing Dilution Controlled Low Temperature Combustion”, SAE paper 2009-01-1446, 2009.

26. Kim, D., Ekoto, I., Colban, W.F. and Miles, P.C., ”In-Cylinder CO and UHC Imaging in a Light-Duty Diesel Engine During PPCI Low-Temperature Combustion”, SAE paper 2008-01-1602, 2008

27. Lechner, G., Jacobs, T., Chryssakis, C., Assanis, D. et al., "Evaluation of a Narrow Spray Cone Angle, Advanced Injection Timing Strategy to Achieve Partially Premixed Compression Ignition Combustion in a Diesel Engine," SAE Paper 2005-01-0167, 2005.

28. Okude, K., Mori, K., Shiino, S., and Moriya, T., "Premixed Compression Ignition (PCI) Combustion for Simultaneous Reduction of NOx and Soot in Diesel Engine," SAE Paper 2004-01-1907, 2004.

29. Noehre, C., Andersson, M., Johansson, B., and Hultqvist, A., "Characterization of Partially Premixed Combustion," SAE Paper 2006-01-3412, 2006.

30. Lewander, M., Ekholm, K., Johansson, B., Tunestål, P. et al., "Investigation of the Combustion Characteristics with Focus on Partially Premixed Combustion in a Heavy Duty Engine," SAE Int. J. Fuels Lubr. 1(1):1063-1074, 2009.

31. Kimura, S., Aoki, O., Kitahara, Y., and Aiyoshizawa, E., "Ultra-Clean Combustion Technology Combining a Low-Temperature and Premixed Combustion Concept for Meeting Future Emission Standards," SAE Technical Paper 2001-01-0200, 2001

32. Kimura, S., Aoki, O., Ogawa, H., Muranaka, S. et al., "New Combustion Concept for Ultra-Clean and High-Efficiency Small DI Diesel Engines," SAE Technical Paper 1999-01-3681, 1999.

33. Johansson, B., “Förbränningsmotorer”, division of combustion engines, LTH Sweden, 2006.

34. Aronsson, U., Solaka, H., Chartier, C.,Andersson, Ö., Johansson, B., ”Impact of Mechanical Deformation due to Pressure, Mass, and Thermal Forces on the In-Cylinder Volume Trace In Optical Engines of Bowditch Design”, Submitted to SIAT 2011, paper no. 119.

35. Aronsson, U., Solaka, H., Lequien, G., Andersson, Ö., Johansson, B.,“Analysis of Errors in Heat Release Calculations due to Distortion of the In-Cylinder Volume Trace from Mechanical Deformation in Optical Diesel Engines”, Submitted to International Journal of Engine Research, 2011.

36. Stone, R., “Introduction to Internal Combustion Engines”, Antony Rowe Ltd, Chippenhham Wiltshire, UK, 1999.

37. Smoke meter information sheet from AVL available at https://www.avl.com/c/document_library/get_file?uuid=3b281792-57db-4654-87dc-e6592e8f4846&groupId=10138, 14/03/2012

38. F.W. Bowditch, ” A New Tool for Combustion Research, A Quartz Piston Engine”, SAE paper 610002, 1961.

39. Colban, W., Kim, D., Miles, P., Oh, S. et al., "A Detailed Comparison of Emissions and Combustion Performance Between Optical and Metal Single-Cylinder Diesel Engines at Low Temperature Combustion Conditions," SAE Int. J. Fuels Lubr. 1(1):505-519, 2009, doi:10.4271/2008-01-1066.

40. Eckbreth, A.C., “Laser Diagnostics for combustion temperature and species”, Second edition, Gordon and Breach Publishers, 1996.

41. Singh, S., Musculus, M.P.B and Reitz, R.D, “Mixing and flame structures inferred from OH-PLIF for conventional and low-temperature diesel engine combustion,” Combustion and Flame 156 (2009), pp. 1898-1908, 2009

42. Higgins, B. S., and Siebers, D. L.,”Measurement of the Flame Lift-Off Location on DI Diesel Sprays Using OH Chemiluminescence” SAE paper 2001-01-0918, 2001

43. Kohse-Höinghaus, K. “Laser techniques for the quantitative detection of reactive intermediates in combustion systems”. Progress in Energy and Combustion Science, 20, 203-279, 1994

44. J. E. Dec, A. O. zur Loye, D. L. Siebers, ”Soot Distribution in a D.I. Diesel Engine Using 2-D Laser-Induced Incandescence Imaging”, SAE paper 910224, 1991

45. J. E. Dec, ” Soot Distribution in a D.I. Diesel Engine Using 2-D Laser-Induced Incandescence, Elastic Scattering, and Flame Luminosity”, SAE paper 920115, 1992

46. Bobba, M. K. and Musculus, M. P. B., ”LII Spectra and Simultaneous Imaging with 532 and 1064 nm Excitation at LTC Diesel Engine Conditions”, Fall Technical Meeting of the Combustion Institute, 2009

47. Idicheria, C.A. and Pickett, L.M, “Formaldehyde Visualization Near Lift-Off Location in a Diesel Jet”, SAE paper 2006-01-3434, 2006

48. Yamada, H. and Goto, Y., "Formation Process of Soot Precursors in a Laminar Flow Reactor," SAE Paper 2007-01-0061, 2007

49. Egnell, R., “Combustion Diagnostics by means of Multizone Heat Release Analysis and NO Calculation”, SAE paper 981424, 1998.

50. Solsjö, R., Jangi, M., Chartier, C., Andersson, Ö., Bai, X.S., “Lift-off and stabilization of n-heptane combustion in a diesel engine with a multiple-hole nozzle injector”, The Combustion Institute, 34th International Symposium on Combustion, PROCI-D-12-00837, 2012.

51. Bruneaux, G., “Mixing Process in High Pressure Diesel Jets by Normalized Laser Induced Exciplex Fluorescence. Part II: Wall Impinging Versus Free Jet”, SAE paper 2005-01-2097, 2005.

52. Pickett, L.M., López, J.J., “Jet-Wall Interaction Effects on Diesel Combustion and Soot Formation”, SAE paper 2005-01-0921, 2005.

53. Musculus, M. P. B., Lachaux, T., Pickett, L. M., and Idicheria, C. A., "End-of-Injection Over-Mixing and Unburned Hydrocarbon Emissions in Low- Temperature-Combustion Diesel Engines," SAE Paper 2007-01-0907, SAE Transactions, 116, No. 3, pp. 515-541, 2007

54. Pacaud, P., Perrin, H., Laget, O., ”Cold Start on Diesel Engine: Is Low Compression Ratio Compatible with Cold Start Requirements?”, SAE paper 2008-01-1310, 2008

55. Pischinger, S., Grütering, U., Graf, M., Adomeit, P., Schmid, L., ”Ignition of Diesel Fuel at Low Temperatures”, MTZ 01/2008 volume 69

56. Lai, M.C., Henein, N.A., Xie, X., Chue, T.H., Itoh, Y, Bryzik, W, ”Diesel Cold-Starting Using Optically Accessible Engines”, SAE paper 952366, 1995

57. Tomoda, T., Ohki, H., Koyama, T., Fujiwara, K., “Study of Diesel Combustion Improvement for Ultra Low Compression Ratio”, Aachener Kolloquium Fahrzeug- und Motorentechnik :371-388, 2010.

58. Genzale, C.L., Reitz, R.D., and Musculus, M.P.B., “Effects of Jet-Bowl and Jet-Jet Interactions on Late- Injection Low-Temperature Heavy-Duty Diesel Combustion”, Proceedings Thiesel 2008, 2008.

59. Bobba, M. K., Musculus, M. P. B., and Neel, W., “Effect of Post Injections on In-Cylinder and Exhaust Soot for Low-Temperature Combustion in a Heavy-Duty Diesel Engine”, SAE Paper 2010-01-0612, 2010.

60. Payri, F., Benajes, J., Pastor, J. V., and Molina, S., “Influence of the Post-Injection Pattern on Performance, Soot and NOx Emissions in a HD Diesel Engine”, SAE Paper 2002-01-0502, 2002.

61. Dronniou, N., Lejeune, M., Balloul, I., and Higelin, P., “Combination of High EGR Rates and Multiple Injection Strategies to Reduce Pollutant Emissions”, SAE Paper 2005-01-3726, 2005.

62. Husberg, T., Denbratt, I., and Karlsson, A., “Analysis of Advanced Multiple Injection Strategies in a Heavy-Duty Diesel Engine using Optical Measurements and CFD-Simulations”, SAE Paper 2008-01-1328, 2008.

63. Roth, P.; von Gersum, S. “High Temperature Oxidation of Soot Particles by O, OH and NO.” In: Turbulence and Molecular Processes in Combustion, Takeno, T. [Editor], Elsevier, Tokyo, 1993.

Summary of papers

7.1 Paper I

Analysis of Smokeless Spray Combustion in a Heavy-Duty Diesel Engine by Combined Simultaneous Optical Diagnostics

Clément Chartier[1], Ulf Aronsson[1], Öivind Andersson[1], Rolf Egnell[1], Robert Collin[2], Hans Seyfried[2], Mattias Richter[2], Marcus Aldèn[2]

[1]*Division of Combustion Engines, Lund University, Sweden*
[2]*Division of Combustion Physics, Lund University, Sweden*

SAE Technical Paper 2009-01-1353

A heavy-duty diesel engine operating case producing no engine-out smoke was studied using combined simultaneous optical diagnostics. The case was close to a typical low load modern diesel operating point without EGR. Parallels were drawn to the conceptual model by Dec and results from high-pressure combustion vessels. Optical results revealed that no soot was present in the upstream part of the jet cross-section. Enhanced air entrainment in the jet prior to the lift-off region was identified as the main factor leading to the non-sooting nature of the investigated jet.

Experiments were carried out together with Ulf Aronsson, Robert Collin, Hans Seyfried and Mattias Richter. I analyzed the data and wrote the paper together with Öivind Andersson.

7.2 Paper II

Effect of Injection Strategy on Cold Start Performance in an Optical Light-Duty DI Diesel Engine

Clément Chartier, Ulf Aronsson, Öivind Andersson, Rolf Egnell

Division of Combustion Engines, Lund University, Sweden

SAE International Journal of Engines, March 2010 2:431-442

This paper investigates stability after start at low ambient temperatures in an optical light-duty diesel engine. The optical engine setup was modified in order to simulate the low temperatures without compromising the optical access. Using natural luminescence imaging, it was found that combustion is localized to the spray close to the glowplug in cold conditions. Identification of the effects of cooled down engine parts on combustion properties was then performed. Furthermore, different injections strategies were investigated in order to enhance fuel evaporation and ignition in the whole combustion chamber. Promising results were obtained with several pilot injections and adjustment of the fuel mass injected between the pilots.

Experiments were carried out together with Ulf Aronsson. I post-processed the data and wrote the paper together with Öivind Andersson.

7.3 Paper III

Effects of Post-Injection Strategies on Near-Injector Over-Lean Mixtures and Unburned Hydrocarbon Emission in a Heavy-Duty Optical Diesel Engine

[1]Clément Chartier, [1]Öivind Andersson, [1]Bengt Johansson
[2]Mohan K. Bobba, [2]Mark P. Musculus

[1]*Division of Combustion Engines, Lund University, Sweden*
[2]*Sandia National Laboratories Livermore, CA, United States*

SAE International Journal of Engines, June 2011 4:1978-1992

In this third paper, post-injection strategies aimed at reducing engine-out emissions of unburned hydrocarbons were investigated for low load LTC cases. Exhaust gas measurements showed that a carefully selected post injection reduced engine-out UHC emissions by 20 % compared to operation with a single injection at the same load. Simultaneous planar laser-induced fluorescence of OH and PLIF of combined formaldehyde and polyaromatic hydrocarbons were employed. The laser diagnostics show that without a post injection, regions close to the injector show formaldehyde fluorescence late in the cycle without detectable OH fluorescence, indicating that these regions do not achieve second-stage ignition, and therefore likely contribute to UHC emissions. With a carefully selected post injection, strong OH fluorescence appears in the near-injector regions, indicating that they are likely enriched by the post-injection such that they reach second-stage ignition and more complete oxidation. The reduction observed in the

exhaust UHC emission is therefore attributed to the enrichment mechanism of the near-injector regions by the close-coupled post-injection.

Experiments were carried out together with Mohan Bobba and Mark Musculus. I post-processed the data. I wrote the paper together with Mark Musculus and Öivind Andersson.

7.4 Paper IV

Influence of Jet-Jet Interactions on the Lift-Off Length in an Optical Heavy-Duty DI Diesel Engine

Clément Chartier, Ulf Aronsson, Öivind Andersson, Rolf Egnell, Bengt Johansson

Division of Combustion Engines, Lund University, Sweden

This forth paper deals with interactions between burning fuel jets in a heavy-duty engine. The effect of inter-jet angle on lift-off length was investigated using symmetric and asymmetric nozzle cups. Decreasing the inter-jet angle produces shorter lift-off length. The lift-off length showed a weaker dependence on the ambient temperature in the engine than predicted by an empirical expression established in a constant-volume combustion vessel. The findings in this paper indicate that experiments in such vessels may not capture all features of the conditions in engines.

Submitted to International Journal of Engine Research

Experiments were carried out together with Ulf Aronsson. I post-processed the data. I wrote the paper together with Öivind Andersson.

7.5 Paper V

Air Entrainment in Wall-Jets using SLIPI in a Heavy-Duty Diesel Engine

Clément Chartier[1], Johan Sjöholm[2], Elias Kristensson[2], Yann Gallo[1], Öivind Andersson[1], Mattias Richter[2], Marcus Aldén[2] and Bengt Johansson[1]

[1]*Division of Combustion Engines, Lund University, Lund, Sweden*
[2]*Division of Combustion Physics, Lund University, Lund, Sweden*

Mixing in wall-jets was investigated in an optical heavy-duty diesel engine with several injector configurations and injection pressures. Laser induced fluorescence (LIF) was employed in non-reacting conditions in order to quantitatively measure local equivalence ratios in colliding wall-jets. A novel laser diagnostic technique, Structured Laser Illumination Planar Imaging (SLIPI), was successfully implemented in an optical engine and permits to differentiate LIF signal from multiply scattered light. It was found that in the tested conditions, increased injection pressure does not imply increased mixing in wall-jets. The confined nature of the wall-jet in the optical engine is suspected to be the reason for these observations compared to results obtained in a combustion vessel with impingement on a flat wall where area increase of the jet is larger. Furthermore, comparisons with free-jet predictions indicate that mixing in wall-jets is lower than in free-jets for identical conditions.

Submitted to SAE Powertrains, Fuels & Lubricants Meeting, September 18-20, 2012, Malmo, Sweden

Experiments were carried out together with Elias Kristensson and Johan Sjöholm. Johan Sjöholm and I post-processed the data. I wrote the paper together with Öivind Andersson.

7.6 Paper VI

Planar Laser-Diagnostics of Soot and OH with Post-Injections in a Heavy-Duty LTC Diesel Engine

Mohan K. Bobba[1], Clément Chartier[2], Bengt Johansson[2], Öivind Andersson[2], and Mark P. B. Musculus[1]

[1]*Sandia National Laboratories Livermore, CA, United States*
[2]*Division of Combustion Engines, Lund University, Sweden*

In this sixth publication, planar laser-induced incandescence of soot and planar laser-induced fluorescence of OH were employed to better identify the in-cylinder mechanisms of soot reduction by post injections. The planar-imaging data shows that for an early main injection, very little soot from the main injection enters the squish region into which the late post injection is directed. Consequently, although the post-injection burns largely soot free and generates significant late-cycle OH that could help oxidize soot, very little main-injection soot is available in the squish region for oxidation. In contrast, a large fraction of the late main-injection soot spills into the squish region. Therefore the OH field generated by the post-injection combustion fills much of the sooty squish region from the main

injection, so that in-cylinder and exhaust soot are reduced below the levels of the main injection only.

Proceedings of THIESEL 2010 Conference on Thermo- and Fluid Dynamic Processes in Diesel Engines, Valencia, Spain, September 14-17 2010.

Experiments were carried out together with Mohan Bobba and Mark Musculus. I assisted Mohan in the data post-processing. Mohan wrote the paper together with Mark Musculus.

Paper I

2009-01-1353

Analysis of Smokeless Spray Combustion in a Heavy-Duty Diesel Engine by Combined Simultaneous Optical Diagnostics

Clément Chartier, Ulf Aronsson, Öivind Andersson, Rolf Egnell
Division of Combustion Engines, Lund University

Robert Collin, Hans Seyfried, Mattias Richter, Marcus Aldén
Division of Combustion Physics, Lund University

ABSTRACT

A heavy duty diesel engine operating case producing no engine-out smoke was studied using combined simultaneous optical diagnostics. The case was close to a typical low load modern diesel operating point without EGR. Parallels were drawn to the conceptual model by Dec and results from high-pressure combustion vessels. Optical results revealed that no soot was present in the upstream part of the jet cross-section. Soot was only observed in the recirculation zones close to the bowl perimeter. This indicated very slow soot formation and was explained by a significantly higher air entrainment rate than in Dec's study. The local fuel-air equivalence ratio, Φ, at the lift-off length was estimated to be 40% of the value in Dec's study. The lower Φ in the jet produced a different Φ -T-history, explaining the soot results. The increased air entrainment rate was mainly due to smaller nozzle holes and increased TDC density. Furthermore, increased injection pressure was believed to reduce the residence time in the jet, thus reducing the soot formation. OH was detected at the periphery of the jet, upstream of the location where fuel started to react on the jet centerline. The OH region extended relatively far into the jet, further supporting the conclusion of a less fuel-rich jet in the current case. Partially oxidized fuel (POF) was found at the center of the jet, downstream of the lift-off position. This indicated that the temperature needed to start chemical reactions inside the jet had not been obtained at the lift-off position. The high-temperature reaction zone at the periphery thus added heat over a distance before POF was observed on the centerline.

BACKGROUND

The diesel engine is the dominating power source for heavy road transports. The last decade has brought a tremendous development in diesel engine technology. The dilemma between nitrous oxides and soot particles emissions is still present but has significantly improved with e.g. cooled exhaust gas recirculation (EGR), elevated injection pressures and, eventually, particle filters. Increasingly stringent emissions regulations continue to force continuous improvement in engine-out emissions. Much of the current diesel engine research is aimed at different types of premixed combustion modes, ranging from homogeneous charge compression ignition (HCCI) to less radical low temperature combustion concepts (see e.g. [1]). These alternatives are capable of simultaneously reducing both soot and NOx formation. Nevertheless, most heavy duty diesel engines in production still use more classical strategies, e.g. using dilution of the charge by EGR to meet the regulation levels. The typical, heavy load duty cycles of these engines are characterized by large fuelling rates and long injection durations. Under those conditions the major part of combustion takes place during the mixing-controlled burn. Therefore, a quasi-stationary jet is a useful picture for analyzing the combustion in heavy duty engines.

The well established, so-called conceptual model describes a quasi-stationary jet in a heavy duty diesel engine. It is based on pioneering laser-diagnostic work by John Dec more than a decade ago [2]. It exposes the different characteristic regions of the burning jet, see Figure 1, and serves as a mental image of diesel spray combustion that dominates in the diesel community today. This model showed a liquid-fuel penetration length much shorter than what had previously been thought. Furthermore, no droplets were present in the combustion zone, only fully vaporized fuel. Just downstream of the liquid part of the spray a rich premixed combustion zone appeared. After that point soot was present throughout the section of the jet, growing in size and volume fraction as it was transported downstream. A diffusion flame was present at the periphery of the jet and corresponded to the region where soot was oxidized and NOx was formed. This model is henceforth referred to as the conceptual model.

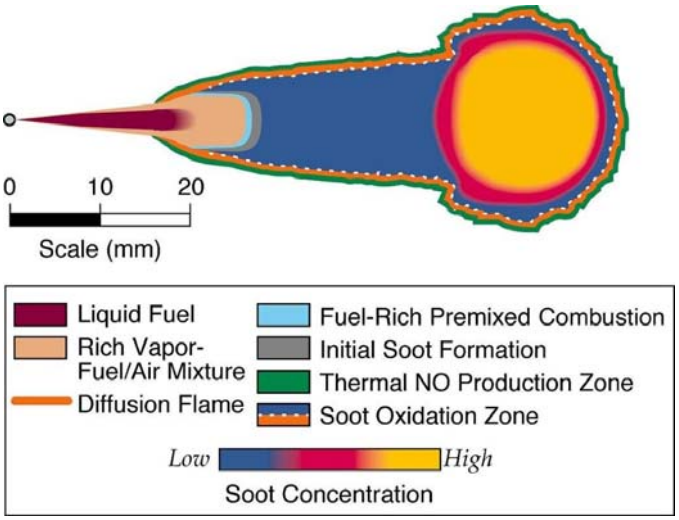

Figure 1 Reproduced from Dec [2]. A schematic of the conceptual model.

A parameter of interest in this quasi-stationary jet is the lift-off length, i.e. the distance between the nozzle hole and the upstream most part of the turbulent diffusion flame. This is the distance available for most entrainment of surrounding air into the jet. Air entrained downstream of the lift-off length reacts in the diffusion flame. The entrainment into the jet interior is thus very limited in the reacting part of the jet. The more air entrained into the spray up to the lift-off length, the lower the equivalence ratio inside the jet and thus less soot formation [3].

Most lift-off investigations have been performed in pressurized vessels; see e.g. [3, 4, 5, 6, 7]. Although few lift-off studies have been performed in optical engines, it is of interest to do so due to the differences that can be expected. Parameters such as pressure and temperature are varying during combustion in an engine, due to the limited volume of the combustion chamber and to the piston movement. In combustion vessels the volume is usually so large in relation to the injected fuel amount that combustion takes place at constant pressure and, thus, constant ambient temperature. Other effects that are difficult to capture in a vessel are fuel jets interacting with the in-cylinder flow and with other jets, which may introduce cycle-to-cycle variations e.g. in lift-off length [8]. In the current study the jet-jet spacing is rather large, but other investigations with the same hardware shows that variations still can be expected [14].

The case presented in the current study can be classified as classical diesel combustion. The injection starts five crank angle degrees (CAD) before top dead center (BTDC) and the major part of the combustion takes place during the injection period. More than half the heat is released by the end of injection. Furthermore, the charge was not diluted using EGR. Despite the fact that it was not a low temperature combustion strategy for soot reduction, no smoke was produced at all. Non-sooting mixing controlled combustion has previously been demonstrated in a pressurized combustion vessel when the equivalence ratio, Φ, falls below approximately 2 [7,9]. However, demonstrations of this combustion mode in an optical engine has not been found in the literature. The current study should be seen as a complement to the previous studies in combustion vessels. The conceptual model is used as a reference for comparison.

EXPERIMENTAL SETUP AND DIAGNOSTICS

OPTICAL ENGINE - The presented investigations were performed on a six cylinder Scania D12 truck sized diesel engine modified for optical access using a Bowditch design. Engine specifications are given in Table 1.

The engine was running in single cylinder operation meaning that only one cylinder was operational while the five other ones were motored.

The top part of the cylinder liner is replaced with a steel ring containing two quartz windows, see Figure 3. This modification reduces the optical access compared to a full quartz ring but is more robust to high pressures and pressure rise rates. Furthermore, a surface treatment absorbs reflections from the laser and from the combustion luminosity, giving a better signal-noise ratio compared to a full quartz ring.

The engine was operated at low load at a speed of 1200 revolutions per minute. The inlet air was conditioned in terms of pressure and temperature by an independent two-stage screw-compressor and an electrical heater. The injector used was equipped with a three-hole nozzle. This choice was motivated by the improved quality of the optical measurements by providing a free path of the laser to the jet of interest.

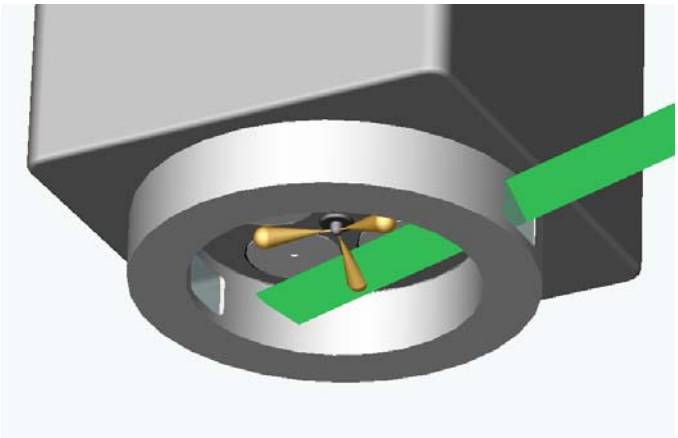

Figure 2 Representation of the optical access with side windows and the path of the laser sheet.

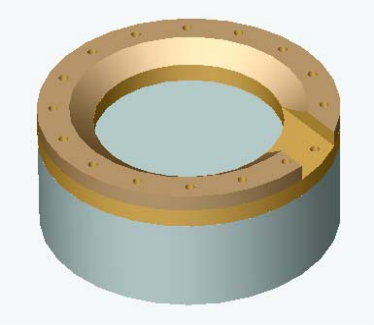

Figure 3 Representation of the piston bowl cut out for improved optical access close to TDC.

The small number of holes and their small diameters resulted in relatively long injection durations even at this low load condition. Furthermore, the injection timing was adapted to the limitations of the measurement techniques. By phasing the combustion late it was possible to access the combustion chamber with the laser sheets from the side at CA50 without the piston blocking the side windows. Injection settings are given in Table 2.

A titanium crown was mounted on the top of the flat optical piston to reproduce a reasonable piston bowl geometry. This crown featured a cut out to improve the optical access from the side windows when the piston was close to top dead center, as illustrated in Figure 3.. Due to the piston blocking the side windows full laser-access to the jet was not possible between -12 and 12 CAD ATDC. A summary of the operating conditions is presented in table 1.

Table 1 Engine specifications

ENGINE SPECIFICATIONS	
Engine type	**Scania D12**
Cycle	**4 stroke**
Number of cylinders	**1**
Number of intake valves	**2**
Number of exhaust valves	**2**
Bore (mm)	**127**
Stroke (mm)	**154**
Bowl width (mm)	**80**
Displacement (liters)	**1.95**
Compression ratio	**15.1:1**
INJECTOR	
Type	**Cummins Common Rail**
Number of holes	**3**
Orifice diameter (mm)	**0.1**

The fuel used in this study is a mixture of 69.3% n-heptane, 29.7% isooctane and 1% of a transparent lubricant, Chevron Synfluid. The lubricant is used to prevent excessive wear of the fuel pump and the injector. This fuel mixture is commonly used in optical experiments since it has a well known composition, as opposed to commercial diesel fuels, and does not generate fluorescence when using laser based measurement techniques. The cetane number of this fuel is estimated to be 42.5 and thus very close to a commercial U.S. diesel fuel. Furthermore, the reference fuel used by Dec has the same cetane number [2]. The boiling points of n-heptane and iso-octane are both 98 °C. It is significantly lower than diesel fuels.

Table 2 Operating conditions

OPERATING CONDITIONS	
IMEP (bar)	**5.5**
Injection pressure (Bar)	**1700**
SOI (CAD BTDC)	**5**
EOI (CAD ATDC)	**25**
Inlet pressure (kPa absolute)	**203**
CA50 (CAD ATDC)	**17**
Inlet Temperature (K)	**373**
O2 Inlet (%)	**21**
Motored TDC pressure (MPa)	**7.0**
Estimated motored TDC temperature (K)	**865**
Estimated motored TDC density (kg/m3)	**27.4**

OPTICAL SETUP –The combustion process is governed by a variety of parameters. Some of them are not controlled, such as variations in the in-cylinder flow, the precise amount of rest gases, and cavitation in the injector. These cycle to cycle variations may have an impact on the spatial and temporal distribution of the species. In order to understand the mechanism of the combustion with optical diagnostics it is necessary to capture these variations. Therefore, the different measurement techniques in this study were performed simultaneously in pairs. Partially oxidized fuel, the high temperature diffusion flame (OH radicals), and the soot formation process were captured in three pairs of combinations.

OH - The OH radicals were excited through the $Q_1(8)$ transition near 283 nm in the v" = 0 → v' = 1 band of the $A^2\Sigma \leftarrow X^2\Pi$ system using a frequency doubled dye laser pumped by the second harmonic of a Nd:YAG laser. The output pulse energy from the laser was approximately 25 mJ near 283 nm.

The resulting OH fluorescence was detected at around 310 nm. A long pass filter was used to isolate this OH emission from elastically scattered laser radiation at 283 nm. To filter out background fluorescence a band-pass filter, UG11, was employed. Further information about OH LIF can be found in the review article by Kohse-Höinghaus [10].

Partially oxidized fuel - For the 355 nm-LIF the third harmonic of a Nd:YAG laser was used with a pulse energy of approximately 75 mJ. LIF was detected using a GG395 Schott-filter combined with a 500 nm short-pass filter.

A large variety of species can be excited at 355 nm. As mentioned previously the fuel does not fluoresce, but some hydrocarbon intermediates may do so. With this set-up the signal was mainly expected to come from ketones, aldehydes (e.g formaldehyde), and polyaromatic hydrocarbons (PAH). However, without a complementary measurement technique, such as a spectroscopic study of the signal, it is not possible to differentiate between these. Therefore, the fluorescence signal collected was referred to as "partially oxidized fuel" (POF), i.e. intermediate species between fuel and carbon monoxide. The simultaneous measurements of OH and POF follow the scheme described by Collin *et al.* [11].

Soot - Measurements of soot were performed using laser-induced incandescence (LII) using a Nd:YAG laser source operating at 1064 nm with 80 mJ per pulse. At this power level, and a focused sheet thickness of approximately 0.5 mm, the laser sheet fluence within the cylinder was maintained well within the LII plateau region. In this region, the soot incandescence is independent of the laser power.

The LII signal was short-pass filtered at 450 nm, with an additional, heat-absorbing Schott filter (KG3) to further attenuate longer wavelengths. Further information about the LII technique can be found in [12, 13].

The simultaneous measurement techniques were performed using two laser sources fired with a time separation of 500 ns. The laser beams from the two laser sources were combined and thereafter shaped into a laser sheet using the same optics (a -100 nm cylindrical lens and a +300 nm spherical lens, see Figure 4).

The two laser beams were combined into a horizontal laser sheet with a width of 22 mm aligned through the centerline of the injected spray. It illuminated a region between 18 and 40 mm downstream from the injector, as illustrated in Figure 5.

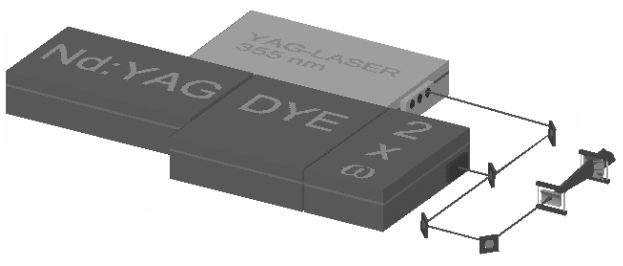

Figure 4 Laser sources and laser beam combination for simultaneous measurements.

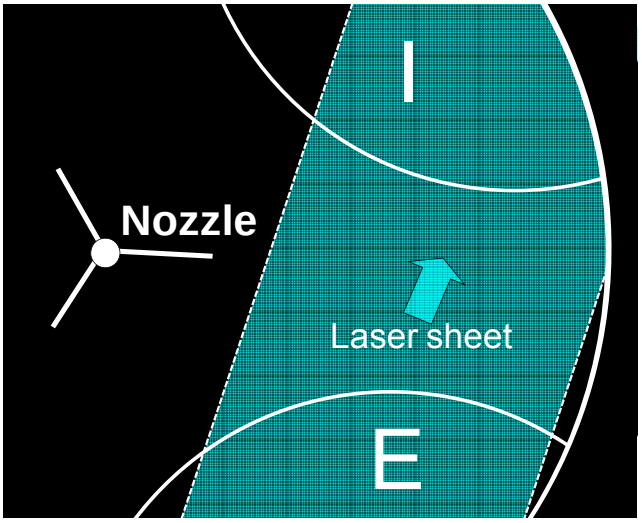

Figure 5 Schematic of the laser path in the combustion chamber intersecting one of the three jets. The inlet (I) and exhaust (E) valves are indicated.

In each simultaneous pair of measurements the two signals were spectrally separated using a mirror. For the combination of OH- and POF-LIF, as well as the OH and LII combination, a high-reflective mirror centered at 308 nm was used. For the combination of POF LIF and LII the signals were separated using a 50% beam splitter dividing the signal equally between the two detectors.

Two ICCD-camera systems (Princeton Instruments PI-MAX), equipped with UV-lenses (Nikon, f =105 mm, f# = 4.5) were used to collect the signals, see Figure 6.

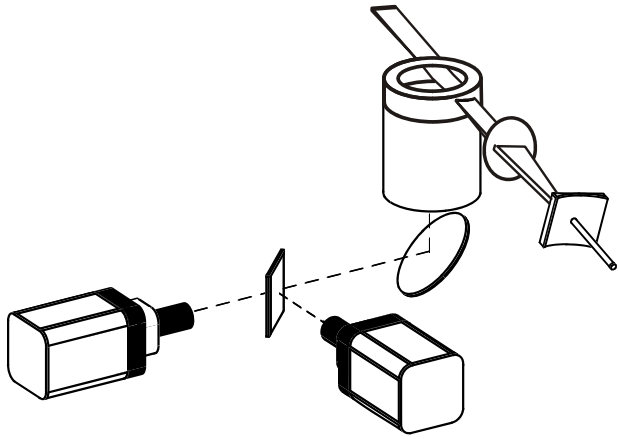

Figure 6 Schematic of the optical setup for simultaneous signal acquisition.

High speed video - Line of sight measurements were also employed during this study. They provided a more global overview of the combustion event than the 2D measurements, showing only a section through the jet. A Phantom 7.1 high speed video camera was used together with a Hamamatsu image intensifier and a LaVision stereoscope. This configuration made it possible to simultaneously record natural luminescence from the combustion and OH-chemiluminescence.

Natural luminescence mostly comes from black body radiation from heated soot particles. OH-chemiluminescence was monitored through a band-pass filter centered at 310 nm, transmitting wavelengths between 305 and 315 nm. This filter absorbs 86% of the incoming light intensity and could cause an unbalanced exposure between the two channels of the stereoscope. To avoid this problem, and to prevent damaging the image intensifier, an OD4 filter was used for the natural luminescence channel. This filter was made of glass and did not transmit light in the UV. This ensured that the natural luminescence images did not contain signal from OH-chemiluminescence. However, given the broadband spectrum of black body radiation there is no doubt that some natural luminescence signal was present on the OH-chemiluminescence images.

The lift-off lengths presented in this paper were measured in these line of sight OH-chemiluminescence images. In the OH-LIF measurements the laser sheet was placed downstream of the liquid penetration length, i.e. close to the lift-off length. Therefore, the natural OH chemiluminescence was judged to provide more certainty in the lift-off length determination. The lift-off length was determined by evaluating the averaged signal strength as a function of radial distance from the injector within a sector containing one spray. The radial position where this signal exceeded a certain threshold value was defined as the lift-off position. The threshold value was set to 100 on a scale from 0 to 255.

Mie scattering- The liquid penetration length of the jet was measured using Mie scattering. The laser beam of a Nd:YAG laser was expanded in the horizontal direction with a negative, f = -40 mm, cylindrical quartz lens before it entered the engine. This ensured that the entire fuel jet was illuminated by the laser beam. The experimental setup is further described in [14]. The engine was run with pure iso-octane and thus without combustion in this case in order to improve the quality of the measurements. A Princeton PI-MAX camera with a 1024 by 1024 CCD chip was used.

The Mie scattering signal was averaged as a function of radial distance from the injector within a sector containing one of the sprays. The position where this averaged signal dropped below a threshold value was defined to be the liquid penetration length. Selecting a threshold value was fairly easy as the Mie scattering generally is several orders of magnitude stronger as compared to the Rayleigh scattering of the surrounding gas phase.

RESULTS

The combustion characteristics of the examined case are presented in Figure 7 and Figure 8. The pressure data was averaged over 200 cycles. The timing for image acquisition of the laser-based diagnostics is indicated on both figures.

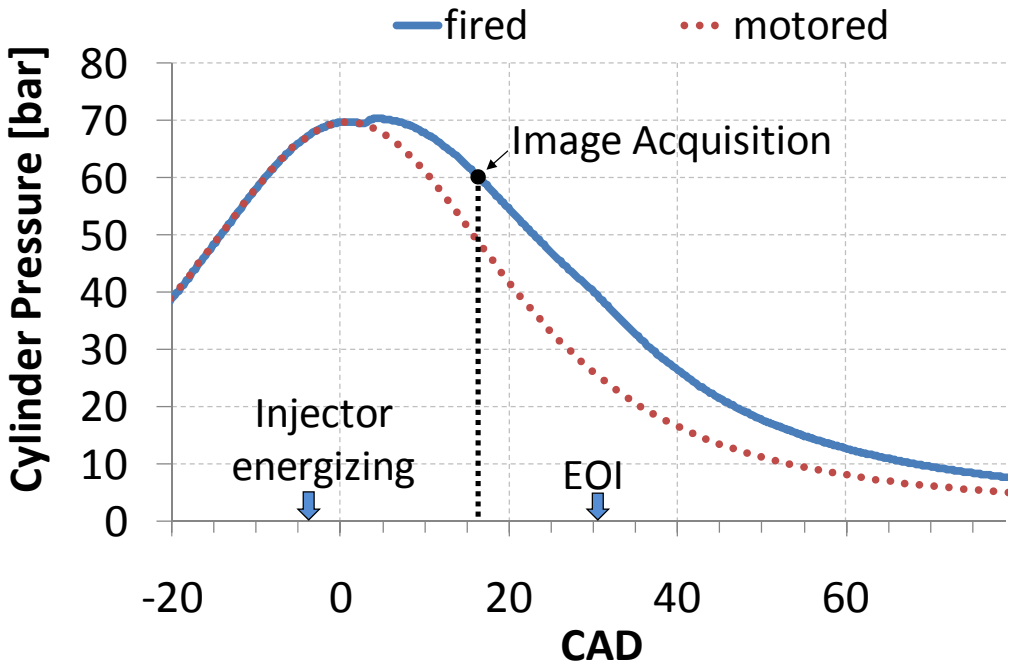

Figure 7 Pressure traces for motored and fired condition. The timing for image acquisition for the laser-based diagnostics is mentioned.

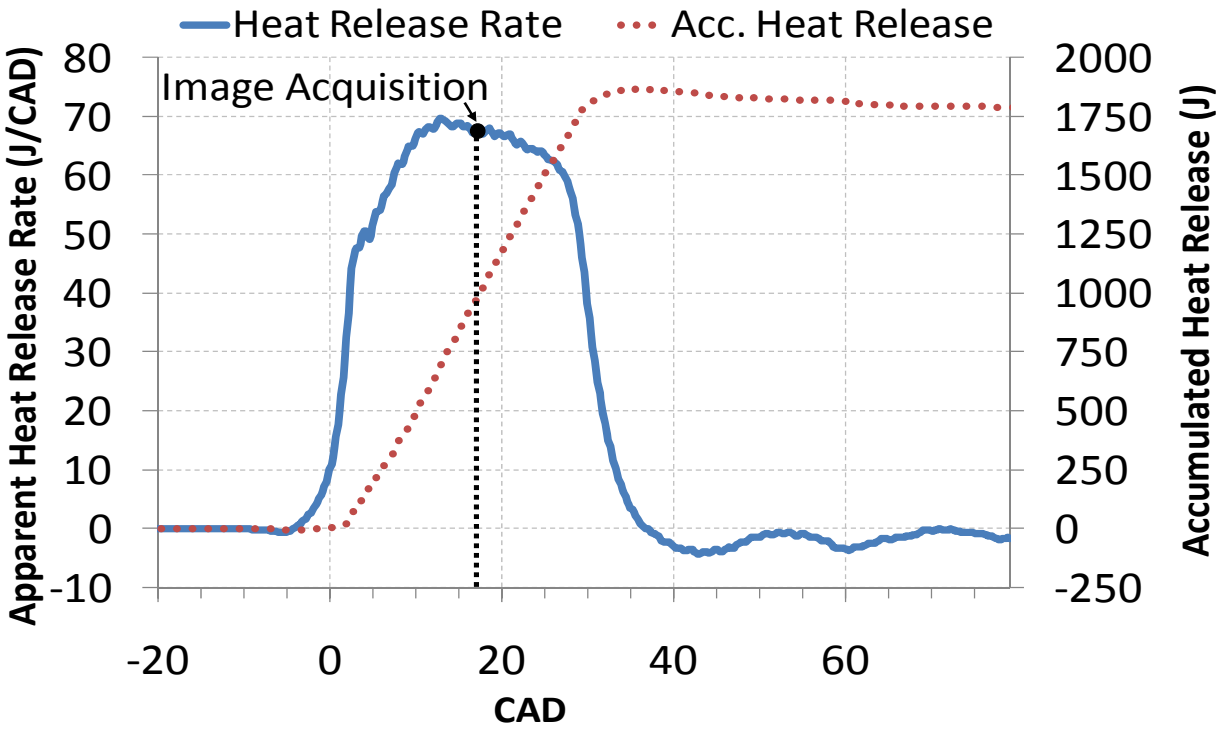

Figure 8 Apparent heat release rate and accumulated heat release for the presented case. The timing for image acquisition for the laser-based diagnostics is mentioned.

SMOKE LEVEL AND LINE OF SIGHT DIAGNOSTIC - Repeated smoke measurements showed a filter smoke number (FSN) of zero, i.e. no soot particles were detected in the exhaust pipe. However, line-of-sight natural luminescence images of the whole combustion chamber showed that soot was present in the downstream jet region. Figure 9 was acquired at 17 CAD ATDC (i.e. at CA50). It shows that the natural luminescence signal was significant in the left image. This signal is mainly due to black body radiation from soot particles showing that soot was produced in the present case. This is further supported by the fact that the glass piston had to be cleaned regularly because of significant soot deposits on its surface.

The soot signal in Figure 7 resides close to the bowl perimeter, whereas the OH signal extends back toward the injector to a point close to the liquid penetration length. This picture was typical for the major part of the combustion process. The temporal history of the OH and soot signals can be described as follows. OH first appeared in the head vortex of the developing jet, at a location midway between the bowl perimeter and the point where the lift-off length later established itself. The OH signal coincided with the heat release rate turning positive. Within 1.5 CAD it was stabilized at the lift-off position. It remained there until about 18 CAD ATDC, i.e. shortly after CA50. This period is referred to as the quasi-stationary jet phase, and corresponds to approximately 50% of the heat release. After this the OH signal moved downstream and vanished completely at 30 CAD ATDC. Soot first appeared in the head vortex of the developing jet, just before it reached the bowl perimeter. This occurred when the lift-off position already was established. As the jet reached the wall, the soot signal temporarily extended up to a point 26 mm from the nozzle. It immediately moved downstream as the jet started to spread along the bowl wall. The soot signal then remained in the vicinity of the wall until approximately 23 CAD ATDC, when it vanished. The two images in Figure 9 are thus typical for the larger part of the combustion process.

If the natural luminescence from soot leaks through the filters used in the laser diagnostic measurements, false conclusions may be drawn. Therefore, background measurements were performed for the different optical setups to rule out the risk of misinterpreting the signals. This was done by switching off the lasers and acquiring the natural luminosity from the combustion passing through the respective filters.

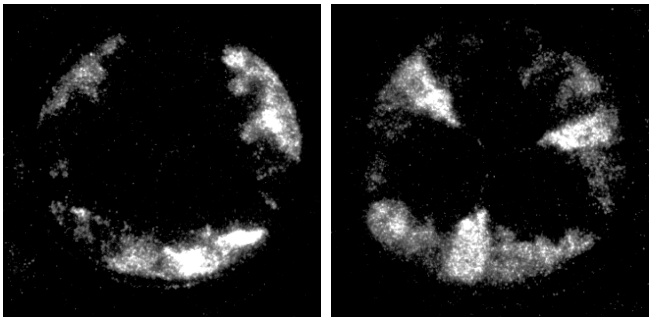

Figure 9 Simultaneous line of sight imaging of the quasi-steady state mixing-controlled combustion. Left, natural luminescence. Right, OH-chemiluminescence.

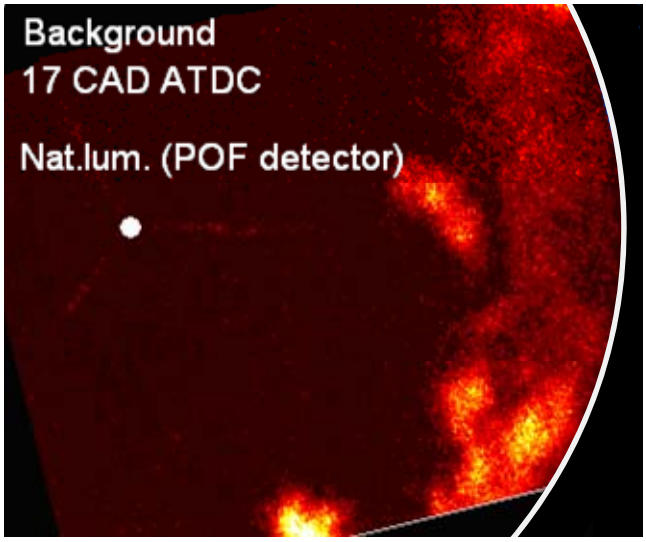

Figure 10 Significant background luminosity level on the POF detector.

Even though the optical setup is made to remove as much background luminosity as possible, the Planck radiation from heated soot particles is very broadband and thus difficult to remove completely. The gating width of the ICCD was optimized to 30 ns in order to reduce the background luminosity. Background measurements for LII and OH-LIF produced no signal above the detector noise level. For POF-LIF, however, a significant background signal was detected through the filters. The background luminosity is mainly located far downstream in the jets and along the piston bowl wall, see Figure 10. Therefore, the POF-LIF data must be interpreted with care at the downstream locations. Figure 10 shows a partial view of the combustion chamber as illustrated in Figure 5.

LASER MEASUREMENTS - The results from the laser diagnostics will be presented with pairs of simultaneous single shot images as well as averaged images for each measurement technique. Single shot images representative for the set of data were chosen. All images were taken at 17.1 CAD ATDC while the combustion phasing (50% burned) was at 17 CAD ATDC. The injector was energized 5 CAD BTDC and the end of injection took place at 25 CAD ATDC. The simultaneous laser imaging results are presented in Figure 11. The data was acquired with two cameras simultaneously for each measurement technique. Then, each pair of images was assembled into one. Signals from the different techniques are color-coded in the images. OH-radicals are represented in blue, POF in green, and soot in red. The laser sheet illuminated a region extending from the bowl wall to 18 mm from the injector. This assured that no droplets were present in the measurement zone, since the liquid penetration length had been measured to be 17 mm using Mie scattering.

As seen in the upper pictures of Figure 11 the signals from OH-LIF and POF-LIF do not overlap spatially, but show a relatively good spatial match. OH, indicating the high temperature diffusion flame, is forming a mantle around the partially oxidized fuel and is beginning upstream of the POF region. POF signal is showing a higher level downstream in the jet, close to the piston bowl wall. Part of the far downstream POF signal can be attributed to a background from soot as seen previously. A noticeable feature is the presence of OH signal on the right hand side of the jet in the downstream direction. The background measurements previously showed that the OH-LIF images are free from background luminosity. The signal therefore indicates the presence of OH radicals in the recirculation zone. It is reasonable to assume that the jet structure is symmetrical and that a similar recirculation zone exists outside of the observation region.

The middle pictures in Figure 11 shows OH radicals and LII signal from soot. The OH-radicals show a similar structure to the previous pictures. However, the most noticeable feature is that no soot is detected in the section of the jet, as would be expected from the conceptual model. The LII signal is very weak, comparable to the noise level of the detector and appeared stochastically from shot to shot. Severe signal trapping was not expected, leading to the conclusion that soot levels in the laser-illuminated section through the jet were very low. It should be noted, however, that in a few images the OH signal in the recirculation zone was accompanied by small specks of LII signal, as showed on the right hand picture. Hence, on the few occasions that soot was detected it was only detected in the recirculation zone.

The bottom picture represents simultaneous POF and LII. As in the middle picture, no soot signal was detected. The POF signal was comparable to the upper images although the region along the wall showed a lower signal level. This can be explained by the different signal division methods between the two cases. A 50% beam splitter was used for simultaneous POF-LIF and LII while a high-reflective mirror centered at 308nm was used for the two other pairs. It does not affect the results to a large extent, apart from the lower picture containing less background luminosity.

Figure 12 presents the averaged signal over a hundred cycles for each measurement technique separately. The OH-LIF averaged signal in the upper picture shows a very similar structure to the single cycle images indicating a relative stability between the cycles.

The POF averaged signal presented in the middle picture was obtained through the 50% beam splitter. Therefore it does not show high signal levels along the bowl wall. However, a strong POF concentration is located in the downstream section of the jet.

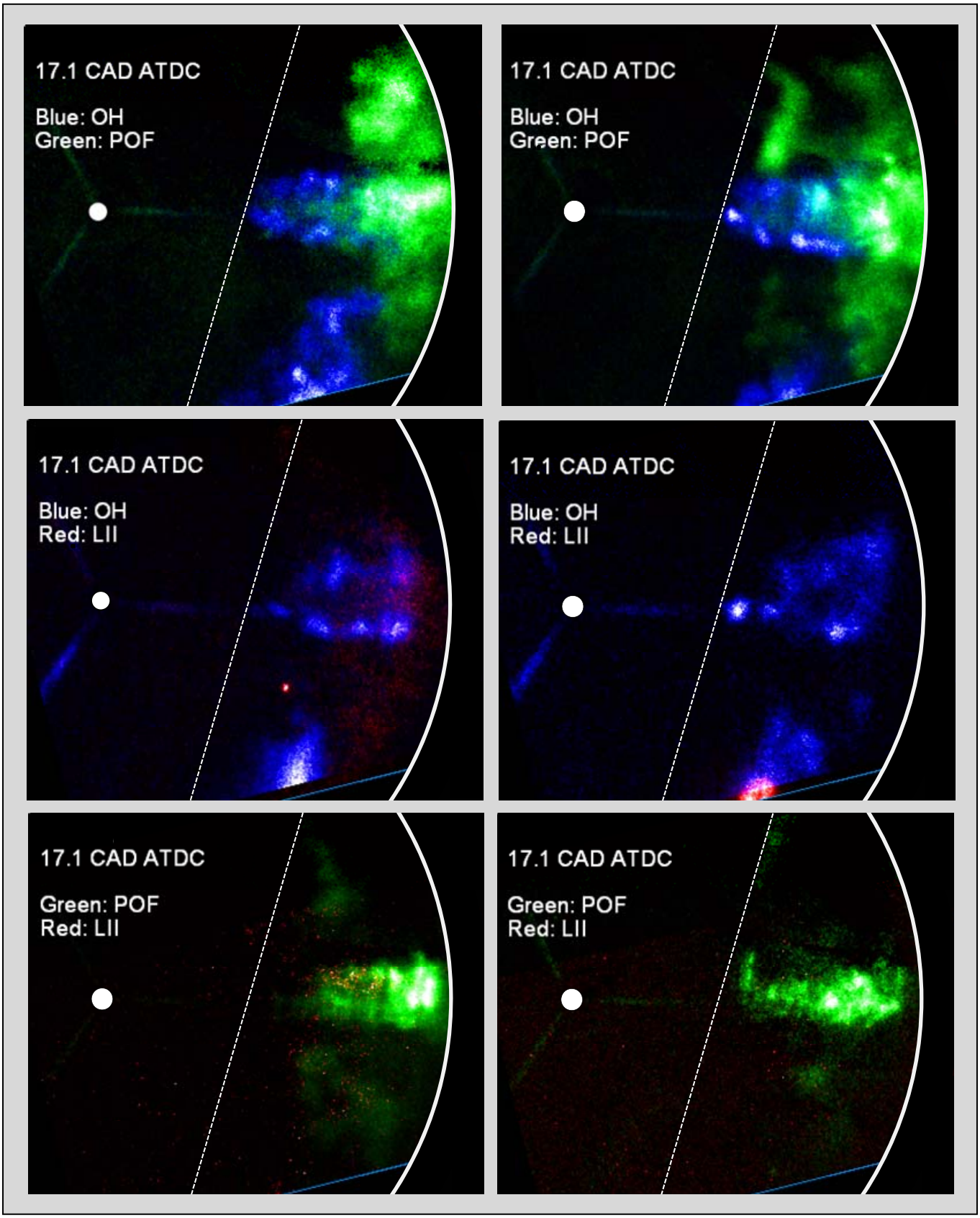

Figure 11 Pairs of single shot images of the quasi-stationary burning jet. Top: simultaneous OH-LIF (blue) and POF-LIF (green). Middle: simultaneous OH-LIF (blue) and LII (red). Bottom: simultaneous POF-LIF (green) and LII (red). The dashed line represents the upstream border of the laser sheet.

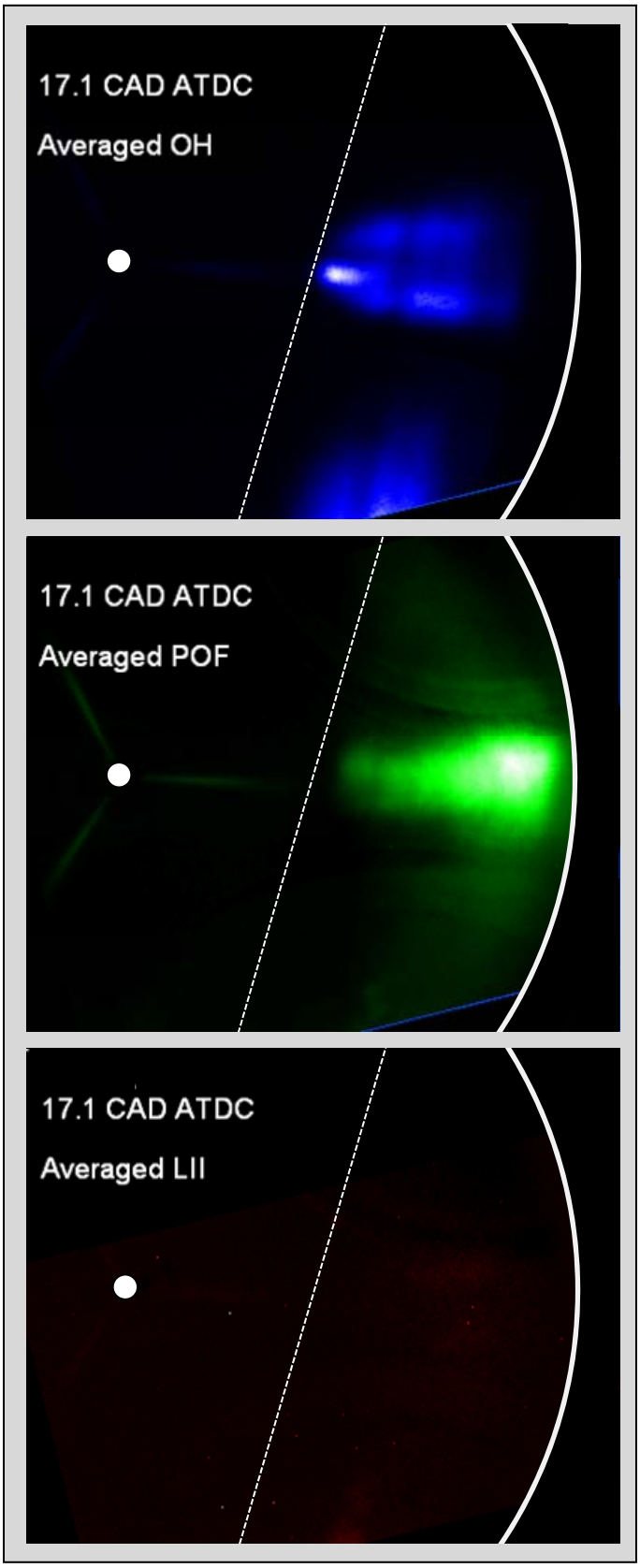

Figure 12 Averaged signal over 100 cycles for each laser-based technique. Top: OH-LIF. Middle: POF-LIF. Bottom: LII. The dashed line represents the upstream border of the laser sheet

Finally, the bottom picture shows the averaged LII signal. No signal was recorded over a hundred cycles. It is obvious that no soot is formed in the observed section of the jet and it rejects the possibility that the observation is due to cycle-to-cycle variations in soot production.

ANALYSIS

A major difference between the current results and the conceptual model is the total absence of soot in the laser-illuminated section of the jet. Dec's LII measurements showed soot formation beginning a few millimeters downstream of the liquid part of the spray. In the current investigation no LII signal was detected, indicating that soot formation does not occur in this region of the jet during the major part of combustion. The natural luminescence images, however, show significant signal close to the perimeter of the bowl. This signal is mainly due to soot luminosity. Therefore, soot must be formed in some region outside the laser sheet in the jet. Most likely this region is located close to the piston glass under the spray centerline as illustrated in Figure 13.

Soot formation depends strongly on the local equivalence ratio, Φ, and the temperatures in the interior of the jet [15]. The absence of soot in the jet can therefore be understood by analyzing factors affecting the air entrainment into the spray. Up to the lift-off length the air entrainment can be described as an adiabatic mixing process. The evaporated fuel is mixed with and heated by hot ambient air. Downstream the lift-off position the air entrainment is impeded by the diffusion flame. It is therefore reasonable to assume that the air entrainment before lift-off is limiting for Φ after the lift-off position.

POF signal appears downstream of the lift-off length. If low temperature or high temperature reactions had occurred in the jet interior at this position a POF signal would have been produced. This indicates that the amount of entrained air was insufficient to reach the low temperature reaction limit (i.e. about 800 K) at the lift-off position. Between the lift-off position and the point where fuel starts to react inside the jet, however, the high temperature reaction zone will mix hot burnt gases into the jet. Over this distance Φ essentially remains constant while the flame zone adds the heat needed to start chemical reactions inside the jet. This idea is schematically described in Figure 14.

As previously mentioned it is not possible to discern between different species contributing to the POF signal with the setup used, neither can low temperature reactions be discerned from high-temperature reactions. It can be noted that the POF LIF images were acquired using a high detector gain setting and a 30 ns gate. Still, a background from natural luminescence is present in the images. This indicates that the POF signal is weak. Since PAH fluorescence typically is strong, the POF-

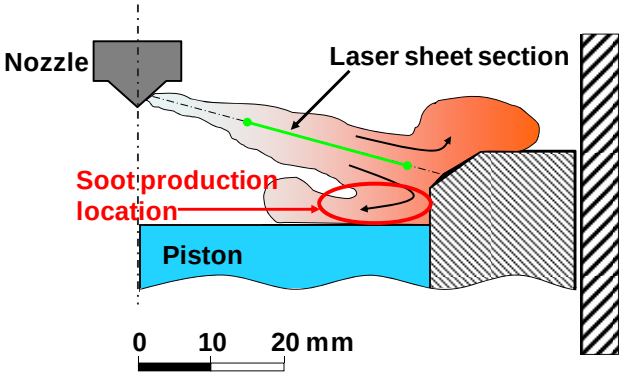

Figure 13 Schematic of the jet representing the soot formation location.

signal is not likely to be dominated by PAH. Also, PAH in the flame would be accompanied by soot, as they are known to be soot precursors. In summary, the observations seem to indicate that the POF signal is dominated by other species than PAH.

Incidentally, when comparing Figure 1 with Figure 14, it is noted that fuel on the jet centerline starts to react downstream the lift-off position in Dec's model as well. The premixed reaction zone located just upstream of the soot formation region in the conceptual model was not based on direct measurements, however, but was only assumed to be there.

To obtain a more quantitative estimate of the effect on air entrainment the spray model by Naber and Siebers can be used [16]. It describes the mean cross-sectional equivalence ratio in an idealized model-jet. As function of distance, x, from the nozzle it varies as

$$\overline{\Phi} = \frac{2\left(A/F\right)_s}{\sqrt{1+16\left(\frac{x}{x^+}\right)^2}-1}, \qquad (1)$$

where the nominator contains the stoichiometric air-fuel ratio and the denominator contains the characteristic length, x^+.

$$x^+ = \sqrt{\frac{\rho_f}{\rho_a}}\frac{\sqrt{C_a}d}{\tan\left(\alpha/2\right)}, \qquad (2)$$

where ρ_f and ρ_a are the fuel and ambient densities, respectively. C_a is the area contraction coefficient of the nozzle, d is the nozzle hole diameter, and α is the jet spreading angle. The spreading angle is given by

$$\tan\left(\alpha/2\right) = a\,c_1\left(\left(\frac{\rho_a}{\rho_f}\right)^{0.19} - c_2\sqrt{\frac{\rho_f}{\rho_a}}\right), \qquad (3)$$

Where a is a constant with a recommended value of 0.75, c_1 is an orifice dependent constant in the range of 0.26-0.40, and c_2 is 0.0043 for a vaporizing jet.

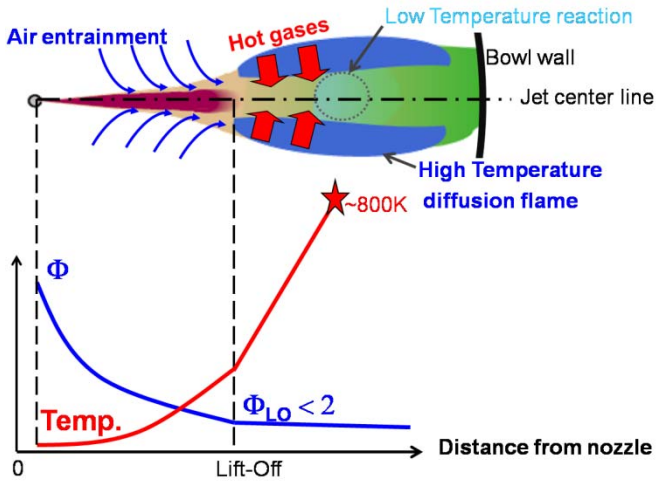

Figure 14 Schematic of smokeless combustion for the present case with Φ-T evolution along the centerline of the jet.

The calculated mean Φ values from the current investigation and Dec's study are given in Figure 15 for the region around the lift-off length. The 0-value on the abscissa represents the measured lift-off lengths in the respective studies. The present study has a mean Φ value that is only 32% that of Dec's value at lift-off. This is due to the combination of smaller nozzle orifices and higher ambient density, but the density effect is estimated to be an order of magnitude smaller than the orifice effect.

Jet spacing has an effect on the lift-off length [8]. This is probably due to the hot products between the jets resulting in higher temperatures of the gas entrained close to the nozzle. For a three-hole nozzle, with large jet-jet spacing, a longer lift-off length is therefore expected. The case presented here shows a lift-off length with variations between 16 and 17 mm obtained from the line of sight OH-chemiluminescence images. This length is similar to the one presented by Dec although he used an 8-hole nozzle in his study. Reduced hole diameter and higher ambient density seems to have counterbalanced the effect of jet-jet spacing.

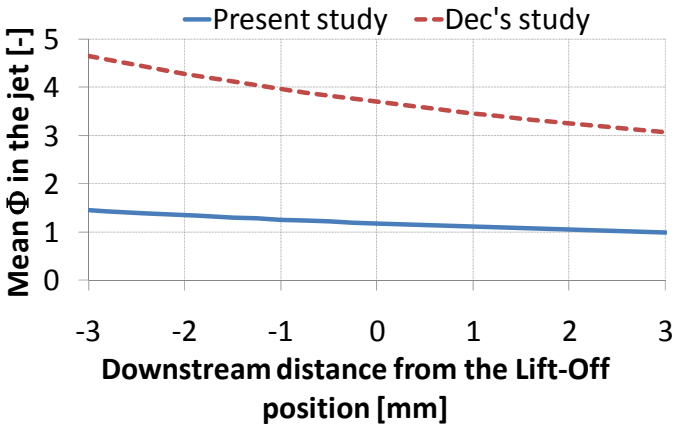

Figure 15 Calculated mean Φ over the jet cross section as function of the axial distance from the lift-off length for the two studies.

Pickett and Siebers showed that when the equivalence ratio at lift-off decreases the soot signal is displaced downstream. When Φ is lower than approximately 2, no soot is formed at all [17]. This is most probably due to oxidation of soot precursors at an early stage in the jet, before soot is even formed [3]. The same trend is obviously observed here. This is further supported by the OH signal extending relatively far into the jet, indicating a low equivalence ratio [3].

The low Φ value at the lift-off location causes the soot formation process to take place far downstream in the jet. Natural luminosity from soot is only observed at the bowl perimeter, presumably close to the bowl floor. This could indicate that the oxidation of soot precursors is impeded in this region. As the jet is in contact with the bowl wall and floor, air entrainment is locally blocked in this region. The soot formed here can then be oxidized in the recirculation zone where oxygen is available again. As no smoke is detected in the exhaust gases, the oxidation is obviously complete.

Apart from the local Φ, also injection pressure has a major impact on the soot formation process. When following the path of a fuel element in the Φ-T space, the time spent at a given location determines the amount of soot formed. It has been shown that increasing the injection pressure results in a decrease in residence time, due to higher jet velocities. Thus, an increased injection pressure will result in less soot formation [17].

SUMMARY AND CONCLUSIONS

A study of direct-injected heavy duty diesel combustion was performed using multiple simultaneous laser diagnostic techniques and high speed video. The case studied was close to a typical low load modern diesel operating point without EGR. Parallels were drawn to the conceptual model by Dec and results from high-pressure combustion vessels. The conclusions can be summarized as follows:

1. The case studied produced no engine-out smoke. No soot was detected in the laser-illuminated section of the jet. Soot was, however, observed in the recirculation zones close to the bowl perimeter. This indicated very slow soot formation.

2. The absence of soot in the jet is explained by a significantly higher air entrainment rate than in Dec's study. This is confirmed by calculations using the air entrainment model by Naber and Siebers. The lower Φ in the jet produces a different Φ-T-history, explaining the soot results.

3. The increased air entrainment rate is mainly due to smaller nozzle holes and increased TDC density. Furthermore, the increased injection pressure is believed to reduce the residence time in the jet, thus reducing the soot formation.

4. OH was detected at the periphery of the jet, upstream of the location where fuel starts to react on the jet centerline. The OH region extends relatively far into the jet, further supporting the conclusion of a less fuel-rich jet in the current case.

5. Partially oxidized fuel (POF) was found at the center of the jet, downstream of the lift-off position. This indicates that the temperature needed to start chemical reactions inside the jet had not been obtained at the lift-off position. The high-temperature reaction zone at the periphery thus adds heat over a distance before POF is observed on the centerline.

ACKNOWLEDGEMENTS

The authors gratefully acknowledge the Swedish Energy Agency for their support and express their gratitude to John Dec, Lyle Pickett, and Mark Musculus for fruitful discussions on the preliminary results.

REFERENCES

1. Musculus, M.P.B, "Multiple Simultaneous Optical Diagnostic Imaging of Early Injection Low Temperature Combustion in a Heavy Duty Diesel Engine", SAE paper 2006-01-0079, 2006.

2. Dec, J.E., "A Conceptual Model of DI Diesel Combustion Based on Laser-Sheet Imaging", SAE paper 970873, 1997.

3. Pickett, L.M. and Siebers, D.L., "Soot Formation in Diesel Fuel Jets Near the Lift Off Length", Proceedings of IMechE IJER03505 vol 7: pp103-130.

4. Siebers, D.L. and Higgins,B., "Flame Lift-Off on Direct-Injection Diesel Sprays Under Quiescent Conditions", SAE paper 2001-01-0530, 2001.

5. Higgins, B. and Siebers, D.L., "Measurement of the Flame Lift-Off Location on DI Diesel Sprays Using OH Chemiluminescence", SAE paper 2001-01-0918, 2001.

6. Pickett, L.M., Siebers, D.L., and Idicheria,C.A., "Relationship Between Ignition Process and the Lift-Off Length of Diesel Fuel Jets," SAE paper 2005-01-3843, 2005.

7. Idicheria, C.A. and Pickett, L.M, "Formaldehyde Visualization Near Lift-Off Location in a Diesel Jet", SAE paper 2006-01-3434, 2006.

8. Musculus, M.P.B, "Effects of the In-Cylinder Environment on Diffusion Flame Lift-Off in a DI Diesel Engine," SAE paper 2003-01-0074, 2003.

9. Pickett, L.M. and Siebers,D.L., “Non Sooting, Low Flame Temperature Mixing-Controlled DI Diesel Combustion”, SAE paper 2004-01-1399, 2004.

10. Kohse-Höinghaus, K., “Laser Techniques for the Quantitative Detection of Reactive Intermediates in Combustion Systems”, Progress in Energy and Combustion Science, 20, 203-279, 1994.

11. Collin R., Nygren J., Richter M., Aldén M., Hildingsson L., and Johansson B., “Studies of the Combustion Process with Simultaneous OH- and Formaldehyde-PLIF in a Direct-Injected HCCI engine”, Proceedings of the Sixth International Symposium on Combustion Diagnostics and Modeling of Combustion in Internal Combustion Engines (COMODIA), August 2-5, Yokohama, Japan, 311-317, 2004.

12. Hofmann M., Bessler W.G., Schulz C., and Jander H., “Laser-Induced Incandescence for Soot Diagnostics at High Pressures”, Appl. Optics Vol. 42, No. 12, 2052-2062, 2003.

13. Axelsson B., Collin R., and Bengtsson P. -E. “Laser-Induced Incandescence for Soot Particle Size Measurements in Premixed Flat Flames”, Appl. Optics 39:3683-3690, 2000.

14. Aronsson, U., Chartier, C., Andersson, Ö., Egnell, R., Sjöholm, J., Richter, M., and Aldén, M., “Analysis of the Correlations Between Engine Out Particulates and Local Φ in the Lift-Off Region of a Heavy Duty Diesel Engine Using Raman Spectroscopy”, SAE paper to be presented at SAE World Congress 2009.

15. Akihama, K., Takatori, Y., Inagaki, K., Sasaki, S., and Dean, A.M., “Mechanism of the Smokeless Rich Diesel Combustion by Reducing Temperature”, SAE paper 2001-01-0655, 2001.

16. Naber, J.D. and Siebers, D.L., “Effect of Gas Density and Vaporization on Penetration and Dispersion of Diesel Sprays”, SAE paper 960034, 1996.

17. Pickett, L.M., Caton, J.A., Musculus, M.P.B., and Lutz, A.E., “Evaluation of the Equivalence Ratio-Temperature Region of Diesel Soot Precursor Formation Using a Two-Stage Lagrangian Model”, Proceedings of IMechE IJER00606 vol 7: pp349-370, 2006.

CONTACT

Clément Chartier
Department of Energy Sciences
Lund University
Box 118, S221 00 Lund, Sweden
clement.chartier@energy.lth.se

Paper II

2009-24-0045

Effect of Injection Strategy on Cold Start Performance in an Optical Light-Duty DI Diesel Engine

Clément Chartier, Ulf Aronsson, Öivind Andersson, Rolf Egnell
Division of Combustion Engines, Lund University

ABSTRACT

The present study investigates cold start at very low temperatures, down to -29 deg C. The experiments were conducted in an optical light duty diesel engine using a Swedish class 1 environmental diesel fuel. In-cylinder imaging of the natural luminescence using a high speed video camera was performed to get a better understanding of the combustion at very low temperature conditions. Combustion in cold starting conditions was found to be asymmetrically distributed in the combustion chamber. Combustion was initiated close to the glow plug first and then transported in the swirl direction to the adjacent jets. A full factorial study was performed on low temperature sensitivity for cold start. The effects of cooling down the engine by parts on stability and noise were studied. Furthermore, different injection strategies were investigated in order to overcome the limited fuel evaporation process at very low temperatures. A strategy with 3 pilot injections and increasing fuel quantity for each injection gave a more homogeneous combustion. The natural luminescence was symmetrically distributed in the piston bowl and all the jets contributed to the combustion. Significant improvements in combustion stability, load level and potential for load increase were observed as well.

INTRODUCTION

Cold start at very low ambient temperatures is an important aspect of diesel engine development. At ambient temperatures down to -25 °C it is difficult to auto-ignite the charge, and even more so to ignite it in every cycle. The latter problem is referred to as intermittent combustion [1]. Cold starting represents only a minor part of the engine utilization. Demands on cold starting performance may still compromise the development of other aspects of the engine.

There is a general trend towards lower compression ratios. This is due to ever higher specific powers [2] and more stringent emission legislations, especially for NO_x. This poses even greater challenges for cold start performance.

Lower compression ratios mean lower pressure and temperature levels in the cylinder at start of injection (SOI). This leads to fuel evaporation issues. It has been demonstrated that as much as 80% of the injected fuel mass does not burn during a cycle [3]. Most of it adheres to the cold surfaces and is difficult to vaporize.

A typical cold start for diesel engines is presented in Figure 1 and can be divided into five phases. First, the glowplug is glowing during a given period, here 10 seconds. After this, the starter motor is activated and the engine is cranked up to 200 rpm until the combustion takes over. Cranking time is longer at lower temperatures. At engine start an engine speed overshoot is typically observed. It is due to a steep load increase during the first combustion cycles. Load can be in the range of 8-11 bar IMEP in this third phase.

Friction losses are very high due to the low temperature of the lubricant in the engine and gearbox. The engine speed is then unstable for a limited period of time where load and combustion phasing variations are large. During this after-start phase loads typically average 4-5 bar IMEP. It is this specific phase that is investigated in the present study. The last phase commences when engine speed stabilizes at the nominal idle speed.

The glowplug plays a central role in cold starting. It locally heats up the air which speeds up the fuel evaporation and starts the fuel oxidation process. Today, ceramic glowplugs are becoming increasingly common. They provide higher temperatures (>1200°C) than metal glowplugs (~950°C). Built-in controllers make them reach a stable working temperature [4].

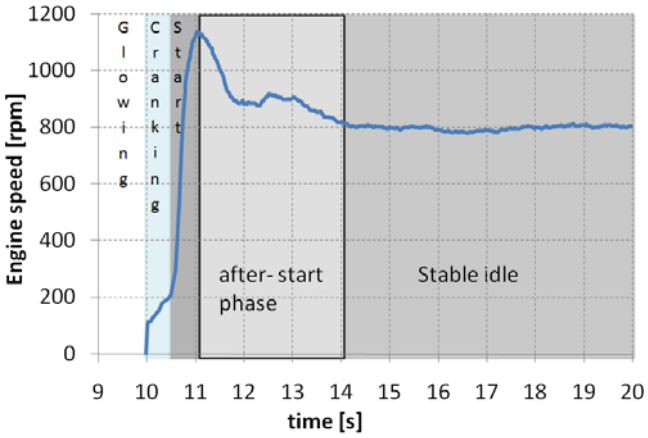

Figure 1 A typical cold start sequence.

Most Diesel engines are equipped with sophisticated injection systems. Especially common rail systems provide a large flexibility in the choice of injection strategy for a wide variety of conditions. All phenomena caused by advanced injection strategies are not fully understood. A number of investigations have demonstrated that adjusting the injection strategy can compensate for lower compression ratios during cold start [3,5,6]. Split-main injection strategies may improve startability (i.e. reduce cranking time) and at the same time reduce the injected fuel mass and unburned hydrocarbon emissions by almost 50% [7]. Although cold startability is improved, poor after start stability may still be a problem [6].

A certain fuel mass is required to start the engine. However, increasing the injected fuel mass above a certain level may deteriorate the starting performance. Contrary to intuition, more fuel mass may lead to lower loads and unstable combustion [8]. This problem is due to fuel evaporation issues and must be solved in order to quickly reach idle speed.

Overfuelling leads to a successively increasing effective compression ratio, since some fuel is left in the piston bowl from cycle to cycle. Eventually, the highly fuel rich mixture ignites and consumes most of the fuel leading to violent intermittent combustion [9]. The following cycle again has too low compression ratio leading to misfire or low load during a few cycles.

No study dedicated to combustion behavior and stability after start has been found in the literature. Apart from reduced cranking time, the stability of the engine speed after start and the potential load increase are important aspects of a successful cold start. This study consists of three parts:

- The first part investigates the differences between starts at normal and low temperature conditions for a baseline case. This is done to extract the main characteristics and patterns from each case.
- In the second part a designed experiment is used to separate the effects of three factors on after start stability. The factors are the engine block temperature, the fuel temperature, and the inlet air temperature.
- In the third part the effects of the injection strategy on after-start stability is investigated. Six different strategies are investigated and a best case is proposed based on a thermodynamic analysis.

EXPERIMENTAL SETUP

OPTICAL ENGINE SETUP - The study was conducted in a on optical HSDI diesel engine based on the Volvo D5. It featured a Fused Silica piston with realistic bowl geometry as seen in Figure 2. The piston rings are made of Fluorflon 412 for dry lubrication usage. The engine was equipped with a piezo-electric common rail injection system from Bosch. The rail pressure was kept constant at 460 bar for all cases studied. This pressure level is typical for start conditions. Engine operating conditions are presented in Table 1. The glowplug used in this study was a ceramic, 7V type from Bosch. Swedish environmental Class 1 Diesel fuel, MK1, was used. The distillation curve is presented in Figure 3.

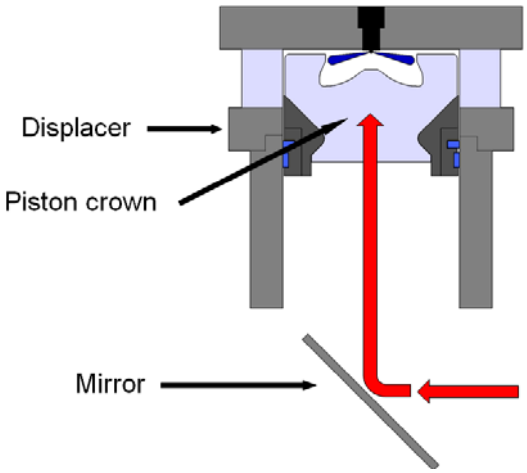

Figure 2 Schematic of the optical access on the D5.

Images of natural luminescence were recorded using a high speed video Phantom V7.1. The natural luminescence mainly originates from soot radiation. The camera was equipped with a UV-Nikkor lens of focal length 105mm and f/2.5. The frame rate was 7200 frames per second, equivalent to one image per crank angle degree (CAD) at 1200 rpm. The camera resolution was 512x512 pixels and an 80µs exposure time was used. This exposure time made it possible to detect the first combustion luminosity. Furthermore, with appropriate lightning, the liquid sprays could be observed as well.

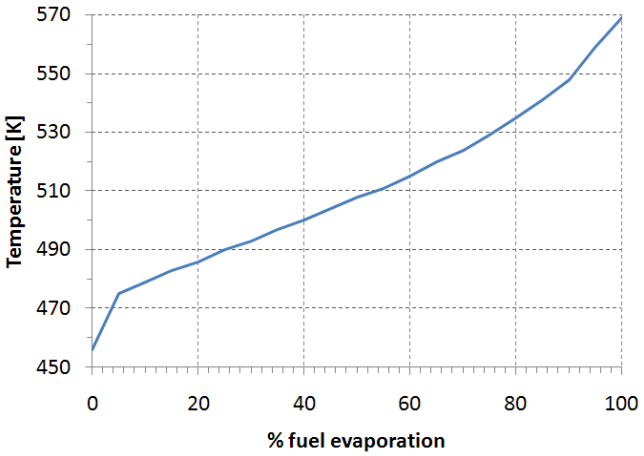

Figure 3 Distillation curve for MK1 fuel.

Figure 4 shows the positions of the glowplug and pressure transducer between the inlet valves. In this engine, the pressure transducer is normally placed in the glowplug hole. The new location of the pressure transducer is not expected to have an impact on the pressure measurement.

Table 1 Engine and fuel injection system specifications.

Engine Specifications	
Number of cylinders	1
Number of intake valves	2
Number of exhaust valves	2
Displacement vol. [l]	0.48
Bore [mm]	81
Stroke [mm]	93.2
Connecting rod [mm]	147
Effective Compression ratio	16.8
Swirl ratio	2.0
Fuel injection system	
Type	Common-rail
Injector type	Piezoelectric
Number of holes	7
Included angle [°]	150
Orifice diameter [mm]	0.140
Rail pressure [bar]	460

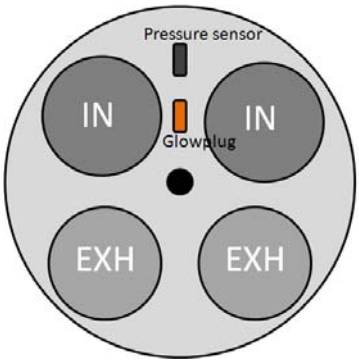

Figure 4 Schematic of the cylinder head with glowplug and pressure transducer positions.

COOLING CIRCUIT - To perform investigations at low temperatures, the engine cooling circuit was modified. A domestic freezer was filled with 160 liters of coolant liquid, consisting of 50% glycol and 50% water. This setup could provide a coolant temperature of -28°C.

To provide a fully flexible system, the cooling circuit was divided into three independent paths:

- The cylinder head and liner
- The fuel
- The intake air

To reproduce cold ambient conditions, the coolant was circulated in the cylinder head and liner by means of a pump submerged in the freezer. The fuel was cooled down between the fuel tank and the high pressure pump using a copper coil submerged in the coolant bath. The low pressure fuel pump assured constant flow through the cooling device. Finally, the intake air was taken from the lab's supply of dehumidified shop air. Dehumidified air prevents ice clogs from forming in the hoses or heat exchangers. The air was cooled using two EGR-coolers mounted in series, submerged in the coolant bath. Coolant was circulating through the EGR-coolers by means of the submerged pump.

The fuel, inlet air or engine coolant flows could independently be set to bypass the cooling device at any time to run at normal conditions. All hoses going to or from the freezer were isolated using a thick rubber insulation hose. This increased the cooling capacity of the system and extended the time of use at optimal conditions.

To prevent frost from forming on the mirror surface and optical piston bottom (see Figure 2) dehumidified shop air was constantly blown towards the mirror.

TEST PROCEDURE – The investigated phase of cold start is after-start stability. Therefore, the engine was not cranked as shown in Figure 1, but motored at 1200 rpm prior to first injection. To obtain a stable rail pressure at first injection, the engine was run for a short period before cooling down the system. During this time the rail pressure was adjusted to 460 bar, and it remained at this level during cool-down.

Figure 5 shows the temperature history during the cooling down period. The optimal cooling down duration turned out to be 25 minutes. After this the temperature of the displacer started to increase due to the engine working as a heat sink for the laboratory air.

Shop air was blown through the cooling system and escaped by a valve just before entering the inlet manifold. By doing so, the hoses were cooled down and low temperatures could be obtained from the start. After 20 minutes of cooling down, the mirror and piston elongation were cleaned from ice.

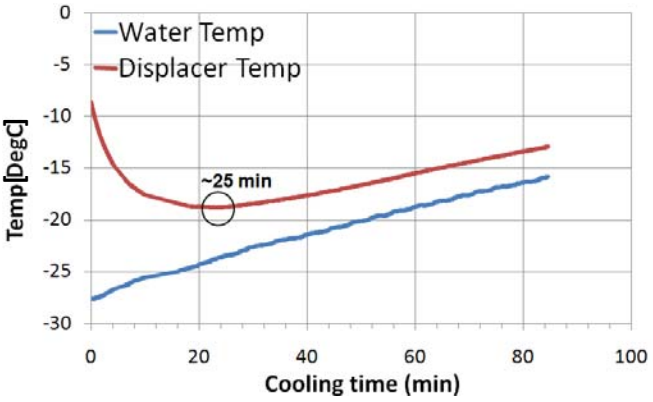

Figure 5 Temperature of the coolant and of the displacer during the cooling down process.

START PROCEDURE – After the cooling down procedure described above, the engine was motored for approximately 45 seconds in order to adjust the common rail pressure to the desired level. Then, fuel injection was switched on and pressure traces were acquired. No skip fire strategy was employed, i.e. every cycle was fired. The first ten fired cycles are presented here in the results. The coefficient of variation for the indicated mean effective pressure is calculated from these ten cycles.

RESULTS AND DISCUSSION

NORMAL VS. LOW TEMPERATURE START – Figure 8 shows images extracted from a high speed video movie of an engine start at 20°C. The case presented is a baseline with two pilot injections and a main injection. The total injected fuel mass of 12mg is divided between the injections as follows: 30% in pilot 1, 30% in pilot 2, and 40% in the main injection. The injection timing corresponds to the fourth from the top in Figure 17. One of the sprays was aimed directly in the direction of the glowplug during this comparison. The number indicated in the upper left corner of each frame is the crank angle position at which the image was acquired. The glowplug position is indicated in the first frame. The glowplug seems to have little influence on the onset of combustion. At -2 CAD, multiple ignition kernels can be seen throughout the combustion chamber. The seven burning jets are then developing equally fast.

Figure 9 shows an engine start with the same injection strategy as in Figure 8, but at -20°C. There are large differences between the two cases. Visible reactions occur 2 CAD later in the cold case at a position next to the glowplug, downstream in the swirl direction. They remain close to the glowplug and later spread in the swirl direction. The combustion does not spread to other jets and involves only a small portion of the piston bowl. Six jets are not involved in the combustion process, probably due to poor evaporation in these regions.

Swirl seems to be a factor of interest when looking at the transport of the reacting area and mixture passing the glowplug during the combustion. To investigate the effect of swirl, the swirl ratio was switched between 2.0 and 2.6 by means of a control valve in one of the inlet ports.

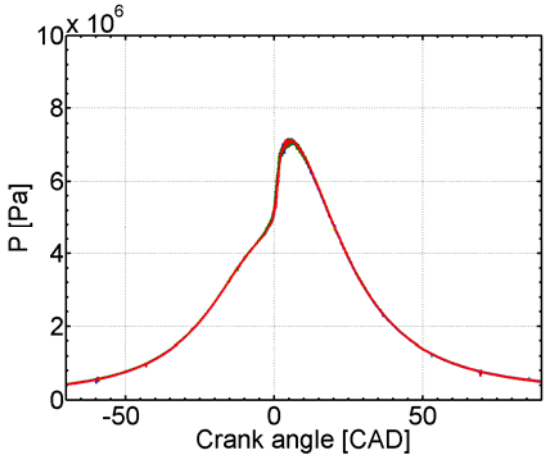

Figure 6 Pressure trace at normal temperature for the baseline case.

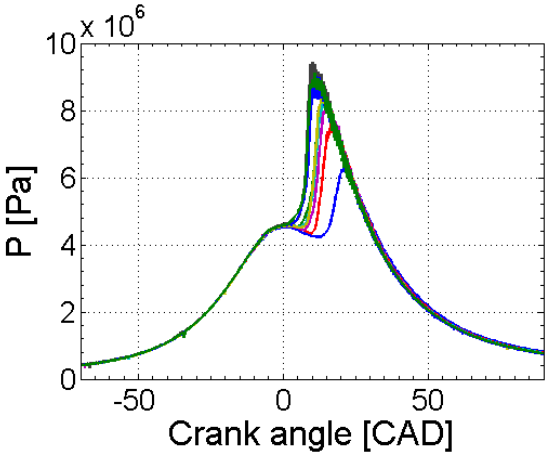

Figure 7 Pressure trace at low temperature for the baseline case.

The sequence presented in Figure 10 represents the same case as in Figure 9 but at the higher swirl ratio. It shows no major difference to the prior sequence. Aiming one spray directly towards the glowplug is, however, not typical of a production engine. A slight rotation of the injector against the swirl direction might have produced different results.

Figure 6 shows pressure traces for 10 cycles acquired at the same conditions as in Figure 8. Apparently, the combustion is very stable from cycle to cycle. Figure 7 shows on the other hand pressure traces for the low temperature case. Cold conditions lead to a longer ignition delay and more late-cycle combustion compared to ambient temperature. The peak pressure is higher for cold conditions as a result of the longer ignition delay.

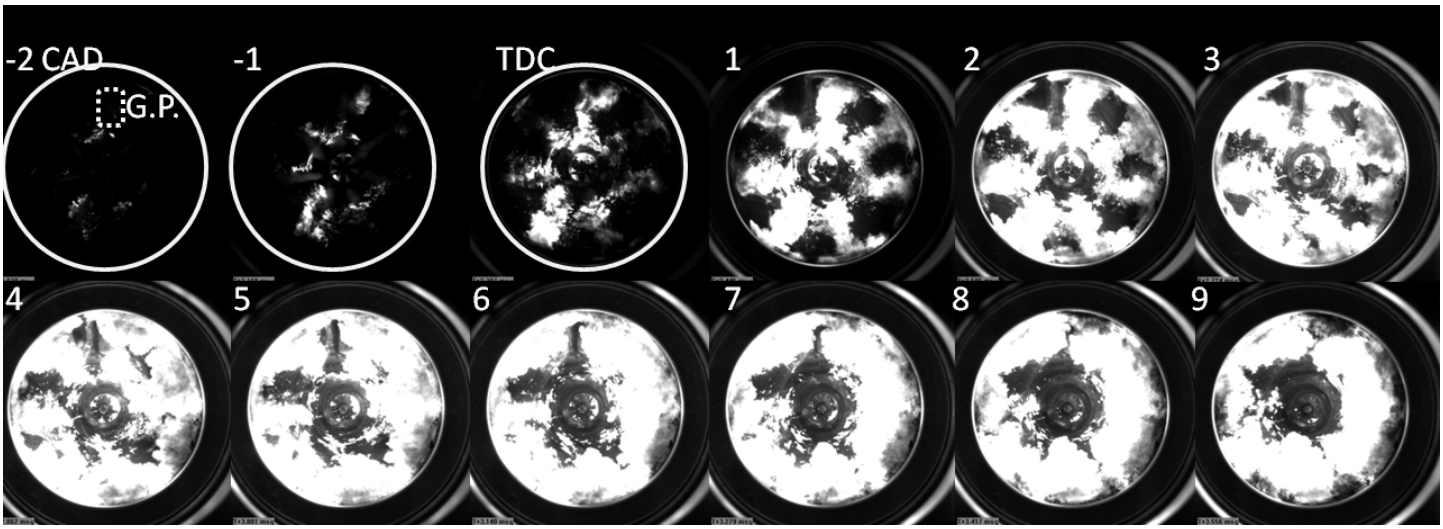

Figure 8 Start at normal temperature (+20°C).

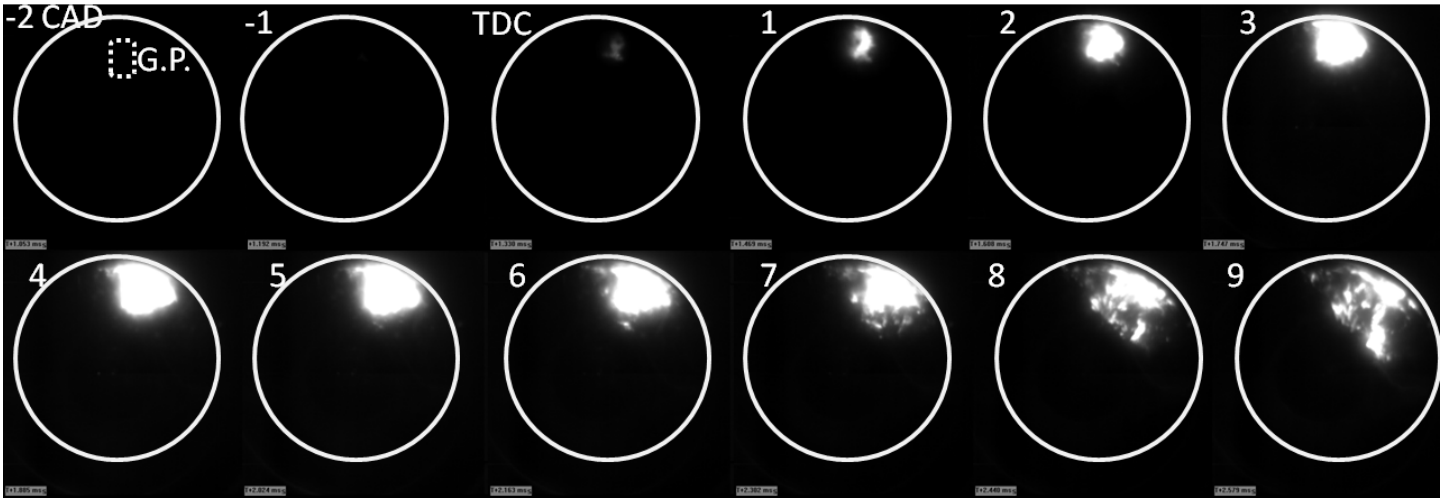

Figure 9 Start at low temperature (-20°C) with swirl ratio 2.0.

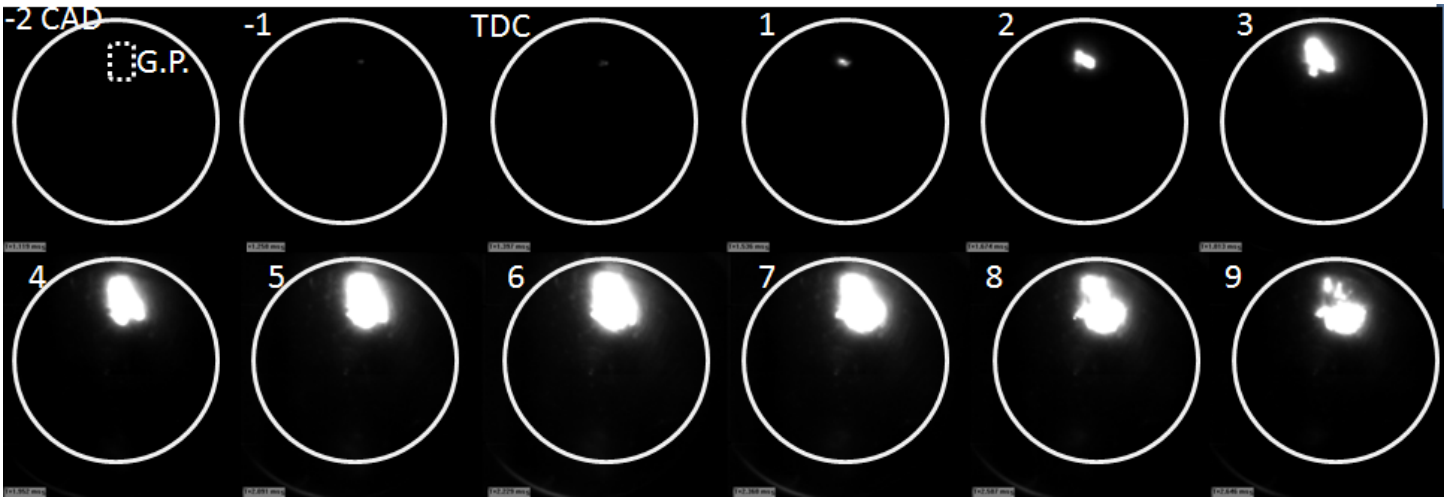

Figure 10 Start at low temperature (-20°C) with swirl ratio 2.6.

FACTORIAL EXPERIMENT – A full factorial experiment was designed to separate the effect of temperatures in the three circuits of the cooling system. The flexibility of the setup allows independent cooling down of the cylinder head and liner, the inlet air, and the fuel. The design is a two-level full factorial experiment with three factors. Testing all combinations results in eight experimental runs.

Table 2 gives the factor levels in coded form. Snowflakes indicate that cooling is switched on in the circuit, a plus sign that cooling is switched off. The coded values represent the following values (low/high) in physical units:

- Engine: -20 and +40°C
- Fuel: -10 and +23°C
- Inlet air: -15 and +25°C

The measured responses were:

- Indicated Mean Effective Pressure (IMEP)
- Coefficient of Variance (CoV) of IMEP
- 50% burn angle (CA50)
- Standard deviation for CA50
- Maximum pressure derivative dp/dCAD

In traditional experiments only one factor is varied at a time. As a result they do not provide information on factor interactions. This means that they assume that the effect of one factor is independent of the settings of other factors. Interactions are likely to be observed in many complex systems. Apart from testing all combinations of factors, factorial experiments detect such factor interactions. All experiments were replicated three times for evaluating the experimental error.

Figure 11 shows an interaction plot for IMEP vs. inlet temperature at two levels of engine temperature. At high engine temperature, the effect of inlet temperature is limited. However, at low engine temperature the steep slope indicates a strong effect of inlet temperature. There is a strong interaction effect between the two factors since the curves are far from parallel. The effect is explained by the inlet air being heated by the cylinder head while entering the engine. When the cylinder head is cooled, this effect is less apparent.

Table 2 Test matrix for the factorial experiment.

	Engine	Fuel	Inlet air
1	+	+	+
2	❄	+	+
3	+	❄	+
4	❄	❄	+
5	+	+	❄
6	❄	+	❄
7	+	❄	❄
8	❄	❄	❄

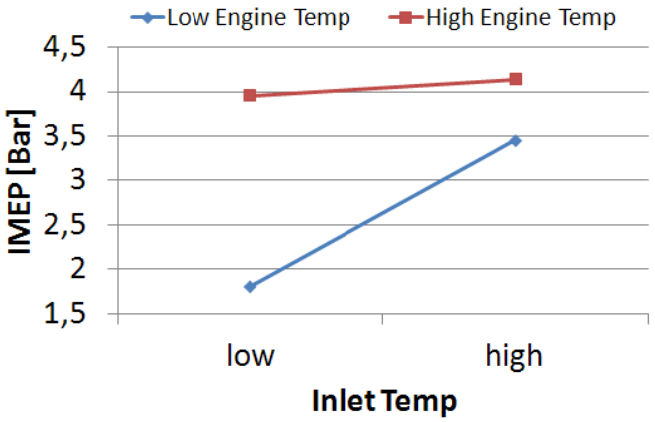

Figure 11 Interaction plot for IMEP.

Figure 12 shows an interaction plot for CoV of IMEP vs. the same factors as previously. CoV of IMEP reflects load variations between cycles and therefore indicates engine speed variations at idle in a vehicle. It was calculated over the first ten fired cycles. Also here, there is a strong interaction effect. The plot shows that inlet temperature has no or limited effect on load stability when the engine block is at normal temperature (20°C). On the other hand, the pronounced slope of the other curve indicates that inlet temperature becomes very important if the engine block is cold (-20°C). In fact, it has been suggested to use an inlet air heater to improve after-start stability [10], a technique that is supported by these results. However, the temperature levels for inlet air and engine block are different. Therefore, the temperature gradient for heat transfer between hot engine and cold inlet air is not the same as for cold engine and ambient inlet air. These differences in temperature gradients are visible in the interaction plots.

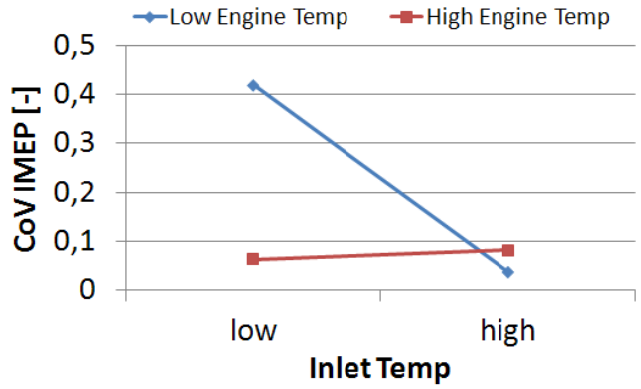

Figure 12 Interaction plot for CoV IMEP.

When analyzing the factorial experiment the effects of the factors are represented by coefficients in a polynomial. The greater the value of the coefficient, the greater the effect of the factor. Figure 13 shows the three coefficients for the response IMEP that are significant.

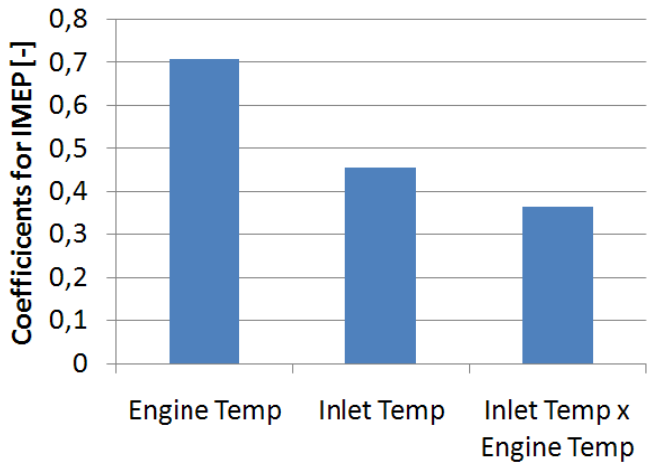

Figure 13 Coefficients for the significant terms for IMEP.

Figure 13 shows the factorial fit coefficients for the response IMEP. The trends in IMEP for engine block temperature and inlet temperature observed previously can be considered as reliable since the coefficients are higher than for other factors. An interaction effect appears as the third most influential cause for IMEP variations. It is an interaction between inlet temperature and engine temperature. However the factorial fit coefficient is much lower than for engine block temperature. As mentioned in the test matrix, fuel temperature was a parameter of the investigation. However, the model regression gave a too low factorial fit coefficient to consider it as significant. Therefore this parameter is no further discussed in this section. A possible explanation of this non-significance of the fuel temperature is that the actual temperature of the fuel at injection is strongly different than when the fuel is fed to the engine.

Figure 14 shows factorial fit coefficient for the response combustion phasing or CA50. Single factor effects are the only significant effects. All factors are significant. Engine block temperature is also the dominant factor for the phasing of the combustion. Lower temperatures cause the combustion to take place later in the cycle.

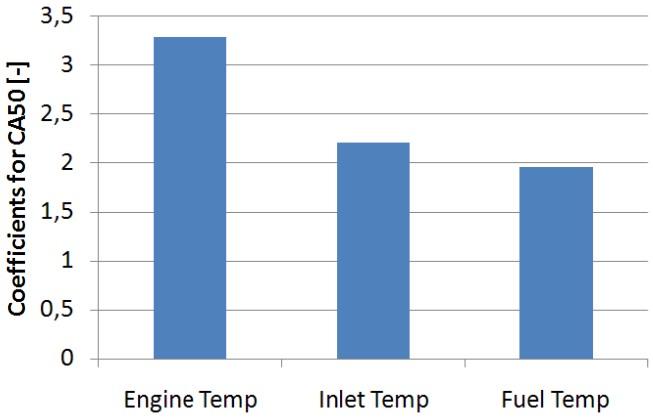

Figure 14 Coefficients for significant terms for CA50.

SPRAY-GLOWPLUG ANGLE - The effect of the position of the spray relative to the glowplug was evaluated using Analysis of Variances (ANOVA). It is a statistical hypothesis test that divides the variation in a data set into a number of components and compares them with the measurement error. Terms that have a significant effect (i.e. are greater than the error) yield a so-called p-value lower than 5%. For clarity, 1-p will be used here, i.e. a higher value is more significant. Two angles between the spray and the glow plug were evaluated; 0° and 15°, as depicted in Figure 15.

Figure 16 shows 1-p values for engine temperature, inlet air temperature and relative angle between spray and glow plug. It can be seen that the angle has a significant effect on all responses except CoV of IMEP. It is the only significant factor affecting the pressure derivative. A likely explanation is that the angle provides more time for the fuel to evaporate and mix with air before reaching the glowplug. It should be noted that the 15° is more typical of production engines than the 0° angle. As has already been noted, inlet air temperature has the greatest effect on engine stability (CoV of IMEP and standard deviation of CA50). Engine temperature is important only for IMEP and CA50.

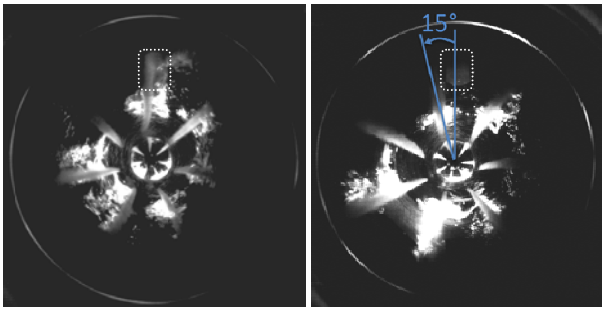

Figure 15 Visualization of the relative spray/glowplug angle.

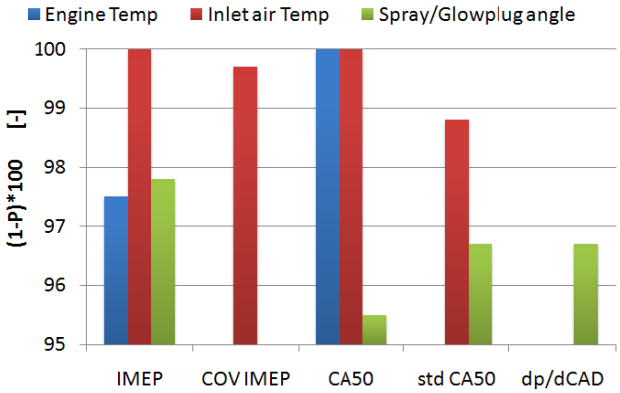

Figure 16 1-p values for all responses.

INJECTION STRATEGY - Different injection strategies were investigated for their stability properties. Also their potential for load increase by increasing the fuelling rate was investigated. Heat release analysis was made for all cases to study the effect on global temperatures within

the cylinder. The total injected fuel mass was kept constant at 12 mg for all 6 cases unless otherwise stated. The different injection strategies are as follows, see Figure 17 for details:

- Only main injection
- Split main injection (Fuel mass: 50%-50%)
- 1 pilot + main (30%-70%)
- 2 pilots + main (30%-30%-40%)
- 4 split main (25%-25%-25%-25%)
- 3 progressive pilots + main (15%-20%-25%-40%)
- 3 progressive pilots + main, with 20% more injected fuel mass in the main injection (12.5%-16.7%-20.8%-50%)

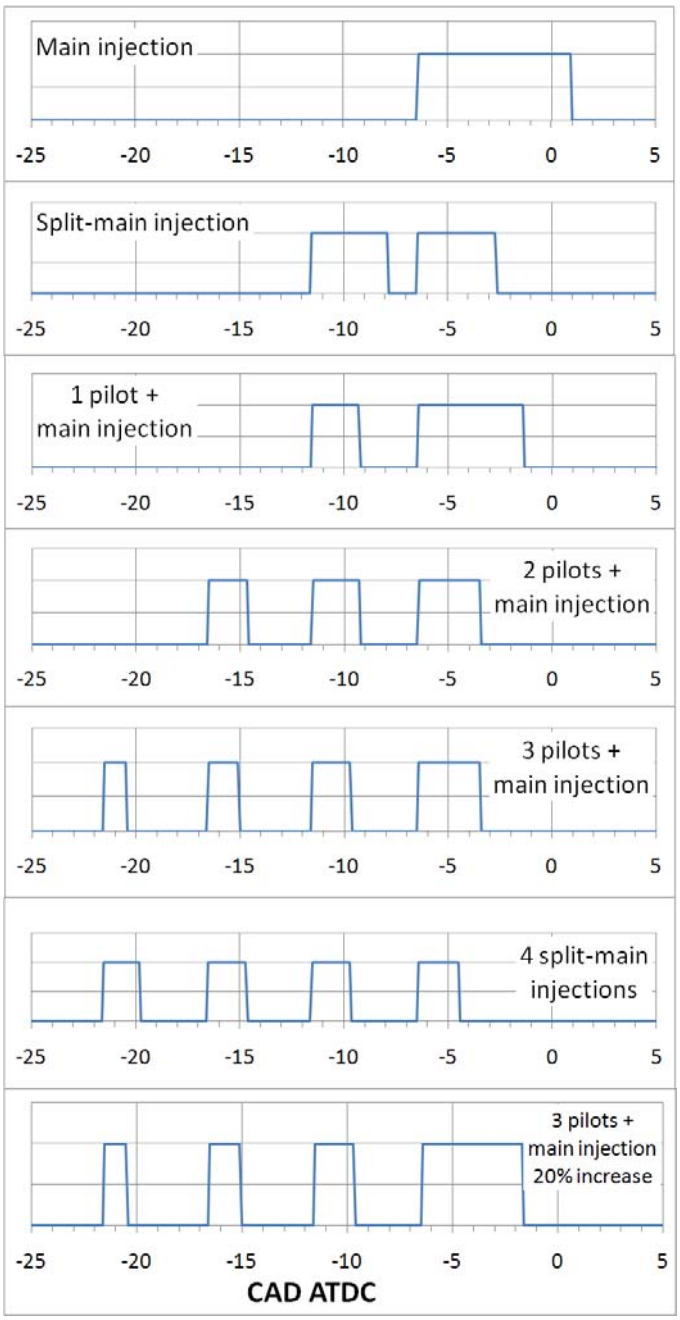

Figure 17 Representation of injector energizing current for all injection strategies.

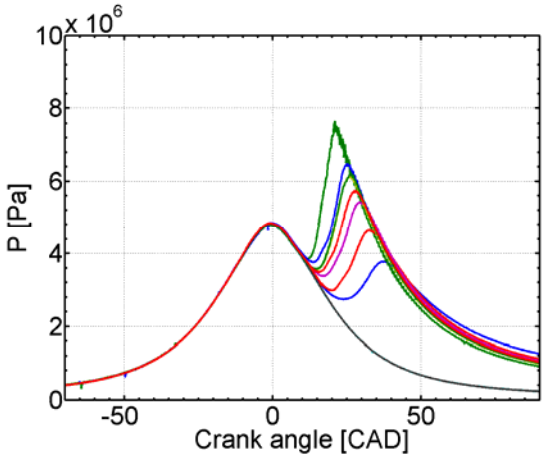

Figure 18 Pressure traces for main injection case.

The first case, a traditional single injection shows large cycle-to-cycle variations in the pressure trace, as seen in Figure 18. The combustion is intermittent and increasing peak pressure and pressure rise rate with time. It is mainly due to a large amount of fuel being injected at once, impeding the evaporation process. Simulations of similar cases have shown that a fuel film is formed on the cold surface of the piston bowl and needs a lot of heat to evaporate [9]. Some of the fuel remains unoxidized by the end of the cycle and remains in the bowl to the next cycle as a fuel film or fuel-rich rest gases trapped during the gas exchange phase. This phenomenon may happen during several cycles until the temperature and equivalence ratio is right for combustion to take place and spread. The fuel mass present in the combustion chamber can be greater than the fuel mass injected in a single cycle due to the transfer between cycles.

An additional effect has been proposed based on the increase in effective compression ratio. This would lead to higher pressure and temperature at SOI and, thus, violent combustion can take place. Once complete high temperature combustion has taken place, most of the fuel is consumed. Rest gases are less loaded with fuel and fuel film negligible. This may lead to misfire for one or several cycles until the phenomenon takes place again, resulting in intermittent combustion [1,9]. However, pressure at TDC in Figure 18 does not show support for this hypothesis in the current data.

The case with one pilot injection (30% fuel mass in the pilot) shows an increase in stability compared to the 'only main' injection strategy, see Figure 19. Combustion phasing is closer to TDC. Some misfire is still observed. Also pressure drops after TDC are observed. These are likely to be caused by competition between combustion (positive heat release) and evaporation (negative heat release).

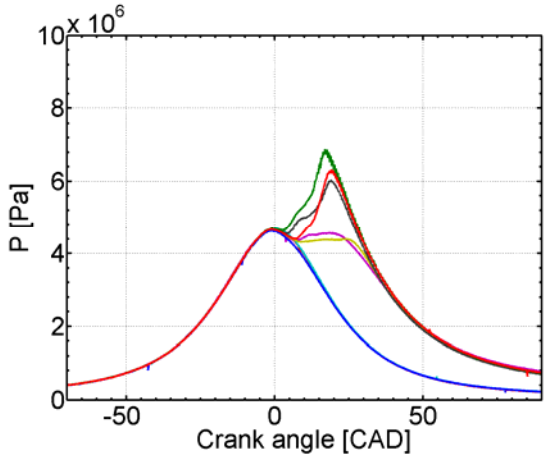

Figure 19 Pressure traces for Pilot + main injection case.

The case with two pilots in Figure 20 is the baseline case, as presented in the first part of this paper. Combustion is phased a bit earlier and the 10 presented cycles are showing less variation. Stability is improved compared with the single pilot case.

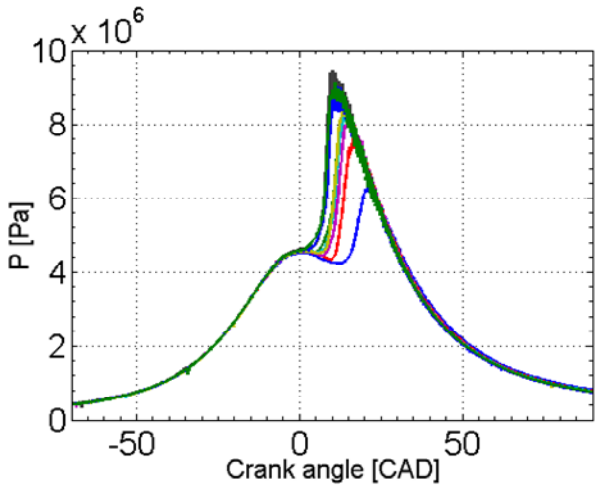

Figure 20 Pressure traces for two pilots + main injection case.

The case with 3 progressively increasing pilot injections (15%-20%-25% and 40% in the main injection) presented in Figure 21 shows improved stability of combustion phasing and peak pressure. The peak pressure is still higher than the reference case at ambient temperature and the late cycle combustion more present but the differences are less visible than the previously tested injection strategies.

Figure 22 shows a case similar to the previous one but the total injected fuel mass is increased by 20%. Higher load is achieved without compromising on the stability. The COV of IMEP for this case is 0.031.

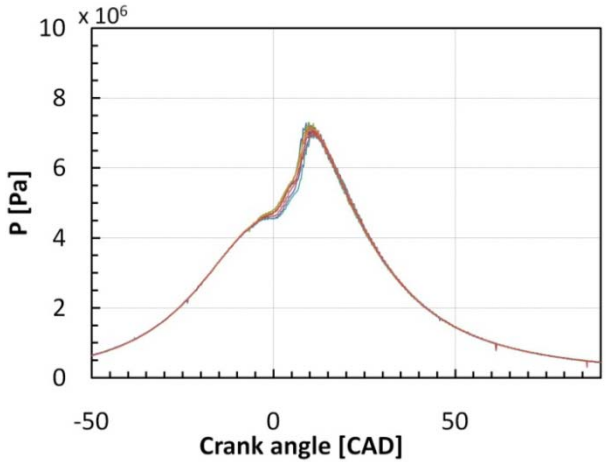

Figure 21 Pressure traces for three pilots + main injection case.

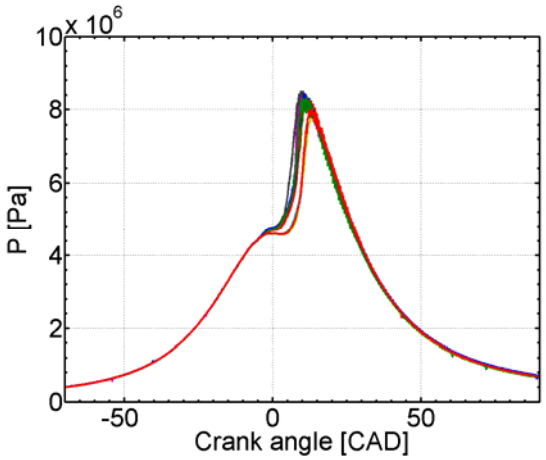

Figure 22 Pressure traces for three pilots + main injection case with 20% total injected fuel mass increase.

Complementing the pressure data analysis, global temperature gives information about the fuel evaporation process in the piston bowl.

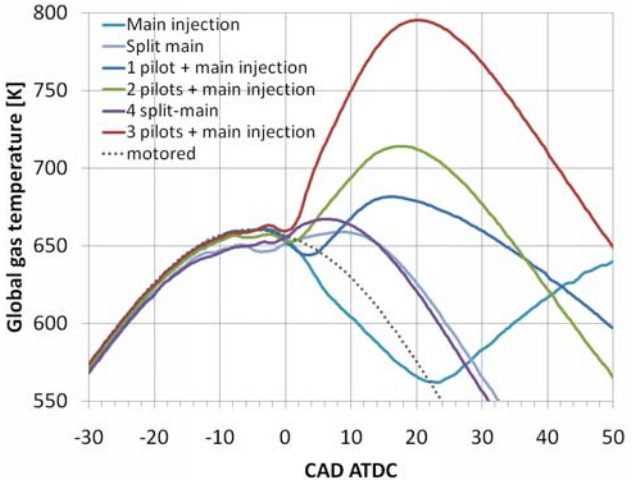

Figure 23 Global temperatures for all cases.

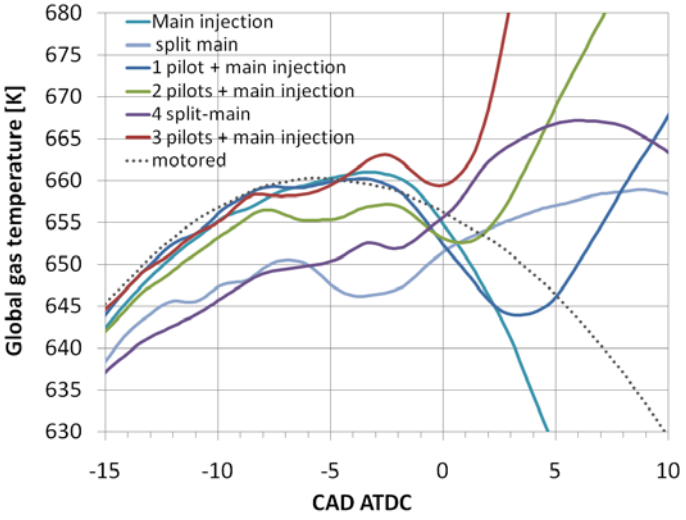

Figure 24 Global temperatures for all cases. Zoomed-in close to TDC.

Figure 23 and Figure 24 show the global temperature data for the different injection strategies. Figure 24 is a closer view of the previous figure. The data presented is the average over the first ten fired cycles. The case without pilot injections obviously shows a large temperature drop due to the large amount of fuel to evaporate at once. Temperature is dropping until 22 CAD ATDC giving a very late combustion phasing. At the end of the temperature drop the temperature is 560K. Previous studies have shown that 550K is the lower boundary for fuel to evaporate and ignite [5]. The case without pilot injections is approaching this lower temperature limit. There is thus obviously a high risk for misfire or limited combustion since the local temperature at the jets reaches lower levels during evaporation.

The split main (-16.5 and -10 CAD) shows a divergence to the motored temperature right after the first injection. The pressure and temperature are too low to assure good fuel evaporation at this stage of the compression stroke. Therefore, a fuel injection of 50% of the total fuel mass phased too early causes evaporation problems. The second injection causes a visible temperature drop as well and the combustion finally takes place, albeit slowly.

The cases with one, two or three pilots show that more pilot injections move the temperature closer to the motored case. It means easier evaporation for each pilot and as seen on the plot, earlier start of combustion. Shorter injections appear to be the key to improved fuel evaporation. Furthermore, short fuel injection pulsations are leading to less wall impingement and less fuel film is formed. If fuel film is formed, the multiple injections can cause so-called 'splashing' phenomenon to remove the fuel from the wall and enhance evaporation [3].However, temperature at the first SOI is important to determine the amount of fuel to inject. In the case of the four split main, 25% of the fuel is injected at 21.5 CAD BTDC and is a handicap for the rest of the cycle.

Evaporation is difficult and pulsations do not overcome the problem of the too large fuel amount injected too early. In the cases with two and three pilot injections it can be seen that the global temperature follows the motored case until the main combustion starts. In order to follow the motored temperature, despite ongoing evaporation of the pilots, heat must be released. Therefore it is reasonable to assume that the pilot injections are contributing with heat release before the main injection. Smaller fuel quantities in the first pilots are favorable for air-fuel mixing and prevent large local temperature drops.

To summarize, the improved evaporation process is due to a combination of three factors. Several injection events create pulsations that remove the fuel film from the piston. They also provide time for the fuel to evaporate during dwell periods. Progressively increasing the fuel amount in the pilot injections also ensures an improved evaporation process as described above.

The effect of the injection strategy can be demonstrated by the rate of heat release for best and worst case showed in Figure 25. Three progressive pilot injections show a premixed peak and a diffusion flame with reasonable timing. The case with only a main injection shows a large negative rate of heat release due to fuel evaporation. It also displays very late diffusion combustion, and the absence of a premixed peak.

The origin of the premixed peak in the best case can be understood by studying the image sequence in Figure 26. Shortly after ignition occurs close to the glow plug two new ignition kernels form on the opposite side of the combustion chamber. Clearly the first ignition event triggers autoignition in premixed portions of the charge that are close to the autoignition temperature. It can be noted that the overall natural luminescence is weaker than in Figure 9 and Figure 10, indicating less soot formation. This is likely due to a more premixed type of combustion than in the previous cases.

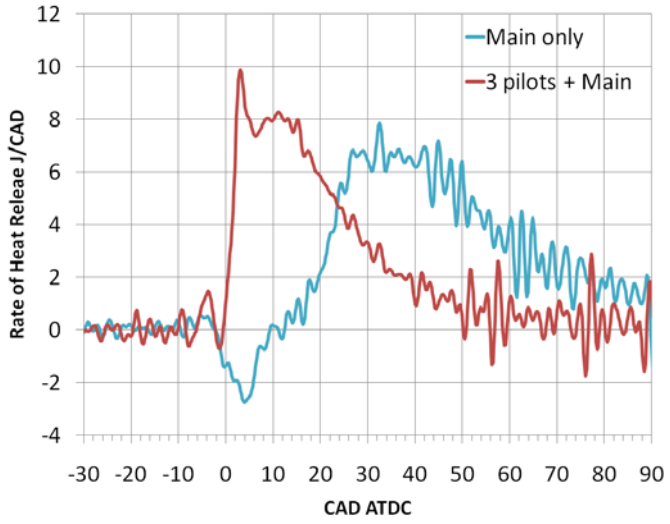

Figure 25 Filtered Rate of Heat Release for best and worst case.

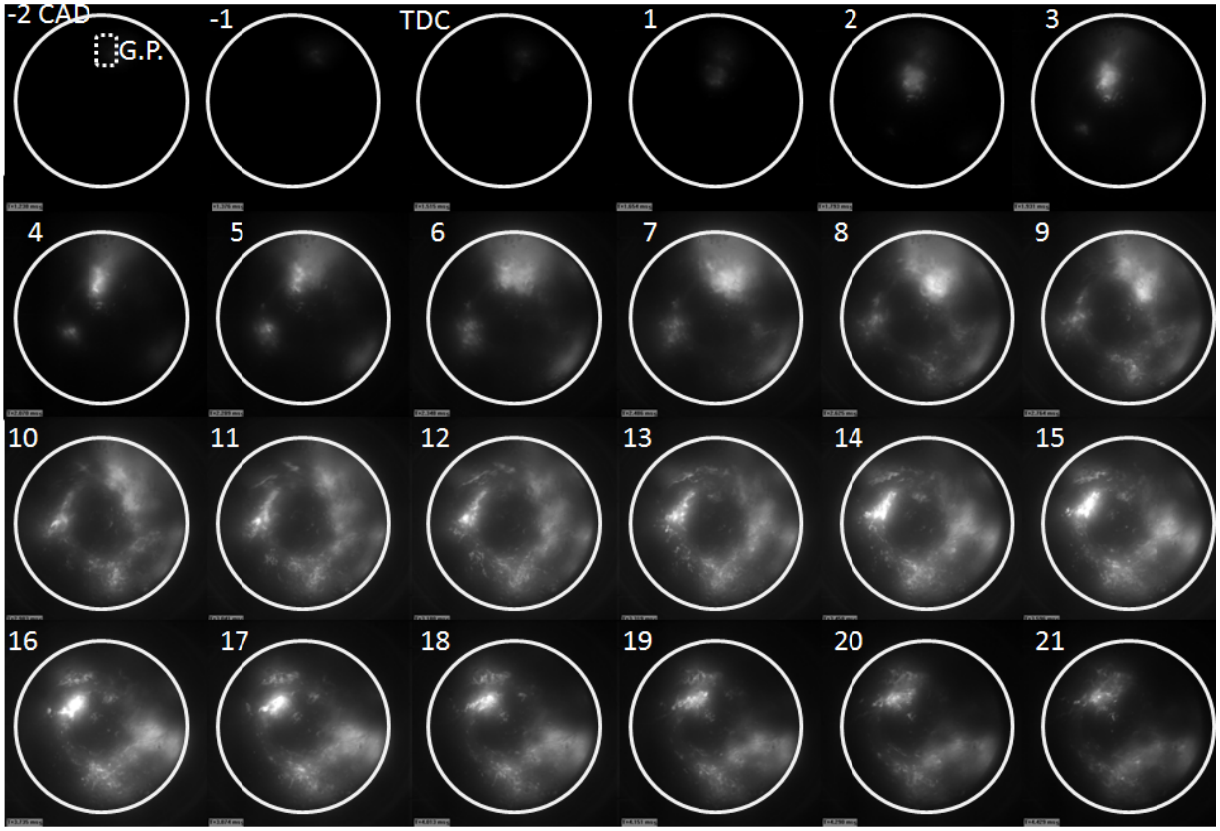

Figure 26 Start at low temperature (-20°C) with three progressive pilots + main injection. Images between 2 CAD BTDC until 21 CAD ATDC. The glowplug location is indicated in the first frame.

CONCLUSION

Cold starting at very low temperatures was investigated in an optical light duty diesel engine. A full factorial study was conducted by cooling down individual engine components and different injection strategies were examined. The following conclusions were reached:

- Fuel evaporation is limited at low temperature; the mixture only ignites close to the glowplug.
- The combustion does not spread to the whole piston bowl during cold start.
- Full factorial study was performed on low temperature sensitivity for cold start. The cooling down of individual engine components has the following effects on combustion stability and noise:
    - Engine block temperature is the dominant parameter for cold start optimization.
    - Inlet temperature strongly affects load stability.
    - Fuel temperature has low significance on most measured parameters.
    - Spray/Glowplug angle affects mainly combustion phasing stability and pressure derivative.
- Injection strategy adaptation for low temperatures gives promising results. A larger number of pilot injections gives a more homogeneous and easy evaporated mixture due to transport by swirl. The best configuration with the present setup was found to be three pilot injections, with increasing fuel mass, and a main injection.
- Gradual increase in pilot fuel quantity seems advantageous for better stability and higher load mainly due to a reduced temperature drop in the cylinder after each injection and more favorable air-fuel mixing. These favorable conditions allow the pilots to react and thus release heat to compensate for the evaporation process.

ACKNOWLEDGMENTS

The authors gratefully acknowledge the Swedish Energy Agency for their support.

REFERENCES

1. Henein, N.A., Zahdeh, A.R., Yassine, M.K, Bryzik, W., “Diesel Engine Cold Starting: Combustion Instability” SAE paper 920005.
2. Fasolo, B., Doisy, A.M., Dupont, A., Lavoisier, F., “Combustion System Optimization of a New 2 Liter Diesel Engine for EURO IV”, SAE paper 2005-01-0652.
3. Stanton, D.W., Lippert, A.M., Reitz, R.D., Rutland, C.J., “Influence of Spray-Wall Interaction and Fuel Films on Cold Starting in Direst Injection Diesel Engines”, SAE paper 982584.
4. Kern, C., Dressler, W., Lindemann, G. and Rothacker, V., “ An Innovative Glow System for Modern Diesel Engines” SAE paper 1999-01-1240.
5. Osuka, I., Nishimura, M., Tanaka, Y. and Miyaki, M., “Benefits of New Fuel Injection System Technology on Cold Startability of Diesel Engines – Improvement of Cold Startability and White smoke Reduction by Means of Multi-injection with Common Rail Fuel System (ECD-U2)”, SAE paper 940586.
6. Pacaud, P., Perrin, H., Laget, O., ”Cold Start on Diesel Engine: Is Low Compression Ratio Compatible with Cold Start Requirements?”, SAE paper 2008-01-1310.
7. Zhong, L.R, Gruenewald, S.,Henein, N.A., Bryzik, W., “Lower Temperature Limits for Cold Starting of Diesel Engine with a common Rail Fuel Injection System”, SAE paper 2007-01-0934.
8. Zhong, L.R, Henein, N.A., Bryzik, W., “Simulation-Based Cold-Start Control Strategy for a Diesel Engine with Common Rail Fuel System at Different Ambient Temperatures”, SAE paper 2007-01-0933.
9. Gonzalez D, M.A., Borman, G.L., Reitz, R.D., “ Astudy of Diesel Cold Starting using both Cycle Analysis and Multidimensional Calculations”, SAE paper 910180.
10. Payri, F., Broatch, A., Serrano, J.R., Rodriguez, L.F. and Esmoris, A., “Study of the Potential of Intake Air Heating in Automotive DI Diesel Engines”, SAE paper 2006-01-1233.

Paper III

SAE International™

Effects of Post-Injection Strategies on Near-Injector Over-Lean Mixtures and Unburned Hydrocarbon Emission in a Heavy-Duty Optical Diesel Engine

2011-01-1383
Published
04/12/2011

Clément Chartier, Oivind Andersson and Bengt Johansson
Lund University

Mark Musculus and Mohan Bobba
Sandia National Laboratories

doi:10.4271/2011-01-1383

ABSTRACT

Post-injection strategies aimed at reducing engine-out emissions of unburned hydrocarbons (UHC) were investigated in an optical heavy-duty diesel engine operating at a low-load, low-temperature combustion (LTC) condition with high dilution (12.7% intake oxygen) where UHC emissions are problematic. Exhaust gas measurements showed that a carefully selected post injection reduced engine-out load-specific UHC emissions by 20% compared to operation with a single injection in the same load range. High-speed in-cylinder chemiluminescence imaging revealed that without a post injection, most of the chemiluminescence emission occurs close to the bowl wall, with no significant chemiluminescence signal within 27 mm of the injector. Previous studies have shown that over-leaning in this near-injector region after the end of injection causes the local equivalence ratio to fall below the ignitability limit. With a carefully selected post-injection, mixtures close to the injector show significant chemiluminescence emission, indicating more complete combustion of those regions, likely due to increased local equivalence ratios.

Simultaneous planar laser-induced fluorescence (PLIF) of OH with 284-nm excitation and PLIF of combined formaldehyde and poly aromatic hydrocarbons (PAH) with 355-nm excitation were employed to identify the regions of first- and second-stage ignition, as well as providing some indication of local equivalence ratios. The laser diagnostics show that without a post injection, regions close to the injector show formaldehyde fluorescence late in the cycle without detectable OH fluorescence, indicating that these regions do not achieve second-stage ignition, and therefore likely contribute to UHC emissions. Persistence of formaldehyde fluorescence late in the cycle is also consistent with fuel-lean mixtures. With a carefully selected post injection, strong OH fluorescence appears in the near-injector regions, indicating that they are likely enriched by the post-injection such that they reach second-stage ignition and more complete oxidation. The reduction observed in the exhaust UHC emission is therefore attributed to the enrichment mechanism of the near-injector regions by the close-coupled post-injection.

INTRODUCTION

The past decade has seen tremendous development in diesel engine technology and performance in response to ever more stringent emissions legislations. Heavy-duty diesel engines have significantly reduced their emissions of nitrous oxides (NO_X) and particulate matter (PM). Low temperature combustion (LTC) is one way of improving the NO_X/PM tradeoff by dilution of the charge with large amounts of cooled exhaust gas recirculation (EGR). The dilution with EGR keeps the adiabatic flame temperature below the thermal NO_X formation temperature region and decreases soot formation [1]. In the lower load range, ignition typically occurs after the end of injection (EOI), so that the ignition dwell, which is the time from EOI to the start of combustion, is positive. The ignition dwell is

usually longer at lower loads, in part because the injection duration is shorter.

Conventional diesel combustion typically has a negative ignition dwell and therefore a significant quasi-steady period [2], where much of the heat release occurs through mixing-controlled combustion during the spray-driven diffusion flame phase. By contrast, for LTC conditions with positive ignition dwells, heat release does not overlap with the fuel injection event, so the quasi-steady jet is not an adequate model for combustion. Instead, as more mixing of air and fuel takes place prior to ignition, more of the heat release is premixed.

The evolution of the local equivalence ratios prior to combustion was investigated in a previous study [3] for a case of LTC combustion. The local fuel concentration within and between two neighboring jets was measured using planar laser-induced fluorescence (PLIF) of a fuel tracer (toluene) under non-reactive conditions. The three images presented in Fig. 1 show equivalence ratio contours corresponding to 12.7% intake oxygen concentration, which were derived from the fuel vapor concentration measurements under non-reacting conditions. The nozzle is located on the left side of the frames and the two studied jets are directed up and to the right and down and to the right of each image.

The first frame presents the results at the end of injection (EOI). The highest local equivalence ratios are located close to the nozzle, as for a quasi-steady jet. 2 crank angle degrees (CAD) after the end of injection (AEI), in the middle image, the mixtures are becoming leaner and close to stoichiometric in the upstream regions. The downstream regions are also becoming leaner but they are now richer relative to the near-nozzle region, which is contrary to the situation at EOI. This leaning trend continues in the bottom frame at 5 CAD AEI, where the mixture close to the nozzle is now below stoichiometric conditions. Formaldehyde imaging has shown that lean mixtures remain stagnant close to the nozzle late in the expansion stroke [4]. At equivalence ratios below 0.5, mixtures are unlikely to ignite or achieve complete combustion. Therefore, very lean mixtures in the near-nozzle region have been identified as potential sources of unburned hydrocarbons (UHC) emissions [3, 4, 5]. Also other studies have pointed out that over-lean mixtures could contribute to explaining the correlation between highly diluted LTC cases and engine-out UHC emissions [6, 7, 8].

The mixtures close to the nozzle shown in Fig. 1 become leaner very quickly after EOI. The air-entrainment rate in the jet after EOI can be compared to a steady jet case. The circled numbers in the top image represent the time needed in CAD for a fuel particle exiting the nozzle to reach the indicated locations in a steady-jet at the measured jet penetration rate. At the position of the second circle, the local equivalence-ratios are in the range 5 to 7. At the same location, i.e. 25 mm from the injector, the equivalence-ratios in the middle frame (2 AEI) are significantly lower, between 2 and 3. In the bottom image (5 AEI) mixtures become closer to stoichiometric in the downstream regions. These observations indicate a faster air-entrainment mechanism after the end of injection compared to a steady-jet.

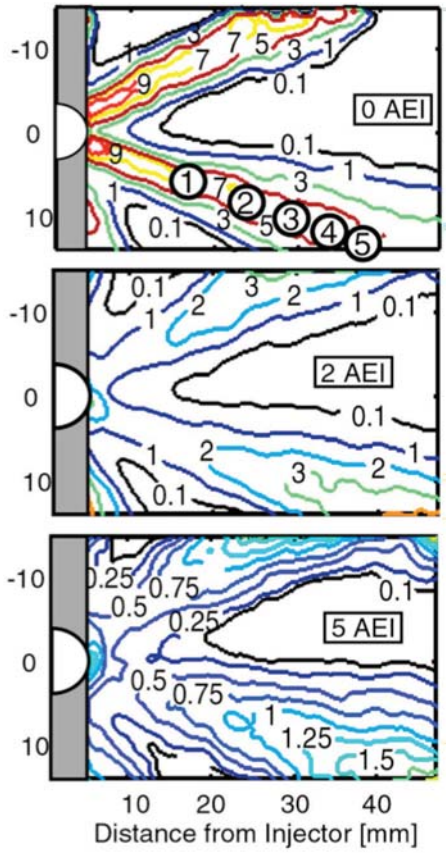

Figure 1. Equivalence ratio contour lines for a portion of the combustion chamber obtained by fuel tracer fluorescence measurements [3]. The nozzle is located on the left side of the frames and two jets are directed up and to the right and down and to the right in the image. The equivalence ratios correspond to 12.7% inlet oxygen. The circled numbers in the top image represent the time needed in CAD for a fuel particle exiting the nozzle to reach the indicated locations at the jet penetration rate.

Previous work also indicates that part of the UHC emissions during low-load LTC operations are caused by stagnant lean mixtures close to the injector after EOI [3]. The goal of this study is to investigate the potential to increase the upstream local equivalence ratios in the jet above the ignitability threshold by a post injection, and thereby reduce UHC emissions.

Toluene fluorescence is strongly affected by collisional quenching due to oxygen, so the technique is typically applied under non-reacting conditions. Non-reactive conditions can be seen as representative until ignition occurs. After ignition, combustion can significantly affect

mixing. To investigate the effects of post-injections on the near-injector equivalence ratios and UHC emissions when ignition occurs near the post-injection event, it is more relevant to study reactive conditions. Therefore, the present investigation of post-injections uses other laser diagnostics for more indirect measurements of mixing.

Imaging of certain combustion intermediates can indicate the progression of two-stage ignition, and may even provide bounds on the local equivalence ratios. For example, Collin *et al*. used combined laser diagnostics to measure the distribution of OH and formaldehyde for HCCI combustion [9]. It was shown that formaldehyde is formed during the first-stage ignition and fills the measurement region in the studied case. When second-stage ignition occurs, OH is detected in small pockets within the formaldehyde region without overlapping. As second-stage ignition continues, OH regions grow and merge while formaldehyde regions are consumed. Therefore, OH- and formaldehyde-PLIF can indicate the ignition-stage that a region of interest goes through.

Similar combined laser diagnostics were employed by Genzale *et al*. on LTC combustion [7]. Observations of the OH and formaldehyde distributions relative to the first- or second-stage ignition were similar to the ones reported previously. Furthermore, toluene-PLIF was used under non-combusting conditions to obtain quantitative information about local equivalence ratios. The comparison between LIF images of OH, formaldehyde, and PAH under reacting conditions with and toluene fluorescence under non-reacting conditions showed how the spatial distribution and temporal evolution of the combustion intermediates can provide boundaries on the local equivalence ratio. Firstly, formaldehyde first appears in regions ranging from from fuel-lean to fuel rich, but it persists late in the cycle only in fuel-lean regions, for which the delay to second-stage ignition is very long. Second, OH concentrations are highest in regions of intermediate stoichiometry, and the OH fluorescence signal should be roughly proportional to its concentration [10], so that OH fluorescence during its initial appearance is strongest in regions that are likely of intermediate stoichiometry. Finally, PAH fluorescence arises in regions that are fuel-rich and later may proceed to soot formation.

In a similar manner, combustion intermediates are used as quantitative indicators of local stoichiometry in the present investigation. Two different post-injection strategies are presented and compared to a single injection in terms of engine-out UHC level, and estimated distributions of near-stoichiometric, lean and potentially rich mixtures derived from laser-induced fluorescence imaging of OH and formaldehyde/PAH. One of the injection strategies is shown to rapidly render the mixture in the upstream regions combustible and thereby decrease load-specific UHC emissions by 20% at approximately the same load as a single injection condition. Rate of injection measurements and sensitivity of the post-injection parameters on UHC reduction are also discussed.

EXPERIMENTAL SETUP AND DIAGNOSTICS

OPTICAL ENGINE

The optical engine is a single cylinder version of a Cummins N-series heavy-duty diesel engine having a bore of 139.7 mm, a displacement of 2.34 liters, and a swirl ratio of 0.5. Other specifications are listed in Table 1. Figure 3 is a schematic showing the extended Bowditch piston with a large flat piston-crown window, small rectangular windows located at the top of the cylinder liner providing cross-optical access for laser-based diagnostics. It has also a small cylinder head window in place of one of the exhaust valves. The piston bowl-rim has a cut-out to allow laser-sheet access to the combustion bowl near top dead center (TDC), see Fig. 2. More details about the optical engine can be found in [2, 11, 12].

The engine is equipped with a Cummins XPI high-pressure, electronically controlled common-rail fuel injector. This injector uses a solenoid-actuated pilot valve and a pressure-balanced needle to control fuel delivery. It is capable of multiple injections at up to 2000 bar fuel-rail pressure. For the experiments presented here, an eight-hole mini-sac injector cup (tip) was employed, having an included angle of 152°. The eight orifices are equally spaced and have a nominal diameter of 0.15 mm.

Exhaust UHC emissions were measured using a 600 series UHC analyzer from California Analytical Instruments. Under skip-fired conditions where the exhaust is significantly diluted, measurement of UHCs can be challenging due to low species concentrations and possible condensation in the exhaust system and sample lines due to the low mean exhaust temperatures. For the conditions tested, UHC emissions were quite high, well above the detection limit of the analyzer, even with skip-firing. To avoid condensation in the exhaust system, the sampling point was located as close to the exhaust valve as possible, in the exhaust manifold. Furthermore, heated sample lines helped to prevent condensation during extraction. The system responded rapidly to transients from fired to non-fired operation, indicating that heavy hydrocarbons had not condensed in the exhaust pipe and released later. Furthermore, a steady level of UHC was reached after a few combustion cycles only and evaluation is based on the steady part of the UHC curve obtained. Although the UHC measurements are reliable, many compromises to the combustion chamber geometry for optical access, such as greatly increased crevice volumes, likely affect UCH emissions. As such, the absolute levels of UHC presented here for the optical engine are not meant to be taken as a quantitative measurement for a practical engine, but rather to indicate the trends and comparisons between different combustion cases.

Table 1. Engine and injector specifications.

Engine base type	Cummins N-14, DI diesel
Number of cylinders	1
Cycle	4-stroke
Number of intake valves	2
Number of exhaust valves	1*
Combustion chamber	Quiescent, direct injection
Swirl ratio	0.5 (approx.)
Bore	139.7 mm
Stroke	152.4 mm
Bowl width	97.8 mm
Displacement	2.34 liters
Connecting rod length	304.8 mm
Piston pin offset	None
Geometric compression ratio	11.2:1
Simulated compression ratio	16:1
Fuel injector type	Common-rail, solenoid actuated
Cup type	Mini-sac
Number of hole	8, equally spaced
Spray pattern included angle	152°
Rail pressure	1600 bar
Orifice treatment	None (square edged)
Nominal orifice diameter	0.15 mm

**In this optically accessible diesel engine, one of the two exhaust valves of the production cylinder head was replaced by a window and periscope.*

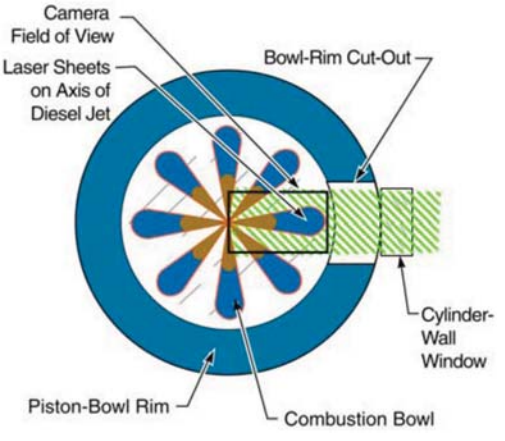

Figure 2. Schematic of the piston with eight-hole injector. The laser sheets enter the combustion chamber from the right side through a cut-out in the bowl rim and follow the jet axis towards the injector nozzle.

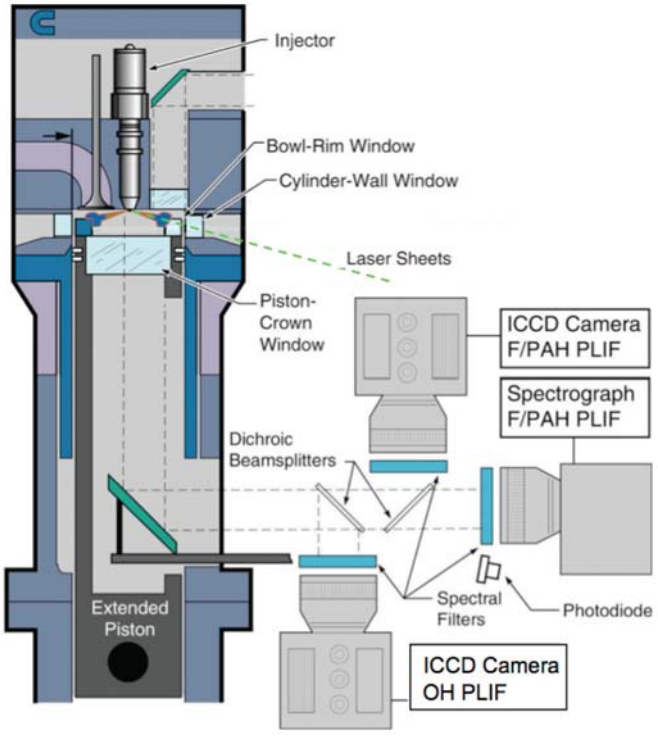

Figure 3. Schematic of the optical heavy-duty diesel engine and layout for the combined laser induced diagnostics.

OPERATING CONDITIONS

The engine operating conditions are summarized in Table 2. To achieve LTC conditions, the oxygen concentration was reduced to 12.7% in the inlet flow. Because the engine is a single-cylinder, and skip-fired for thermal loading reasons, EGR was not available for dilution. Rather, a metered flow of nitrogen was added to the intake stream to dilute the oxygenconcentration to the desired level. At the chosen dilution of 12.7% O_2, the adiabatic flame temperature for a stoichiometric mixture at peak pressure is 2170 K, compared to 2680 K for pure air. Ojeda *et al*. have shown that this level of dilution can comply with the NO_x limit of the US 2010 heavy-duty on-road legislation without NO_x after-treatment for a wide load range by adjusting the injection strategy [13].

The injection parameters are given for the different injection strategies in Table 3. The values for actual start and duration of injection are extracted from injection rate measurements for each strategy. For each of the low load LTC cases investigated, the start of the main injection is −5° ATDC. This particular timing of the main injection gives both a positive ignition dwell (essential for LTC) and a practical combustion phasing for fuel efficiency. Also, for more fundamental reasons, injection starting at −5 ATDC is attractive because the density remains nearly constant before and after injection (little piston motion), so that the data are more easily compared with nearly constant-density constant-volume combustion chamber experiments. The

fuel mass delivered in the post-injection is discussed together with rate of injection results in a later section.

Table 2. Engine operating conditions.

Engine speed	1200 rpm
Intake O_2	12.7%
Common-rail fuel pressure	1600 bar
TDC Motored Density	22.1 kg/m^3
TDC Motored Temperature	837 K
TDC Motored Pressure	54.9 bar
Intake Pressure	214 kPa (abs)
Intake Temperature	78°C

Table 3. Injection parameters for the different strategies.

	Single Main Injection	Main + Small Post Injection	Main + Large Post Injection
Actual Start of Main Injection	-5° ATDC	-5° ATDC	-5°ATDC
Actual Duration of Main	~980 µs	~970 µs	~830 µs
Actual Start of Post Injection	-	3°ATDC	4°ATDC
Actual Duration of Post Injection	-	~200 µs	~560 µs
Total Fuel Injected	39.2 mg	41 mg	44.7 mg
Post-injected fuel	-	1.8 mg	14.6 mg
$IMEP_g$	270 kPa	287 kPa	327 kPa
Indicated efficiency	37.7%	38.3%	40.1%

For all operating conditions, cylinder pressure and fuel rail pressure were digitized and recorded at quarter CAD increments, simultaneously with the acquisition of the optical data. The apparent heat release rate (AHRR) was calculated from ensemble-averaged pressure data using an air-standard first-law analysis (see e.g. [14]). A regular schedule is maintained during these experiments where the engine is motored for 90 seconds before the injecting fuel to minimize variability of results due to transients.

A diesel primary-reference fuel (PRF) mixture was used to avoid unwanted fluorescence interferences from aromatic components in diesel fuel. The PRF mixture is 32.3% n-hexadecane (cetane) and 67.7% heptamethylnonane by volume, giving a defined cetane number of 42.5, which is typical of U.S. diesel fuel [15].

Rate of injection analysis

Multiple injection strategies can possibly affect the dynamics in the injector due to pressure waves in the common rail system. To understand the effects of pressure waves on post injections, the rates of injection for the strategies in Table 3 were measured using a spray-impingement meter [16]. Fig. 4 shows the derived mass rate of injection for all three cases. The rail pressure in the fuel line upstream of the injector is also indicated on the plot. Both parameters are averaged over 100 injections and low-pass filtered using a Butterworth filter with a normalized cutoff frequency of 0.1. The rate of injection was measured with atmospheric back-pressure and the nozzle was heated to 90°C, which corresponds to the nominal temperature of the coolant in the engine cylinder head. The low pressure of the injector test chamber compared to the in-cylinder pressure close to TDC could influence the injection rate measurements. The spray velocity is proportional to the square root value of the pressure difference between the nozzle-sac and the surrounding air. However, Klein-Dowel *et al.* showed that for fully cavitating flows in similar injectors, the mass flow rate was independent of the chamber pressure [17]. Cavitating flow is estimated to occur above 200 bar injection pressure.

It appears clearly on the figure that the delayed post-injection strategy, i.e. actual start of post injection at 4°ATDC, shows a much larger fuel mass in the post-injection compared to the strategy with an earlier post-injection at 3°ATDC. It is important to note that both post-injection strategies had the same energizing time from the injector control system. The two strategies only differ by a delay of 1 CAD in the start of injection command. The main injection duration was reduced in the large post-injection strategy to maintain roughly constant load with the increased post-injected fuel mass. The start of the main-injection was kept unchanged. The results gave 39.2 mg of fuel per injection with a standard deviation of 0.9 mg for the single injection only and 41.0 mg for the main and small post-injection together. The large post-injection strategy resulted in 44.7 mg of fuel per cycle. Analysis of the rate of injection results shows that 14.6 mg of the 44.7 mg are injected in the large post injection with a standard deviation of 0.6 mg. On the other hand, only 1.8 mg of 41.0 mg are post-injected in the small post-injection strategy. The standard deviation for this post injection is 0.4 mg. These values are determined from 100 cycles.

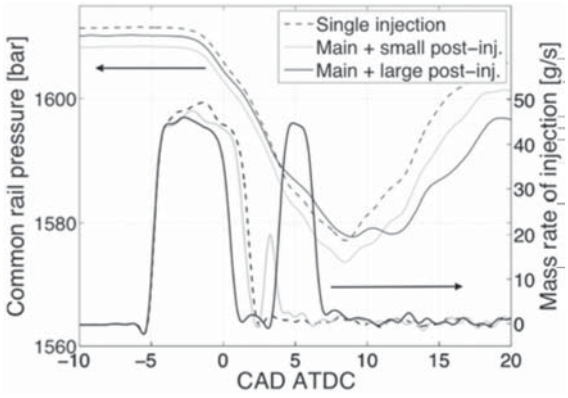

Figure 4. Rate of injection for all three injection-strategies averaged over 100 cycles and low-pass filtered. The fuel pressure in the common rail is also indicated.

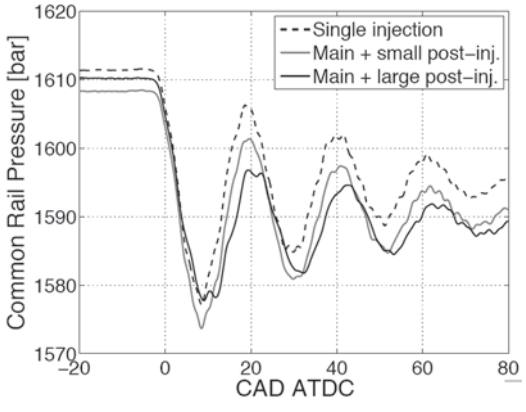

Figure 5. Fuel pressure oscillation in the common rail due to pressure waves in the fuel lines after the different injection strategies.

The mass of post-injected fuel in the small post-injection strategy appears to be very small. However, repeatability tests in the engine and the rather low standard deviation obtained for the post-injected fuel mass indicate that such a small post-injection is achievable.

A reasonable explanation for the large difference in post-injected fuel-mass despite an identical energizing time could be the presence of pressure waves in the high-pressure fuel system generated by the main injection. The change in timing of the post-injection changes the opening time for the injector needle relative to the pressure waves and could cause a variation in the actual injection duration and injected fuel mass.

The fuel pressure before the injector was monitored by a Kistler pressure transducer in the common rail. Fig. 5 shows the fuel pressure in the common rail for the different injection strategies. Significant variations are observed after the main injection. However, the common rail pressure data is also presented in Fig. 4 together with the injection rate data for direct comparison. It appears that the timescale between the main and post-injections is smaller than the dynamics of the fuel system. For both post-injection strategies, SOI for the post-injections is occurring at comparable fuel pressure conditions. Nevertheless, injector and fuel line dynamics are very complex and the conditions depicted at the location of the pressure transducer may be very different from the ones at the nozzle. (Pressure waves within the injector body are very likely to play a role in the opening of the needle as well.)

LASER DIAGNOSTICS

The objective of this investigation is to qualitatively observe the effects of post-injected fuel in the over-mixed near-nozzle region. Two effectively simultaneous planar laser-diagnostics were used to investigate species that mark the progress of a two-stage autoignition process, as well as to provide an indication of mixture stoichiometry (i.e. lean, rich, or intermediate stoichiometry) at their location along the centerline of one of the eight jets. PLIF of OH was employed to identify the regions that have achieved second-stage ignition and to provide an indicator of mixtures that are of intermediate stoichiometry [10]. PLIF at 355 nm was imaged both with a camera and a spectrometer. By spectrally analyzing this fluorescence, the locations of formaldehyde and PAH could be determined. Regions with PAH fluorescence indicate fuel-rich mixtures, while regions with persistent formaldehyde fluorescence late in the cycle indicate fuel-lean mixtures [7].

OH fluorescence (OH-PLIF) was excited near 284 nm using 20 mJ per pulse provided by the frequency-doubled output of an optical parametric oscillator (OPO) pumped by the 355-nm third-harmonic of a Nd:YAG laser. A 105mm UV-Nikkor lens was mounted on a UV camera to collect the fluorescence emission. The positions of the cameras are shown in Fig. 3. To maximize the signal/noise ratio and reject elastic-scattered laser light, several filters were employed. Since OH-fluorescence is narrow-band, a 16nm wide bandpass filter centered at 310 nm was used. A 2-mm thick WG 305 long-wave-pass filter was employed to remove the scattered laser light at 284 nm. Finally, a 358-nm short-pass filter rejected fluorescence from other species and other interference such as black body radiation from soot. Further information about OH-PLIF can be found in [18].

Both formaldehyde and PAH fluorescence (formaldehyde/PAH PLIF) were excited simultaneously by a single 355-nm beam of a frequency-tripled Nd:YAG laser at 60 mJ per pulse. The resulting combination of formaldehyde and PAH fluorescence was imaged by a second camera (see Fig. 3). A CG385 long-pass filter removed the scattered laser-light while a 40-nm wide bandpass filter centered at 408 nm isolated the fluorescence signal of interest from other species. To distinguish formaldehyde fluorescence from that of PAH in the images, the fluorescence emission was spectrally analyzed to discriminate the signatures of

formaldehyde and PAH in the total signal. A beam splitter directed part of the fluorescence emission along the jet axis onto the entrance slit of an Oriel 1/8-meter spectrometer using a 55-mm f/2.5 glass lens, as shown in Fig. 2. A CG375 long-pass colored glass filter was placed in front of the lens to help reject strong elastic scatter from the laser. The fluorescence spectrum was imaged onto an intensified CCD array at the exit of the spectrograph, capturing emission from 380 nm to 450 nm. An Oriel 77298 grating with 1200 lines/mm blazed at 350 nm and a slit opening of 600 µm gave a resolution of 4 nm.

Figure 6. Visualization of the binning zones used for the spectral evaluation of the formaldehyde\|PAH LIF along the jet axis.

The region of the combustion chamber viewed by the spectrograph is a 4.2-mm wide band along the jet axis. As illustrated in Fig. 6, this narrow band was divided into 15 discrete zones in the axial direction. In each zone, the signal captured with the spectrometer was compared to a reference formaldehyde-spectrum. The reference spectrum was extracted from the acquired combustion-spectra at a timing and location dominated by premixed burn. The premixed phase of the combustion is characterized by the presence of formaldehyde. Spectra from different binning zones are presented as examples in Fig. 7 together with a formaldehyde reference-spectrum.

A typical feature of the formaldehyde spectrum is its regular peak spacing. Seven characteristic peaks between 385 and 445 nm can be considered as its fingerprint. In noisy spectra, a bandpass filter can thereby distinguish potential formaldehyde peaks from more broadband features. Fig. 8 presents the signal in Fig. 7 after bandpass filtering. The frequency range employed in the bandpass filter corresponds to the frequency of the regularly spaced peaks in a theoretical formaldehyde spectrum between 385 and 445 nm. The filter was designed using a third-degree polynomial together with a spatial frequency cut-on at 0.04 nm^{-1} and cut-off at 0.21 run^{-1}. The spectral peaks appear clearly in the reference spectrum and the similarity or non-similarity of the reference signal from the signal integrated within each measurement zone becomes more obvious.

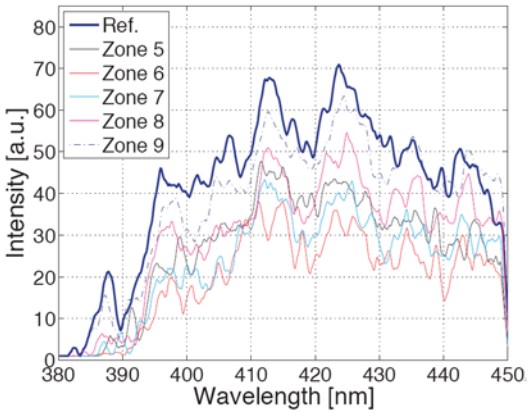

Figure 7. Example of spectral visualization of the formaldehyde\|PAH LIF signal for several binning zones. A reference spectrum is plotted for comparison.

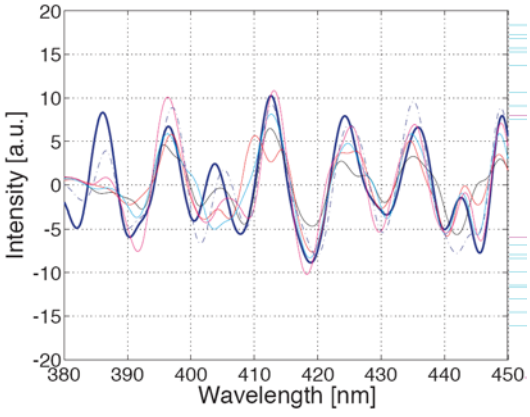

***Figure 8. Bandpass-filtered spectra for the binning zones presented in* Fig. 7**

The spectra are compared using the normalized covariance of the two signals for each zone, similarly to the approach in [19]. The correlation value obtained is between zero (i.e. no correlation to the reference spectrum) and unity (i.e. perfect correlation). The correlation value is visually represented in a color bar placed under the studied spray, see Fig. 9. The bar is divided into 15 zones and the color of each zone reflects the similitude of the fluorescence signal to formaldehyde along the jet axis, with black indicating zero and red indicating unity.

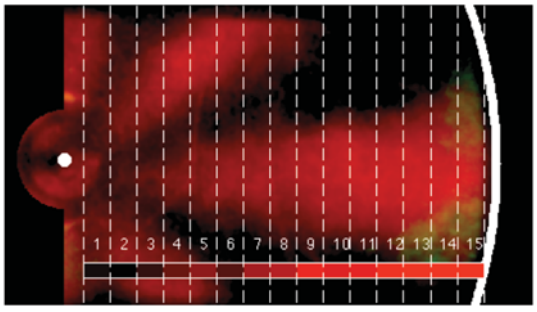

Figure 9. Image resulting front the spectral analysis. The darkest colors in the correlation bar indicate a low correlation with a formaldehyde reference spectrum whereas the brightest color indicate that the LIF signal has a high probability of being formaldehyde-LIF signal.

RESULTS

UHC EMISSIONS FOR LTC CASES

As discussed earlier, EGR-diluted LTC conditions have low combustion temperatures for limiting NOx formation, and they typically have a positive ignition dwell. This is necessary to increase pre-combustion mixing and thereby limit the formation of soot during combustion. Both the ignition dwell, which creates locally lean mixtures, and the lower combustion temperature contribute to UHC emissions. Higher load conditions have longer injection durations and therefore shorter ignition dwells, as well as somewhat higher in-cylinder temperatures because of compression-heating from the rise in pressure from the combustion event. Consequently, UHC emissions are a strong function of load.

Figure 10 shows how the load-specific UHC emissions decrease with increasing gross indicated mean effective pressure (IMEPg) for a load sweep for the single-injection condition in our engine. Only the duration of the main injection was changed during the load sweep, and UHC data are adjusted to account for skip-fired operation mode (the data correspond to continuously-fired operation). The exhaust gases were analyzed with a 600 HFID flame ionization analyzer from California Analytical Instruments. A heated line sampled gas from the exhaust pipe as close as possible to the engine, approximately 20 cm from the exhaust port, to avoid effects of potential condensation of heavier hydrocarbons in the exhaust pipe before the sampling point. Heat insulation material was employed on the exhaust and sampling pipe to further avoid condensation issues of the exhaust gases. For this study, we selected a target load-region around 300 kPa IMEPg for comparison of single-injection with post-injection UHC emissions performance. The specifications of the injection strategies are given in Table 3.

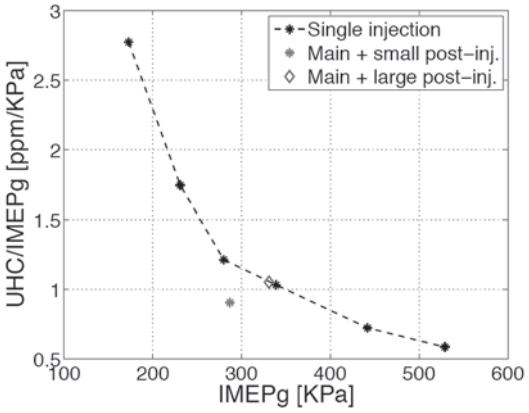

Figure 10. Engine-out UHC measurements versus IMEPg for LTC cases. The result for the investigated post-injection strategies are indicated. The UHC levels presented are corrected for skip-fired operation mode.

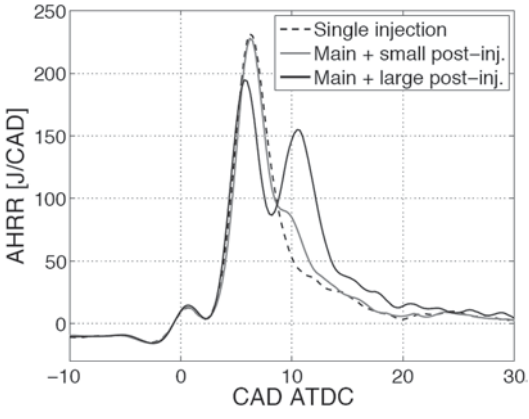

Figure 11. Apparent rate of heat-release for the single injection compared to the investigated post-injection strategies.

The post-injection condition reported in the next sections shows a 20% reduction in load-specific UHC emissions at approximately the same load as the reference case with main injection only. The UHC emissions results for this post-injection strategy are presented in Fig. 10 for direct comparison with the single-injection cases. The apparent heat release rate for both injection strategies is presented in Fig. 11. The start of main injection is identical for both strategies, and the injection duration for the main-only strategy is slightly longer. Therefore, the heat release rate is very similar for both cases regarding the cool flame and the start of combustion. The actual start of the post-injection occurs close to 3 CAD ATDC. The small difference in peak value between the two curves can be explained by the higher fuel mass in the main injection for the single-injection case, as well as the reduction of apparent heat release due to evaporation of the post-injected fuel near the timing of the peak. The evidence of the combustion of the post injection is visible between 9 and 12 CAD ATDC. Thereafter the two curves merge through the end of the combustion event.

The indicated efficiency for the small post-injection case was not decreased compared to the single injection case, see Table 3. It is due to the contribution of the post-injected fuel to the heat release. The fuel mass injected in the post-injection was kept as low as possible. The energizing time employed for the second injection was set as the shortest duration assuring a reasonable cycle-to-cycle repeatability of the injection quantity. Rate-of-injection measurements for the different injection strategies show that a very short (approximately 200 microsecond) post-injection is achieved, as discussed in an earlier section.

LASER DIAGNOSTICS RESULTS

Single injection

The laser diagnostic results presented in Fig. A1 (in the appendix section) show combined images of OH-PLIF (false-colored green) and formaldehyde/PAH-PLIF (red) for the single main injection condition. The data are averaged over twelve separate cycles for a better signal to noise ratio given the rather low cycle to cycle variations in the observed phenomena. The nozzle is located on the left side of the images and the jet of interest is penetrating horizontally from left to right. The bowl wall is indicated in the frames, but it should be noted that a wall cut-out was present at the studied jet to enable laser sheet access, see Fig. 2.

The end of the single injection is visible in the first frame by scattered light from the liquid portion of the jet. The signal is not revealing the presence of OH-radicals in this region since offline images show the same scattered light pattern. Offline images are taken when the laser wavelength is tuned away from the OH excitation lines. The intensity of the scattered light in the liquid spray is lower for the studied jet compared to the neighboring ones. Attenuation of the laser intensity after intersecting with the jet is a plausible explanation for low scattering signal from the horizontal fuel spray.

The formaldehyde/PAH-PLIF signal appears in a jet shape already by EOI. The jet structure is clear and remains for 8 CAD after EOI. The formaldehyde correlation level along the centerline of the jet indicates that the signal in the downstream portion of the jet is highly correlated with the formaldehyde reference spectra. The jet is progressively filled with formaldehyde towards the upstream regions in the following frames.

By five CAD after EOI, OH-LIF signal is detected in the vicinity of the bowl wall. It indicates progression to second-stage ignition and relatively complete combustion in mixtures of intermediate stoichiometry, between fuel-lean and fuel-rich [10]. The regions of OH-fluorescence progress toward the nozzle (to the left) for a short period (6 CAD), after which the fluorescence decreases in intensity.

Formaldehyde fluorescence remains in the region between the nozzle and halfway to the bowl wall throughout the entire combustion event. The presence of formaldehyde indicates regions of partially oxidized fuel that have not yet achieved second-stage ignition. The downstream regions of OH fluorescence do not propagate upstream to the near injector region, indicating that the region of formaldehyde fluorescence late in the cycle is a source of UHC emissions. This observation agrees with previous studies [3, 4, 5] that showed the presence of unburned fuel remaining close to the nozzle due to over-leaning after EOI. Although many possible sources of engine-out UHC exist, such as unburned fuel in the crevices [20], flame quenching at the wall [14] or injector dribble [21] for example, the near-nozzle region is of major interest in the present study.

Small post-injection strategy leading to lowered UHC emissions

The post-injection strategy investigated in this section was previously shown to yield 20% lower engine-out UHC emissions as compared to using only a single injection at the same load (Fig. 10). The laser diagnostic results are presented in Fig. A2 in a similar outline as the single injection case. The scattered light on the liquid part of the jets reveals the end of the main injection by one CAD after TDC. After a one-degree dwell, the post-injection starts. Given the short exposure time of the frames, it can be concluded that the actual duration of the post injection is between one and two CAD (140-280 microseconds), which is consistent with the rate of injection measurements (~200 microseconds).

The initial development of combustion, in terms of formaldehyde and OH-radicals, is similar to the single-injection case previously described. The horizontal jet fills with formaldehyde a few CAD after the end of the main injection and OH is formed in the downstream regions. However, ten degrees after the main EOI (11 ATDC), OH radicals are rapidly formed in the upstream part of the jet, within the field of formaldehyde fluorescence. The following frames show that OH-radicals continue to progressively fill the jet cross-section and propagate upstream. By 10 CAD after the end of the post-injection (14 ATDC), OH radicals are found in the near-nozzle region where only formaldehyde was detected with the single injection. Afterward, the OH signal weakens, and the strongest intensities generally remain downstream. The spatial development of the OH distribution along the jet axis is illustrated in Fig. 12. A threshold intensity of 10 out of the full-scale value of 255 is used to determine the downstream distance of OH from the OH-PLIF images.

The appearance of OH fluorescence in the near-injector regions formerly occupied by formaldehyde implies that the post injection has helped to raise the local equivalence ratio from fuel-lean to more intermediate stoichiometry. The flammable mixture ignites rapidly in the jet and second

stage ignition reaches the near-nozzle region. The present diagnostics do not quantify the effect of the post-injection on upstream UHCs. However, the observation of the increased upstream OH fluorescence together with the exhaust-gas measurements strongly suggest that a significant part of the near-injector UHC were oxidized as a consequence of the post-injection. Significant formaldehyde fluorescence still remains late in the cycle, however, indicating that the small post injection investigated here does not entirely consume the unburned fuel near the injector.

Finally, there are no clear signs of PAH in the 355-nm PLIF data. Therefore, the post-injection is not suspected to create fuel-rich soot-forming zones in the wake of the main injection.

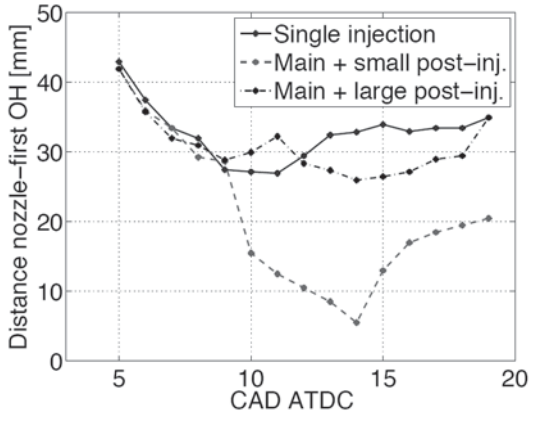

Figure 12. Evolution of the OH-radicals downstream position relatively to the injector nozzle in the jet-axis plane for the single-injection compared to both the investigated post-injection strategies.

Large post-injection strategy leading to unchanged UHC emissions

The small post-injection strategy described in the previous sections, which yields a 20% reduction in UHC emissions, was quite unique, and was discovered by trial and error. In fact, most of the post-injection strategies that we investigated in our parameter sweeps produced little or no reduction of UHC emissions, or even increased UHC emissions at the same load. This section presents one example of an alternative post-injection strategy that does not yield a reduction of UHC emissions. Comparison of this alternative condition with the more optimized post-injection strategy helps to illustrate the sensitivity of the post-injection timing and quantity on UHC emissions as well as to better understand the underlying mechanism. In the alternative strategy, the post-injection was delayed by one CAD compared to the case previously discussed. Because of fuel rail and possibly injector dynamics, the delay caused the post-injection quantity to be increased, even though the command duration was held constant. To offset the increased mass in the post injection so that load could be held constant, the injector solenoid energizing time of the main injection was decreased, while the start of the main injection was kept unchanged.

The exhaust-gas measurements revealed that this large post-injection strategy had no significant effect on UHC emissions compared to a single injection at the same load. The laser diagnostic data for the large post-injection strategy are presented in Fig. A3. Prior to 8 CAD after the main EOI (9 ATDC), the formaldehyde and OH distributions are generally the same as for the other injection strategies. However, scattered light from the liquid sprays reveals a significantly longer post-injection duration than the previous post-injection strategy.

Then, between 10 and 12 CAD after the main EOI, strong formaldehyde/PAH-PLIF signal is visible in the downstream region of the jet. It is reasonable to assume that the post-injected fuel is at the origin of this observation since the region was filled with OH radicals prior to that timing. In the image at 12 CAD ATDC, the formaldehyde correlation coefficient is low in the downstream regions along the jet centerline. It indicates a probable presence of PAH due to locally richer mixtures caused by the large post-injection, which was not observed with the single main injection.

During the same period, the evolution of the OH distribution is different from the small post-injection case. Here, second-stage ignition is not observed in the upstream regions close to the injector. It progresses only slightly upstream, staying in the outer portion of the bowl wall. Late in the cycle, the formaldehyde and OH signals remain separated, with formaldehyde close to the injector and OH close to the bowl wall, with a decreasing intensity in time. This indicates that the mixtures in the upstream regions did not go through second-stage ignition despite the use of a post-injection. The late-cycle formaldehyde distributions near the injector are similar to those of the single injection condition (Figure A1), but the source is some combination of both the main and post injections.

Unfortunately, without some diagnostic to differentiate between fuel from the two injections, it is not possible to quantify the separation of the two contributions. However, we can reason that the post-jet passes through and displaces the lean near-nozzle regions left after the end of the main injection. Therefore, the lean tail of the post-injection likely contributes significantly to the UHC in the large-post case.

Importance of post-injection momentum flux for UHC reductions

Based on the observed differences in the evolution of formaldehyde and OH between the single injection case and the small and large post-injection strategies, the momentum of the post-injection appears to affect the mechanism for

UHC reduction close to the nozzle. With a single injection with a relatively large total momentum, the front of the jet penetrates to the bowl wall, while the upstream wake over-mixes. The upstream mixtures become too fuel-lean to achieve second-stage ignition, so that formaldehyde and UHCs persist late in the cycle. Similarly, for the large post injection, the formaldehyde fluorescence intensity increases at 9 CAD after the main EOI (10 ATDC), and the post-injection jet penetrates toward the bowl wall, pushing the residual OH from the main injection farther downstream. This observation is clear in Fig. 12 where the distance between the nozzle and the first OH signal on the jet axis is compared for all three cases. The downstream movement of OH for the large post injection is apparent in Fig. 12 between 9 and 10 CAD after the main EOI (10-11 ATDC). Additionally, the upstream wake for the large post injection shows formaldehyde persisting late in the cycle, indicating overly lean mixtures and incomplete combustion, similar to the single injection. Later in the cycle, the OH radicals do not interact with the upstream non-oxidized fuel, which explains the results of unchanged exhaust gas UHC content.

For the small post injection, however, the post-injection jet does not displace the OH downstream, so it does not appear to have penetrated to the wall at ignition. Instead, the upstream mixtures achieve second-stage ignition indicated by the upstream appearance of OH, as illustrated in Fig. 12. The upstream appearance of OH strongly suggests that upstream mixtures have been enriched by the small post injection so that chemical kinetics leading to second-stage ignition are accelerated. The low momentum of the small post-injection likely contributes to its ability to enrich the near-injector region without penetrating so far downstream and leaving fuel-lean mixtures in its wake.

The momentum flux in the jet is proportional to the product of the mass flow rate and the outlet velocity. The rate of injection results in Fig. 4 show that the mass flow through the nozzle holes is approximately doubled in the large post-injection compared to the previous one. As a consequence, the momentum is also significantly larger, approximately 14.7 $g.m.s^{-1}$ compared to 1.3 $g.m.s^{-1}$ for the small post-injection. Therefore, for the operating conditions examined here, the post-injection momentum threshold to achieve UHC reduction is apparently somewhere between 1.3 and 14.7 $g.m.s^{-1}$.

SUMMARY/CONCLUSIONS

For diesel LTC, overleaning in the jet during the ignition dwell has previously been identified as a potential source of UHC. The ignition kinetics are too slow in the fuel-lean near-injector regions for combustion to proceed to second-stage ignition and complete combustion in the time available. The present study investigated the potential of a post-injection strategy to enrich the near-injector regions with additional fuel, and thereby hasten the ignition chemistry so that more complete combustion would be achieved and UHC emissions would be reduced. In addition to exhaust-gas UHC measurements, combined laser-diagnostics were employed to identify fuel lean, near stoichiometric, and fuel rich regions along the jet path. The following conclusions can be drawn from the study:

• A post-injection strategy was identified that effectively reduced engine-out UHC emissions by 20% compared to a single injection at the same load.

• For the single-injection condition, PLIF measurements at 355 nm showed formaldehyde fluorescence in the near-injector region late in the cycle, which is indicative of overly fuel-lean mixtures that do not achieve complete combustion. Images of OH-PLIF confirmed that second-stage ignition only occurs farther downstream in the jet where mixtures are likely of more intermediate stoichiometries

• For a small post-injection condition, the energizing time was set to the shortest duration assuring a lift of the injector needle at every cycle. OH-PLIF measurements revealed second-stage ignition occurring in the upstream region of the jet within a few CAD after the post-injection. The post-injection is thereby capable of enriching the local mixtures near the injector so that the chemical kinetics become fast enough to achieve more complete combustion in the time available.

• For an alternative strategy with a smaller main injection and a larger post injection, OH fluorescence did not indicate second-stage ignition occurring in the upstream regions. This observation suggests that the momentum delivered in the post-injection needs to be low so that the penetration is relatively short. Thus, the post-injected fuel remains in the near-injector region to enrich the over-mixed zones that lead to UHC emissions, and is not carried too far downstream by the post-injection momentum.

REFERENCES

1. Kook, S., Bae, C., Miles, P.C., Choi, D., and Pickett, L.M, "The Influence of Charge Dilution and Injection Timing on Low-Temperature Diesel Combustion and Emissions," SAE Technical Paper 2005-01-3837, 2005, doi: 10.4271/2005-01-3837.

2. Dec, J.E., "A Conceptual Model of D.I. Diesel Combustion Based on Laser-Sheet Imaging," SAE Technical Paper 970873, 1997, doi:10.4271/970873.

3. Musculus, M.P.B., Lachaux, T., Pickett, L.M., and Idicheria, C.A., "End-of-Injection Over-Mixing and Unburned Hydrocarbon Emissions in Low-Temperature-Combustion Diesel Engines," SAE Technical Paper 2007-01-0907, 2007, doi:10.4271/2007-01-0907.

4. Lachaux, T. and Musculus, M.P.B., "In-cylinder Unburned Hydrocarbon Visualization during Low-Temperature Compression-Ignition Engine Combustion Using Formaldehyde PLIF," Proc.Combustion.Inst.,2007.

5. Kim, D., Ekoto, I., Colban, W.F. and Miles, P.C., "In-cylinder CO and UHC Imaging in a Light-Duty Engine Diesel Engine during PPCI Low-Temperature Combustion," *SAE Int. J. Fuels Lubr.* **1**(1):933-956, 2008, doi: 10.4271/2008-01-1602.

6. Han, M. Assanis, D.N. and Bohac, S.V., "Sources of Hydrocarbon Emissions from Low-Temperature Premixed Compression Ignition Combustion from a Common Rail Direct Injection Diesel Engine", Combustion Science and Technology, 181: 3, pp. 496-517, 2009.

7. Genzale, C.L., Reitz, R.D., and Musculus, M.P.B., "Effects of Jet-Bowl and Jet-Jet Interactions on Late-Injection Low-Temperature Heavy-Duty Diesel Combustion", Proceedings Thiesel 2008, 2008.

8. Koci, C.P., Ra, Y., Krieger, R., Andrie, M., et al., "Detailed Unburned Hydrocarbon Investigations in a Highly-Dilute Diesel Low Temperature Combustion Regime," *SAE Int. J. Engines* **2**(1):858-879, 2009, doi: 10.4271/2009-01-0928.

9. Collin, R., Nygren, J., Richter, M., Aldén, M., Hildingsson, L., Johansson, B., "Simultaneous OH- and Formaldehyde-LIF Measurements in an HCCI Engine," SAE Technical Paper 2003-01-3218, 2003, doi: 10.4271/2003-01-3218.

10. Singh, S., Musculus, M.P.B and Reitz, R.D, "Mixing and flame structures inferred from OH-PLIF for conventional and low-temperature diesel engine combustion," Combustion and Flame 156 (2009), pp. 1898-1908, 2009.

11. Musculus, M.P.B., Dec, J.E. and Tree, D.R., "Effects of Fuel Parameters and Diffusion Flame Lift- Off on Soot Formation in a Heavy-Duty Diesel Engine," SAE Technical Paper 2002-01-0889, 2002, doi:10.4271/2002-01-0889.

12. Espey, C. and Dec, J.E., "Diesel Engine Combustion Studies in a Newly Designed Optical Access Engine Using High-Speed Visualization and 2-D Laser Imaging," SAE Technical Paper 930971, 1993, doi:10.4271/930971.

13. Ojeda, W., Zoldak, P., Espinosa, R., and Kumar, R., "Development of a Fuel Injection Strategy for Partially Premixed Compression Ignition Combustion," *SAE Int. J. Engines* **2**(1):1473-1488, 2009, doi:10.4271/2009-01-1527.

14. Heywood, J. B., Internal Combustion Engine Fundamentals, McGraw-Hill, Inc., 1988.

15. Bobba, M.K, Chartier, C., Andersson, Ö., Johansson, B., Musculus, M.P.B, "Planar Laser-Diagnostics of Soot and OH with Post-Injections in a Heavy-Duty LTC Diesel Engine", Proceedings Thiesel 2010, 2010.

16. Musculus, M.P.B., "On the Correlation between NOx Emissions and the Diesel Premixed Burn," SAE Technical Paper 2001-01-1401, 2004, doi:10.4271/2004-01-1401.

17. Klein-Douwel, R. J. H., Frijters, P. J. M., Seykens, X. L. J., Somers, L. M. T. and Baert, R. S. G. "Gas Density and Rail Pressure Effects on Diesel Spray Growth from a Heavy-Duty Common Rail Injector," Energy & Fuels 2009, 23, pp. 1832-1842, 2009.

18. Kohse-Höinghaus, K. "Laser techniques for the quantitative detection of reactive intermediates in combustion systems". Progress in Energy and Combustion Science, 20, 203-279, 1994.

19. Genzale, C.L., Reitz, R.D. and Musculus, M.P.B. "Effects of Piston Bowl Geometry on Mixture Development and Late- Injection Low-Temperature Combustion in a Heavy-Duty Diesel Engine," *SAE Int. J. Engines* **1**(1): 913-937, 2008, doi:10.4271/2008-01-1330.

20. Aceves, S.A., Flowers, D.L., Espinosa-Loza, F., Martinez-Frias, J., Dibble, R.W., Christenson, M., Bengt, J., and Hessel, R.P., "Piston-Liner Crevice Geometry Effect on HCCI Combustion by Multi-Zone Analysis," SAE Technical Paper 2002-01-2869, 2002, doi:10.4271/2002-01-2869.

21. Greeves, G., Khan, I.M., Wang, C.H.T., and Fenne, I., "Origins of Hydrocarbon Emissions from Diesel Engines," SAE Technical Paper 770259, 1977, doi:10.4271/770259.

AKNOWLEDGMENT

The optical engine experiments were performed at the Combustion Research Facility, Sandia National Laboratories, Livermore, CA. Support for this research was provided by the U.S. Department of Energy, Office of Vehicle Technologies and the Swedish Energy Agency. Sandia is a multi-program laboratory operated by Sandia Corporation, a Lockheed Martin Company for the United States Department of Energy's National Nuclear Security Administration under contract DE-AC04-94AL85000. The authors express their gratitude to David Cicone and Chris Carlen of Sandia National Laboratories for their great assistance and dedication with maintaining the research engine and the lasers used in these experiments.

APPENDIX

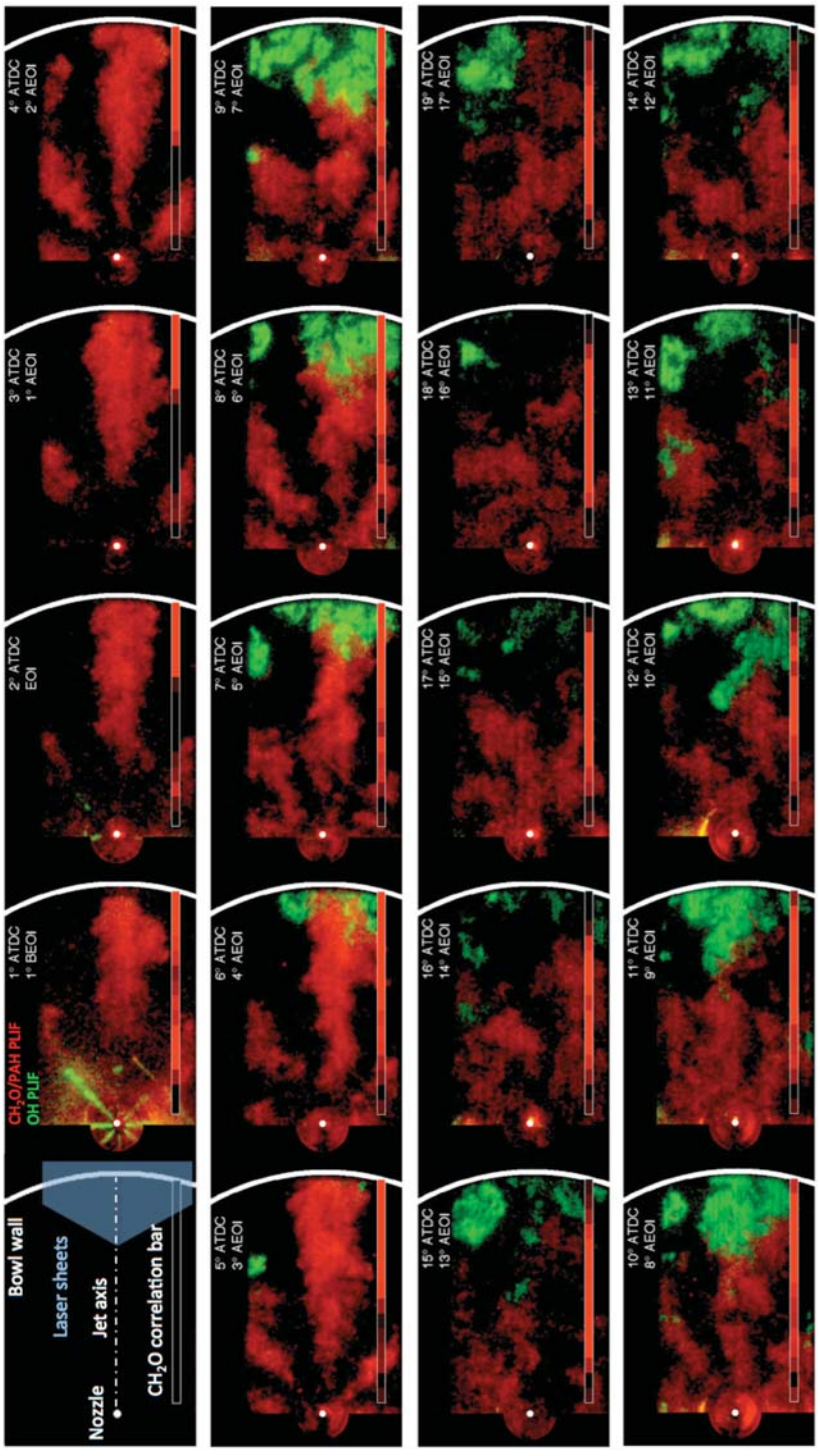

Figure A1. Combined results for OH-PLIF (green) and formaldehyde\|PAH PLIF (red) with single main injection only. The configuration is given in the first frame and the timings indicated are relative to TDC and the main EOI. The formaldehyde correlation bar indicates the similitude of the formaldehyde\|PAH PLIF signal to a formaldehyde reference spectrum. The darkest colors in the correlation bar indicate a low correlation with a formaldehyde reference spectrum whereas the brightest color indicate that the LIF signal has a high probability of being formaldehyde-LIF signal.

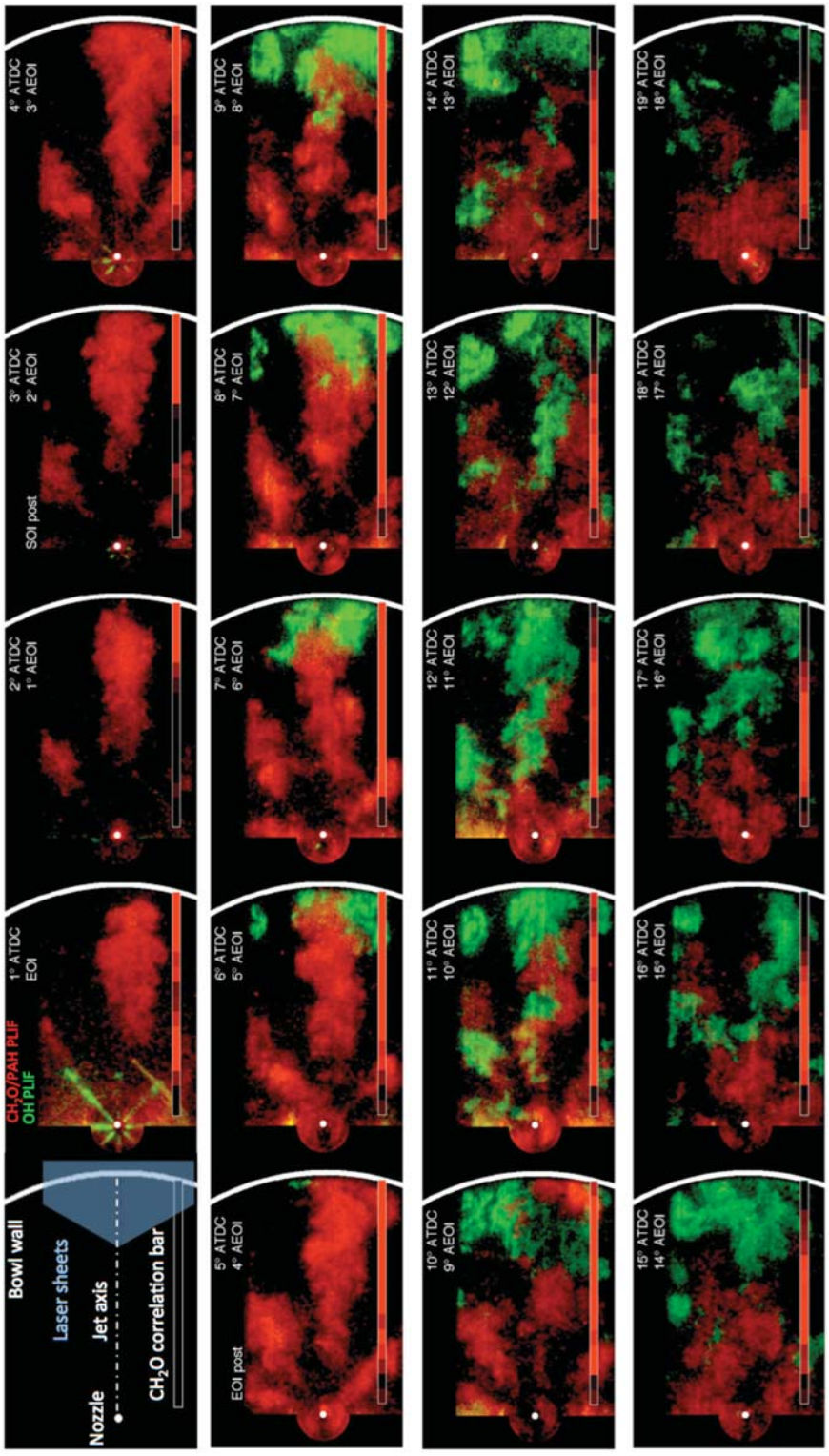

Figure A2. Combined results for OH-PLIF (green) and F\PAH PLIF (red) with main and small post- injection. See Fig. A1 for description of figure annotations.

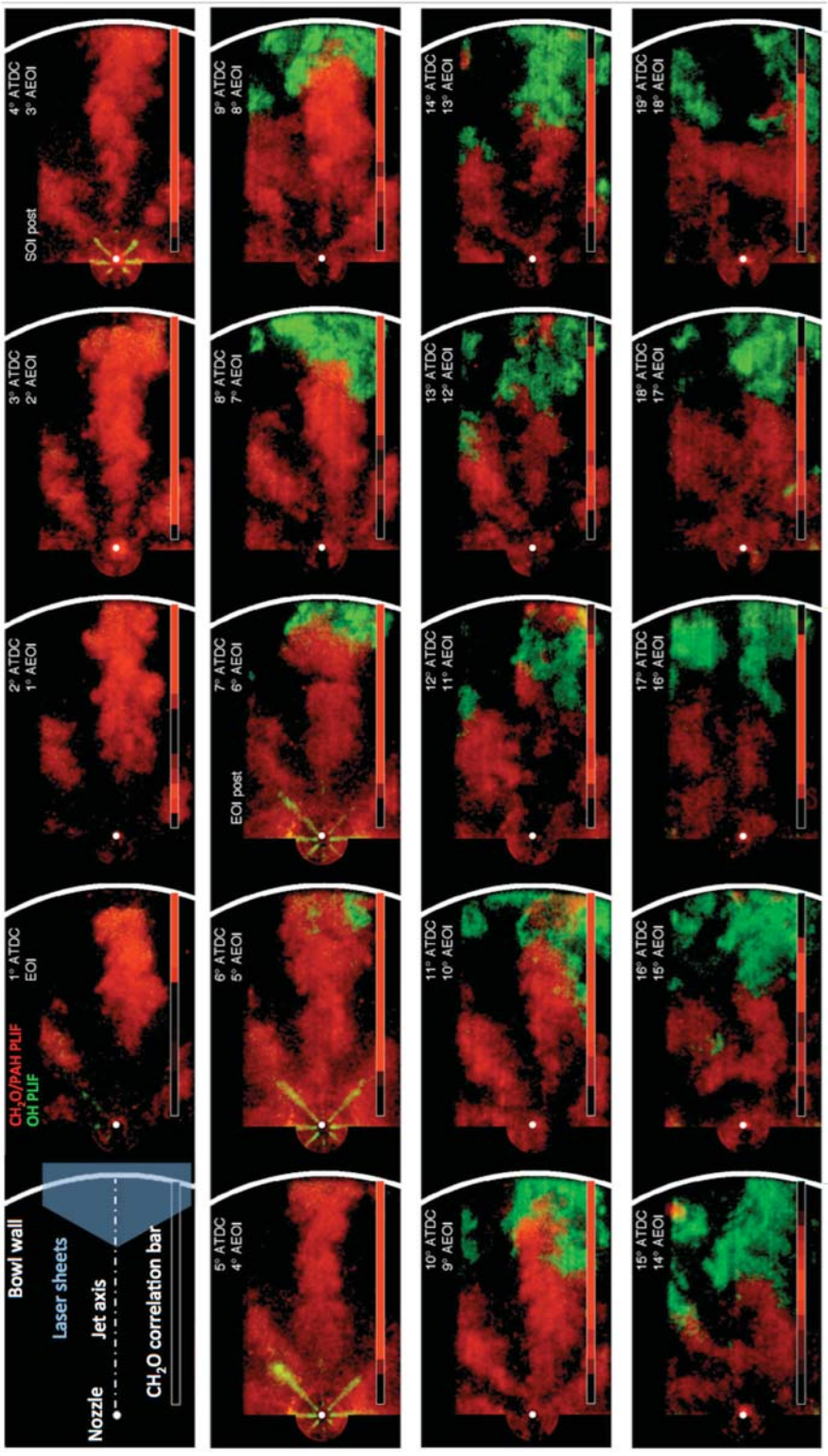

Figure A3. Combined results for OH-PLIF (green) and F\|PAH PLIF (red) with main and large post- injection. See Fig. A1 for description of figure annotations.

The Engineering Meetings Board has approved this paper for publication. It has successfully completed SAE's peer review process under the supervision of the session organizer. This process requires a minimum of three (3) reviews by industry experts.

ISSN 0148-7191

SAE Customer Service:
Tel: 877-606-7323 (inside USA and Canada)
Tel: 724-776-4970 (outside USA)
Fax: 724-776-0790
Email: CustomerService@sae.org
SAE Web Address: http://www.sae.org
Printed in USA

Paper IV

Influence of Jet-Jet Interactions on the Lift-Off Length in an Optical Heavy-Duty DI Diesel Engine

Clément Chartier, Ulf Aronsson, Öivind Andersson, Rolf Egnell and Bengt Johansson
Division of combustion engines, Lund University

ABSTRACT

Several investigations have reported that the lift-off length on diesel jets depends strongly on the ambient temperature. The spacing between adjacent jets is thereby expected to influence the lift-off length, as it affects the amount of hot, burned gases present between the jets. Measurements on an 8-hole nozzle in an optical diesel engine showed that the lift-off length can be transient at all times between the start and end of injection. This is attributed to varying in-cylinder temperature and especially to the presence of hot combustion products in the gases entrained into the jets. The effect of inter-jet angle on lift-off length was investigated using symmetric and asymmetric nozzle cups. Decreasing the inter-jet angle produces shorter lift-off length. The lift-off length showed a weaker dependence on the ambient temperature in the engine than predicted by an empirical expression established in a constant-volume combustion vessel. These findings indicate that experiments in such vessels may not capture all features of the conditions in engines. The lift-off length tended to be 15% shorter on the downswirl (leeward) side of the jet. A strong interaction between the effects of the inter-jet spacing and the inlet temperature on the lift-off length was found. All these effects are attributed to the presence of hot gases between the jets.

1. INTRODUCTION AND BACKGROUND

The past decade has seen a tremendous development in the diesel engine technology and performance [1]. Stringent emission legislations and concern about fuel economy as well as drivability have pushed forward advanced solutions for the compression ignition engine. Simultaneous reduction of NOx and soot emissions usually necessitates both after-treatment and in-cylinder solutions. The latter implies more flexible injection systems and the trend goes towards higher injection pressure capabilities and smaller nozzle orifice sizes. Smaller nozzle holes have been shown to increase air entrainment in jets. The direct effect is a lower local equivalence ratio in the jet. If this value falls below approximately 2 at the lift-off position, the soot production is limited or non-existent [2,3]. Smaller nozzle holes raise other issues, however. To maintain reasonable injection durations at high loads, the number of nozzle holes and the injection pressure must be increased in order to reach a

given injected fuel-mass target. Increasing the number of nozzle holes is not without consequences for the combustion process. It leads to a reduction in the inter-jet spacing. There is thus a trade-off between increasing the air entrainment in each jet through using smaller hole diameter and providing a greater volume of air between the jets.

The soot formation rate in quasi-steady jets is known to be influenced by the amount of air entrained in the jet [3,4]. The lift-off length is a major parameter in this context since a significant part of the total air entrainment in the jet takes place between the nozzle hole and the lift-off region. Numerous studies of the lift-off length in diesel combustion have been performed in constant-volume combustion vessels, see e.g. [3-9]. This type of device is able to accurately reproduce ambient conditions of most automotive diesel operating conditions in terms of temperature, density or degree of dilution. The simulated ambient conditions together with ample optical access give the possibility to investigate spray combustion in detail. However, since the volume of the vessel is larger than that of an actual engine combustion chamber, it does not reproduce some aspects of combustion in engines. First, the larger volume greatly reduces the effect of combustion on ambient pressure and temperature. Secondly, the large distance to the chamber walls removes the wall interaction effect. Finally, since single hole injectors are usually employed, there are no jet-jet interactions. Thus, whereas the combustion vessel is essential in the fundamental investigation of diesel jets, optical engines provide more realistic conditions for investigating jet-jet and jet-wall interactions.

The current study investigates the influence of inter-jet spacing on the lift-off length for quasi-steady jets, to gain insight into the effect of the burned gases recirculated upstream of the lift-off region. An empirical expression by Pickett et al. [9], based on combustion-vessel experiments, is used for lift-off length prediction:

$$H = CT_a^{-3.74}\rho_a^{-0.85}d^{0.34}U^1Z_{st}^{-1}, \qquad \text{(Eq. 1)}$$

where H is the lift-off length, C is a proportionality constant, Ta and ρa are the ambient temperature and density, d is the injector orifice diameter, U is the jet velocity (related to the injection pressure), and Zst is the stoichiometric mixture fraction. This expression indicates that the lift-off length for diesel jets depends strongly on ambient temperature. Due to the large number of jets in a much smaller volume, the influence of combustion on ambient gas temperature is greater in an engine combustion chamber compared to a quiescent combustion vessel. Therefore, comparison of engine and combustion vessel results can give insight into the effect of the on-going combustion on the temperature of the gas entrained into the jet. In a combustion vessel, Ta can reasonably be approximated as the temperature of the unburned gases at a given time. This is close to the temperature of the gases entrained in the jet upstream of the lift-off region. Ta is harder to define in engines since high-temperature burned gas is mixed in an unknown proportion to the unburned gas.

2. EXPERIMENTAL SETUP AND DIAGNOSTICS

2.1 Engine configuration

The presented investigations were performed on a six cylinder Scania D12 truck sized diesel engine modified for optical access using a Bowditch design. Engine specifications are given in Table 1. Only one cylinder was operational while the five others were motored.

The engine was operated at 5 bar IMEP and a speed of 1200 rpm. The inlet air was conditioned in terms of pressure and temperature by an independent two-stage screw-compressor and an electrical heater.

Two different injector configurations were used to study the influence of jet-jet interactions on the lift-off length. One symmetrical and one asymmetrical nozzle were employed, both with four holes. Fig. 1 shows the three resulting inter-jet angles: 45°, 90° and 135°. The images were acquired from below, through the optical piston. In the asymmetric configuration (right-hand side of Fig. 1) the 12 o'clock and 6 o'clock jets were used to study the 45° and 135° cases, respectively. In the symmetric configuration (left-hand side in Fig. 1) the 6 o'clock jet was used to study the 90° case. In addition to these nozzles, an eight hole nozzle was used in the initial stage of this investigation.

The engine was operated at approximately 20% load. Each injector configuration was investigated in nine different operating points in order to draw parallels with theoretical predictions of the lift-off length. Basic characteristics of the operating condition are given in Table 2. The engine coolant was preheated prior to start to ensure thermal stability of the combustion chamber.

Table 1. *Engine characteristics*

Engine Specifications	
Engine type	***Scania D12***
Cycle	***4-stroke***
Number of cylinders	***1***
Number of intake valves	***2***
Number of exhaust valves	***2***
Bore [mm]	***127***
Stroke [mm]	***154***
Displacement [L]	***1.95***
Compression ratio	***15.1:1***
Injector	
Type	***Cummins common-rail XPI***
Number of holes	***8/4***

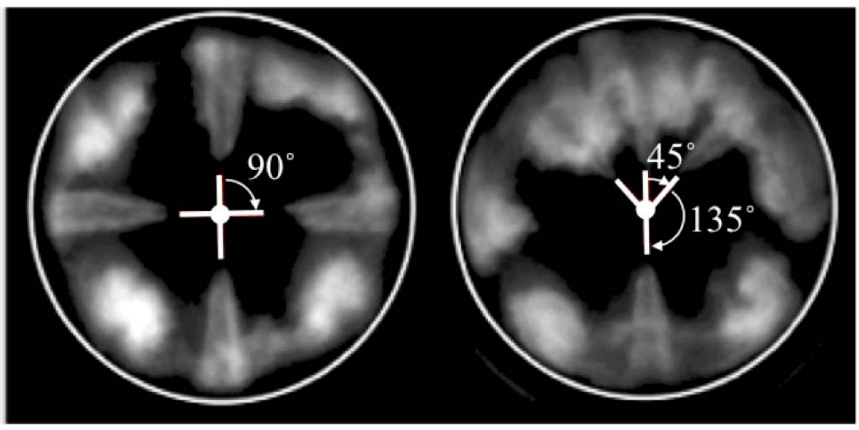

Fig. 1: *Symmetrical and asymmetrical nozzle configurations*

Table 2: *Operating conditions*

Operating conditions	
$IMEP_g$ [bar]	***5***
Engine coolant temperature [K]	***353***
Combustion phasing CA50 [CAD ATDC]	***10***
O_2 inlet [%]	***21***
Estimated motored TDC density [kg/m^3]	***27.4***
Fuel	***n-heptane***

The combustion phasing (CA50) was kept constant for all configurations by adjusting the injection timing in order to ensure similar ambient conditions between the different cases. To maintain a constant load, the injection duration was adjusted in accordance with the different injection pressure levels. Injection durations were on the order of 20 CAD, providing a long quasi-steady jet phase. The density at top dead center was kept constant by adjusting the level of boost pressure for the different inlet temperatures employed.

N-heptane was used as a fuel in this study because it is less sooting than diesel fuel and has a comparable cetane number. It differs from diesel in carbon chain length and boiling point but the overall trends in lift-off length observed with n-heptane are believed to be representative of diesel combustion.

2.2 Experiments

The experimental part of this lift-off length study is divided in two parts. First, the lift-off length was studied with an 8-hole nozzle injector. This configuration was used to study the lift-off stabilisation process. Based on these results, a second set of experiments was performed using both symmetrical and asymmetrical 4-hole injector nozzles in order to gain insight into the effects of jet-jet interactions on the lift-off length. The number of holes was reduced to make the asymmetric configuration possible. The test engine characteristics are the same in both cases, as described in Table 1.

In the second set of experiments, a three-level full factorial experiment was designed to separate the effects of the different factors (rail pressure, inlet temperature and inter-jet angle). Full factorial experiments test all factor combinations. Apart from separating the effects of the factors, these experiments also detect factor interactions. Interactions are common in complex systems and are not discovered in traditional experiments where only one factor is changed at a time. If interactions are present it means that the response to changes in one factor depends on the settings of another factor. All experiments were replicated four times for evaluating the experimental error. Each factor was tested at three levels, as shown in Fig. 2.

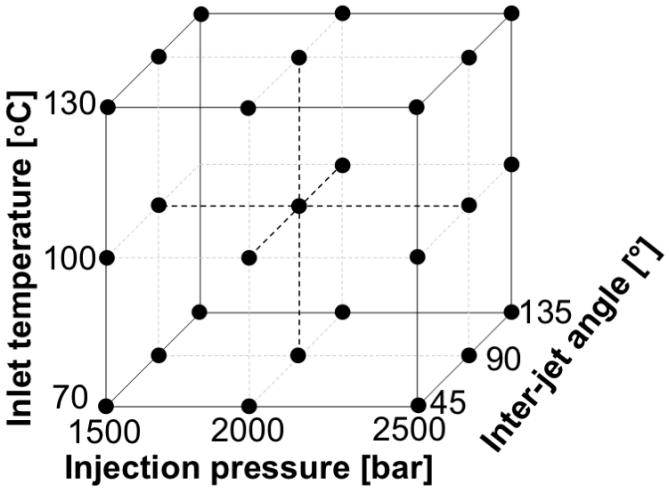

Fig. 2: *Three dimensional representation of the test matrix with tree factors and three levels.*

2.3 Optical diagnostics for lift-off length measurements

Both nozzle configurations were investigated by imaging natural luminescence with a Phantom V7.1 high speed video (HSV) camera. The lift-off length is defined here as the distance between the nozzle and the first appearance of OH radicals in the jet, i.e. the distance to the high temperature mixing-controlled reaction zone. OH-chemiluminescence images were recorded during the quasi-steady stage of the combustion, using an interference filter centred at 310 nm (FWHM 10 nm) in front of a 105 mm UV-Nikkor lens along with a Hamamatsu image intensifier.

Fig. 3 shows an example of a time resolved lift-off measurement from a single cycle with a symmetrical four-hole nozzle cup. The injector nozzle is located at the zero position of the y-axis and the piston bowl wall is 40 mm from the injector. The method for determining lift-off length from the image data is detailed in the next section. At auto-ignition, the flame is close to 15 mm downstream from the injector nozzle, and the lift-off length shortens rapidly to 10 mm. During most of the remaining injection time, the lift-off length oscillates around this position, a state that is also known as the quasi-steady jet phase.

The lift-off length was studied during the quasi-steady jet phase as it is representative of classical diesel combustion in heavy-duty applications. This is because the higher loads typical for such engines imply long injection durations and, thereby, a long quasi-steady phase. As HSV imaging had revealed that a quasi-steady lift-off was reached at 2 CAD ATDC for all cases, all subsequent lift-off determinations were made at this timing. The lift-off length becomes shorter by the end of injection, probably due to enhanced air entrainment at the injector closing and decrease in jet velocity.

When a suitable timing for the measurements had been determined using the HSV camera, the remaining lift-off length measurements were made using a Princeton ICCD camera, equipped with the same interference filter as above. The gain for the camera was set rather high to be able to image the relatively weak OH-chemiluminescence signal in the lift-off region. Strong soot luminosity in the downstream regions for some cases caused local saturation of the detector.

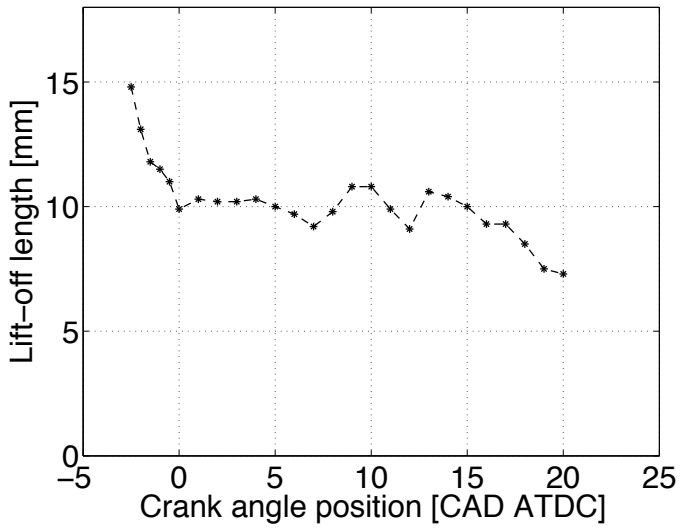

Fig. 3: *Example of time-resolved lift-off length measurement from start of combustion until end of injection. After a transient phase, the lift-off length stabilizes close to TDC.*

2.4 Image processing and data analysis

In each OH-chemiluminescence image, the jet was divided into two pie-shaped examination regions as illustrated in Fig. 4, for separate evaluation of upswirl and downswirl lift-off lengths. The upswirl side of the jet is the side facing the swirl flow. The downswirl side is the opposite side, i.e. the leeward side.

The precise location of the injector on each frame is essential for accurate lift-off length determination. A calibration target was used prior to the measurements but slight changes of the position of the camera relative to the engine can occur when firing the engine. A tracking algorithm was therefore developed in order to locate the injector precisely on each frame. Scattered light from the liquid portion of the jet made the sprays visible in the region nearest to the nozzle. By tracking the small bright lines along a calibration circle drawn around the centre of the image, it was possible to precisely locate the centre of the combustion chamber.

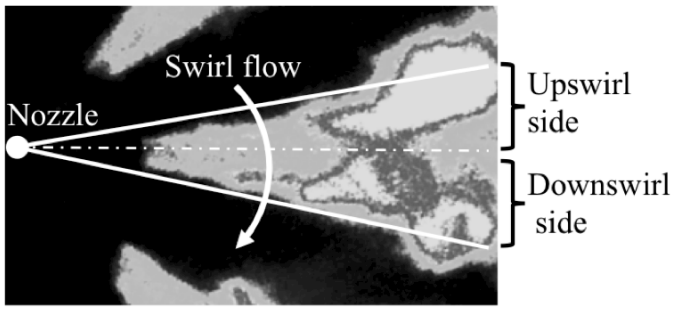

Fig. 4: *Schematic of the two pie-shaped examination regions for lift-off length evaluation on the upswirl and downswirl sides of the jet. The injector is located on the left-hand side of the image.*

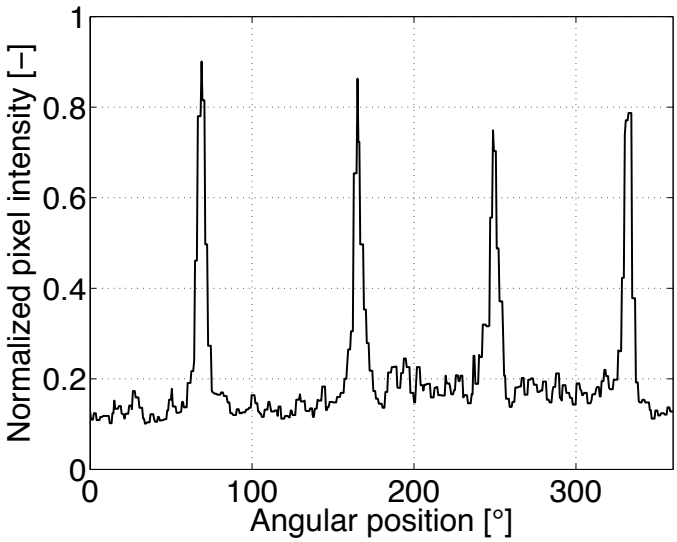

Fig. 5*: Pixel intensity along the calibration circle used to determine the exact nozzle position in every frame. The peaks represent the locations of the liquid portions of the jets.*

An example of pixel intensity along the calibration circle is given in Fig. 5. The angles where the jets intersect the circle are clearly visible on the plot. By extracting the coordinates of the four peak values we obtain four points along the perimeter of the circle. By calculating the equations of the two lines joining the diametrically opposed points, the intersecting point can be determined. This point reveals the actual nozzle position. The new coordinates for the centre are fed to the analysis of the next frame in order to place the centre of the calibration circle closer to the nozzle position.

The scattered light from the liquid sprays is useful in the nozzle tracking procedure, but it can interfere with the lift-off length evaluation since the scattered light intensity is comparable to the OH-chemiluminescence signal level. Therefore, the liquid spray luminosity would pass through the image processing and be present on the final images. A short distance along the jet centre axis was therefore masked in order to eliminate this source of error during lift-off calculations. The mask was applied close to the nozzle position in order to prevent the masking of actual OH signal in short lift-off length cases.

First, the images were digitized by setting all pixels with signal exceeding a certain threshold level to white, and the remaining pixels to black. The threshold was determined using the Matlab function *graythresh*, which is based on Otsu's method. The lift-off length was then calculated by processing each pie-shaped examination region radially from the nozzle toward the bowl wall. The number of white pixels was extracted as a function of radial distance. Fig. 6 presents an example of white pixel count as function of downstream distances from the nozzle.

Some signal from the liquid spray is visible at first but the actual lift-off region appears clearly with an abrupt increase in pixel counts. Given the steep slope of the curve, a threshold method can be used without introducing large errors in the final lift-off length. The threshold was set to 15 pixel counts. Finally, the 15° angle between the firedeck and the jets' central axes was taken into account to correct for the line-of-sight visualization of the jets.

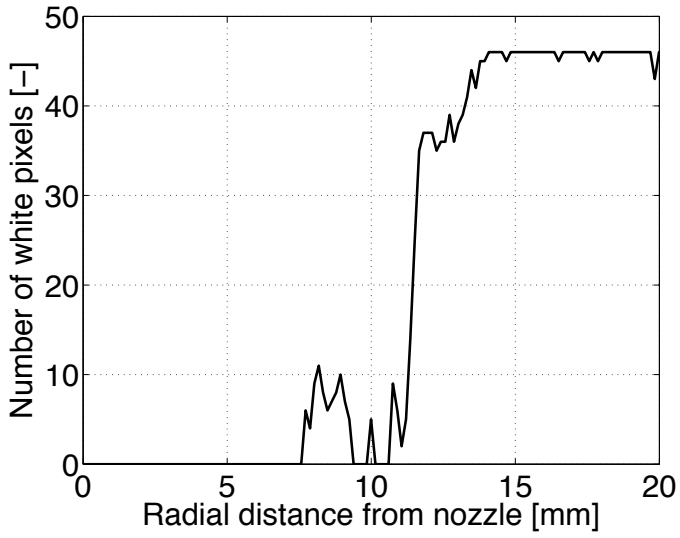

Fig. 6: *Pixel intensity as function of radial distances from the nozzle for lift-off length determination.*

3. RESULTS AND DISCUSSION

3.1 Flame lift-off length, a moving target

Lift-off length measurements were first performed using an 8-hole injector cup. Results for single cycles are presented in Fig. 7 for different injection pressures. The data are plotted from the start of combustion (positive heat release rate value) to the end of injection for each case. The relative positions of the curves do not follow any trend caused by the injection pressure. However, the evolution of the lift-off length position is similar for all five cases.

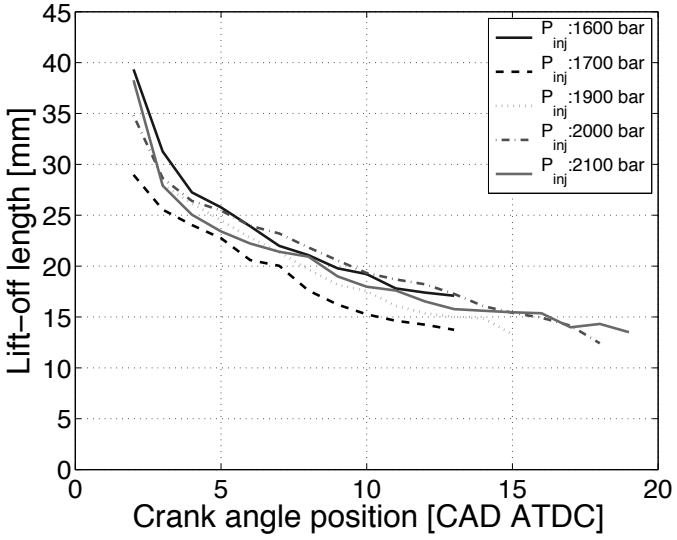

Fig. 7: *Lift-off length measurements for single cycles at several injection pressure levels. The data are plotted from the start of combustion (positive heat release rate value) to the end of injection for each case.*

The start of combustion takes place in the downstream regions, in the vicinity of the bowl wall, and thereafter the lift-off position travels back towards the injector. In this configuration, no quasi-steady phase of the lift-off length is seen. This can be interpreted as an effect of temperature variation in the entrained gas due to jet-jet interactions.

Fig. 8 shows the evolution of the global in-cylinder gas temperature for the same cases calculated using the Ideal Gas Law and the sampled in-cylinder pressure data. Variations of squish height due to pressure forces during compression were taken into account when calculating the volume trace [10]. The temperature data are presented only for the timeframe between the start of combustion and the end of injection, the relevant period when investigating lift-off. As expected, the global temperature increases during the timeframe of observation due to the ongoing combustion. As previously observed for the lift-off length data, the relative positions of the curves do not reveal any effects of interest caused by the injection pressure, but the general trends are of interest.

In order to calculate the mean temperature of the unburned gas, the cylinder content can be divided into two zones; burned and unburned regions [11]. Assuming isentropic compression, the temperature of the unburned zone, T_{unb}, *is given by*

$$T_{unb} = T_{soc}\left(\frac{p}{p_{soc}}\right)^{\frac{n-1}{n}}, \qquad \text{(Eq. 2)}$$

where p is the in-cylinder pressure, T_{soc} and p_{soc} the global temperature and cylinder pressure at the start of combustion, and n the polytropic exponent. The latter was determined from the slope of the in-cylinder pressure trace during compression (in a log p – log V diagram).

By using Eq. 1 backwards it is possible to calculate which T_a is needed to produce the measured lift-off length. This temperature is referred to as T_{needed} and is presented in the plots of Fig. 9 together with the calculated global and unburned gas temperatures for one of the injection pressure cases. The other cases show a similar behavior and, therefore, only one case is presented for clarity.

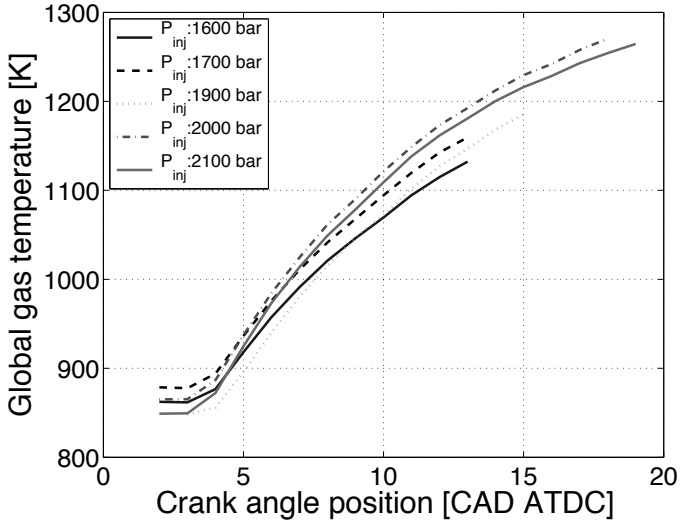

Fig. 8: *Global in-cylinder gas temperature for the different cases. The temperature data are presented only for the timeframe between the start of combustion and the end of injection.*

As seen in Fig. 9, Eq. 1 indicates that the temperature needed to obtain the measured lift-off length, T_{needed}, is close to the global temperature and far from the unburned temperature. Note that T_{needed} is always higher than the global temperature. This observation implies that the gas entrained in the jet along the lift-off distance has a temperature between the global and burned gas temperatures.

This comparison of gas temperatures indicates that burned gases constitute a non-negligible portion of the gas entrained prior to the lift-off region. The gap between T_{needed} and T_{global} in Fig. 9 is decreasing with time during combustion since the fraction of burned gases in the cylinder is increasing. The global temperature thereby gradually approaches the burned gas temperature.

According to this analysis, the decreasing trend in lift-off length observed in Fig. 7 seems to be related to the temperature variation of the entrained gases. It could be argued that this trend could be caused by the behavior of the injector needle, which could affect the rate of injection and therefore other factors in Eq. 1, such as the jet velocity or even the effective hole diameter. However, taking into account the much higher exponent for T_a in Eq. 1, the lift-off length variations seen in Fig. 7 are more likely to be coupled to the large variations of this factor during combustion.

These results show the influence of the temperature of the gas entrained upstream of the lift-off region, which raises the issue of jet-jet interactions. As neighbouring jets collide, i.e. in the region where their recirculation vortices meet along the bowl wall, burned gases are directed towards the centre of the combustion chamber, between the jets. The path taken by burned gases towards the nozzle is shorter the narrower the jets are spaced. This is expected to influence the rate at which burned gas travels towards the nozzle and is mixed into the jet upstream of the lift-off region.

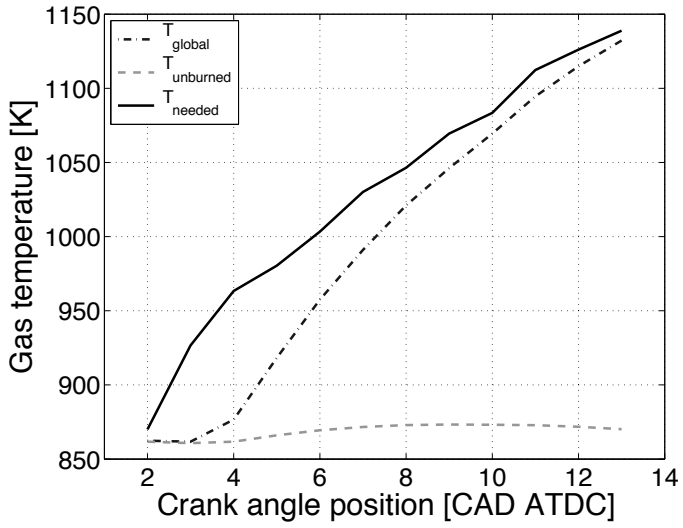

Fig. 9: *Global, unburned and needed temperature for the observed lift-off length at 1600 bar injection pressure. The global temperature is obtained by applying the ideal gas law to the sampled in-cylinder pressure whereas the unburned gas temperature is calculated using the assumtion of an isentropic compression of the unburned gas [11]. The needed temperature is obtained by using Eq. 1 and experimental lift-off length measurements.*

Previous investigations have indicated that the lift-off is not stabilized by flame propagation under diesel conditions. It rather seems to stabilize by a process closer related to auto-ignition [9,12]. Shadowgraph imaging revealed that reservoirs of hot, burned gases are formed at the periphery of the jet. These were believed to aid the lift-off stabilization [12]. Factors affecting the temperature of the burned gases have also been shown to affect the lift-off length [13]. If these conclusions are correct, the inter-jet spacing is expected to affect the lift-off length through its effect on the amount of burned gases between the jets. The experiments in the following sections test the hypothesis that the inter-jet angle affects the lift-off length through this mechanism.

3.2 Effect of inter-jet spacing on lift-off length

The experimental setup used for this part differs from the previous section in terms of injector nozzle. In order to investigate the inter-jet spacing effect on the lift-off length the symmetrical and asymmetrical nozzles described in Fig. 1 were employed. The results presented in Fig. 10 show the lift-off length obtained by varying the inter-jet angle for a fixed inlet temperature and fixed injection pressure. Each point is the average of four measurements and the error bars represent the standard deviation of the data. The effect of inter-jet spacing on the lift-off length is significant. Decreasing the angle between the jets leads to shorter lift-off lengths. This trend supports the hypothesis that jet-jet proximity enhances the recirculation of hot gases.

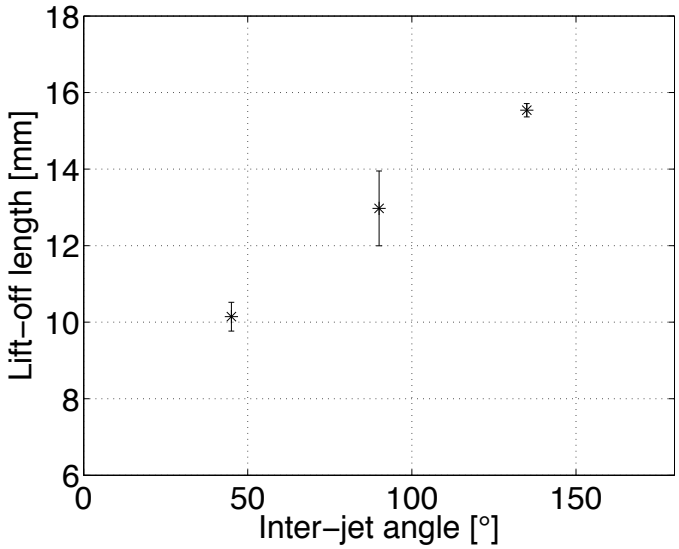

Fig. 10: *Lift-off length as a function of inter-jet angle for fixed injection pressure and inlet temperature conditions. The error bars represent the standard deviation of the measurement data.*

3.3 Inlet temperature effect on lift-off length

The inlet temperature affects the global in-cylinder temperature. Fig. 11 shows how the lift-off length varies with the global temperature, determined at 2 CAD ATDC. The global temperature is used on the abscissa rather than the inlet temperature, to facilitate comparison with Eq. 1.

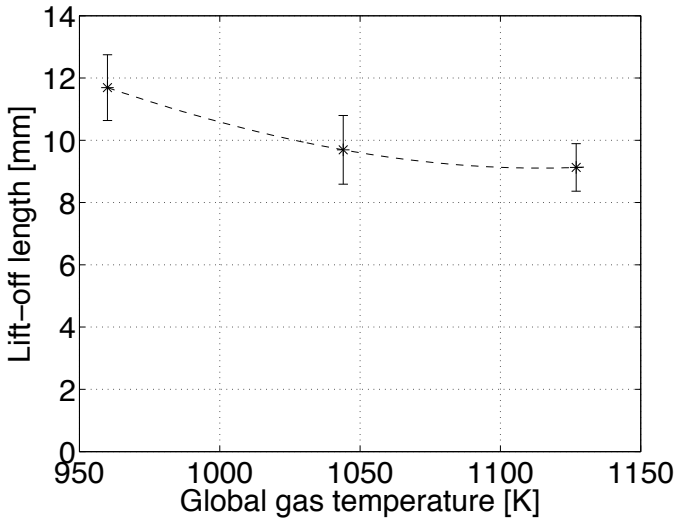

Fig. 11: *Lift-off length as a function of the global gas temperature. The temperature is determined for the timing of image acquisition, i.e. 2 CAD ATDC.*

As expected, the lift-off length shortens with increasing temperature, but the effect is weaker than Eq. 1 predicts. Instead of a temperature exponent of -3.74, the trendline in Fig. 11 has an exponent of -1.55. The standard deviation of the measurement data is relatively large and shows how variable the lift-off stabilisation process is. The data presented in Fig. 11 were obtained under fixed injection pressure and inter-jet spacing conditions.

A plausible explanation of the reduced effect of global gas temperature on lift-off length in the engine is that the global temperature is too general a value compared to the actual temperature of the gas entrained in the upstream regions of the jets. Since burned gases are mixed with fresh air, the local temperature of the entrained gases is expected to be higher than the ambient value.

The difference between global temperature and the one needed to produce the observed lift-off is large. Calculations show that on average, throughout the whole test matrix, 108 K and 85 K higher temperature than global are needed to obtain the measured lift-off lengths for the upswirl and downswirl sides, respectively, at the measurement timing. The constant parameter C in Eq. 1 is calculated based on data from combustion vessel experiments at similar conditions [14].

3.4 Comparison between predicted and measured lift-off length

Fig. 12 shows a scatter plot of measured lift-off lengths versus calculated ones using T_{global} for the current study. If Eq. 1 were applicable to the optical engine data, all points would collapse onto a line with slope 1, which they clearly do not.

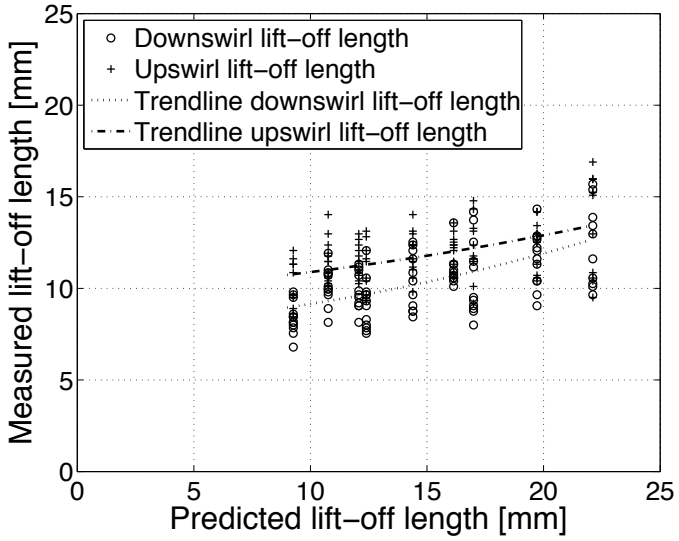

Fig. 12: *Comparison between the measured and predicted lift-off length for all conditions investigated in the factorial study.*

The large variations in the lift-off length data illustrate how sensitive the stabilization process is to disturbances affecting the entrained gas temperature. These phenomena are not completely reproduced in a combustion vessel and can explain the differences observed.

3.5 Asymmetrical lift-off length

Asymmetrical lift-off lengths were observed in the measurement data. Fig. 13 shows a boxplot to compare the distribution and central tendency of the data. The lower and upper ends of the boxes represent the first and third quartiles, respectively. The horizontal line in the middle is the median. The vertical lines, called whiskers, represent the region within 1.5 times the interquartile range over and under the box. Data outside of this range are indicated here with asterisks beyond the whiskers.

The distributions of the upswirl and downswirl lift-off lengths have similar degrees of dispersion and skewness. However, the median value for downswirl measurements is approximately 15% lower than for the upswirl dataset. A similar trend was reported in [15] and was hypothetically attributed to the presence of swirl in the test engine. In that study, the asymmetry was evaluated to be on average 7% with a swirl number of 0.5. In the present study, with a swirl number of 2.18, the asymmetry is close to 15% on average. A plausible explanation for this trend is that the swirl field displaces hot gases around the jet. As mentioned in the experimental hypothesis, Pickett *et al.* [12] suggested that reservoirs of hot gases surrounding the jet stabilize the lift-off length by a process relying on autoignition. In that picture, the asymmetric lift-off would be explained by more hot gases being present on the downswirl side, facilitating autoignition. This is in line with the observation that burned gases affects the lift-off length.

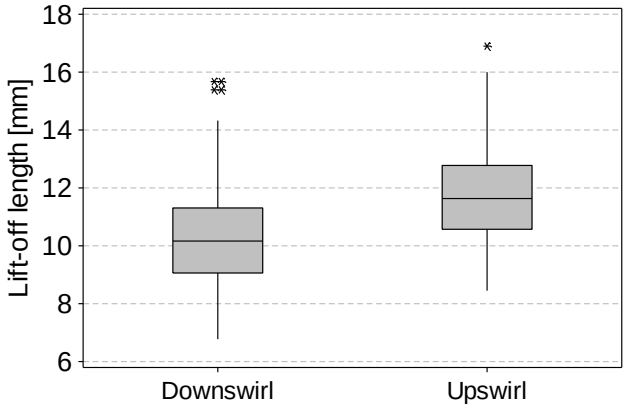

Fig. 13: *Boxplot representation of the lift-off length distribution on the downswirl and upswirl side of the jet.*

3.6 Interactions between inlet temperature and inter-jet spacing

Fig. 14 shows a strong interaction between the inter-jet angle and the inlet temperature on the flame lift-off length. At close inter-jet spacing, the effect of the inlet temperature is surprisingly low. The variation of the lift-off length is very limited despite the large inlet temperature range studied. At large inter-jet spacing, in contrast, the lift-off length becomes very sensitive to the variations in inlet temperature. The plotted data show that the effect of either of these factors on the lift-off length depends on the setting of the other. A plausible explanation is that the gas temperature experienced by the jet at close inter-jet spacing is dominated by the burned gas temperature. The temperature variation in the unburned gas thereby becomes incapable of affecting the lift-off length.

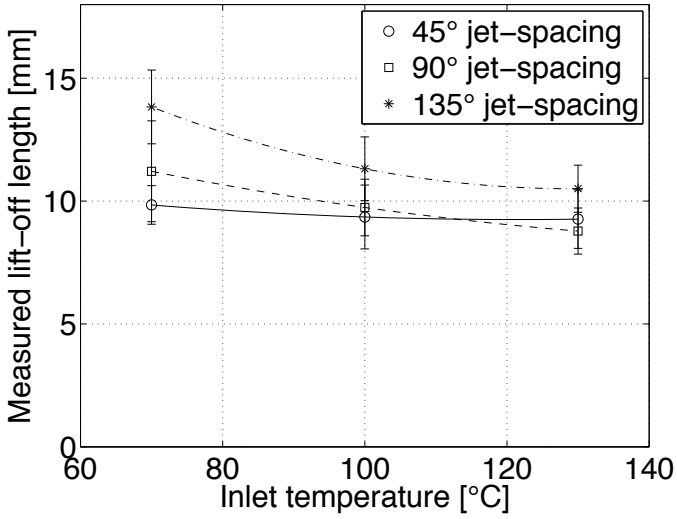

Fig. 14 *Lift-off length vs. inlet temperature and inter-jet angle.*

4. CONCLUSIONS

Lift-off measurements were conducted in an optical heavy-duty diesel engine using several hardware configurations in order to investigate the influence of jet-jet interactions on the lift-off length. The main conclusions can be summarized as follows:

- When using an 8-hole nozzle the lift-off length varies during combustion. It shortens from its initial position, at start of combustion, until the end of injection. Calculations and measurements of the lift-off length for different cases indicate that a significant amount of burned gases is entrained in the jet upstream of the lift-off region.
- Decreasing the angle between jets leads to shorter lift off length. This observation agrees with the hypothesis that hot gas from neighbouring jets is entrained in the lift-off region. This observation is useful for practical applications since the results can be related to the design of diesel combustion systems.
- The lift-off length tends to be longer on the upswirl side of the jet compared to the downswirl side by 15% on average. This is suspected to be caused by swirl-induced displacement of the hot gas reservoirs at the lift-off region to the downswirl side.
- Increasing the ambient gas temperature leads to shorter lift-off length, as expected. However, the influence of the inlet temperature was less important than theoretical calculations would predict. This observation underlines the impact of hot burned gases entrained in the jet prior to the lift-off region.
- A strong interaction was found between inlet temperature and inter-jet spacing since they both influence the temperature of the entrained gases upstream of the lift-off region.
- The poor correspondence between predicted and measured lift-off length shows that some aspects of combustion in engines, such as jet-jet interactions, are not reproduced in a combustion vessel. This has consequences for the lift-off predictions in engines.

ACKNOWLEDGMENTS

The authors gratefully acknowledge the Swedish Energy Agency for their support.

REFERENCES

1. **Andersson, Ö.,** ”Diesel Combustion”, in Lackner, Winter, Agarwal (Eds.): Handbook of Combustion Vol. 3, pp. 415-440, Wiley-VCH Verlag GmbH & Co. KGaA, Weinheim, 2010.
2. **Chartier, C., Aronsson, U., Andersson, Ö., Egnell, R., Collin, R., Seyfried, H., Richter, M. and Aldén, M.** Analysis of smokeless spray combustion in a heavy duty diesel engine by combined simultaneous optical diagnostics. SAE paper 2009-01-1353, 2009.
3. **Pickett, L.M. and Siebers, D.L.** Soot formation in diesel fuel jets near the lift-off region. Proceedings of IMechE JER03505 vol.7: pp 103-129, 2006.
4. **Pickett, L.M., Caton, J.A., Musculus, M.P.B. and Lutz, A.E.** Evaluation of the Equivalence Ratio-Temperature Region of Diesel Soot Precursor Formation Using a Two-Stage Lagrangian Model. Proceedings of IMechE IJER00606 vol 7: pp349-370, 2006.
5. **Siebers, D.L. and Higgins,B.** Flame Lift-Off on Direct-Injection Diesel Sprays Under Quiescent Conditions. SAE paper 2001-01-0530, 2001.

6. **Higgins, B. and Siebers, D.L.** Measurement of the Flame Lift-Off Location on DI Diesel Sprays Using OH Chemiluminescence, SAE paper 2001-01-0918, 2001.
7. **Pickett, L.M., Siebers, D.L. and Idicheria,C.A.** Relationship Between Ignition Process and the Lift-Off Length of Diesel Fuel Jets. SAE paper 2005-01-3843, 2005.
8. **Idicheria, C.A. and Pickett, L.M**. Formaldehyde Visualization Near Lift-Off Location in a Diesel Jet. SAE paper 2006-01-3434, 2006.
9. **Pickett, L.M., Siebers, D.L., and Idicheria,C.A.** Relationship Between Ignition Process and the Lift-Off Length of Diesel Fuel Jets. SAE paper 2005-01-3843, 2005.
10. **Aronsson, U., Solaka, H., Chartier, C., Andersson, Ö., Johansson, B.** Impact of Mechanical Deformation Due to Pressure, Mass, and Thermal Forces on the In-Cylinder Volume Trace in Optical Engines of Bowditch Design. SAE technical paper 2011-26-008
11. **Egnell, R.** Combustion Diagnostics by means of Multizone Heat Release Analysis and NO Calculation, SAE paper 981424, 1998.
12. **Pickett, L.M., Sanghoon , K., Persson, H. and Andersson, Ö.** Diesel fuel jet lift-off stabilization in the presence of laser-induced plasma ignition. Proceedings of the Combustion Institute 32: pp.2793-2800, 2009.
13. **Persson, H., Andersson, Ö. and Egnell, R.** Fuel effects on flame lift-off under diesel conditions. Combustion and Flame **158** pp.91-97, 2011.
14. Lift-off length database available online at the Engine Combustion Network. (http://www.sandia.gov/ecn/)
15. **Musculus, M.P.B**. Effects of the In-Cylinder Environment on Diffusion Flame Lift-Off in a DI Diesel Engine, SAE paper 2003-01-0074, 2003.

Paper V

SAE draft #12FFL-0272

Air-entrainment in wall-jets using SLIPI in a heavy-duty diesel engine

Clément Chartier, Yann Gallo, Öivind Andersson, Bengt Johansson
Division of combustion engines, Lund University

Johan Sjöholm, Elias Kristensson, Mattias Richter, Marcus Aldén
Division of combustion physics, Lund University

ABSTRACT

Mixing in wall-jets was investigated in an optical heavy-duty diesel engine with several injector configurations and injection pressures. Laser induced fluorescence (LIF) was employed in non-reacting conditions in order to quantitatively measure local equivalence ratios in colliding wall-jets. A novel laser diagnostic technique, Structured Laser Illumination Planar Imaging (SLIPI), was successfully implemented in an optical engine and permits to differentiate LIF signal from multiply scattered light. It was used to quantitatively measure local equivalence ratio in colliding wall-jets under non-reacting conditions. Mixing phenomena in wall-jets were analyzed by comparing the equivalence ratio in the free part of the jet with that in the recirculation zone where two wall-jets collide. These results were then compared to ϕ predictions for free-jets. It was found that under the conditions tested, increased injection pressure did not increase mixing in the wall-jets. Comparisons with free-jet predictions further indicated that mixing in wall-jets is less effective than in free-jets for identical conditions and downstream distances. The confined nature of the wall-jet in the optical engine is suspected to be the reason for these observations. A rapid leaning-out of the jet after end of injection was observed for all cases, but this enhanced mixing was not transmitted to the wall-jet.

INTRODUCTION

Soot formation in diesel engines is highly related to the local fuel-to-air equivalence ratio between fuel and air in the fuel jet. Generally, the more air that is entrained in a diesel jet, the weaker the soot formation is [1]. Extensive research has been performed on air-entrainment in fuel jets at high injection pressures leading to a general understanding of the mechanisms involved [2-6]. The main focus of these previous works has been to estimate the local stoichiometry in the jet at the lift-off region in order to predict the soot formation tendency. This relies on the observation that oxygen-entrainment in the jet downstream of the lift-off region is decreased compared to the upstream region of the jet, due to the presence of the high temperature diffusion flame that surrounds the jet and consumes most of the entrained oxygen. However, oxygen entrainment is also important in the parts of the jet that are downstream of the lift-off region to ensure efficient oxidation, which relies upon access to O_2 and OH radicals [7].

Furthermore, the diesel jet geometry is complex due to the presence of the bowl-wall in the downstream region, typically 40 mm from the nozzle in a heavy-duty diesel engine. When the jet reaches the bowl wall it is diverged into wall-jets. As the wall-jets travel along the bowl wall, they are confined between the piston floor and the firedeck, roughly 15 mm apart at top dead center in a heavy-duty diesel engine. When two neighboring wall-jets eventually collide they form a recirculation zone, as will be shown later in the results section.

Although most air-entrainment investigations in combustion vessels are performed on free jets, Bruneaux *et al.* placed a flat wall about 30 mm downstream of the nozzle to study the air-entrainment in an impinging fuel jet [8]. Results showed an increased air-entrainment after the wall impact compared to the free jet. Furthermore, higher equivalence ratios were observed in the free-jet just before the wall impact. At an injection pressure of 1500 bar, these two effects were equally strong, thus canceling one another and leading to the same total-air-entrainment as in a free-jet. However, at 2000 bar injection pressure the air-entrainment after the wall impact was substantially enhanced, resulting in higher total air entrainment as compared to a free-jet.

The current study aims to determine if similar trends can be observed in a diesel engine. Two hypotheses are investigated. The first enhanced mixing in the wall-jet and recirculation zone could be due to increased turbulence. Increasing injection pressure would increase turbulence in the wall-jet due to the higher impact momentum and higher average flow speeds. If this hypothesis was to be confirmed, the same effect would be observed in the optical engine as in the combustion vessel used by Bruneaux *et al.* [8].

The second hypothesis is that the effects observed in the combustion vessel are mostly due to an increase in surface-area of the fuel-jets after interaction with the flat wall. A larger area available for mixing would then imply a greater air-entrainment rate. If this is a major mechanism behind the trends observed in the combustion vessel the effect will be substantially weaker in the engine, as the jet is more confined than in a combustion vessel and the surface area of the jet cannot increase as much.

In order to test the above hypotheses, experiments were carried out in an optical engine where the wall-jet is expected to behave essentially as it does in a real engine. Injection pressure and inter-jet angle were varied to observe their effects on air-entrainment in the wall-jet. The local equivalence ratio was measured using quantitative laser induced fluorescence (LIF) of a fuel tracer (acetone). A novel technique called Structured Laser Imaging Planar Illumination (SLIPI) [9,10,11] was used in order to remove multiply scattered light from the actual fluorescence signal.

EXPERIMENTAL SETUP

Optical engine and operating conditions

The presented investigations were performed on a six cylinder Scania D12 truck sized diesel engine modified for optical access using a Bowditch design. Engine specifications are given in Table 1. Only one cylinder was operational while the five others were motored. The engine was operated at a speed of 1200 rpm. The inlet air was conditioned in terms of pressure and temperature by an independent two-stage screw-compressor and an electrical heater. The inlet oxygen concentration was lowered below 5% by leading the exhaust gases from an external diesel furnace to the inlet of the optical engine, producing

non-reacting jets. As reacting jets would produce a range of fluorescing species interfering with the fuel signal, using non-reacting jets was necessary to quantitatively determining the mixing.

Two different injector configurations were used to study the effect of inter-jet spacing on mixing in the recirculation zones. One symmetrical and one asymmetrical nozzle were used, both with four holes. Figure. 1 shows schematics of the fuel jets. The resulting inter-jet angles were 45°, 90° and 135°. The latter was not investigated in this study.

Apart from inter-jet angle, the effect of injection pressure was also studied. Injection commands were adjusted to ensure identical start and end of injection for the different injection pressures. These parameters were confirmed using scattered laser light on the liquid fuel at the nozzle exit. Inlet temperature was set at 398 K in order to ensure complete vaporization of the fuel when port-injection was used for calibration purposes, as explained below. The main operating conditions are summarized in Table 2. A diesel furnace working at stoichiometric conditions provided external exhaust-gas recirculation.

Table 1. *Engine characteristics*

Engine Specifications	
Engine type	**Scania D12**
Cycle	**4-stroke**
Number of cylinders	**1**
Number of intake valves	**2**
Number of exhaust	**2**
Bore [mm]	**127**
Stroke [mm]	**154**
Displacement [dm^3]	**1.95**
Compression ratio	**15.1:1**
Swirl number	**2.18**
Injector	
Type	**Cummins common-rail**
Number of holes	**4**
Orifice diameter [µm]	**100**
Inter-jet angles [°]	**45 and 90**

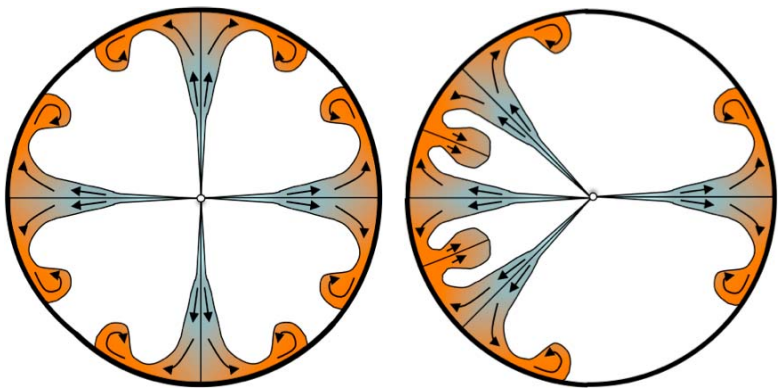

Figure 1: *Schematic of the symmetrical (left) and asymmetrical (right) nozzle configurations.*

Table 2 *Operating conditions*

Operating conditions	
Engine speed	**1200 rpm**
Inlet temperature	**398 K**
Inlet pressure	**1.6 bar (a)**
Inlet O_2	$<$ **5%**
Actual start of injection	**-7.5 CAD ATDC**
Actual end of Injection	**7.7 CAD ATDC**
Injection pressure	**1500-2000-2500 bar**
Fuel	**90% iso-octane/10% acetone**
Estimated TDC temp.	**896 K**
Estimated TDC density	**21 kg/m^3**

Fuel-tracer planar laser induced fluorescence

Planar LIF is a common method to measure the fuel distribution in a combustion engine. Most commercial fuels contain several species that naturally fluoresce upon UV excitation and that can be used for LIF measurements [12]. However, when several species with different transport, evaporation, quenching and fluorescence properties fluoresce at the same time, quantification of the fluorescence intensities in order to get local equivalence ratios is extremely difficult. LIF measurements of commercial fuels are thus most often limited to qualitative measurements.

Therefore, fuel tracer LIF, where a florescent tracer is added to a non-fluorescing base fuel, is usually employed for quantitative measurements. This allows control of the tracer concentration, and simplifies the pressure and temperature dependencies of the signal. A comprehensive summary of quantitative fuel tracer-LIF in practical combustion systems can be found in [13].

Acetone was selected as fuel tracer in the present study due to its low pressure dependency on the combined absorption cross-section and fluorescence quantum yield [12]. The injection event occurred around top-dead center in order to further reduce pressure and volume variations during the measurements. Furthermore, acetone is not prone to pyrolysis at temperatures below 1000 K [14]. The experimental conditions in this setup fulfill this criterion. Furthermore, the low intake oxygen mole fraction of the charge was used together with iso-octane as fuel to ensure non-reacting conditions and to avoid oxygen quenching of the acetone LIF signal.

Only a brief overview of the optical measurement techniques employed will be given in this section. Details about the laser-diagnostic aspects of the present investigation are presented in [11].

In order to relate the fluorescence signal intensity to fuel-air ratios, calibration measurements were conducted using port-injected fuel (90% iso-octane/10% acetone). Corrections for ambient pressure and temperature as well as laser fluence variations were made account to ensure the fidelity of the quantitative measurements.

Structured Laser Illumination Planar Imaging (SLIPI)

Quantitative fuel-tracer LIF measurements are difficult to perform in combustion engines. One important issue concerns the subtraction of background that is due to light scattered around the combustion chamber. Scattered laser light gives rise to secondary fluorescence from walls and regions outside the laser sheet, which is not easily subtracted as it overlaps spectrally with the signal. Detection of this secondary fluorescence will lead to inaccuracy in the measurements.

By using Structured Laser Illumination Planar Imaging (SLIPI) it is possible to remove these scattered light effects. SLIPI is based on laser sheets that are spatially modulated with a sinusoidal pattern, $\mathrm{E_{laser}} = \mathrm{E_0}\,(1 + \sin(\omega x + p))$. The detected signal, I_1, from one laser sheet is then

$$\mathrm{I_1} = \mathrm{I_B} + \mathrm{I_S}[1 + \sin(\omega x + \mathrm{p_1})] \qquad (1)$$

where I_s is the amplitude of the modulation and I_B is the background offset arising from e.g. from scattering and reflections. Figure 2 shows an example of a raw data image with a modulated laser sheet in homogeneous conditions (port fuel injection).

Combining three measurements with different phases, i.e. p = 0°, 120°, 240°, it is possible to reconstruct how the image would look without the modulation. More significant, however, is that I_s can also be retrieved from these three measurements according to Eq. 3 [11]. SLIPI can thus suppress the background I_B from the images and reveal the signal originating from the laser sheet without any background due to scattered or reflected light.

$$I_s = \frac{\sqrt{2}}{3}\sqrt{[(I_1 - I_2)^2 + (I_1 - I_3)^2 + (I_2 - I_3)^2]} \qquad (3)$$

The condition of the phases being 0°, 120° and 240° is essential for a correct image reconstruction using Eq.3. However, in the case of measurements in engines, vibrations can be transmitted to the optical setup and slightly alter the phases. In these cases, Eq. 4 can be used since it is able to account for erroneous phase shifts. This equation was used in the present study due to identified phase shifts in the collected data Further details regarding the SLIPI technique can be found in [10, 15].

$$I_s = \frac{1}{2\left|\sin\left(\frac{p_1 - p_3}{2}\right)\right|}\left|(I_3 - I_1) + i\left\{\frac{I_1 - I_2}{\tan\left(\frac{p_1 - p_2}{2}\right)} - \frac{I_2 - I_3}{\tan\left(\frac{p_2 - p_3}{2}\right)}\right\}\right| \qquad (4)$$

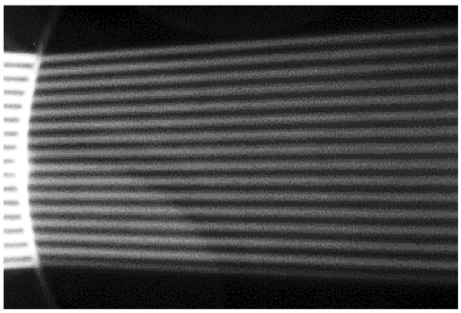

Figure 2: *LIF image of a homogeneous case with port fuel injection using a modulated laser sheet, the signal was collected from below. The laser sheet enters the piston bowl from the left side through the quartz piston crown that can be seen as a stronger signal.*

Optical setup

The laser (Continuum Powerlite DLS 9010) used in this setup generated 170 ±3 mJ of 266 nm radiation. The beam was sent through an expanding telescope and an aperture in order to get a top hat beam profile before the grating as illustrated in Figure 3. The 3 mm thick quartz plate was rotated between three different positions to produce a horizontal shift of the modulated laser sheet corresponding to the phases p=0°, 120° and 240°.

The structured laser-sheet entered the combustion chamber horizontally via a side-window in the cylinder liner and passed through the side of the fully optical piston top. The laser sheet was cropped to a width of 28 mm by the window in the liner, corresponding to 16 modulation periods. The vertical position of the laser sheet was fixed at the point where the centerline of the jet intersected the bowl wall, i.e. 1.4 mm above the flat bowl floor at TDC. Figure 4 shows the path of the laser sheet in the piston bowl. The red rectangle indicates the imaged area. The laser sheet was positioned horizontally in order to fully capture the impact of the free-jet on the wall together with the wall-jet and recirculation zone. The whole free part of the jet could therefore not be observed given the umbrella angle of the nozzle orifices.

Light was detected from below through the quartz piston via the 45° mirror using a Princeton PI-MAX II ICCD camera (1024 x 1024 pixels) with a UV-acromatic lens (B. Halle, f = 100 mm, f# = 2). The pixels were binned 2 by 2 on chip (yielding 512 x 512 pixels) in order to increase the frame rate to >10 Hz. A long pass liquid filter before the camera lens (12 mm thick, N,N-dimetylformamid) was used to block elastically scattered laser light (a transmission curve can be found in [6]). Even though the fully optical piston enables a large optical access, the region within 1 mm from the bowl wall could not be properly imaged due to a rather sharp radius between the bottom of the piston bowl and the vertical bowl wall as a result of the quartz-piston machining process.

In theory, single shot SLIPI measurements are possible. This would, however, require the use of three individually structured laser sheets (using three separate lasers) that are sent almost simultaneously through the combustion chamber. Additional beam filtering, and beam stabilization optics are also needed [16]. This high level of complexity was not deemed feasible for measurements in the optical engine at the time of the experiments. Therefore, average imaging SLIPI was used. 350 images were acquired for each of the three phases during one engine run. Applying Eq. 3 to these three average images then resulted in one SLIPI image corresponding to, in total, 1050 engine cycles.

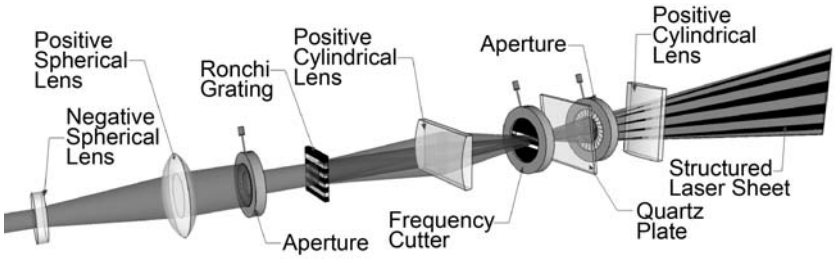

Figure 3: *Detailed illustration of the optics for SLIPI measurements.*

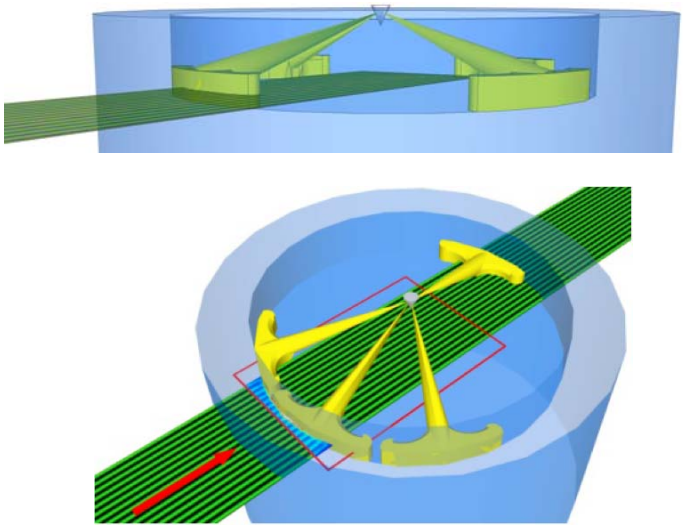

Figure 4: *Sketches of the full-optical piston (blue), structured laser sheet (green), fuel-jets (yellow) and the imaged area (red rectangle).*

RESULTS AND ANALYSIS

The results in this section are divided into three categories. First, time-resolved measurements of local equivalence ratios will be presented. Secondly, analysis of the mean equivalence ratio before impact on the bowl wall and at the end of the wall-jet, i.e. at the start of the recirculation zone, will be analyzed. Finally, the trends showing rapid leaning-out in the jet after end of injection will be discussed.

Evolution of colliding wall-jets

The fuel-LIF measurements were performed over a large timespan from start of injection until late after end of injection in order to capture the different phases of the fuel jet. Figure 5 shows the resulting LIF images, using SLIPI and Eq. 3, for the asymmetrical nozzle at 2000 bar injection pressure. The timings of the frames are indicated in the upper right corner relative to the start of injection (aSOI). End of injection (EOI) occurs at 2.11 ms aSOI. As scattered light from the liquid parts of the jets is suppressed, the positions of the nozzle and of the four jets are illustrated by the “chicken foot” in white on the right side of the images. For the asymmetrical configuration shown in Figure 5, the central and partially the upper jet from the group of three were observed.

At 0.49 ms aSOI, the head of the free-jet first intersects the laser sheet at a small distance from the bowl wall, located to the left in the images. The upper jet is partly visible at the upper edge of the laser sheet right at the top of the frames. The jet has reached the wall by 0.76 ms aSOI but the wall-jet traveling upwards in the images along the bowl wall is not clearly visible until the next frame (1.04 ms aSOI). The two wall-jets, from the central and upper jet, meet to form an inward-moving recirculation zone around 1.32 ms aSOI. The recirculation grows in the next couple of frames until the end of injection at 2.11 ms aSOI.

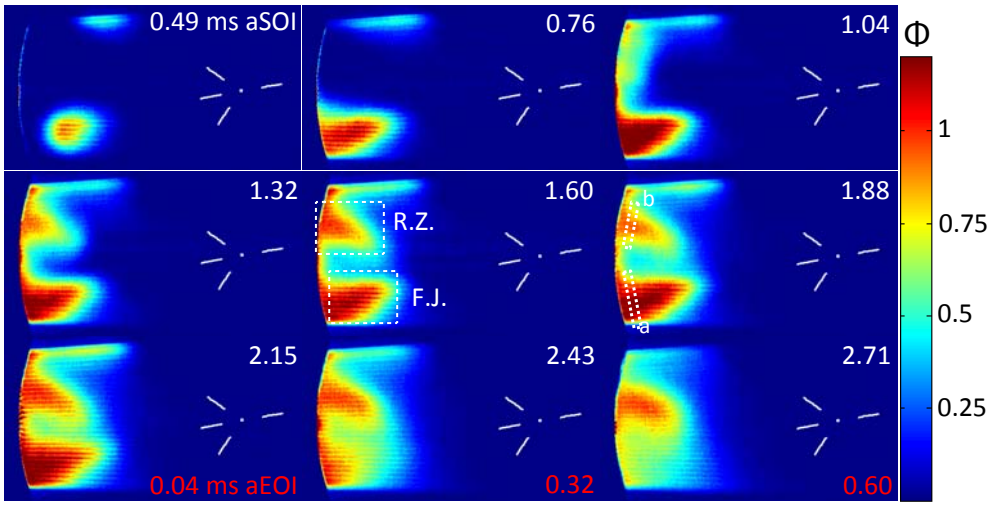

Figure 5: *Evolution of* the ϕ*-distribution in colliding wall-jets with an asymmetrical four-hole nozzle at 2000 bar injection pressure. The time of acquisition is indicated in each frame relative to the start of injection (aSOI) and end of injection (aEOI) when relevant. The free part of the jet and the whole recirculation zone are indicated in the center frame as "F.J." and "R.Z." respectively. The color scale show the local equivalence ratio (ϕ) as indicated by the color bar to the right.*

The structures of the different parts of the jet are fairly unchanged immediately after the end of injection (0.04 ms aEOI). At later timings however, the part of the jet upstream of the wall quickly becomes leaner and is probably moved along the wall to the growing recirculation zone. Since the formation of the recirculation zone at 1.32 ms aSOI, it has steadily grown and moved downwards in the frames, which corresponds to the direction of the swirl in the engine. Note, that these images are averaged over a large number of single shots.

Similar structures and chains of events are observed for the 1500 and 2500 bar injection pressures as well as for the symmetrical injector. However, in the case of the symmetrical injector, the wall-jets travel a longer distance before colliding with the adjacent wall-jet. Due to these similarities, only the frames seen in Figure 5 are shown in this section. However, the detailed analysis of the equivalence ratios in the next section is presented for all cases.

Mixing in wall-jets

The main objective of this study is to test if air-entrainment is changed in wall-jets compared to free-jets. Therefore, the average cross-sectional equivalence-ratio of the jet is analyzed before and after the wall-jet. By comparing these results with ϕ predictions for free-jets according to Siebers [3,4], the influence of the wall-jet on mixing processes can be estimated.

The average cross-sectional equivalence-ratio of the free-jet was extracted from the fuel-LIF results 3 mm upstream of the bowl-wall over a 0.2 mm thick region. This region is illustrated in the sixth frame of Figure 5 marked with an "*a*". The equivalence-ratio at the point where the recirculation-zone is formed was determined in an identical way over a 0.2 mm thick section where the colliding wall-jets are deflected inward, as indicated by a "*b*" in the same frame.

The results presented in Figure 6 show the evolution of the local equivalence ratio in the free portion of the jet (upstream of the impact on the bowl-wall) for the 45° inter-jet angle configuration at all three injection pressures. The standard deviations indicated in the figures were obtained for 14 consecutive identical runs at the downstream distances of interest. First, a highly transient phase is observed between 0.76 and 1.04 ms aSOI with an increase in ϕ when the free-jet impinges the wall. This trend is observed for all injection pressures and was also observed by Bruneaux for impingement on a flat wall in a combustion vessel [8].

After this initial transient phase, the 1500 bar case shows a rather stabilized trend in Φ with values around 1.2 up to EOI. However, for the higher injection pressures, 2000 and 2500 bar, an increasing trend is observed up to EOI. The slope and amplitude of this increase is almost identical for both cases. An explanation for this bump in ϕ can be found in the second row of images in Figure 5. The recirculation zone grows with time and is transported towards the free part of the jet by the swirl motion. On average there is an interaction between the recirculation zone and the free part of the jet by 1.88 ms aSOI. This indicates that the air-fuel mixture from the recirculation zone is being entrained in the jet prior to wall-impingement instead of air only. As a consequence, the local equivalence ratio in the jet should increase. At 1500 bar, the inward motion of the recirculation zone is slightly smaller compared to the other injection pressures and therefore this phenomenon is not observed.

These experiments are performed in non-reacting conditions and therefore the fuel survives all the way from the nozzle to the tip of the recirculation zone. In reacting conditions, fuel molecules are not expected to be re-entrained as such in the incoming jet. However, it is reasonable to assume that hot burned products would follow the same path from the recirculation zone into the free-jet. The low oxygen content of burned products would contribute to higher ϕ values in the jet and probably changes in soot concentration, both due to increased soot formation rates (increasing ϕ and temperature) and impeded soot oxidation rates (increasing ϕ). Furthermore, inclusion of hot gases in the free part of the jet is expected to shorten the lift-off length and further enhance the soot formation process. Pickett and López showed similar mechanisms in confined jets, where hot burned-gas recirculation upstream in the jet shortened the lift-off length and gave a significant effect on soot formation [17].

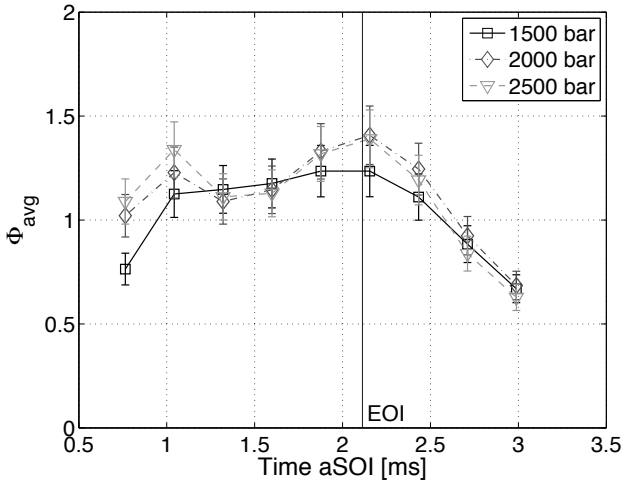

Figure 6: *Evolution of the local equivalence ratio in the free portion of the jet, prior to wall impact, for the 45° inter-jet angle configuration as a function of time aSOI.*

The results presented in Figure 6, considering the recirculation process described above, show that the effect of injection pressure on the equivalence ratio of the jet before impingement is not significant. This result is expected according the free-jet scaling laws proposed by Siebers [4].

The same type of processing is applied to obtain the average cross-sectional equivalence-ratio for the start of the recirculation zone. For all injection pressures, similar values and trends in ϕ are obtained until EOI, as seen in Figure 7. Given that increasing injection pressure is expected to increase turbulence in the wall-jet and therefore the mixing rate, this similarity is rather unexpected. Based on Siebers free-jet studies [3,4], the jet speeds before impingement in the present conditions are estimated to be 52, 60.3 and 67.6 m/s for 1500, 2000 and 2500 bar respectively.

There is a clear difference between these results and the results by Bruneaux [8] where the impingement on a flat wall provided increased mixing with increasing injection pressure. However, the wall-jet in that study was not confined and could therefore expand in a circular pattern on the surface. The wall-jet in the engine's combustion chamber in this study is much more confined with only 15 mm from the bowl floor to the firedeck at TDC.

In this geometry, the fuel jet is essentially divided into two wall-jets. Air entrainment only occurs on the side of the wall-jet not facing the bowl-wall. This would yield a surface area for air entrainment more similar to a free jet than to a flat-wall-jet.

A similar bump in ϕ to the one described earlier in Figure 6 is observed in Figure 7 slightly after EOI. This indicates that the enriched mixtures seen in the free-part of the jet for 2000 and 2500 bar injection pressure travels along the bowl wall and are found at a later time in the recirculation zone. Based on image processing of the data, the wall-jets are estimated to travel at average speeds of 26, 29 and 33 m/s, for 1500, 2000 and 2500 bar injection pressure respectively. These values correlate with the square root of the injection pressures, as is expected for a free-jet.

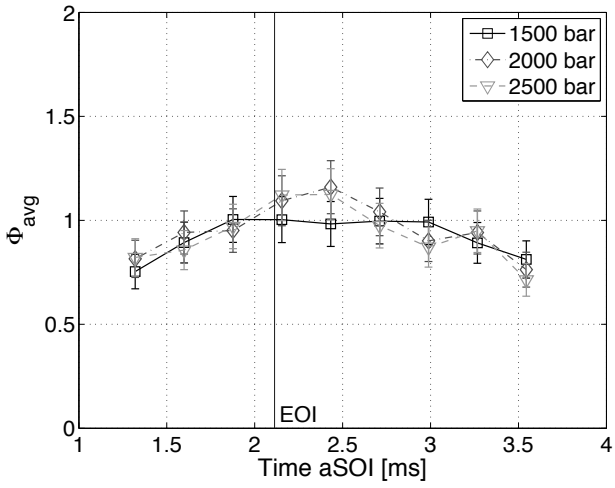

Figure 7: *Evolution of the local equivalence ratio at the start of the recirculation zone for the 45° inter-jet angle configuration as a function of time aSOI.*

The same analysis as presented above for the asymmetrical injector with an inter-jet spacing of 45° was also performed on the results for the symmetrical injector with 90° inter-jet spacing. As seen in Figure 8, these results show larger variations in the ϕ values compared to Figure 6 during the injection period. However, no clear conclusions can be drawn about the effect of injection pressure on the local equivalence ratio before impingement.

The larger spacing between the jets removes the interaction between the recirculation zone and the free-part of the jet as observed previously for the 45° inter jet angle case. The 63 mm traveling distance along the bowl-wall between two neighboring impingement points delays the formation of the recirculation zone to after EOI. The ϕ values at the start of the recirculation zone presented in Figure 9 show no clear correlation to the injection pressure, thus corresponding to the trends seen in Figure 7. The results indicates that, regardless of the inter-jet spacing, the injection pressure does not affect the mixing rates in confined wall-jets.

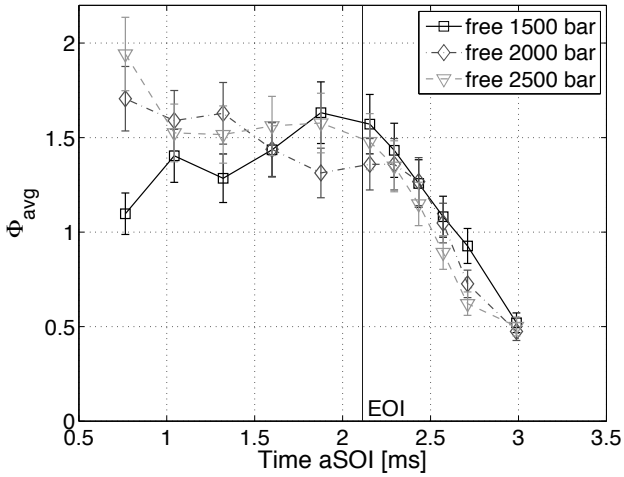

Figure 8: *Evolution of the local equivalence ratio in the free portion of the jet prior to impact against the bowl wall for the 90° inter-jet angle configuration as a function of time aSOI.*

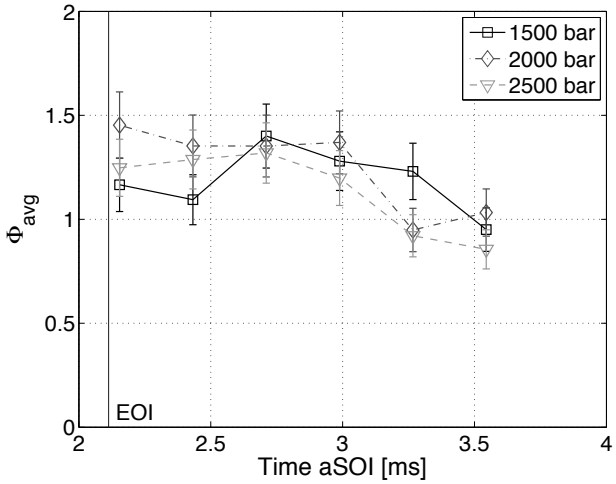

Figure 9: *Evolution of the local equivalence ratio at the start of the recirculation zone for the 90° inter-jet angle configuration as a function of time aSOI.*

Equivalence ratio predictions according to the model by Siebers [4] can be performed in order to compare a free-jet and a wall-jet more precisely in terms of mixing. The experimental data shown in Figures 6 to 9 provides the cross-sectional average ϕ values for each frame at the two locations of interest: the free-jet prior to impingement and the start of the recirculation zone. These results can be combined to the equivalence ratio predictions in order to perform this comparison.

Several of the constants needed to determine the effective orifice diameter (d_f) and the spreading angle of the model fuel jet (a) are not available and therefore, the characteristic length (x^+) used in [4] could not be calculated *a-priori*. However, the known ϕ in the jet prior to impingement (37 mm from the nozzle) makes it possible to empirically determine the value of the characteristic length for each case. Hence, the theoretical local equivalence ratio in a free jet under identical conditions can be calculated.

Figure 10 thus shows the ratio between the measured and the predicted ϕ values at the start of the recirculation zone for different cases. Note that the downstream distance differs between the 45° and 90° inter-jet spacing cases due to the longer distance travelled along the wall-jet prior to the recirculation zone in the 90° case (53 mm from the nozzle to the recirculation zone for 45° and 74 mm for 90° inter-jet angle).

The 90° inter-jet angle case with a longer portion of wall-jet has a significantly higher ϕ at the start of the recirculation zone compared to the free-jet predictions, in the range of 45% higher. The same trend is observed with the 45° inter jet-angle but to a lesser degree due to the shorter wall-jet section before the recirculation zone is formed. This implies a lower air entrainment rate in the wall-jet compared to free-jets. This observation goes against the hypothesis of increased mixing rates in wall-jets compared to a free jet.

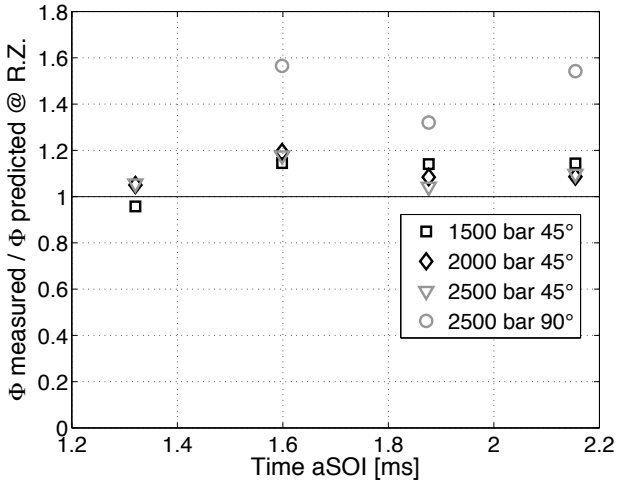

Figure 10: *Ratio between the measured ϕ values after the wall-jet and predicted ϕ values in a free-jet according to Siebers model at the same downstream distance corresponding to the beginning of the recirculation zone. The predicted values use the measured ϕ values from the free jet prior to wall impingement to calculate x^+.*

Rapid leaning-out after end of injection

The trends in ϕ, observed in Figure 6 and 8, after end of injection are interesting in terms of mixing process. A rapid decrease in average ϕ is noticed in the free part of the jet after end of injection for both injectors and all injection pressures. This trend appears before the tail of the jet would normally reach the bowl-wall after end-of-injection (about 0.5 ms aEOI). This indicate a rapid leaning-out of the jet after end-of-injection as observed in other studies [18,19,19]. An entrainment wave [19] has been shown to travel downstream in the jet faster than the jet speed and increase air entrainment by a factor up to 2.5 after end-of-injection compared to a quasi-steady jet. The same phenomenon seems to be observed here. Although variations in ϕ were observed before EOI, the curves are surprisingly gathered and monotonous after EOI. However, this phenomenon is not observed at the start of the recirculation zone, see Figure 7 and 9.

This observation implies that the enhanced mixing effect associated with the end of the fuel injection is not transmitted through to the wall-jet after the wall impingement. The mixtures in the wall-jet and in the recirculation zones are therefore not affected by this mixing enhancement, which could otherwise be beneficial for soot oxidation.

CONCLUSIONS

Mixing in wall-jets was investigated in an optically accessible heavy-duty diesel engine for several injector configurations and injection pressures. Acetone-LIF was employed under non-reacting conditions in order to quantitatively measure local equivalence ratios in colliding wall-jets. SLIPI was successfully implemented in an optical engine and permits to differentiate LIF signal from multiply scattered light thus increasing the measurement accuracy. The mixing in the wall-jets was evaluated by analyzing the equivalence ratio before impingement and at the point where the recirculation zone is formed after the wall-jet. These results were then compared to ϕ predictions for free-jets. The following conclusions were reached:

1. No significant differences between the average ϕ values for different injection pressures were observed, either at the bowl wall or in the recirculation zone. The previous observations of increased mixing in wall-jets, especially at higher injection pressures, was thus not confirmed for the conditions of this investigation. The confined nature of the wall-jet in the engine was suspected to be the reason for these observations.

2. At 45° inter-jet angle, significant interaction between the recirculation zone and the free part of the jet was noticed. This gave an enrichment of the mixture in the free-jet due to entrainment of fuel mixtures from the recirculation zone. This increase in ϕ was further transmitted to the recirculation zone.

3. In the engine configuration used in the present study, air entrainment in the wall-jet was lower compared to a free-jet prediction. The 90° inter-jet angle case with a longer portion of wall-jet has a significantly higher ϕ at the start of the recirculation zone compared to the free-jet prediction (ca. 45%). The same trend is observed with the 45° inter jet-angle but to a lesser degree (ca. 15%) due to the shorter wall-jet section before the recirculation zone.

4. A rapid decrease in average ϕ values is noticed in the free part of the jet after end of injection. This trend appears before the tail of the jet would normally reach the bowl-wall after end of injection and seems to indicate a rapid leaning-out of the jet after end of injection. This enhanced mixing is however not transmitted passed the wall impingement and through the wall-jet to the recirculation zone.

ACKNOWLEDGMENTS

The authors gratefully acknowledge the Swedish Energy Agency for their support.

REFERENCES

1. Pickett, L.M. and Siebers, D.L. “Soot formation in diesel fuel jets near the lift-off region.” Proceedings of IMechE JER03505 vol.7: pp 103-129, 2006.

2. Pickett, L.M., Siebers, D.L., and Idicheria,C.A. “Relationship Between Ignition Process and the Lift-Off Length of Diesel Fuel Jets.” SAE paper 2005-01-3843, 2005.

3. Naber, J.D. and Siebers, D.L., "Effects of Gas Density and Vaporization on Penetration and Dispersion of Diesel Sprays," SAE Paper 960034, SAE Transactions, 105, No. 3, pp. 82-111, 1996.

4. Siebers, D.L., ”Scaling Liquid-Phase Fuel Penetration in Diesel Sprays Based on Mixing-Limited Vaporization”, SAE paper, 1999-01-0528, 1999.

5. Siebers, D.L., “Liquid-Phase Fuel Penetration in Diesel Sprays,” SAE Technical Paper 980809, 1998.

6. Aronsson, U., Chartier, C., Andersson, Ö., Egnell, R. et al., "Analysis of the Correlation Between Engine-Out Particulates and Local Φ in the Lift-Off Region of a Heavy Duty Diesel Engine Using Raman Spectroscopy," *SAE Int. J. Fuels Lubr.* 2(1):645-660, 2009.

7. Eismark, J., Balthasar, M., Karlsson, A., Benham, T. et al., "Role of Late Soot Oxidation for Low Emission Combustion in a Diffusion-controlled, High-EGR, Heavy Duty Diesel Engine," SAE Technical Paper 2009-01-2813, 2009.

8. Bruneaux, G., "Mixing Process in High Pressure Diesel Jets by Normalized Laser Induced Exciplex Fluorescence Part II: Wall Impinging Versus Free Jet," SAE Technical Paper 2005-01-2097, 2005.

9. Berrocal, E., Kristensson, E., Richter, M., Linne, M. and Aldén, M., “Application of structured illumination for multiple scattering suppression in planar laser imaging of dense sprays,” Opt. Express, 16, 17870-17881, 2008

10. Kristensson, E., “Structured Laser Illumination Planar Imaging, SLIPI, Applications for spray diagnostics”, doctoral thesis, Lund University 2012.

11. Sjöholm, J., Chartier, C., Kristenson, E., Berrocal, E., Gallo, Y., Richter, M., Andersson, Ö., Aldén, M., Johansson, B., “Quantitative in-cylinder fuel measurements in a heavy duty diesel engine using Structured Laser Illumination Planar Imaging (SLIPI)”, COMODIA 2012.

12. Fansler, T. D., French, D. T. and Drake, M. C., “Fuel Distributions in a Firing Direct-Injection Spark-Ignition Engine Using Laser-Induced Fluorescence Imaging”, SAE Technical Paper 950110, (1995).

13. Schulz, C. and Sick, V., “Tracer-LIF diagnostics: quantitative measurement of fuel concentration, temperature and fuel/air ratio in practical combustion systems”, Progress in Energy and Combustion Science, 31, (1), 75-121 (2005)

14. Yip, B., Miller, M. F, Lozano, A., Hanson, R. K, “A combined OH/acetone planar laser-induced fluorescence imaging technique for visualizing combusting flows”, Experiments in Fluids, Vol. 17,1994,.pp 330-336.

15. Neil, M. A. A., Juskaitis, R. and Wilson, “Method of obtaining optical sectioning by using structured light in a conventional microscope T.,” Opt. Lett., 22, 1905-1907 (1997).

16. Kristensson, E., Berrocal, E., Richter, M. and Aldén, M., “Nanosecond structured laser illumination planar imaging for single-shot imaging of dense sprays,” Atomization Sprays, 20, 337-343, 2010.

17. Pickett, L. and López, J., "Jet-Wall Interaction Effects on Diesel Combustion and Soot Formation," SAE Technical Paper 2005 -01-0921 , 2005

18. Musculus, M., Lachaux, T., Pickett, L., and Idicheria, C., "End-of-Injection Over-Mixing and Unburned Hydrocarbon Emissions in Low-Temperature-Combustion Diesel Engines," SAE Technical Paper 2007-01-0907, 2007.

19. Musculus, M. and Kattke, K., "Entrainment Waves in Diesel Jets," *SAE Int. J. Engines* 2(1):1170-1193, 2009.

Paper VI

Planar Laser-Diagnostics of Soot and OH with Post-Injections in a Heavy-Duty LTC Diesel Engine

Mohan K. Bobba[1], Clément Chartier[2], Bengt Johansson[2], Öivind Andersson[2], and Mark P. B. Musculus[1]

[1]Combustion Research Facility, Sandia National Laboratories,
7011 East Avenue, Livermore, CA, USA.

E-mail: mkbobba@sandia.gov
Telephone: +(1) 925 294 3691
Fax: +(1) 925 294 1004

[2]Division of Combustion Engines, Lund University,
P.O. Box 118, SE-221 00 Lund, Sweden.

E-mail: clement.chartier@energy.lth.se
Telephone: +(46) 46 222 49 25
Fax: +(46) 46 222 47 17

Abstract. Multiple fuel-injections during a single engine-cycle can reduce combustion noise and improve pollutant emissions tradeoffs. Our previous work has shown that the reduction of exhaust soot depends on the timing of both the main and the post injections, with greater soot reductions for late main-injections. Complementary in-cylinder soot radiometry using the two-color method suggested that the exhaust soot reductions were due to improved oxidation of soot in the squish region by the late post injection. However, limitations of the two-color technique left significant uncertainty about the chemical and fluid-mechanical interactions between the post injection and residual soot from the main injection. In the current study, we employ planar laser-induced incandescence of soot and planar laser-induced fluorescence of OH to better identify the in-cylinder mechanisms of soot reduction by post injections. Two medium-load low-temperature combustion conditions (12.7% intake oxygen) are examined in a heavy-duty diesel engine, with either an early (-18°ATDC) or a late (2°ATDC) main injection. A late post-injection at 36°ATDC yielding maximum impact on exhaust smoke is used at both the conditions. The planar-imaging data show that for an early main injection, very little soot from the main injection enters the squish region into which the late post injection is directed. Consequently, although the post-injection burns largely soot free and generates significant late-cycle OH that could help oxidize soot, very little main-injection soot is available in the squish region for oxidation, and the exhaust soot emissions with the post injection are no lower than for the main injection alone. In contrast, a large fraction of the late main-injection soot spills into the squish region. Therefore the OH field generated by the post-injection combustion fills much of the sooty squish region from the main injection, so that in-cylinder and exhaust soot are reduced below the levels of the main injection only.

1. Introduction

Stringent pollutant emissions regulations for on-road heavy-duty diesel engines have required significant reductions of nitrogen oxides (NOx) and particulate matter (PM) emissions. The NOx emissions can be controlled by using exhaust-gas recirculation (EGR) to achieve low temperature combustion (LTC) conditions. However, EGR can adversely affect other emissions, including soot, a prime component of PM. One way to offset the increase in soot emissions with EGR is to use multiple fuel-injections during a single engine cycle [8]. Specifically, a combination of high EGR (over 40%) and post injections is an effective way to reduce soot emissions while maintaining low NOx emissions [6,13,16]. Post-injection strategies seem to work best at medium to high-loads and high EGR conditions where effective utilization of in-cylinder air is critical [6,18]. Ojeda et al. [15] showed that post injections help to extend the load limits of clean combustion (NOx level of 0.2g/hp-hr and an after treatment-tolerant soot level) from 10 bar to 16.5 bar brake mean-effective pressure (BMEP) in a medium-duty diesel engine at a LTC condition having an EGR rate of 44%.

Exhaust-emissions with post injections are sensitive to the delay from main injection and the fraction of fuel injected in the post [2,16]. For example, figures 1 and 2 show previous measurements

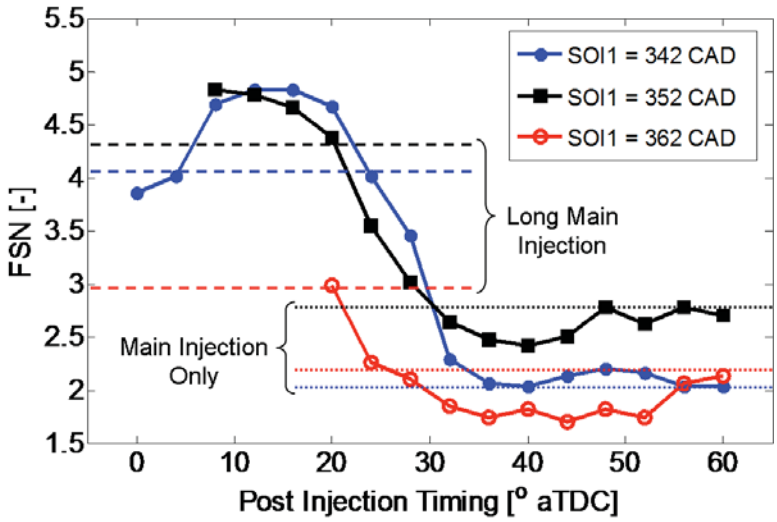

Figure 1. Variation of exhaust smoke as post-injection timing is delayed into the power stroke for three main injection timings, reproduced from [2]. Smoke emissions for the main-injection only and for a longer main-injection with the same total fuel mass as with a post injection are also shown in the figure with dotted and dashed lines, respectively

of exhaust smoke and total in-cylinder soot-mass for mid-load operation, using the same optical heavy-duty diesel engine as the current study [2]. Figure 1 shows the variation of exhaust smoke with post-injection timing for a LTC condition with 12.7% intake oxygen (corresponding to an EGR rate of approximately 55%). A fuel injection pressure of 1600 bar was employed in this previous study, with an included cone angle of 152° between the fuel jets. The post-injection sweeps are shown for three different starts of main injections between –18º and 2º after top-dead center (ATDC). Also shown are smoke levels for reference cases of the main-injection alone and a longer main-injection matching total fuel-mass in the main and post injections combined.

For the conditions in figure 1, close-coupled post-injections increase the engine-out smoke, even above that of the long main-injection. But with sufficient post-injection retard, the exhaust smoke drops below the long main-injection levels, and in some cases, even drops below the soot produced by the standard main-injection alone. The maximum soot-reduction benefit is realized when the post injection is introduced near 40°ATDC, irrespective of the timing of the main injection. Such a retarded post injection has a significant fuel economy penalty (7-8%), though the load increases by 13% because of the additional 17% fuel in the post injection.

For an early main-injection timing (SOI1) of -18ºATDC, smoke emissions with post-injections at best drop to essentially the same value as the main-injection only case. Similar observations were reported in other studies by Han [7] and Desantes et. al. [5], who concluded that the main and post injections can be treated as independent, which Desantes called “split-flame” behaviour. In contrast, for later main injections (especially for SOI1=2ºATDC), the smoke emissions dip below that of the main-injection only by as much as 15% at the optimal retarded post-timing. Clearly, for late main injections, the post injections eliminate some of the soot produced from the main injection, implying some sort of interaction between injections, as also argued by Chen [3] and Hotta et al. [12]. According to them, enhanced late-cycle fuel-air mixing by the post-injection could improve soot oxidation and thereby eliminate some soot from the main-injection. Hence, previous research offers two somewhat contradictory descriptions for the role of post injections in exhaust soot emissions.

Previous research in the optical engine used in the current study has also demonstrated similar trends for in-cylinder soot. The variation of total in-cylinder soot mass, measured optically by the 2-color method [2] is shown in figure 2 with either the early (SOI1=-18ºATDC) or the late (SOI1=2ºATDC) main-injection timings from figure 1. The measurements are for both the region in and directly above the piston bowl (top) and for the squish region (bottom), so both together are representative of the total soot mass in the engine cylinder.

For the early main-injection, the piston-bowl soot-mass shows a distinct second bump just after the post injection. This second bump abruptly disappears for post injections later than 24ºATDC [2], indicating that for the longer delays, the post injection does not produce any additional piston-bowl

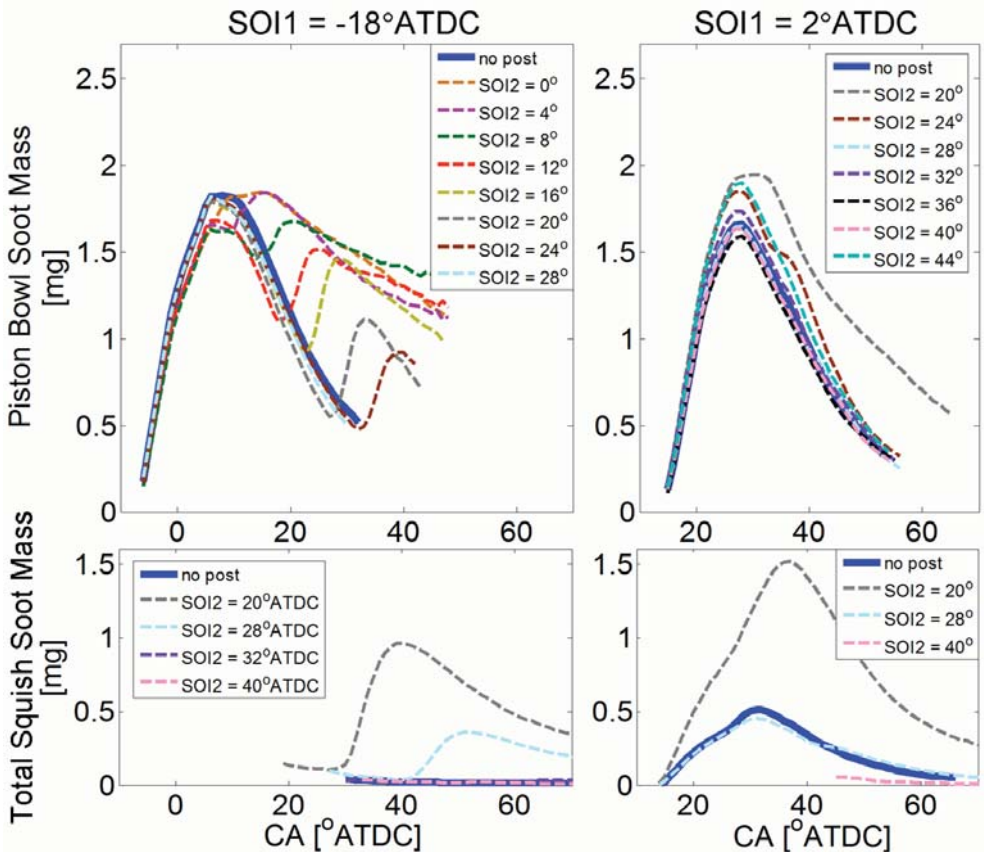

Figure 2. Evolution of in-cylinder soot mass measured in the region within and directly above the piston bowl (top) and in the squish region (bottom) for early and late main-injection timings and a range of post injection timings adapted from [2]. A reference case with no post injection is also included in each plot

soot, at least not that can be measured by the 2-color soot diagnostic[†]. In the squish volume, significant soot is detected as late as 28ºATDC, but the post injection does not produce any measurable soot for timings at 32ºATDC and later. This is consistent with the sudden decrease in exhaust smoke noted with early main-injection for post timings after 24ºATDC.

The late main-injection data show only a relatively modest increase in piston-bowl soot due to the post injection at small delays. Instead, much soot appears in the squish volume (comparable to the soot levels in the bowl) for a short delay between the main and post injections in this case. As the post injection is further delayed, however, soot in the squish region decreases to the level of only the main-injection by 28ºATDC. Further retarding the post injection to 40ºATDC significantly reduces detectable soot in the squish region. These in-cylinder measurements suggest that for the late main injection, a late post injection timing (SOI2) of 40ºATDC not only burns soot-free but also helps to oxidize soot in the squish volume from the main injection (or prevents its formation), consistent with the exhaust measurements.

While the 2-color optical data are consistent with exhaust measurements, the conclusions that may be drawn from the data are limited by the shortcomings of the 2-color technique. Specifically, the technique is line-of-sight integrated and is strongly biased to the hotter, more brightly radiating soot, so that the contributions from colder soot may not be fairly represented. As a potential consequence, under some conditions, evaporative cooling and mixing induced by the post injection could sufficiently cool the soot from the main injection so that it is not detectable by the 2-color technique, even though a significant amount of cooled soot may remain. Furthermore, the technique provides only indirect information about important soot oxidizer species such as OH, which are likely crucial for the in-cylinder mechanisms of soot reduction by post-injections. Consequently, the in-cylinder mechanisms responsible for soot reductions for early and late main-injection timings are not well revealed by the 2-color technique.

[†] A detailed discussion about the 2-color soot diagnostic, and explanations for the range limits of the data presented in figure 2 measured using this technique, is included in [2].

To provide a more complete picture of the in-cylinder evolution of soot and reaction zones for post-injection conditions, the current study uses planar laser diagnostics, with simultaneous imaging of soot laser-induced incandescence (LII) and OH laser-induced fluorescence (OH-LIF). These measurements show how OH radicals produced by the post injection interact with the main injection soot. To complement the laser diagnostics, the evolution of soot in the cylinder is also visualized using high-speed imaging of natural soot-luminosity. Throughout the experiments, the fuel mass in each injection, rather than engine load, is held constant, so that the fundamental fluid-mechanical effects of post injections may be studied.

2. Experimental Setup

2.1 Optical Engine

A single-cylinder, direct-injection (DI), 4-stroke diesel engine based on a Cummins N-series production engine was used in this investigation. A schematic of the engine is shown in figure 3 and its specifications are summarized in Table 1. A brief description of the engine is provided here, while a complete account is available in Refs. [4,14]. The Cummins N-series engine is typical of heavy-duty size-class diesel engines, with a bore of 140 mm and a stroke of 152 mm, yielding a displacement of 2.34 liters per cylinder. To provide optical access, the engine is equipped with an extended piston and a flat piston-crown window. A window replaces one of the two exhaust valves in the cylinder head to provide imaging access to the squish region. Several windows are also located around the top of the cylinder-wall for introduction of coplanar laser light for OH-PLIF and LII measurements as will be discussed later.

The engine is equipped with a Cummins XPI common-rail fuel injector. The mini-sac injector cup (tip) has an included angle of 152° (14° down-angle from the firedeck) with eight equally spaced 0.15-mm diameter fuel orifices. The rail pressure used in this study is 1600 bar. Specifications for the

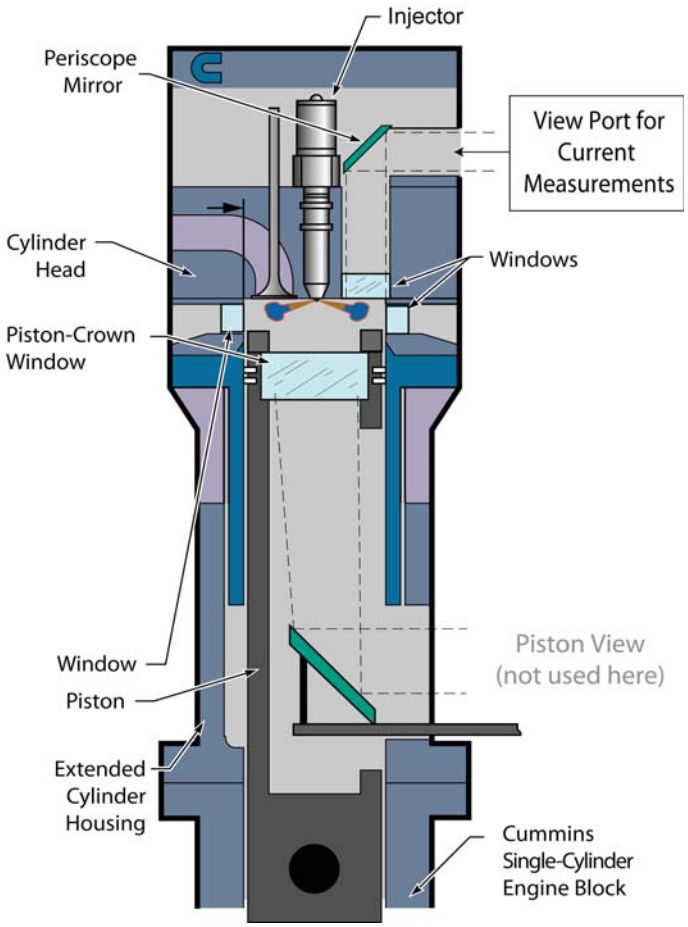

Figure 3. Schematic of the optical heavy-duty DI diesel engine facility

Table 1. Engine and injector specifications

Engine base type	Cummins N-14, DI diesel
Number of cylinders	1
Cycle	4-stroke
Number of intake valves	2
Number of exhaust valves	1*
Intake valve opening	17° BTDC Exhaust‡
Intake valve closing	195° ATDC Exhaust‡
Exhaust valve opening	235° BTDC Exhaust‡
Exhaust valve closing	27° ATDC Exhaust‡
Combustion chamber	Quiescent, direct injection
Swirl ratio	0.5 (approx.)
Bore	139.7 mm [5.5 in]
Stroke	152.4 mm [6.0 in]
Bowl width	97.8 mm [3.85 in]
Displacement	2.34 liters [142 in^3]
Connecting rod length	304.8 mm [12.0 in]
Piston pin offset	None
Geometric compression ratio	11.2:1
Simulated compression ratio	16:1
Fuel injector type	Common-rail, solenoid actuated
Cup (tip) type	Mini-sac
Number of holes & arrangement	8, equally-spaced
Spray pattern included angle	152°
Orifice treatment	None (square-edged)
Nominal orifice diameter	0.15 mm

*In this optically accessible diesel engine, one of the two exhaust valves of the production cylinder head was replaced by a window and periscope (see figure 3).
‡All valve timings correspond to the crank angle when the valve first starts to move from fully closed.

fuel injector are included in Table 1. This injector uses a solenoid-actuated pilot valve and a pressure-balanced needle to control fuel delivery.

2.2 Engine Operating Conditions

The engine operating conditions employed here to investigate changes in soot formation with post injections are listed in Table 2. The top dead center (TDC) conditions (27.7 kg/m^3 and 914 K) correspond to medium-boost operation in production 16:1 compression-ratio diesel engines. The nominal TDC conditions listed in the table were calculated using a classical polytropic compression from the intake manifold conditions as described in [17].

Due to compromises necessary to implement optical access in the engine, the geometric compression ratio of the optical engine is about 11.2:1, compared to 16:1 in the production engine. As a result, elevated intake air temperatures and pressures are required to yield charge conditions at TDC typical of those in a production diesel engine. The intake pressure and temperatures required for a 16:1 compression ratio engine to achieve the same TDC charge conditions are also listed in Table 2 for reference. Although the thermodynamic conditions at TDC are representative of production hardware, the temperature and density of the air charge in the optical engine are slightly higher than in the

Table 2. Engine operating conditions

Engine Speed	1200 RPM
Engine Load Range	9-10 bar gIMEP
Intake O_2	12.7% (Sim. 55% EGR)
Fuel Pressure	1600 bar
TDC Motored Density	27.7 kg/m^3
TDC Motored Temperature	914 K
TDC Motored Pressure	74.3 bar
Intake Pressure	276 kPa (abs)
Intake Temperature	116.5°C
(16:1 Compression Ratio Intake Pressure)	170 kPa (abs)
(16:1 Compression Ratio Intake Temperature)	70°C
Command Start of Main Injection (SOI1)	-18 and 2° ATDC
Command Duration of Main Injection (DOI1)	1500µs (~11 CAD)
Post-Injection Timing (SOI2)	32 to 40°ATDC
Fraction of Fuel in Post Injection	17% (~25 mg/stroke)

production engine at crank positions where the piston is away from TDC, because of the lower geometric compression ratio. For all operating conditions, cylinder pressure and fuel rail pressure were digitized and recorded at quarter crank angle degree increments, simultaneously with the acquisition of the optical data. The apparent heat release rate (AHRR) was calculated from ensemble-averaged pressure data using an air-standard first-law analysis (e.g., Heywood [10]).

Imaging measurements were performed in the engine for the early and late main-injection timings at -18 and 2°ATDC respectively. Post-injection timings from 32 to 40°ATDC have been used, which reduce exhaust smoke for both the main-injection timings as shown in figure 1. All the timings mentioned above refer to the command start of the injection. For each injection, the delay between the command start of injection and the actual start of fuel injection (i.e., when fuel first emerges from the injector) is approximately 460 microseconds, or 3.3 CAD at 1200 crankshaft rotations per minute (RPM).

The 1500-microsecond (11 CAD at 1200 RPM) command-duration of the main injection (DOI1) delivers 115 mg of fuel. The nominal 400 microsecond post-injection command-duration is adjusted to account for rail dynamics so that the injected mass remains approximately constant at 25 mg of fuel, corresponding to 17% of the total fuel mass injected during the entire engine cycle. Ideally, we would have preferred to explore a smaller post-injection mass, but stable injector performance could not be maintained for post-injection masses smaller than 25 mg. When using multiple injections, pres-

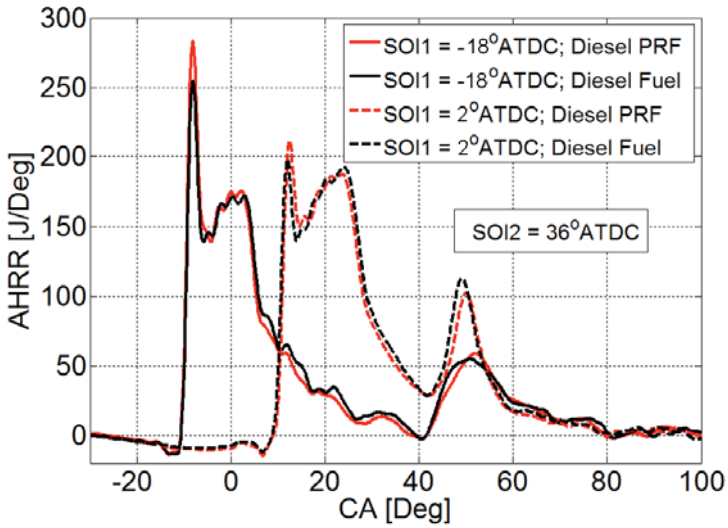

Figure 4. Heat Release Rate (AHRR) variation for diesel fuel and the diesel PRF fuel mixture at the early and late main-injection timings of -18° and 2°ATDC. Post-injection timing for all the cases presented is 36°ATDC

sure oscillations triggered by the nozzle closure after each injection can induce disturbances in the fuel injection profiles during subsequent injections, thereby altering the fuel mass in the post injection as the dwell between injections is varied [1]. Hence, to be able to study the effect of post injections on engine performance at constant fuel mass as desired, the amount of fuel injected during the post injection is monitored using the rail-pressure correlation described in Ref [2]. The post-injected fuel mass is held constant by making small changes to its command duration according to the rail-pressure analysis. With this methodology, the injected fuel mass is held constant to within 3mg.

All the tests are performed at an intake oxygen concentration of 12.7% (corresponding to an EGR rate of approximately 55% for a 16:1 compression ratio engine). Based on earlier studies (for example, Ojeda et al. [15], Helmantel [9], and Horibe et al. [11]), the exhaust NOx emission at these high EGR rates (although not measured directly), is expected to be sufficiently below the US 2010 heavy-duty truck limit of 0.2 g/bhp-hr. To avoid thermal loading problems in the optical engine, the engine was skip-fired, so that fuel injection occurred in every 10^{th} engine cycle. As a result, the use of real EGR is not a practical option to dilute the oxygen in the intake stream to the low levels used in this study. Rather, the intake stream was diluted with a metered flow of nitrogen to achieve the desired intake oxygen concentrations to simulate dilution by EGR. A regular schedule is maintained while performing these experiments, where the engine is motored for 90 seconds before the start of fuel injection to minimize variability of results due to transients.

Ultra-low sulfur No. 2 Diesel fuel (cetane number of 42.5) is used for the natural soot-luminosity imaging measurements presented in this paper. For the laser-induced incandescence and fluorescence measurements, a diesel primary-reference fuel (PRF) mixture was used to avoid unwanted fluorescence interferences from aromatic components in diesel fuel. The PRF mixture consists of a mixture of 32.3% n-hexadecane (cetane) and 67.7% hepta-methyl nonane by volume, and matches the ignition characteristics of the diesel fuel. The apparent heat-release rate characteristics for the two main-injection timings of -18° and 2°ATDC and a post-injection timing of 36°ATDC are presented in figure 4 for both of these fuels. The diesel PRF mixture yields nearly identical ignition timings and heat-release rate profiles as the diesel fuel for both the main-injection timings.

2.3 Optical Diagnostics Setup

OH fluorescence (OH-PLIF) is excited near 284 nm at 20 mJ per pulse with the frequency-doubled output of an optical parametric oscillator (OPO), pumped by the 355-nm third-harmonic of a Nd:YAG laser. Laser-induced incandescence of soot is excited using the Nd:YAG fundamental at 1064-nm with 500 mJ per pulse from a second laser system. Both beams are formed into coplanar laser-sheets using the combination of a spherical and a cylindrical lens with focal lengths of 500 and -90 mm respectively. This lens combination expands both beams into sheets that overfill the engine window so that only the central portion of the sheets (50% of the total pulse energy), which is relatively uniform in intensity, enters the engine cylinder. The laser sheets are limited to 30 mm by the width of the cylinder window. The thickness of the LII beam at 1064-nm is approximately 0.3 mm, yielding an estimated mean laser fluence of 2.7 J/cm^2 in the engine cylinder. The laser-sheets are introduced into the engine parallel to the firedeck of the cylinder head (see figure 5) and are aligned with one of the eight fuel jets inline with the cylinder-wall window. Because of the 14° downward tilt of the diesel jet from the cylinder head and the laser sheet, the recorded images are within a plane at an angle of 14° relative to the jet axis. Simultaneous LII and OH-PLIF measurements are performed at two different sheet heights of 15 and 29 mm from the cylinder head, as illustrated in figure 5.

The laser-induced signals from the engine cylinder are passed upwards through the cylinder-head window, which provides a view of the squish region, along with a small portion of the piston bowl. Using a periscope mirror, a dichroic beam splitter directs the UV and visible-light signals to two UV-enhanced, gated, intensified CCD cameras, as shown in figure 5a. The camera receiving the visible-light LII signal is equipped with a 50 mm focal length f/1.2 commercial glass camera lens and is positioned head-on with the periscope port. The LII signals were spectrally filtered using a BG-39 and short-pass Corion LS 450 filters, which along with the glass camera lens provide a band pass spectral range of 380-450 nm. The second camera receiving the UV light from OH fluorescence is equipped with a 35-mm focal length Hamamatsu f/3.5 UV lens. The intensifier gate width on both cameras is set to the practical minimum of approximately 100 ns. The OH fluorescence was isolated from elastic scattering and other interference by a 2-mm thick WG 305 long-wave-pass colored-glass filter, a 16-nm wide bandpass filter (BPF) centered at 312 nm, and a 358-nm short-pass filter. Both laser-induced imaging measurements are performed nearly simultaneously with the OH laser delayed by 1 microsecond from the LII laser pulse. The 1 microsecond separation is short compared to the relevant flow

and chemical timescales in the engine, but the separation is long compared to the duration of the laser-induced emission.

A series of 30 images of LII and OH-LIF signal were acquired at each crank angle of interest for each experimental run, followed by 10 background images acquired with the lasers blocked. Background images at each of the measurement timings show intensities 16 times weaker than with the LII-laser switched on, indicating that the contribution of non laser-induced emissions like natural soot luminosity and chemiluminescence to the LII signal are insignificant at the late cycle conditions explored here. Images were also acquired with the OPO laser tuned off the OH excitation line to investigate possible fluorescence interferences from other species for each run. The OH-offline images acquired at all the conditions were also very weak (OH-online images are 36 times stronger than the OH-offline images), indicating the signal observed in the OH-LIF images is primarily from OH fluorescence. Representative images of OH-LIF and LII are chosen based on manual inspection in each case and are presented as composite images later in the paper, with the OH-LIF false-colored in green and the LII shown in red. Any regions where OH and soot coexist would therefore appear yellow (secondary color for red and green).

In addition to the single-shot laser-based imaging, natural soot-luminosity in the squish region is imaged by an IDT-XS-4 high-speed digital CMOS camera (manufactured by Integrated Design Tools, Inc.) in place of the LII camera in figure 5a. The high-speed soot luminosity imaging data provide high-speed visualization of the soot luminosity in the squish region to complement the laser diagnostics, which can provide only a single snapshot per cycle.

3. Results and Discussion

The spatial evolution of soot and reaction zones are imaged for two limiting main-injection timings of -18 and 2°ATDC, referenced as the early-main and late-main injections throughout the rest of the paper. The in-cylinder soot distribution is visualized by imaging of natural luminosity and laser induced incandescence from soot, while the reaction zones are visualized using planar laser-induced fluorescence of OH radicals.

3.1 Early Main-Injection Case (SOI1=-18ºATDC)

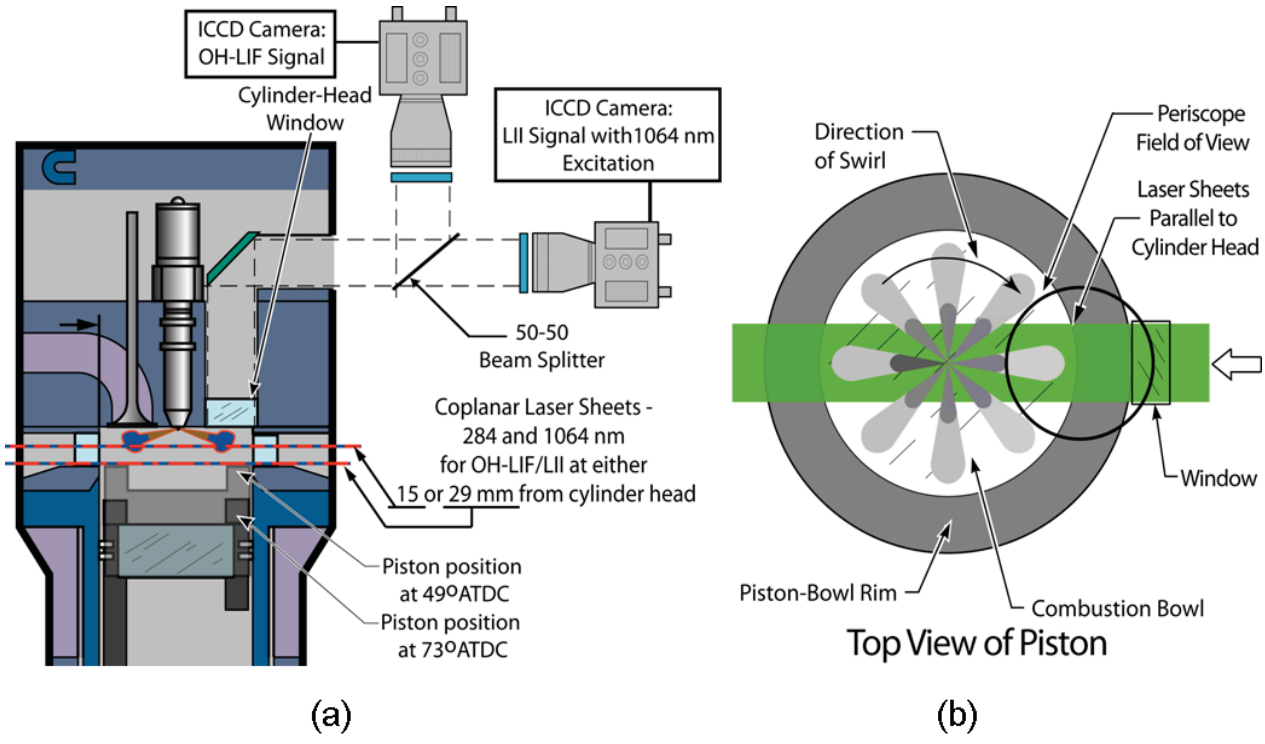

Figure 5. (a) Top and (b) side views of the piston showing laser-sheet illumination, and field of view for imaging setup

Figures 6-7 show images from high-speed movies of natural soot-luminosity for two early-main injection conditions. Figure 6 is for a post-injection timing of 32°ATDC (adapted from [2]), where the post injection could be clearly discerned because the post-injection creates some soot. As a result, the exhaust smoke is marginally higher than a main-injection-only condition. Figure 7 is for a more optimal post-injection timing of 40°ATDC, where the post-injection is less obvious because it creates little soot luminosity of its own. In each case, post-injection image sequences (left) are compared to the reference case with the same main injection timing but without a post injection (right). The camera gain for the visualization was intentionally set high enough to be able to discern the weak luminosity of the post injection, but this gain level partially saturates the earlier images.

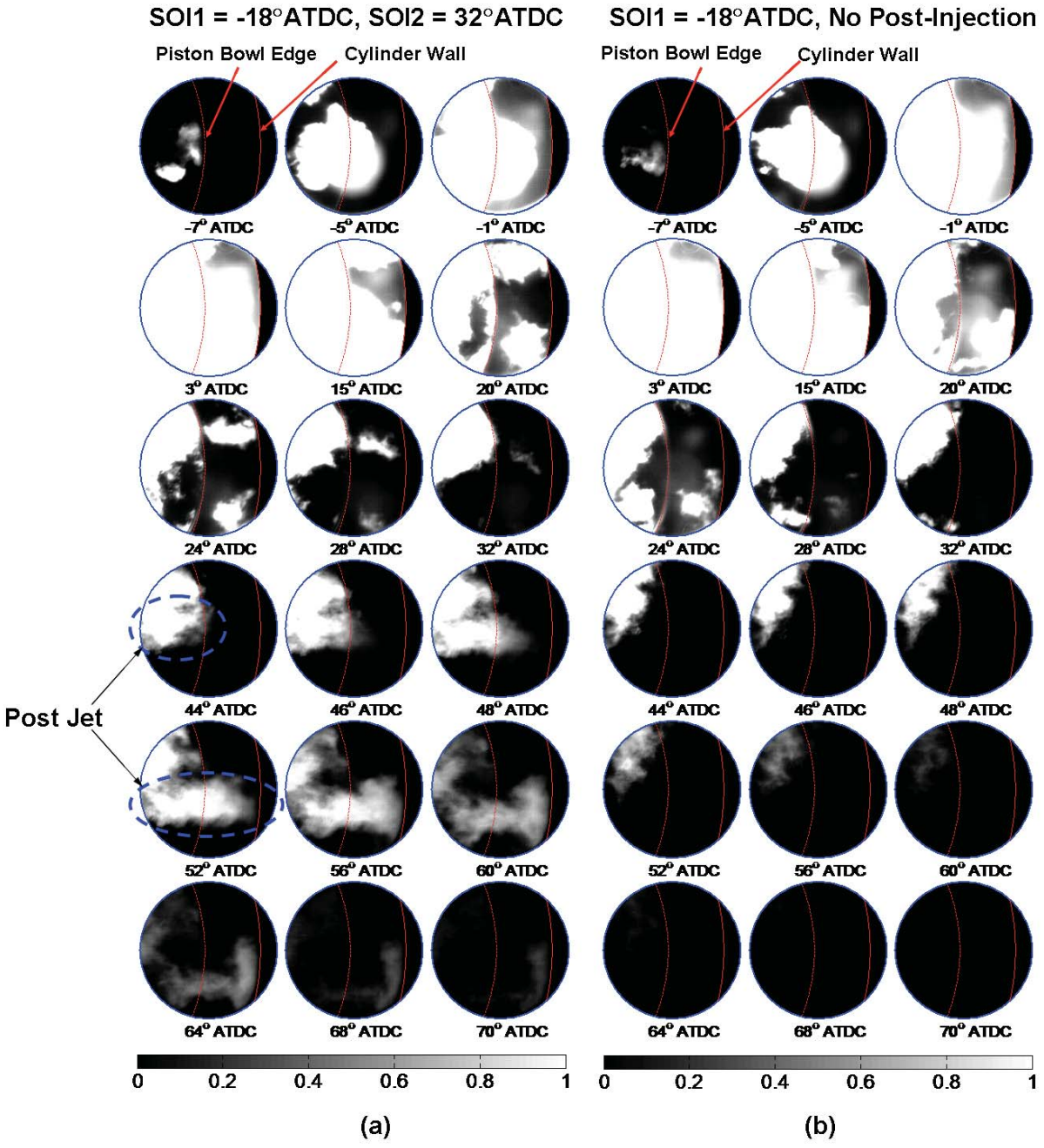

Figure 6. Sequential high-speed natural soot luminosity images for an early main-injection (SOI1=-18°ATDC) with (left) and without (right) a post injection at 32°ATDC (adapted from [2]). The locations of piston bowl edge and the cylinder wall are indicated by curved red lines in each of the images. The crank position when each image was acquired is also displayed at the bottom of each image

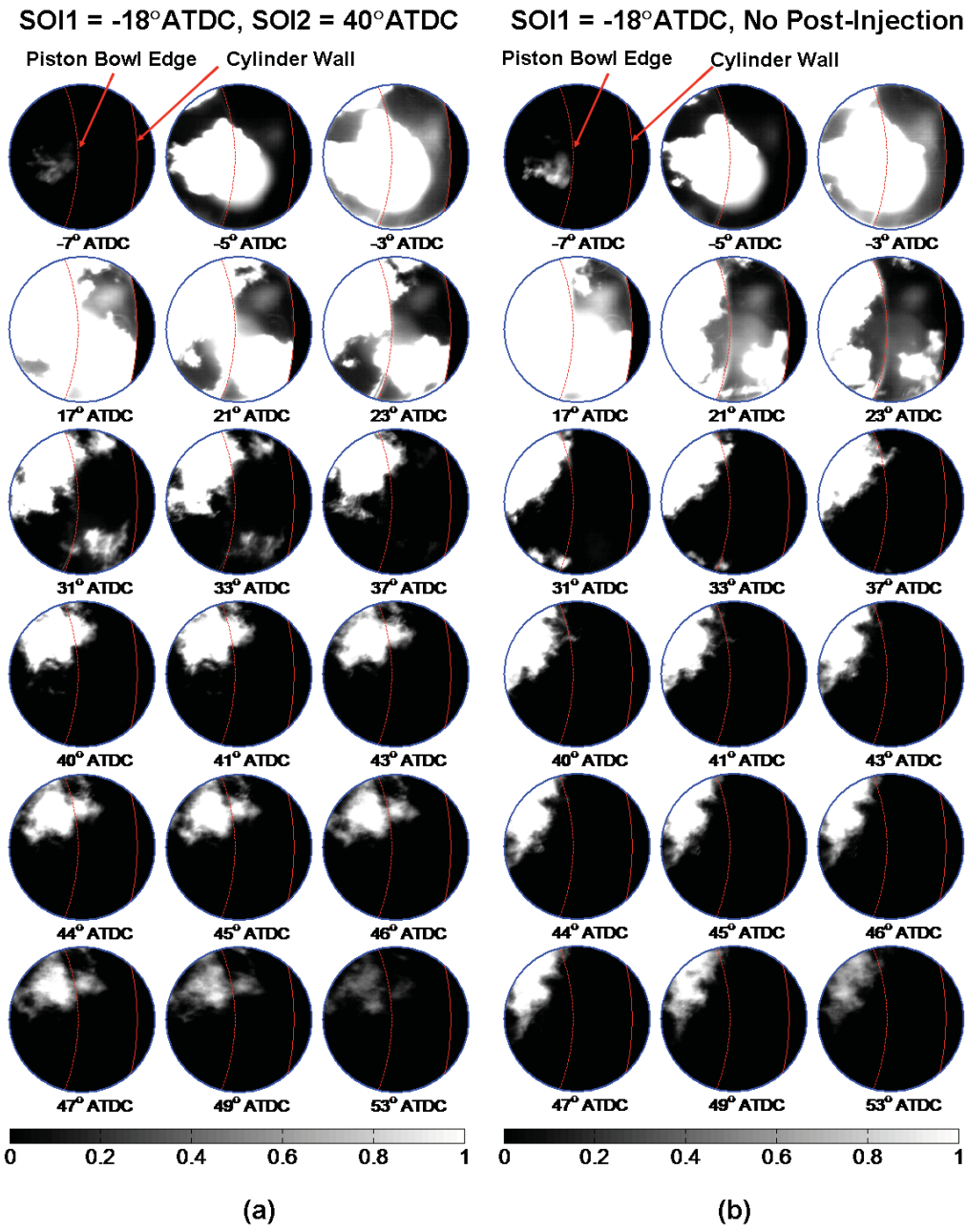

Figure 7. Sequential high-speed natural soot luminosity images for a case with an early main-injection (SOI1=-18°ATDC) with (left) and without (right) a post injection at 40°ATDC

The images were acquired through the cylinder head window (figure 5b), providing a view of part of the bowl and squish volume. The images are bounded by the round perimeter of the cylinder window on the top, left, and bottom, and by the cylinder wall (140-mm bore) on the right (curved red line). The position of the edge of the piston bowl (90-mm diameter) also is shown as a curved red line through the middle of each image. The piston bowl is to the left of the piston bowl-edge, while the squish volume is to the right of the piston bowl-edge, up to the cylinder wall. Each image captures a single diesel jet, propagating horizontally from the left to right. The injector is 27 mm to the left of the edge of the window, so it is not visible in the images. The crank angle position at which the image was taken is shown at the bottom of each image.

For the first case with SOI2 = 32°ATDC in figure 6, soot luminosity is first detectable at -7°ATDC, very close to the edge of the piston bowl. Over the next 38 CAD (from -6 to 32°ATDC), soot luminosity from the main injection remains mostly contained within the piston bowl, though some soot spills into the squish region. During the sequence, the clockwise swirl in the engine cylinder also carries the main-injection soot from the neighboring jet slightly downward. Figure 6 shows that the early evolution of the main injection is reasonably similar to the case with no-post injection (minor changes

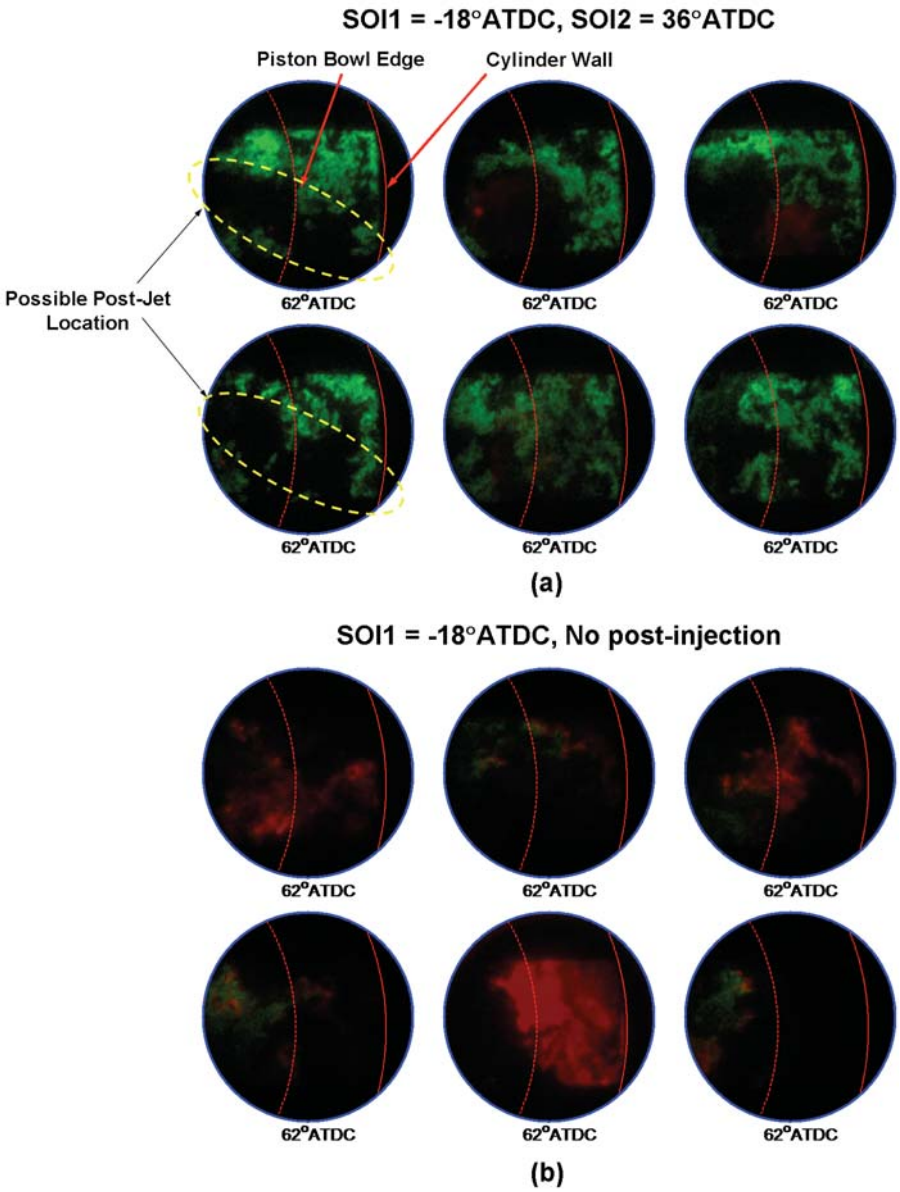

Figure 8. Simultaneous single-shot soot-LII and OH-PLIF images acquired at 62°ATDC for an early main-injection case (a) with and (b) without a post injection at 36°ATDC. The OH-LIF signal is false-colored in green, while soot-LII is shown in red in the images. Any spatial overlap of soot-LII and OH-PLIF appears yellow

in soot distribution are due to engine cycle-to-cycle variation). The post injection at 32°ATDC is evident in the soot luminosity images starting at about 44°ATDC, as marked in the figure. The post jet at this timing fully enters the squish volume, reaching all the way to the cylinder wall, as indicated by the weak jet-like structure in the soot luminosity images.

Figure 7 shows soot luminosity images for the same main injection, but a later post injection at 40°ATDC where the exhaust smoke is the same as the main-injection alone. The ignition delay for the post-injected fuel is relatively long and the jet is directed largely into the squish volume. Figure 7 shows that the early evolution of the main injection is reasonably similar to the case with no-post injection, as observed also in figure 6. The distribution of main-injection soot is similar to that of the no-post case, even late into the expansion stroke, which indicates that the post-injection does not significantly interact with the remnants of the main injection. Also, there is little or no soot luminosity visible in the post jets for this case (bearing a close resemblance to the case with no post injection), suggesting fuel from the post injection might be burning soot-free. However, it might also be possible that the soot is relatively cold after mixing with the colder squish-gases, and thereby does not emit appreciable natural luminosity. A better visualization of soot within the jet cross section can be provided by planar laser-induced incandescence imaging, which is less sensitive to relevant temperatures, along with simultaneous measurement of reaction zones using OH-PLIF in the engine cylinder.

Figure 8 shows simultaneous single-shot images of combined LII (red) and OH PLIF (green) from six different cycles at 62°ATDC for the early main injection case, both with (a) and without (b) a post injection at 36°ATDC. This post-injection timing lies in between the post timings for which natural soot-luminosity images are presented earlier (figure 6 and 7) and would yield exhaust smoke comparable to cases with main-injection alone. The chosen timing of 62°ATDC is late in the engine cycle, but well before exhaust-valve opening (at 125°ATDC). Therefore, the images shown illustrate the state of late-cycle soot long after the post-injection. These images were acquired in a plane 15 mm below the firedeck with the same field of view as the natural luminosity images in figures 6 and 7.

Overall, the case with a post injection shows significantly higher OH-PLIF signal, with much lower LII signal. Without a post injection, the residual OH-PLIF from combustion of main injection fuel is visible only in the upstream regions of the field of view. The weak OH-PLIF without a post injection is likely due to, at least in part, reduced OH concentrations because of lower in-cylinder temperatures in the expansion stroke, as previous 2-color soot measurements indicated [2]. Additionally, the OH signal with a post injection is widely distributed through most of the sheet, whereas only small pockets of weak OH-PLIF are apparent without a post injection.

The dark zones within the OH-PLIF distributions possibly represent regions of unmixed ambient fluid, unburned fuel, or either fuel-lean or fuel-rich pockets where OH concentrations are low. Some cycles with a post injection in figure 8a show weak soot LII within some of the dark regions suggesting that these pockets are likely fuel-rich. In addition, the similarity of the slightly downward-tilting “jet-like” dark zones, as marked in figure 8a, with the natural soot-luminosity images from 60-70°ATDC in figure 6a, further suggest that some of the dark zones are fuel-rich pockets in the post-injection jet that may form soot in some cycles. However, although the post-jet injected at 32°ATDC (figure 6a) has significant soot luminosity, the LII images for post jet at 36°ATDC show relatively weak LII signal, which is more similar to the soot luminosity images for post jet at 40°ATDC (figure 7a). The LII data, along with the soot luminosity imaging, confirm that the post jets at the later “optimal” timings are burning relatively soot-free. The post injections also clearly affect residual soot from the main injection. In images for the case without a post injection (figure 8b), the LII images show significant soot remaining from the main injection. With a post injection, the soot LII signal is considerably weaker, and generally more restricted to a central region of the post-injection jet.

While single-shot images like those in figure 8 are valuable because they portray the actual, instantaneous jet dynamics, it is difficult to make clear conclusions about the effects of post-injections on in-cylinder soot because of substantial variability from one-cycle to the next. A better understanding of the general evolution of soot and reaction zones with and without post injections can be gained from observations of ensemble-averaged LII and OH-PLIF images. Figure 9 shows a progression of ensemble-averaged soot (LII) and reaction zones (OH-PLIF) averaged over 30 cycles. The images are acquired at two laser-sheet heights of 15 and 29 mm from the firedeck, for the early main injection with a post injection at 36°ATDC. The figure also compares images to the case with a main-injection alone. For operation without the post injection, some soot resides close to the cylinder wall by 46°ATDC and spreads over most of the squish region by 62°ATDC at both the sheet heights. The OH-LIF signal on the other hand is primarily limited to upstream regions of the jet (left side of the field of view) and is distributed across the laser sheet in these average images.

Prior to 50°ATDC, when the post jet reaches the field of view, the LII and OH PLIF images look very similar with or without the post injection. Beyond 50°ATDC, the post-injection case has a stronger OH-PLIF signal at both sheet heights. In the plane 15 mm from the cylinder head, the OH distribution is asymmetric, and the center of the post jet is visible as a weak downward tilting darker region in the OH image, similar to that observed in the instantaneous frames of figure 8a. OH radicals from the neighboring jet seem to be carried down into the field of view by the clockwise swirl in the engine cylinder. In the plane 29 mm from the cylinder head, which is approximately 10 mm below the intersection of the nominal jet axis and the cylinder wall, the OH-PLIF is more evenly distributed across the field of view. Although a few cycles occasionally show strong instantaneous soot LII (see figure 8), in these averaged images, the soot LII is weak in the squish region (compared to the late main-injection case presented later in the paper), even without a post injection. With the introduction of a post injection, the soot LII signal is almost non-existent. Although the post injection fills the squish region with OH radicals for this early main-injection case, there is not much soot-oxidation interaction between the injections due to low-levels of soot in the squish. Most of the soot from the main injection in this case is contained within the piston bowl [2], while the post injection is largely directed into the squish region. Therefore, without potential for significant interaction, addition of the post injection can at most reduce exhaust soot down to the level of the main injection only, consistent with the exhaust smoke measurements in figure 1.

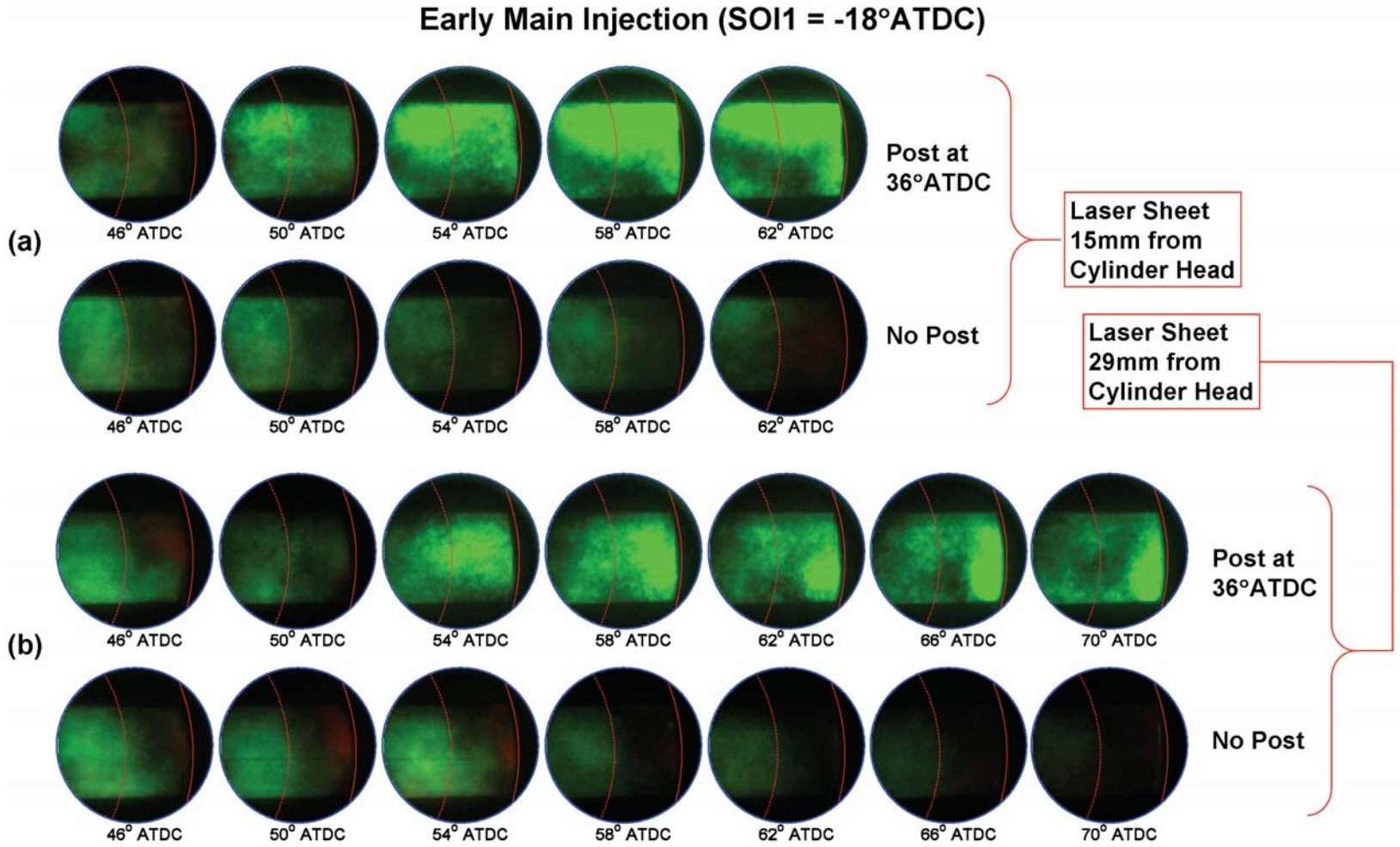

Figure 9. Ensemble averaged soot LII (red) and OH PLIF (green) through the expansion stroke for an early main-injection of -18ºATDC with and without a post injection for two sheet heights of (a) 15 and (b) 29 mm from the cylinder head

3.2 Late Main-Injection Case (SOI1=2ºATDC)

Figure 10 shows images from high-speed movies of natural soot luminosity for a late main injection at 2°ATDC and a post injection at the "optimal" timing of 40°ATDC (adapted from [2]). Similar to figure 7 for the early main-injection, the post-injection image sequences (left) are compared to the reference case with the same main-injection timing but without a post injection (right). In figure 10, the soot luminosity first appears at 14 ATDC, and with the top of the piston 5 mm below the firedeck, a significant portion of the soot (luminosity) from the main injection enters the squish volume. This also is reflected in the in-cylinder soot mass measurements from figure 2 (right), where the peak squish soot-mass without a post injection is almost a third of that found in the piston bowl.

At the post-injection timing of 40°ATDC, the nominal jet axis is well above the piston bowl edge so that the post-jet can enter the squish volume. The post-jet has very little soot luminosity and, hence, cannot be clearly seen in the luminosity image sequence in figure 10. Rather, evidence of the effect of the post injection is primarily manifest in the reduction of soot luminosity remaining from the main injection. Starting near 40º ATDC, when the post injection is introduced, the soot luminosity from

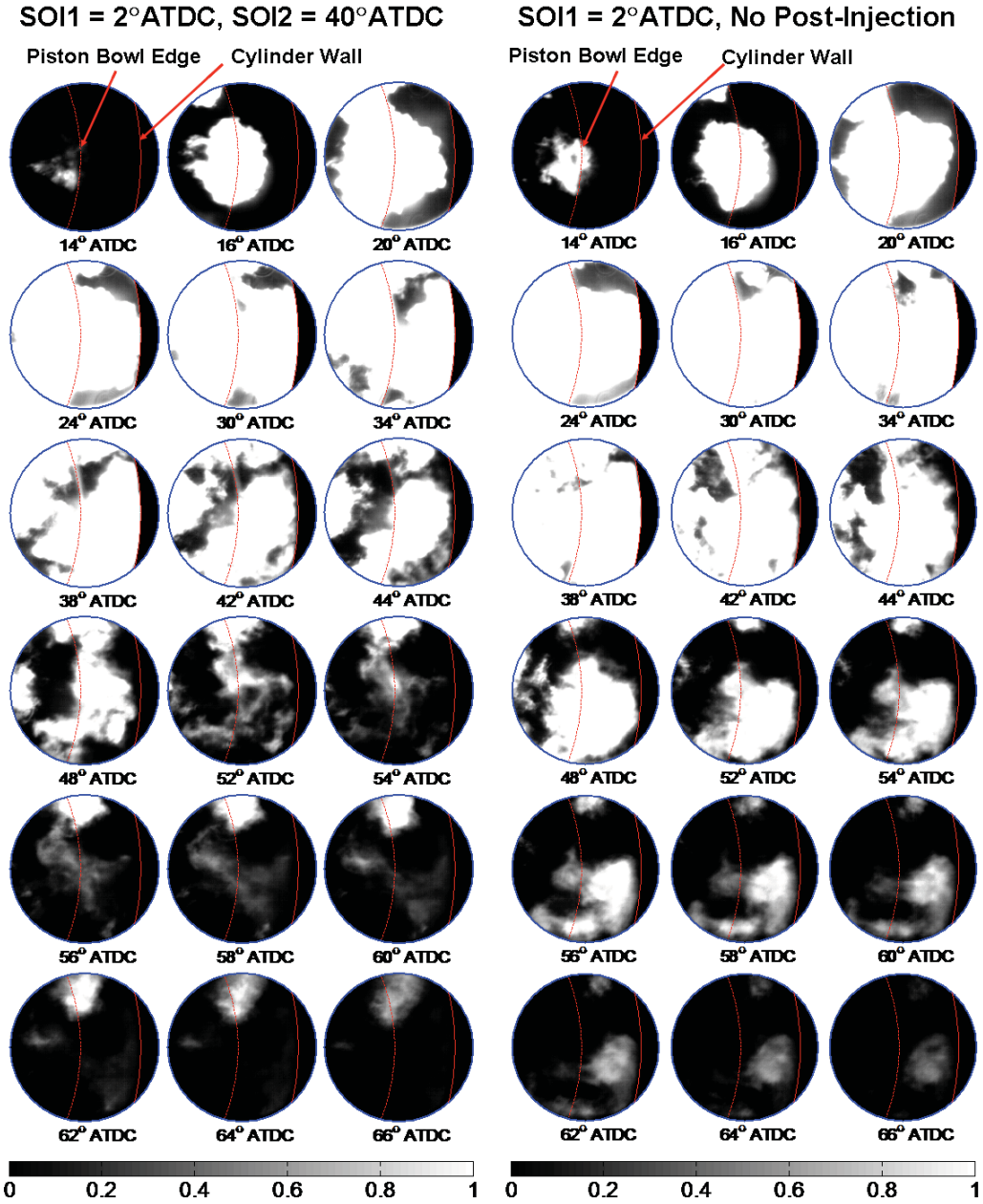

Figure 10. Sequential high-speed natural soot luminosity images for the late main injection (SOI1=2°ATDC) case with (left) and without (right) a post injection at 40°ATDC (adapted from [2])

the main injection starts to decrease at the center of the image when compared to the no-post injection case shown on the right. A weak outline of the post jet is visible in soot-luminosity images from 58º to 62º ASI, as the post jet impinges on the cylinder wall after interacting with the soot from the main injection. The post jet is tilted slightly downwards due to the action of the clockwise in-cylinder swirl. This weak soot luminosity in the lower half of the image is however significantly reduced by 66°ATDC while some soot luminosity from the main-injection that is outside of the path of the post injection remains at the top of the image (compare to no-post case on the right). As discussed earlier, the reduction in natural soot-luminosity from the main-injection soot could be due to enhanced oxidation by the post injection, but mixing from the post injection could also cool the soot and hence reduce the luminosity. To better determine the effect of the post injection on in-cylinder soot independent of soot temperature, soot-LII and OH-PLIF images are compared.

A few selected frames of soot-LII and OH-PLIF images acquired at 62°ATDC, with and without the post injection at 36°ATDC, are shown in figure 11 for the late main-injection case. These images are acquired with the laser sheets positioned 15 mm below the cylinder head. Images for the case with main-injection alone show bright soot-LII, mainly near the piston-bowl edge and in the squish regions. Weak OH-PLIF from the combustion of the main-injection fuel is also still present at these late timings.

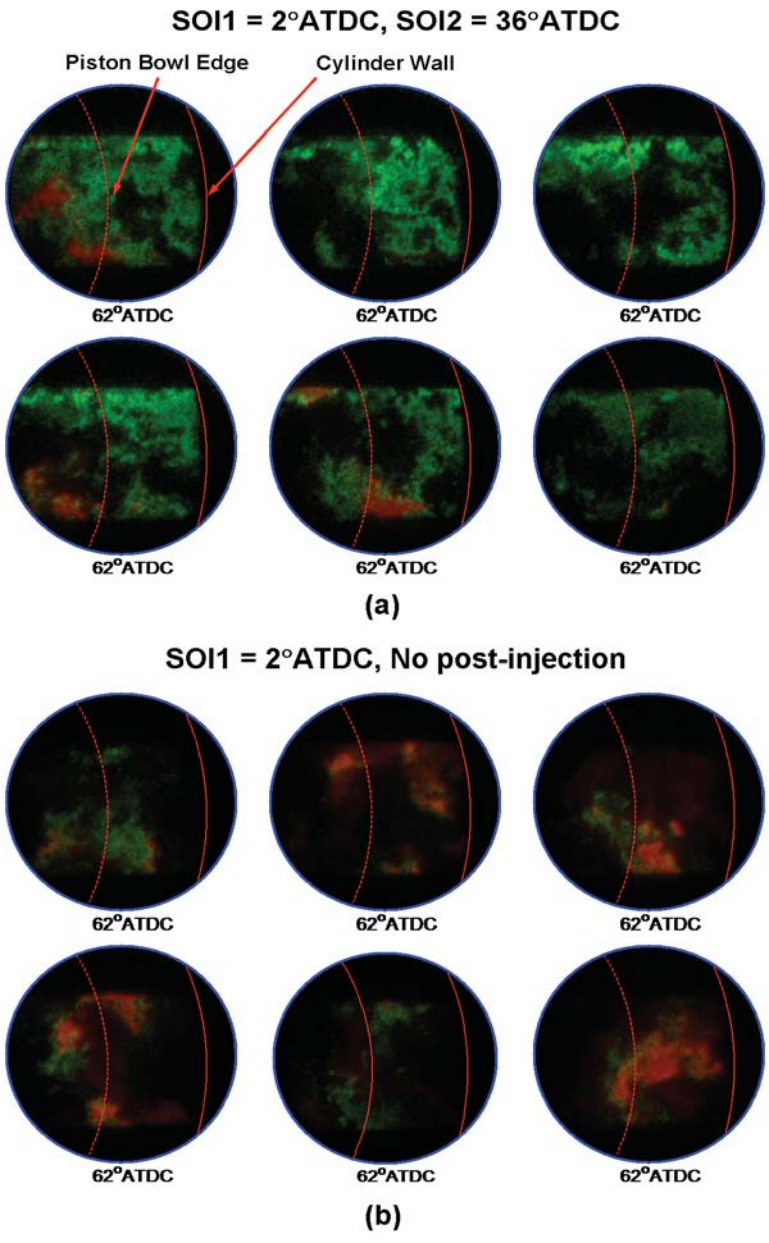

Figure 11. Simultaneous single-shot LII (red) and OH-PLIF (green) images acquired at 62°ATDC for the late main-injection case (a) with and (b) without a post injection at 36°ATDC.

The OH-PLIF signals are very stochastic, however, and are not confined to specific regions of the field of view. In comparison, images with a post injection show strong OH-PLIF over most of the laser sheet, with some intermediate dark zones. As with the early main-injection (figure 8), these dark regions possibly represent regions of unmixed ambient fluid, unburned fuel, or either fuel-lean or fuel-rich pockets where OH concentrations are low. Also, much like the early main injection case, some of the dark regions show soot-LII, indicating a portion of the post-injected fuel is burning fuel-rich above the sooting threshold at this condition. A portion of the fuel from the late main-injection spills over into the squish region (see figure 10) probably rendering richer stoichiometries in this region compared to an early main-injection case. Hence, when the post jet is injected into this region, it likely burns slightly richer producing some soot of its own. However, the soot-LII is significantly weaker than without a post injection.

The general evolution of soot and reaction zones is further studied with the help of ensemble-averaged LII and OH-PLIF images at the two laser sheet heights of 15 and 29 mm from the cylinder head, presented in figure 12. (The reader is cautioned that while the regions of LII (red) and OH-PLIF (green) overlap significantly in the averaged images (to yield yellow regions), instantaneous images (e.g. figure 11) show very narrow regions of overlap). For the baseline case without a post injection, stronger soot-LII is present in the squish region compared to the early main-injection case at both the sheet heights. The soot-LII in the 15-mm sheet height is mostly along the edge of the piston bowl at 46°ATDC, which is consistent with the natural-luminosity frames shown in figure 10 for the no-post case. Late in the cycle, by 62°ATDC, most of the field of view is filled with soot at both the sheet heights, on average. The soot-LII is stronger in the upper plane (15 mm from firedeck), which is close to the height where the nominal jet axis intersects with the cylinder wall. Even late in the cycle, the soot-LII signals in the lower plane remain relatively low as the piston descends, perhaps indicating that soot near the top of the in the squish region is not transported downward with the piston by the reverse-squish flow.

The addition of the post injection drastically alters the spatial extent of the soot-LII and OH-PLIF for this late main-injection case. Near 50°ATDC, the post injection starts to appear in the images in the form of the green OH-LIF region. Later, by 62°ATDC, the OH-PLIF distribution in the 15-mm sheet is asymmetric, with higher LIF signal at the top of the image. This is most likely due to clockwise swirl transporting some of the OH radicals into the middle of the field of view from the perimeter of the post jet or from the neighboring jet. As the OH-PLIF signal propagates across the image in the later frames, the soot-LII is almost completely absent by 60°ATDC at both the sheet heights, and OH-PLIF fills the field of view in the ensemble-averaged images. With this late main-injection, the post-injection directly interacts with a significant amount of soot left behind in the squish region from the main injection, as indicated by the yellow regions. The strong post-jet OH-PLIF signal indicates that soot oxidation is likely enhanced by increased OH, while further soot formation also may be prevented because the mixtures are more quickly leaned out (as evidenced by widespread OH formation).

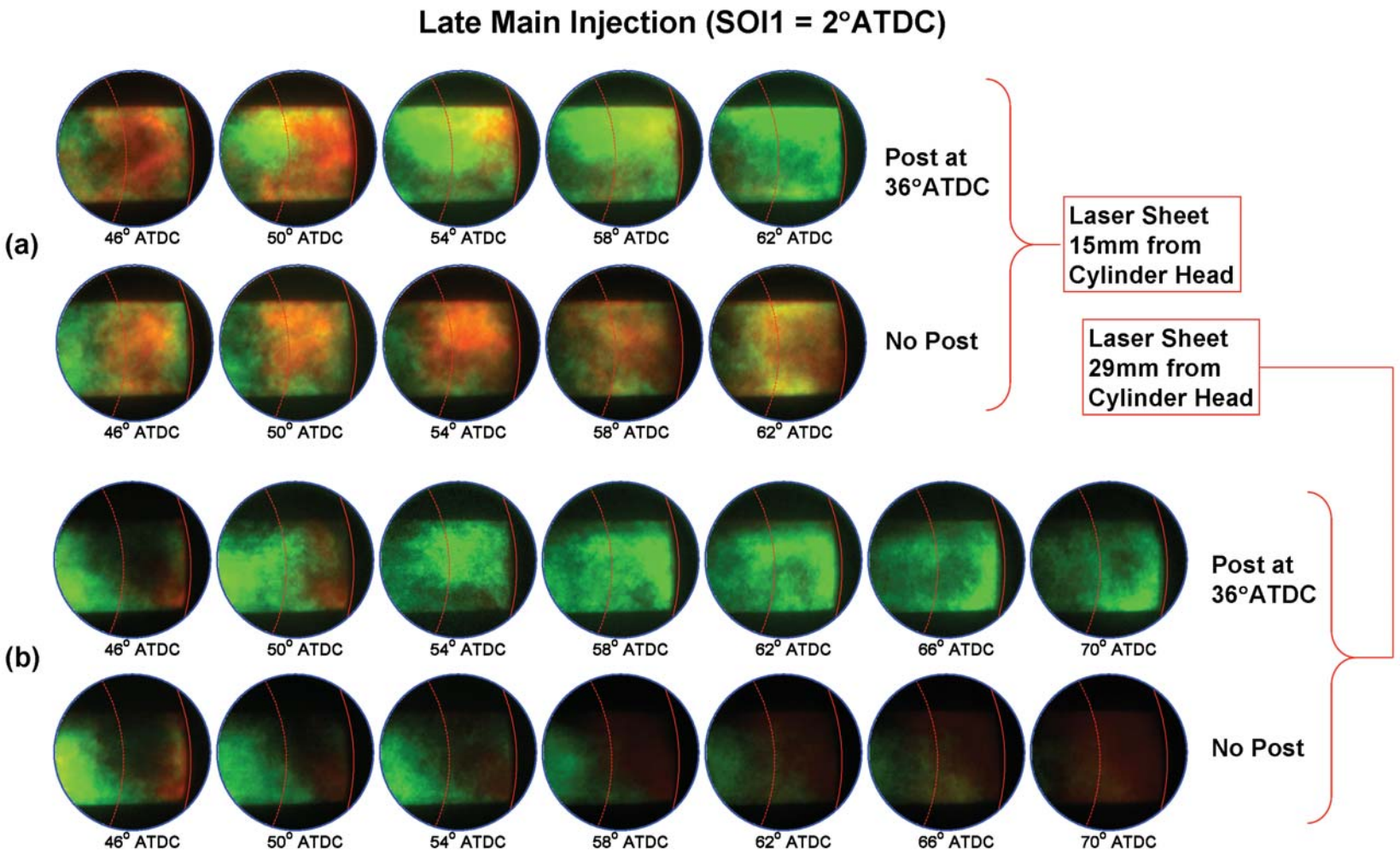

Figure 12. Ensemble averaged soot-LII (red) and OH-PLIF (green) images through the expansion stroke for a late main-injection of 2ºATDC with and without the post injection for two sheet heights of (a) 15 and (b) 29 mm from the cylinder head

Conclusions

The effects of post-injections on in-cylinder soot and OH distributions were examined using simultaneous imaging of planar laser-induced incandescence (LII) of soot and planar laser-induced fluorescence (PLIF) of OH in a single-cylinder optical heavy-duty diesel engine at mid-load low-temperature combustion (LTC) operating conditions. Late post injections with timings optimized to minimize exhaust soot were examined for two limiting cases: (1) an early main-injection for which the post injection did not decrease exhaust soot, and (2) a late main-injection for which the post-injection reduced the exhaust soot below the value of the main injection only.

For the early main injection, the soot-LII images show that, on average, very little soot from the main injection enters the squish region, and OH-PLIF signals become relatively weak late in the cycle. With the addition of a late post injection into the squish region, some additional soot appears within the post-jet on some cycles, but late-cycle OH-PLIF signals increase markedly on all cycles relative to the cases without post injections. Later in the cycle, the PLIF signal from soot-oxidizing OH remains much higher than for cases without a post injection, and soot-LII becomes very low. However, even though the post-injection burns largely soot free and generates significant late-cycle OH that could help oxidize soot, with early main-injection, very little main-injection soot is available in the squish region for oxidation.

For the late main injection, the soot-LII images show that, on average, a large fraction of soot from the main injection enters the squish region, and without a post injection, soot-LII within the squish region persists while the OH-PLIF intensity decreases late in the cycle. With the addition of a late post-injection into the squish region, the OH-PLIF intensity increases markedly while the soot-LII decreases. Late in the cycle, the OH-PLIF signal remains much higher and the soot-LII becomes much lower than for the case without a post injection. With significant residual soot from the main injection in the squish region, the post injection for the late main injection reduces in-cylinder soot considerably. The large increase in the OH-PLIF intensity coupled with the rapid decrease of soot-LII suggests that relatively soot-free combustion of the post-injection at an optimal timing helps to oxidize soot that is targeted by the post-injection in the squish region.

Acknowledgements

The optical engine experiments were performed at the Combustion Research Facility, Sandia National Laboratories, Livermore, CA. Support for this research was provided by the U.S. Department of Energy, Office of Vehicle Technologies. Sandia is a multi-program laboratory operated by Sandia Corporation, a Lockheed Martin Company for the United States Department of Energy's National Nuclear Security Administration under contract DE-AC04-94AL85000. The authors express their gratitude to David Cicone of Sandia National Laboratories for his assistance with maintaining the optical-access research engine used in these experiments.

References

1. Baratta M., Catania A. E., and Ferrari A. (2006), Hydraulic Circuit Design Keys to Remove the Dependence of the Injected Fuel Amount on Dwell Time in Multi-Jet C. R. Systems, ASME IC Engine Spring Conference, ICES 2006-1426.
2. Bobba M. K., Musculus M. P. B., and Neel W. (2010), Effect of Post Injections on In-Cylinder and Exhaust Soot for Low-Temperature Combustion in a Heavy-Duty Diesel Engine, SAE Paper 2010-01-0612.
3. Chen S. K. (2000), Simultaneous Reduction of NOx and Particulate Emissions by Using Multiple Injections in a Small Diesel Engine, SAE Paper 2000-01-3084, SAE Transactions, Vol. 109(3), pp 2127-2136.
4. Dec, J. E. (1997), A Conceptual Model of D.I. Diesel Combustion Based on Laser-Sheet Imaging, SAE Paper 970873, SAE Transactions 106(3), pp 1319-1348.
5. Desantes J., Arregle J., Lopez J. J., and Garcia A. (2007), A Comprehensive Study of Diesel Combustion and Emissions with Post-Injection, SAE Paper 2007-01-0915, SAE Transactions 116(3), pp 542-550.
6. Dronniou N., Lejeune M., Balloul I., and Higelin P. (2005), Combination of High EGR Rates and Multiple Injection Strategies to Reduce Pollutant Emissions, SAE Paper 2005-01-3726.

7. Han Z., Uludogan A., Hampson G. J., and Reitz R. D. (1996), Mechanism of Soot and NOx Emission Reduction Using Multiple-Injection in a Diesel Engine, SAE Paper 960633, SAE Transactions 105(3), pp 837-852.
8. Hardy W. L. and Reitz R. D. (2006), An Experimental Investigation of Partially Premixed Combustion Strategies Using Multiple Injections in a Heavy-Duty Diesel Engine, SAE Paper 2006-01-0917, SAE Transactions 115(3), pp 514-531.
9. Helmantel A. (2008), Reduction in NOx Emissions from a Light Duty DI Diesel Engine in Medium Load Conditions with High EGR Rates, SAE Paper 2008-01-0643.
10. Heywood J. B. (1988), Internal Combustion Engine Fundamentals, McGraw-Hill, Inc.
11. Horibe N. and Ishiyama T. (2009), Relations among NOx, Pressure Rise Rate, HC and CO in LTC Operation of a Diesel Engine, SAE Paper 2009-01-1443.
12. Hotta Y., Inayoshi M., Nakakita K., Fujiwara K., and Sakata I. (2005), Achieving Lower Exhaust Emissions and Better Performance in an HSDI Diesel Engine with Multiple Injection, SAE Paper 2005-01-0928, SAE Transactions 114(3), pp 883-898.
13. Husberg T., Denbratt I., and Karlsson A. (2008), Analysis of Advanced Multiple Injection Strategies in a Heavy-Duty Diesel Engine using Optical Measurements and CFD-Simulations, SAE Paper 2008-01-1328.
14. Musculus M. P. B., Dec J. E. and Tree D. R. (2002), Effects of Fuel Parameters and Diffusion Flame Lift-Off on Soot Formation in a Heavy-Duty Diesel Engine, SAE Paper 2002-01-0889, SAE Transactions 111(3), pp 1467-1489.
15. Ojeda W., Zoldak P., Espinosa R., and Kumar R. (2009), Development of a Fuel Injection Strategy for Partially Premixed Compression Ignition Combustion, SAE Paper 2009-01-1527, SAE International Journal of Engines 2(1), pp 1473-1488.
16. Payri F., Benajes J., Pastor J. V., and Molina S. (2002), Influence of the Post-Injection Pattern on Performance, Soot and NOx Emissions in a HD Diesel Engine, SAE Paper 2002-01-0502.
17. Sjöberg M. and Dec J. E. (2004), An Investigation of the Relationship between Measured Intake Temperature, BDC Temperature, and Combustion Phasing for Premixed and DI HCCI Engines, SAE Paper 2004-01-1900, SAE Transactions 113(3), pp 1271-1286.
18. Tow T. C., Pierpont D. A., and Reitz R. D. (1994), Reducing Particulate and NOx Emissions by Using Multiple Injections in a Heavy Duty D.I. Diesel Engine", SAE Paper 940897, SAE Transactions 103(3), pp 1403-1417.